UC Berkeley
UC Berkeley Electronic Theses and Dissertations

Title

Formal Developments for Hadronic Reactions with Quantum Computers

Permalink

https://escholarship.org/uc/item/0hs1z1gp

ISBN

9798173789723

Author

Burbano Aldana, Ivan Mauricio

Publication Date

2026-08-10

Peer reviewed|Thesis/dissertation

eScholarship.org Powered by the California Digital Library
University of California

Formal Developments for Hadronic Reactions with Quantum Computers

by

Ivan Mauricio Burbano Aldana

A dissertation submitted in partial satisfaction of the

requirements for the degree of

Doctor of Philosophy

in

Physics

in the

Graduate Division

of the

University of California, Berkeley

Committee in charge:

Doctor Christian W. Bauer, Co-Chair
Professor Raúl A. Briceño, Co-Chair
Professor Luca Victor Iliesiu
Professor Michael Lindsey

Summer 2026

Formal Developments for Hadronic Reactions with Quantum Computers

Copyright 2026
by
Ivan Mauricio Burbano Aldana

Abstract

Formal Developments for Hadronic Reactions with Quantum Computers

by

Ivan Mauricio Burbano Aldana

Doctor of Philosophy in Physics

University of California, Berkeley

Doctor Christian W. Bauer, Co-Chair

Professor Raúl A. Briceño, Co-Chair

Lattice quantum chromodynamics provides a systematically improvable, first-principles framework for studies of nonperturbative strong-interaction physics. Although largely successful on traditional computing platforms, conventional lattice quantum chromodynamics has not yet furnished a way to study general reactions with arbitrary particle multiplicities and kinematics. In this dissertation, we present the Real-Time Estimators for Scattering Observables proposal for the study of general scattering amplitudes using implementations of lattice quantum chromodynamics on quantum computers. We show, to all orders in perturbation theory and at a fixed non-zero regulator, that the finite-volume effects in this proposal are exponentially suppressed. Realizing this program requires a formulation of quantum chromodynamics amenable to quantum computation. As a step in this direction, we also provide a fully gauge-fixed Loop-String-Hadron basis for pure SU(2) Yang–Mills theory, a simpler theory that shares key structural features with the gauge sector of quantum chromodynamics. The resulting basis uses discrete labels that facilitate truncations for weak-coupling studies. Accompanying these advances, this dissertation includes a pedagogical introduction to lattice quantum field theory, with an emphasis on explicit calculations in exactly solvable models.

Dedication

Para El Hijo, gracias por acompañarme en cada segundo de mi vida.

Contents

1 Towards Hadronic Reactions with Quantum Computers **1**
- 1.1 Why Hadronic Reactions? . . . 1
- 1.2 Why Lattice Quantum Chromodynamics? . . . 3
- 1.3 Some Successes of Lattice Quantum Chromodynamics and the Need for Quantum Computers . . . 5
- 1.4 Some Successes of Quantum Computers for the Study of Particle Physics . 7
- 1.5 Reading Guide . . . 8

2 Loop-String-Hadron Formulation for Fully Gauge-Fixed SU(2) **Lattice Gauge Theory** **11**
- 2.1 Yang-Mills Theory . . . 12
  - 2.1.1 Euclidean Theory . . . 12
  - 2.1.2 Kogut-Susskind Hamiltonian . . . 19
  - 2.1.3 Magnetic Bases . . . 26
  - 2.1.4 Electric Bases . . . 28
- 2.2 Yang-Mills on General Graphs . . . 34
  - 2.2.1 Basics of Graph Theory . . . 34
  - 2.2.2 Classical Aspects . . . 36
  - 2.2.3 Quantum Aspects and Symmetries . . . 39
- 2.3 Examples of Graph-Coarsening . . . 41
  - 2.3.1 Point-Splitting . . . 41
  - 2.3.2 Maximal-Tree Gauge Fixing . . . 45
  - 2.3.3 Plaquette Flower . . . 47
  - 2.3.4 Branch . . . 49
- 2.4 Loop-String-Hadron Formulation on General Graphs . . . 51
  - 2.4.1 Loop-String-Hadron on Half-Edges . . . 53
  - 2.4.2 Loop-String-Hadron on Corners . . . 57
  - 2.4.3 Loop-String-Hadron on Links . . . 58
  - 2.4.4 Loop-String-Hadron on Trajectories . . . 62
  - 2.4.5 Loop-String-Hadron on Vertices . . . 65

2.5 Loop-String-Hadron on Branches . . . 69
2.5.1 States on the Branch . . . 69
2.5.2 Magnetic Hamiltonian . . . 72
2.5.3 Ultralocal Electric Hamiltonian . . . 75
2.5.4 Comments on Nearest Neighbor Interactions . . . 77
2.5.5 Examples . . . 77

3 Scattering in Finite Volumes 82
3.1 The S-matrix . . . 82
3.2 Single-Particle States . . . 84
3.3 Exciting Single-Particle States . . . 85
3.4 LSZ Reduction Formula . . . 87
3.5 $2 \to 2$ Scattering . . . 89
3.6 Real-Time Estimators for Scattering Observables . . . 93
3.6.1 Spectral Structure of Estimators . . . 94
3.6.2 The Proposal . . . 96
3.6.3 Finite-volume Effects on Feynman Diagrams . . . 97
3.6.4 Bubble Diagrams . . . 102
3.6.5 Applications to Traditional Lattice QCD . . . 103

4 Conclusions and the Path Forward 112

A Introduction to Lattice Quantum Field Theories 114
A.1 Path Integrals . . . 115
A.2 Time Evolution Operator . . . 117
A.3 Path Integral Quantization . . . 122
A.4 Comments on Renormalization . . . 125
A.5 Schwinger-Dyson Equations . . . 126
A.6 Spectrum in a Euclidean Finite Volume . . . 128
A.7 1D Ising Model . . . 129
A.7.1 Classical Statistical Mechanical Interpretation . . . 130
A.7.2 Hamiltonian . . . 132
A.7.3 Renormalization . . . 135
A.7.4 Operators . . . 137
A.7.5 Correlation Functions . . . 138
A.7.6 First quantization . . . 139
A.7.7 Quantum Implementation . . . 142
A.8 Harmonic Oscillator . . . 144
A.8.1 Hamiltonian . . . 146
A.8.2 Renormalization . . . 148

A.8.3 Operators 151
A.8.4 Correlation Functions 152
A.9 2D Ising Model 155
A.9.1 Hamiltonian 156
A.9.2 Diagonalization of the Hamiltonian 158
A.9.3 Spectrum 164
A.9.4 Renormalization 168

List of Figures

1.1 Relative error in the N-th partial sum of (1.3), when compared to a direct numerical evaluation of (1.2). 4

2.1 The oriented link $\ell = (b, a)$. 29
2.2 (b) shows a vertex in a graph $\mathrm{G}_{\mathrm{red}}$ that has valency n. (a) shows the graph G obtained by point splitting $\mathrm{G}_{\mathrm{red}}$, which has now a vertex of valency $n-1$ and one of valency 3. From the point of view of this dissertation $\mathrm{G}_{\mathrm{red}}$ is obtained from G using graph coarsening with the trajectories $v_1 w$ and $v_2 w$. 42
2.3 (a) A maximal tree in a square lattice is shown in blue. We can find labelled one of the links ℓ that is not on the maximal tree, its source $s(\ell)$ and target $t(\ell)$ vertices, and a choice of root $\star$ for the maximal tree. The trajectory γ_ℓ is shown in red. It is explicitly shown in its decomposition $\gamma_{\star \leftarrow t(\ell) \ell \gamma_{s(\ell) \leftarrow \star}}$, with the factors separated by the vertices $s(\ell)$ and $t(\ell)$. (b) The flower obtained by coarse graining the square lattice through the trajectories obtained for each choice of ℓ not within the maximal tree. 44
2.4 The trajectory $\gamma^{-1}_{(\boldsymbol{x}+e_2)_1} \gamma_{\boldsymbol{x}_1}$ is shown, showing that the Wilson loop on it is equivalent to that of the plaquette $\boldsymbol{x}_{12}$. 46
2.5 Generic loop in the construction leading to a flower whose links correspond to plaquettes. 48
2.6 Trajectory built out of trajectories in T' with the same Wilson line as the trajectory shown in Fig. 2.3a. 48
2.7 Branch G with $P = 9$ leaves. Its maximal tree highlighted in blue. In red is shown an example γ_4 of the trajectories in T for which the coarse-graining procedure leaves to a flower $\mathrm{G}_{\mathrm{red}}$ as the one shown in Fig. 2.3b. 50
2.8 i-th leaf of a branch. 50
2.9 Trajectory $\gamma_{p_4 \leftarrow p_8} \ell_8^{-1} \gamma_{p_8 \leftarrow p_4} \ell_4$ carrying the same Wilson loop as $\gamma_8^{-1} \gamma_4$. . . . 52
2.10 Embedding of a branch in a $d = 2$ lattice compatible with the plaquette flower construction. 52

2.11 The orientation on a pair of leaves in a branch is shown. The arrows on each link determine our convention for their orientation, so that loops are oriented clockwise, horizontal links from left to right and vertical links from bottom to top. Additional guiding arrows show the orientation of each vertex, so that their half-edges are oriented clockwise. 69
2.12 Labeling of the corners on the i-th leaf compatible with the vertex orientation choices in Fig. 2.11. 70
2.13 Spin labels counting the number of fluxes through each edge (2.304). 72
2.14 Labelling convention for the branch half-edges. 73
2.15 Energy levels measured with respect to the ground state are shown in solid lines. The one with transparency corresponds to a truncation into the Hilbert space with a maximum $n = 2^4$. The one without has a maximum $n = 2^7$. Dashed lines correspond to the exact solutions at $g = 0$ and at strong coupling. 79
2.16 (a) A two-plaquette chain with a choice of half-edges H_T with the maximal tree compatible with Fig. 2.3a. The trajectories in T are shown in blue and red colors. (b) A $P = 2$ branch, whose loops are color coded to indicate correspondence to those on (a). 79
2.17 Spectrum for the two plaquette system. Dashed lines correspond to both the $g \to 0$ limit and the leading order strong-coupling expansion. Colors were chosen arbitrarily to gather states with a similar behavior at small g. These were obtained using sparse matrices. The truncation was chosen so that $N(n_i) \leq 2^6$ and $L \leq 3$. 81

3.1 Example of a trajectory $\mathcal{C}$ that can be smoothly deformed to an infinitesimal loop around z without going through the positive real line. 95
3.2 Bubble diagram. 102
3.3 Finite-Volume effects for the bubble diagram in Fig. 3.2 in $D = 2$ with $\boldsymbol{n} = 1$. Calculations were done in the CM frame. (a) was done below the two particle threshold $E^* = m < 2m$. The overlapping lines show that the suppression of finite-volume effects is independent of ϵ. (b) was done above the two particle threshold $E^* = 3m > 2m$. Vertical dashed lines correspond to $\epsilon L/E^* = 1$, which marks the transition in which the exponential suppression starts becoming considerable. The Horizontal dashed line is a visual aid. . 104
3.4 $D = 4$ correspondence to Fig. 3.3 with $\|\boldsymbol{n}\| = 1$. Note that the suppression at large L is enhanced by comparison with the $D = 2$ case due to the power law effects. 105

3.5 Finite-volume effects for the bubble diagram in $D = 2$. Black line shows the results in the CM frame for $E_0^* = \sqrt{s_0} = 3m$. Blue dots correspond to averaging over all kinematics of a two-particle state in which none of the particles have momentum higher than $\frac{\pi}{8a}$ and where their corresponding s is within 1% of s_0. The lattice spacing is taken to be $ma = 0.1$ 106
3.6 Approximations to I_L for the bubble diagram Fig. 3.2 at $D = 4$. Calculations were done in the CM frame with $E^\star = 3m$ and $\epsilon = 0$. Blue dots correspond to the naive results, which lead to a divergent series. The red line corresponds to the diagonal elements of the Padé table where the terms have been organized by $\|\boldsymbol{n}\|$. The black horizontal line corresponds to the result through an implementation of the more traditional methods [53]. . . 111

A.1 A generic spacetime $\mathcal{M}$ is shown which is bounded by an initial time slice Σ_i and a final time slice Σ_f. 116
A.2 A spacetime with an incoming boundary Σ_i, an outgoing boundary Σ_f, and a spatial slice Σ. 118
A.3 Subfigure (a) corresponds to a spacetime of the form $\mathcal{M} = [0, T] \times \Sigma$. The time coordinate has the range $0 \leq t \leq T$. Subfigure (b) corresponds to a spacetime of the form $\mathcal{M} = S^1 \times \Sigma$, with a circle of circumference T. In this case the time coordinate has the identification $t \sim t + T$. 120
A.4 A spacetime with spatial slices Σ_i, Σ_1, Σ, Σ_2 and Σ_f, in that temporal order. 124
A.5 Renormalization (A.76) of the coupling of the 1D Ising model as a function of the lattice spacing ϵ. 136
A.6 One point function for the 1D Ising model on a time interval with $mT = 10$ and $\varphi_i = 1$. In solid the continuum result is shown. Scattered points correspond to an Ising chain with $N_t = 20$ links. This corresponds to $K \approx 0.7$. In dashed lines is the result with $T \to \infty$. Letting $t = t_2 - t_1$, these also correspond to $\langle \phi(t_2)\phi(t_1) \rangle$ on this open interval. The $\varphi_f = 1$ curve also yields $\langle \phi(t_2)\phi(t_1) \rangle$ for periodic times. 140
A.7 Transition probability $|\langle 1|U(t)|1\rangle|^2$ in the 1D Ising model. The data were run on `ibm_marrakesh`, with 4096 shots used for each point. 143
A.8 Mass renormalization (A.139) for the harmonic oscillator. 150
A.9 Two-point function for the harmonic oscillator on a periodic time with $mT = 10$. In solid the continuum result is shown. Scattered points correspond to a chain with $N_t = 5$ links. In dashed lines is the result with $T \to \infty$. In crossed markers, we show the naive unrenormalized propagator $m_0 \langle \phi(t)\phi(0) \rangle$ on the chain, had we taken instead $m_0 T = 10$, showing the importance of renormalization in comparing lattice and physical results. 153

A.10 Spectrum of the 2D Ising model in the disordered phase $B/J = 1.25$, with $N_s = 6$. Thin solid and dashed lines correspond to fermionic levels in the NS and R sectors. Scattered points correspond to those states that persist in the 2D Ising model. Scattered squares are the energies E/B of the states in the dual ordered phase with $J/B = 1.25$. The solid curved line corresponds to the dispersion relation of the single particle states. Only states with even total momenta are shown since all the states in the 2D Ising model satisfy this. 166
A.11 Renormalization group flow of the parameters B and J in the disordered phase. 169
A.12 Renormalization group flow of the parameters g and ϵ in the disordered phase. 170

Acknowledgements

This dissertation would not be possible without my mother, Martha Cecilia Aldana Clavijo. She made it a priority to be available for me whenever I needed her, regardless of what was going on in her life. She exemplifies in her day-to-day life what true love looks like, and I count myself lucky to be one of the recipients of her care. Gracias mamá. I hope to live up to the standard you set every day.

I would also like to thank my advisors, Raúl Briceño and Christian Bauer. Their guidance, not only in our specific research projects, but more broadly in how to become a good scientist, will always stay with me. They taught me what it looks like to bring out the best in people in a caring, thoughtful and humane way. If I am fortunate enough to manage my own research group in the future, I will strive to mirror their mentorship with my students.

The welcoming and nurturing environment they have created within their research groups was essential for me. I would like to thank everyone in these groups for everything they taught me. In particular, postdoctoral researchers like Felipe Ortega-Gamma, Anthony Ciavarella, Dimitra Pefkou, Jesse Stryker, Thomas Richardson and Zack Hall were integral throughout my studies. I hope to also mirror their mentoring now that I will also be starting my postdoctoral journey.

Finally, I would also like to thank the community of Berkeley. The love and support Alice Lily Schmitz, the band Casachanclas, and the UC Berkeley Salsa group were fundamental. I would also like to highlight the support of my fellow physics colleages, including Nicole Farias, Joseph Slivka, Joseph Moscoso, Anna Coerver, Marco Carrillo, and in general everyone that danced, played games, shared music and laughed with me. You will all be in my heart forever.

Chapter 1

Towards Hadronic Reactions with Quantum Computers

1.1 Why Hadronic Reactions?

We have been able to identify four fundamental interactions in nature. These are the gravitational, electromagnetic, weak and strong interactions. The Standard Model (SM) of particle physics is our best theory for the last three. The SM has passed a wide range of precision tests [1]. For example, agreement between experimental and theoretical determinations of the anomalous magnetic moment of the electron has been demonstrated at approximately one part in 10^{12} [2].

There are, however, regimes in which SM predictions are difficult to calculate. This makes comparisons with experiment challenging. In the SM, quantum chromodynamics (QCD) describes quarks and gluons as the fundamental particles participating in the strong interactions. These have a property known as color charge. A phenomenon known as confinement, however, prevents colored particles from being observed in isolated asymptotic states. Instead, at ordinary temperatures and densities, they are confined within color-neutral particles known as hadrons [3]. Through a mechanism we will illustrate in Section 1.2, SM predictions at hadronic energy scales are particularly challenging. This dissertation develops formal tools for the calculation of such hadronic reactions with quantum computers. The long-term goal is to make these predictions feasible, so that more stringent tests on the SM can be performed and the frontiers of validity of the theory can be clarified.

The existence of these frontiers has been established experimentally, showing that the SM is incomplete. Physics beyond the Standard Model (BSM) is therefore required. Direct evidence for it comes from neutrino oscillations. These indicate that neutrinos are massive [4], which the minimal SM does not accommodate. Astrophysical observations also provide compelling evidence for dark matter and dark energy, whose microscopic origins

are not described by the SM. Other unsolved problems include the strong CP problem [5] and the matter-antimatter asymmetry we observe in the universe [6]. Many experiments probing these questions require precise SM predictions to distinguish BSM physics from the SM background. In several examples, these involve many-body hadronic reactions.

To make this concrete, let us consider the Deep Underground Neutrino Experiment (DUNE). It will characterize differences between the behavior of neutrinos and antineutrinos [7]. This could inform the origin of the prevalence of matter over antimatter that we see in the universe [8]. The principal detection mechanism will be the scattering of neutrinos and antineutrinos with a liquid argon target [9]. Electroweak interactions with the neutrino beam will produce hadronic transitions in the argon nuclei. The initial and final nuclei are many-body systems, composed of several protons and neutrons, collectively known as nucleons. Furthermore, final states in these transitions could contain other hadronic byproducts. For these reasons, as well as the presence of electroweak mediators, this is precisely a many-body hadronic reaction [10].

Another example is neutrinoless double beta decay. Observation of this reaction would confirm the Majorana nature of neutrinos, so that they would be their own antiparticles [11]. As in the case of DUNE, this would play an important role in our understanding of matter-antimatter asymmetry [12]. The more traditional two-neutrino double beta decay acts as a background SM effect. Both of these are hadronic transitions mediated by electroweak currents. A pair of neutrons within the initial nuclear environment will end up decaying into a pair of protons in the final state.

Besides BSM physics, the phenomenology of strong interactions is in itself rich and interesting. As a first example of this, let us consider nucleons themselves, the principal hadronic constituents of ordinary matter. Initial attempts at understanding these in terms of the constituent quark model painted a picture in which nucleons were bound states of three quarks [13]. It is now clear, however, that this is incomplete. Instead, nucleons are complex *soups* of strongly interacting quarks and gluons [14]. One of the objectives of the Electron-Ion Collider (EIC) will be to map out this structure and understand how nuclear properties arise from QCD. The main experimental probe at the EIC will be the scattering of electrons off nuclei, producing a variety of hadronic byproducts [15]. This will therefore be yet another example of a many-body hadronic reaction mediated by electroweak interactions.

Let us conclude our motivation by noting that the hadronic spectrum extends far beyond nucleons and nuclei. Conventional hadrons of the quark model have quantum numbers consistent with composites of a quark-antiquark pair or three quarks. There are, however, exotic hadrons that do not conform to this norm. Potentially, there could be glueballs, whose predominant components would be gluons [16, 17]. Furthermore, tetraquarks [18], pentaquarks [19], hexaquarks, and so on, are also possible. Rather than occurring only as bound states, these exotic hadrons also tend to appear as resonances, which are short-lived intermediate states in scattering processes. Thus, theoretical studies

of exotic hadrons require predictions for these reactions [20]. These often involve several particles, with examples given by the decays $X(3872) \to J/\psi\pi^+\pi^0\pi^-$ [21] and $d^*(2380) \to NN\pi\pi$ [22]. External probes, such as electroweak and gravitational currents [23, 24], can provide additional structural information on the nature of these resonances. This is therefore yet another situation in which many-body strong reactions are required.

1.2 Why Lattice Quantum Chromodynamics?

The main analytic tool we have for the extraction of predictions from the SM is perturbation theory. In it, couplings g are identified which characterize the strength of the interactions. Predictions are made by initially considering the $g = 0$ case in which the theory is free. After this initial solution, the effects of $g \neq 0$ are incorporated slowly into the solution, order by order in g. Schematically, this yields answers in the form of power series in g

$$\text{prediction} = \sum_{n=0}^{\infty} a_n g^n. \tag{1.1}$$

As a simple example of how these predictions come about, consider the integral

$$I = \int \mathrm{d}x\, e^{-\frac{1}{2}x^2 + \frac{g}{4!}x^4}. \tag{1.2}$$

This integral is convergent for $g \leq 0$, but diverges for $g > 0$. Accordingly, a power series expansion (1.1) for the solution could potentially fail. Indeed, if it converges, it would have to do so within a disk centered at $g = 0$. But given that for $g > 0$ the integral is divergent, unless there is an analytic continuation of it, we conclude that the radius of this disk must be 0.

To make this concrete, we expand the integrand in powers of g, exchange the order of summation and integration, and employ Wick's theorem (which will be explained in Section A.5), yielding the series expansion

$$I = \sum_{n=0}^{\infty} \frac{g^n}{n!4!^n} \int \mathrm{d}x\, e^{-\frac{1}{2}x^2} x^{4n} = \sqrt{2\pi} \sum_{n=0}^{\infty} \frac{(4n-1)!!}{n!4!^n} g^n. \tag{1.3}$$

The error in the partial sums of this series is shown in Fig. 1.1 for three values of the coupling. This exemplifies a common behavior of perturbation theory [25]. If one adds a few terms, one can approximate the answer quite well. But if we start adding too many the result will begin to get worse.

In general, the degree of precision one can achieve with perturbation theory heavily depends on the magnitude of g. For g small, one can obtain many terms in perturbation theory before the result starts getting worse, thus allowing accurate predictions. However,

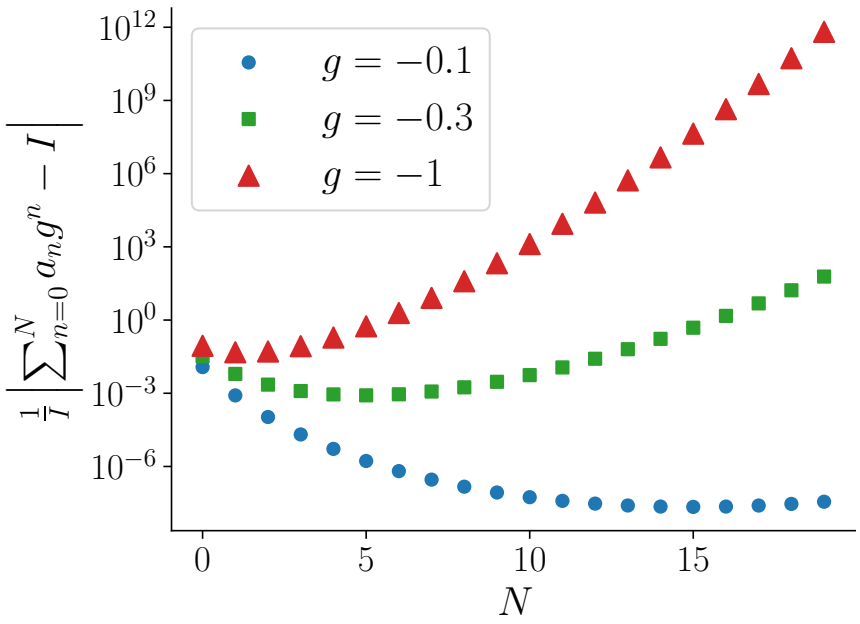


Figure 1.1: Relative error in the N-th partial sum of (1.3), when compared to a direct numerical evaluation of (1.2).

it is a generic feature of quantum field theories, such as the SM, that predictions (1.1) for phenomena at different energies require perturbation theory with different couplings g. In particular, in a regime in which the coupling g is large, it might be that no terms in (1.1) approximate the correct answer faithfully.

The sector of the SM that describes strong interactions is known as Quantum Chromodynamics (QCD). At high energies, the coupling constant of QCD is small, a phenomenon known as asymptotic freedom [26, 27]. In these regimes, perturbation theory can be used reliably. However, at the energy scales relevant to the reactions discussed in Section 1.1, the coupling g of the strong interactions grows. At this point, the theory becomes nonperturbative, and we must therefore search for a different tool for its analysis. The most broadly applicable, first-principles, systematically improvable framework for the exploration of QCD in the nonperturbative regime is Lattice Quantum Chromodynamics (LQCD) [28, 29]. In terms of our running example, traditional LQCD aims to directly compute the integral (1.2) through numerical methods.

It should be noted in passing that there are resummation techniques that can be used to improve the convergence of (1.1). An example of this is Padé summation, which will be discussed in Section 3.6.5. For the simple toy model (1.3), this technique produces the correct answer for all negative values of the coupling. It is, however, not expected that such techniques will allow one to resolve the strongly-coupled hadronic regime from perturbative methods.

1.3 Some Successes of Lattice Quantum Chromodynamics and the Need for Quantum Computers

In its traditional incarnation, meaning its implementation on traditional computing resources, LQCD relies on a crucial relation between quantum theories and classical statistical ones. This is often known as Wick rotation, and the equivalence between the two is abstractly ensured by the Osterwalder-Schrader axioms [30]. Practical examples of this relation form one of the central subjects of Chapter A. Classical statistical theories are well-suited for numerical exploration on traditional computing platforms, which made LQCD possible. The price to be paid, however, is that the outcomes of these calculations are most closely related to the classical statistical theory, not the quantum one. On top of this, due to the restrictions inherent to computational methods, the results have to be extracted on a finite volume. Thus, additional work is required to create dictionaries translating these results to the infinite-volume quantum theory.

For certain finite-volume observables of the quantum theory, such as single-particle energy levels and their equal-time matrix elements, this dictionary is simple. This is shown in Section A.6. Indeed, one of the major successes of LQCD has been the prediction of the masses of the low-lying stable states of QCD [31]. A classic result in [32] shows

that such masses only suffer exponentially suppressed finite-volume effects, so that they can be reliably extracted from finite-volume energy levels. Other applications of LQCD include the calculation of nonperturbative matrix elements that can be combined with perturbative calculations to obtain QCD predictions. A prime example of this is the recent role LQCD has played in alleviating the long-standing tension between experimental measurements and theoretical predictions of the muon anomalous magnetic moment in [33]. Other important examples include the determination of lattice constraints of several parton distribution functions and related quantities [34].

The main focus of this dissertation is, however, on reactions, which are inherently dynamical processes. These are particularly difficult to study through traditional LQCD for two reasons. First, in the transition to the classical statistical theory, Lorentzian spacetime gets replaced by a Euclidean one. This obscures the flow of time, making dynamical information harder to extract. Second, scattering processes require asymptotic states, states in which particles are sufficiently separated so that their interactions are negligible. In a strict sense, this is only achievable once the particles are infinitely far from each other, which is impossible in a finite volume. In practice, the propagation of intermediate on-shell states in finite distance is responsible for the power-law finite-volume effects that will be seen in Chapter 3.

Surprisingly, in [35] it was realized that finite volumes, rather than being obstacles in the study of scattering, can be used as a tool for the calculation of scattering amplitudes. This was first worked out for elastic scattering processes of the form $2 \to 2$, after which it received several extensions to multichannel systems and systems with bound states [36–44]. It is applicable only to low center-of-momentum (CM) energies, so that intermediate on-shell states with more than two particles are not allowed. Since then, external probes $\mathcal{J}$ such as electroweak currents have been included in these dictionaries, under similar kinematic restrictions. This has opened up the possibility of studying reactions of the form $\mathcal{J} \to 2$, $1 + \mathcal{J} \to 2$, $2 + \mathcal{J} \to 2$, $\mathcal{J} \to 2 + \mathcal{J}$, $1 + \mathcal{J} \to 2 + \mathcal{J}$ and $\mathcal{J} + \mathcal{J} \to 2$, through LQCD [45–56]. Extensions have also been able to push past the three-particle threshold, allowing studies in which no more than three-particle intermediate states can go on shell. For example, methodologies for the study of $3 \to 3$ processes below the four-particle threshold have been developed [57–65]. Representative LQCD determinations of scattering and transition amplitudes include [66–79].

Let us describe a common structure shared by many of these mappings in further detail. Roughly speaking, they all have two ingredients. The first is an infinite-volume component, in which the principles of S-matrix theory, such as unitarity, analyticity and cluster decomposition, are employed to parametrize scattering amplitudes in terms of simpler functions with well-understood analytic properties. The second is a finite-volume component, where a bridge between infinite-volume scattering amplitudes, and finite-volume energy levels and matrix elements, is drawn. The same interactions responsible for scattering dynamics determine how energy levels are shifted due to the interactions between particles in a finite

volume. For the energy levels, these usually come in the form of quantization conditions that the finite-volume spectrum has to satisfy. For matrix elements, these are generalizations of the Lellouch-Lüscher relation for the process $1 + \mathcal{J} \to 2$ [46]. Once these two ingredients are in place, one can fit parametrizations of scattering amplitudes which best reproduce observed finite-volume data coming from LQCD calculations.

As we explained in Section 1.1, there are several reactions for which we need theoretical predictions but which lie beyond the scope of the dictionaries mentioned above. Generalizing these dictionaries has been a major roadblock in the prospect of applying LQCD to these reactions. This is where quantum devices come in. In Section 3.6 we will present the proposal, now known as the Real-Time Estimators for Scattering Observables (RESOs), that aims to access generic scattering amplitudes in general kinematical regimes [80–83]. We will, in particular, show that at all orders in perturbation theory the finite-volume effects are exponentially suppressed through the introduction of a non-zero regulator.

1.4 Some Successes of Quantum Computers for the Study of Particle Physics

The basic unit of information stored in a quantum computer is a qubit[1]. The space of states in which a qubit can be is given by a two-dimensional complex Hilbert space $\mathbb{C}^2$. If a quantum device has N qubits, its memory is given by the tensor product Hilbert space $(\mathbb{C}^2)^{\otimes N}$. In the digital paradigm, quantum computers are capable of applying unitary gates affecting one or more of these qubits. Feynman noticed that, by embedding the space of states of a physical system into the one of a quantum computer $(\mathbb{C}^2)^{\otimes N}$, and by choosing gates in our quantum computer that approximate the time evolution of our system of interest, quantum computers are the ideal platforms for the numerical study of quantum systems [84, 85]. This program thus offers the opportunity to perform real-time simulations of quantum fields and particle physics [86].

At the time of the writing of this manuscript, we are in the era of Noisy Intermediate-Scale Quantum (NISQ) devices [87]. There has neither been a simulation of $3 + 1$ QCD, nor of a scientifically useful quantum advantage over efficient classical methods for LQCD. Nevertheless, important algorithmic and experimental steps have been undertaken in the construction of a pipeline that will eventually permit quantum advantage for QCD simulations. The first is in the encoding of the degrees of freedom of QCD within those of a quantum computer [88–102]. Chapter 2 is amongst these contributions, and a detailed discussion of the requirements for this is given in Sections 2.1.3 and 2.1.4. The second is in the preparation of vacua [103–106], hadrons [107, 108] and wave packets in quantum

[1]More general qudits are also possible but, for simplicity of exposition, we will stick to qubits in this dissertation

field theories [109–112]. The third is in the development of circuits of quantum gates that accurately approximate time evolution in gauge theories [113–117].

By having access to real-time evolution, quantum simulation opens the opportunity to directly scatter wave packets [118, 119]. The tools developed above have led to experimental demonstrations of this on quantum hardware [120–125]. The potential of these has also been demonstrated classically for $1 + 1$ theories in which tensor network methods are efficient [126, 127]. It is however not yet clear how this methodology will scale to $3 + 1$ dimensions, in which the scaling of the number of lattice sites with distance is worse, making it more difficult to accommodate non-interacting wave packets. Moreover, the usefulness of these simulations is not clear for high-energy reactions involving high particle multiplicities, which, as explained in Section 1.1, is the focus of this dissertation.

Alternatively, there is the Real-Time Estimators for Scattering Observables (RESOs) proposal [80–83]. In RESOs, the Lehmann-Symanzik-Zimmermann (LSZ) reduction formula, which is reviewed in Section 3.4, is applied to finite-volume time-ordered correlation functions. To our knowledge, RESOs is presently the only proposal for which a systematically improvable, finite-volume-controlled route to general scattering observables across general reactions and kinematics has been established. Through the inclusion of a regulator shifting the energy slightly into the complex plane, Section 3.6 shows that these correlators only have exponentially suppressed finite-volume effects. It is also explained how averaging over different boosts leads to a partial restoration of Lorentz symmetry which further diminishes these finite-volume effects. This establishes the relation between the results of RESOs and the target infinite-volume scattering amplitudes. A discussion of quantum algorithms for the extraction of scattering amplitudes through LSZ reduction is found in [128, 129].

1.5 Reading Guide

Before this PhD, we contributed to the following publications:

[130] A. P. Balachandran et al. "Emergent Gauge Symmetries and Quantum Operations". In: *J. Phys. A* 53.6 (2020), 06LT01. DOI: 10.1088/1751-8121/ab6143. arXiv: 1906.05464 [quant-ph]

[131] Ivan M. Burbano, T. Rick Perche, and Bruno de S. L. Torres. "A path integral formulation for particle detectors: the Unruh-DeWitt model as a line defect". In: *JHEP* 03 (2021), p. 076. DOI: 10.1007/JHEP03(2021)076. arXiv: 2012.14912 [hep-th]

During this PhD we contributed to the following publications:

[132] Ivan M. Burbano and Francisco Calderón. "Self-Normalizing Path Integrals". In: *Found. Phys.* 54.5 (2024), p. 60. DOI: 10.1007/s10701-024-00779-1. arXiv: 2109.00517 [hep-th]

[133] Ivan M. Burbano, Justin Kulp, and Jonas Neuser. "Duality defects in E_8". In: *JHEP* 10 (2022), p. 186. DOI: 10.1007/JHEP10(2022)187. arXiv: 2112.14323 [hep-th]

[100] Ivan M. Burbano and Christian W. Bauer. "Gauge loop-string-hadron formulation on general graphs and applications to fully gauge fixed Hamiltonian lattice gauge theory". In: *JHEP* 12 (2025), p. 060. DOI: 10.1007/JHEP12(2025)060. arXiv: 2409.13812 [hep-lat]

[134] Anthony N. Ciavarella, Ivan M. Burbano, and Christian W. Bauer. "Efficient truncations of SU(Nc) lattice gauge theory for quantum simulation". In: *Phys. Rev. D* 112.5 (2025), p. 054514. DOI: 10.1103/ylqb-phv5. arXiv: 2503.11888 [hep-lat]

[83] Ivan M. Burbano et al. "Real-time estimators for scattering observables: A full account of finite-volume errors for quantum simulation". In: *Phys. Rev. D* 113.7 (2026), p. L071502. DOI: 10.1103/dc17-4zjy. arXiv: 2506.06511 [hep-lat]

The last three in particular pertain to the subject of this dissertation.

Rather than a transcription of all of these papers, in this dissertation we have decided to focus only on [83, 100]. We have included complete rewrites of these two papers, including more background information and expanding on their results. In order to keep the reader on their toes, we have decided to completely change the notation and conventions used between [100] and Chapter 2. This is a joke. In reality, we believe that the conventions used here are more intelligible and lead to a cleaner presentation. All the results presented have been rederived for this dissertation, along with the code used to implement them. This code is found in [135].

Chapter 2 presents the formulation of SU(2) Yang-Mills theory, a theory closely related to QCD, combining the loop-based approaches of [94, 98, 99] with the Loop-String-Hadron [95, 96] approach. This leads to a formulation that is particularly well suited for analysis of the continuum limit in quantum devices that permit simulations of non-local interactions.

Chapter 3 presents RESOs and gives an all-orders perturbation theory proof that it is able to access general reactions in generic kinematical regimes with controlled finite-volume errors. It also includes an introduction to the relevant scattering theory required to understand the result.

Restricting to a subset of publications also allowed the writing of Chapter A. This is an introduction to lattice quantum field theories as a whole. It is intended for mathematically-oriented students, giving first a general exposition to the mathematical structure of QFT, which is later supported by explicitly worked out examples of exactly solvable models. In

these we can obtain analytic solutions without the use of computers and are therefore useful to learn the subject and develop intuition. They also contain a few exercises if the reader desires to acquire some more practice. Working through these exactly solvable theories can be a good entry point to Yang-Mills theory on the lattice, presented in Section 2.1.

Chapter 2

Loop-String-Hadron Formulation for Fully Gauge-Fixed SU(2) Lattice Gauge Theory

In this chapter we will present a basis for quantum-computing implementations of SU(2) Yang-Mills theory, which is different from the more standard magnetic and electric bases [88] that will be discussed in Sections 2.1.3 and 2.1.4. It will be a mixture of both, combining several of their advantages:

1. Like certain magnetic bases, we will have a fully gauge-fixed basis. Accordingly, it minimizes the number of qubits required, for the encoded Hilbert space is already the full physical Hilbert space without any further Abelian or non-Abelian Gauss law constraints. Furthermore, by not encoding any unphysical states, errors characteristic of the NISQ era of quantum devices cannot drift states into an unphysical sector.

2. Like electric bases, it will be described in terms of quantum numbers that are discrete. Therefore, it is particularly well-suited to digitization into a qubit representation.

3. Like magnetic bases, these quantum numbers are well-suited for explorations towards the continuum limit. Indeed, the quantum numbers will be isolated into sectors, where the majority can be truncated harshly without jeopardizing this limit.

However, as we will further explain in Section 2.1.3, having a fully-gauge fixed basis signifies that we will lose manifest locality. Indeed, we will have pairwise-interactions across all the degrees of freedom.

This chapter expands upon the material first presented in [100] written in conjunction with Christian W. Bauer. That paper built strongly on the mixed-basis approach presented

in [98, 99]. Moreover, our results greatly overlap with [94]. We were unaware of this previous work during most of our investigation, but similar results were obtained through independent methodologies. Furthermore, in our results we were able to incorporate the Loop-String-Hadron (LSH) formalism, which was developed posteriorly in [95, 96]. We also developed a general understanding of lattice gauge theories on general graphs, which heavily informed our reasoning and could potentially do the same for subsequent developments. The presentation in this dissertation is more concrete than the one in the first publication. It also includes a general introduction of some standard facts of Yang-Mills theory in Section 2.1, which is complemented by the general introduction to lattice quantum field theories in Chapter A. We recommend that the reader that can use a refresher on the transfer matrix formalism reads this section concurrently with Chapter A.

2.1 Yang-Mills Theory

We first discuss the basics of Yang-Mills theory in general. This is the theory that describes the force carriers of the SM. In fact, rather than a single theory, it is a family of theories parametrized by a choice of group G. The electroweak sector, describing photons and the W and Z bosons, has $G = \mathrm{U}(1) \times \mathrm{SU}(2)$. The strong nuclear force, whose force carriers are gluons, has $G = \mathrm{SU}(3)$.

The Yang-Mills theory of the non-Abelian sectors of the electroweak and strong forces is rather similar in principle. At low energies, however, they behave differently due to the Higgs mechanism which affects the electroweak sector but not the strong one. For example, while both weak and strong nuclear interactions are short ranged, they are so for different reasons. In the strong case, the strength of interactions between the gluons grows as we look at the theory at lower energy scales, which heuristically leads to the phenomenon of confinement. This in turn leads to massive pions which mediate a strong nuclear force with a finite range. In the weak case, instead, the W and Z bosons themselves acquire mass through the Higgs mechanism, which kicks in before confinement does.

This section and, in fact, most of this chapter, will be focused on general Yang-Mills theories with a non-Abelian Lie group G. Our main results however, will only be applicable to $G = \mathrm{SU}(2)$. Since we will not consider a Higgs mechanism, the resulting theory is qualitatively similar to the $G = \mathrm{SU}(3)$ theory of the strong interactions. History showed for traditional LQCD that studying $G = \mathrm{SU}(2)$ first is an important milestone on the path to $G = \mathrm{SU}(3)$. The same is likely to be true for implementations on quantum computers.

2.1.1 Euclidean Theory

Consider a spacetime $\mathcal{M}$ and a Lie group G with Lie algebra $\mathfrak{g}$. The field of this theory can be locally represented by a Lie-algebra valued 1-form $A(x) = A_\mu(x)\,\mathrm{d}x^\mu \in \Omega^1(\mathcal{M}) \otimes \mathfrak{g}$,

with $A_\mu(x) = A^a_\mu(x)T_a$ in terms of a basis T_a. It is however crucial to remark that this representation is redundant and local, as we will soon see.

In order to clarify the meaning of this field, consider an infinitely heavy particle moving along a trajectory $\mathcal{C}$ on $\mathcal{M}$. Its interaction with the Yang-Mills field is determined by the choice of a representation of G. The particle will then have internal degrees of freedom described by a wave function ψ in this representation. Given a parametrization $x^\mu : [0,T] \to \mathcal{M}$ of $\mathcal{C}$, the time evolution of these internal degrees of freedom is given by a Hamiltonian $-i\dot{x}^\mu A_\mu(x)$. In other words, the wave function satisfies the Schrödinger equation

$$\frac{\mathrm{d}\psi}{\mathrm{d}\tau} = -\dot{x}^\mu A_\mu(x)\psi. \tag{2.1}$$

Thus, the field A transports the internal degrees of freedom of this particle.

The parametrization of $\mathcal{C}$ is unimportant, as can be seen by writing the Schrödinger equation in the form

$$\mathrm{D}\psi = 0, \tag{2.2}$$

having introduced the covariant derivative $\mathrm{D} := \mathrm{d} + A$. Furthermore, as with any other Schrödinger equation with a time-dependent Hamiltonian, this is formally solved by $\psi(T) = u(\mathcal{C})\psi(0)$, in terms of the Wilson line $u(\mathcal{C}) \in G$. It is defined as the solution $u(\mathcal{C}) := u(T)$ of the differential equation

$$\frac{\mathrm{d}u(\tau)}{\mathrm{d}\tau} = -\dot{x}^\mu A_\mu(x)u(\tau) \tag{2.3}$$

with initial conditions $u(0) = 1 \in G$. Locally, the solution is given in terms of the path-ordered exponential

$$u(\mathcal{C}) = \mathcal{P}\exp\left(-\int_0^T \mathrm{d}\tau\, \dot{x}^\mu A\right) = \mathcal{P}\exp\left(-\int_{\mathcal{C}} A\right). \tag{2.4}$$

This operator is known as the Wilson line on $\mathcal{C}$.

The key foundational principle is that we want physics to be invariant under a transformation $g \in C^\infty(\mathcal{M}, G)$, mapping

$$\psi(\tau) \mapsto \tilde{\psi}(\tau) = g(x(\tau))\psi(\tau). \tag{2.5}$$

These are known as gauge transformations. Under this transformation the Schrödinger equation remains invariant as long as

$$\mathrm{D} \mapsto g\,\mathrm{D}g^{-1}. \tag{2.6}$$

This yields the transformation property of the field

$$A \mapsto gAg^{-1} + g\,\mathrm{d}g^{-1}. \tag{2.7}$$

Alternatively, the Wilson line transforms as

$$u(\mathcal{C}) \mapsto g(y)u(\mathcal{C})g(x)^{-1}, \tag{2.8}$$

where $y = x(T)$ and $x = x(0)$ are the ending and starting points of $\mathcal{C}$.

The field A is only a local description of the theory. Several interesting configurations cannot be described through a well-defined field A on all of $\mathcal{M}$, such as that of a magnetic monopole for $G = \mathrm{U}(1)$. On the overlap of two different A's describing the same configuration, we demand that they are related to each other by a gauge transformation. These are not to be understood as symmetries of the theory. Instead, they are redundancies in the description. Accordingly, A is not a physical observable. All physical observables must be invariant under these transformations.

Our starting point for the construction of observables will be Wilson lines, for their transformation properties are much simpler. In particular, for loops $\mathcal{C}$ starting and ending at the same point x, these transform under the adjoint representation of the gauge group G at x. Thus, we can build observables by taking the trace of the associated Wilson line in a representation R of G

$$w_R(\mathcal{C}) = \mathrm{tr}_R\, u(\mathcal{C}). \tag{2.9}$$

These are known as Wilson loops.

While observable, they are inherently non-local, being supported on $\mathcal{C}$. We can however obtain a local observable by studying the behavior of the Wilson loop as we shrink $\mathcal{C}$ down to x. Since this is local, we might as well restrict to $\mathcal{M} = \mathbb{R}^D$ with standard basis e_μ. Let us consider the infinitesimal square $x \mapsto x + \epsilon e_\mu \mapsto x + \epsilon e_\mu + \epsilon e_\nu \mapsto x + \epsilon e_\nu \mapsto x$, for $\mu \neq \nu$. We will denote it as $x_{\mu\nu}$. Let us compute the Wilson line $u(x_{\mu\nu})$ on it to order ϵ^2.

From its interpretation as an evolution operator, it is clear that Wilson lines along a trajectory can be computed by composing the different Wilson lines on subsegments. We focus first on the evolution due to the trajectory $x \mapsto x + \epsilon e_\mu$, which we will denote as [1] x_μ. The first non-trivial term in the expansion of the path ordered exponential yields

$$-\int_0^\epsilon \mathrm{d}t\, A_\mu(x + te_\mu) = -\epsilon A_\mu(x) - \frac{1}{2}\epsilon^2 \partial_\mu A_\mu(x) + \mathcal{O}(\epsilon^3). \tag{2.10}$$

[1] This is not to be confused with the μ-th component of x, which is x^μ. Since the points in $\mathcal{M}$ are not vectors, it does not make sense to raise and lower their indices. Thus, in this dissertation there will be no room for ambiguity.

The second term yields

$$\begin{aligned}
&\frac{1}{2}\mathcal{P}\int_0^\epsilon \mathrm{d}t_1 \int_0^\epsilon \mathrm{d}t_2\, A_\mu(x+t_1 e_\mu)A_\mu(x+t_2 e_\mu) = \\
&\int_0^\epsilon \mathrm{d}t_1 \int_0^{t_1} \mathrm{d}t_2\, A_\mu(x+t_1 e_\mu)A_\mu(x+t_2 e_\mu) = \\
&\frac{1}{2}\epsilon^2 A_\mu(x)A_\mu(x) + \mathcal{O}(\epsilon^3).
\end{aligned} \tag{2.11}$$

The remaining terms will be of order $\mathcal{O}(\epsilon^3)$ so that

$$u(x_\mu) = 1 - \epsilon A_\mu(x) - \frac{1}{2}\epsilon^2 \partial_\mu A_\mu(x) + \frac{1}{2}\epsilon^2 A_\mu(x)A_\mu(x) + \mathcal{O}(\epsilon^3). \tag{2.12}$$

For the trajectory $x + \epsilon e_\mu \mapsto x + \epsilon e_\mu + \epsilon e_\nu$ we have the Wilson line

$$u((x+\epsilon e_\mu)_\nu) = u(x_\nu) + \epsilon \partial_\mu u(x_\nu) + \mathcal{O}(\epsilon^3). \tag{2.13}$$

In here we note that the derivatives of $u(x_\mu)$ are of order ϵ. For the trajectory $x + \epsilon e_\mu + \epsilon e_\nu \mapsto x + \epsilon e_\nu$, we should have the inverse evolution to the opposite trajectory $x + \epsilon e_\nu \mapsto x + \epsilon e_\mu + \epsilon e_\nu$. We thus conclude that the associated Wilson line is

$$\begin{aligned}
u((x+\epsilon e_\nu)_\mu)^{-1} &= (u(x_\mu) + \epsilon \partial_\nu u(x_\mu) + \mathcal{O}(\epsilon^3))^{-1} \\
&= u(x_\mu)^{-1} - \epsilon u(x_\mu)^{-1}\partial_\nu u(x_\mu) u(x_\mu)^{-1} + \mathcal{O}(\epsilon^3) \\
&= u(x_\mu)^{-1} - \epsilon \partial_\nu u(x_\mu) + \mathcal{O}(\epsilon^3).
\end{aligned} \tag{2.14}$$

And for the final trajectory $x + \epsilon e_\nu \mapsto x$ we simply have $u(x_\nu)^{-1}$.

We thus conclude that

$$\begin{aligned}
u(x_{\mu\nu}) &= u(x_\nu)^{-1} u((x+\epsilon e_\nu)_\mu)^{-1} u((x+\epsilon e_\mu)_\nu) u(x_\mu) \\
&= u(x_\nu)^{-1} u(x_\mu)^{-1} u(x_\nu) u(x_\mu) - \epsilon \partial_\nu u(x_\mu) + \epsilon \partial_\mu u(x_\nu) \\
&\quad + \mathcal{O}(\epsilon^3).
\end{aligned} \tag{2.15}$$

In the derivative terms, only the $\mathcal{O}(\epsilon)$ terms in $u(x_\mu)$ contribute

$$-\epsilon \partial_\nu u(x_\mu) + \epsilon \partial_\mu u(x_\nu) = -\epsilon^2(\partial_\mu A_\nu(x) - \partial_\nu A_\mu(x)). \tag{2.16}$$

For the local term we need to use

$$u(x_\mu)^{-1} = 1 + \epsilon A_\mu(x) + \frac{1}{2}\epsilon^2 \partial_\mu A_\mu(x) + \frac{1}{2}\epsilon^2 A_\mu(x)A_\mu(x) + \mathcal{O}(\epsilon^3). \tag{2.17}$$

Thus, since they appear with opposite signs, the terms linear in A of the local product vanish. The quadratic terms yield

$$\begin{aligned} &u(x_\nu)^{-1}u(x_\mu)^{-1}u(x_\nu)u(x_\mu) - 1 \\ &= \epsilon^2 A_\nu(x)A_\mu(x) - \epsilon^2 A_\mu(x)A_\mu(x) - \epsilon^2 A_\nu(x)A_\mu(x) - \epsilon^2 A_\mu(x)A_\nu(x) \\ &\quad - \epsilon^2 A_\nu(x)A_\nu(x) + \epsilon^2 A_\nu(x)A_\mu(x) + \frac{1}{2}\epsilon^2 A_\mu(x)A_\mu(x) \\ &\quad + \frac{1}{2}\epsilon^2 A_\nu(x)A_\nu(x) + \frac{1}{2}\epsilon^2 A_\mu(x)A_\mu(x) + \frac{1}{2}\epsilon^2 A_\nu(x)A_\nu(x) + \mathcal{O}(\epsilon^3) \\ &= -\epsilon^2[A_\mu(x), A_\nu(x)] + \mathcal{O}(\epsilon^3). \end{aligned} \tag{2.18}$$

With this we find that to leading order

$$u(x_{\mu\nu}) = 1 - \epsilon^2 F_{\mu\nu}(x) + \mathcal{O}(\epsilon^3), \tag{2.19}$$

in terms of the local

$$F_{\mu\nu} := \partial_\mu A_\nu - \partial_\nu A_\mu + [A_\mu, A_\nu]. \tag{2.20}$$

This defines a Lie-algebra valued 2-form $F = \frac{1}{2}F_{\mu\nu}\,\mathrm{d}x^\mu\,\mathrm{d}x^\nu \in \Omega^2(\mathcal{M}) \otimes \mathfrak{g}$, related to A via

$$F = \mathrm{d}A + \frac{1}{2}[A, A]. \tag{2.21}$$

It inherits its transformation behavior through that of the Wilson line

$$F \mapsto gFg^{-1}. \tag{2.22}$$

Several gauge invariant actions can be built from this operator. On a manifold of even dimension D one can consider the $D/2$-fold wedge product of F with itself, which yields a differential form that can be integrated over $\mathcal{M}$. Combining this with an invariant polynomial on $\mathfrak{g}$ of degree $D/2$ leaves us with an action. This leads to the θ-terms, and their associated Chern-Simons actions on manifolds of dimension $D-1$. These are notoriously difficult to simulate classically, for they have a severe sign problem. Indeed, at no point did we use a metric to define them. They are topological. In particular, considering Euclidean spacetimes does nothing to the exponent in the path integral. Along with their physical importance, ranging from the CP-problem in high-energy physics, to the classification of topological phases of matter, they are a prime candidate for simulation on quantum computers.

Nevertheless, for the purposes of scattering theory, it is more pressing to consider a different kind of action, which is available once we equip $\mathcal{M}$ with a metric $\mathrm{d}s^2 = g_{\mu\nu}\,\mathrm{d}x^\mu\,\mathrm{d}x^\nu$. For the moment we will assume this to be a Euclidean metric. With this we can build an integration form $\mathrm{d}^D x\,\sqrt{g}$ and a quadratic function $F_{\mu\nu}F^{\mu\nu} = g^{\mu\rho}g^{\nu\sigma}F_{\mu\nu}F_{\rho\sigma}$. Accordingly,

if we choose positive-definite invariant pairing $\langle \bullet, \bullet \rangle$ on $\mathfrak{g}$ we are left with the Yang-Mills action

$$S = \frac{1}{4g^2} \int \mathrm{d}^D x \, \sqrt{g_{\bullet\bullet}} \, \langle F_{\mu\nu}, F^{\mu\nu} \rangle \, . \tag{2.23}$$

In this dissertation we will mostly focus on $G = \mathrm{SU}(N_c)$, which has a compact simple Lie algebra. Up to an overall constant, which we absorb into the definition of a coupling constant g, for these Lie algebras we can without loss of generality build this pairing using the trace in any non-trivial representation

$$\langle \bullet, \bullet \rangle := -2 \, \mathrm{tr}(\bullet\bullet). \tag{2.24}$$

This leads to

$$S = -\frac{1}{2g^2} \int \mathrm{d}^D x \, \sqrt{g_{\bullet\bullet}} \, \mathrm{tr}(F_{\mu\nu} F^{\mu\nu}). \tag{2.25}$$

The additional minus sign appears since, in the conventions that will be used throughout this dissertation, namely that $\mathfrak{su}(N_c)$ is the Lie algebra of antihermitian $N_c \times N_c$ matrices, this leads to a positive-definite action.

This convention is unimportant if we choose a basis T_a for $\mathfrak{g}$. Choosing an orthonormal basis $\langle T_a, T_b \rangle = \delta_{ab}$, which in the trace formulation reads

$$\mathrm{tr}(T_a T_b) = -\frac{1}{2} \delta_{ab}, \tag{2.26}$$

the action takes the form

$$S = \frac{1}{4g^2} \int \mathrm{d}^D x \, \sqrt{g_{\bullet\bullet}} F^a_{\mu\nu} F^{a\mu\nu}. \tag{2.27}$$

This leads to an action with a $1/2$ normalization

$$S = \frac{1}{2g^2} \int \mathrm{d}^D x \, \sqrt{g_{\bullet\bullet}} \partial_\mu A^a_\nu \partial^\mu A^{a\nu} + \cdots . \tag{2.28}$$

A canonical normalization can be obtained by simply reabsorbing g into A. We will however not do that throughout this dissertation.

We now consider the discretization of this theory on a lattice $\epsilon\mathbb{Z}^D$, considered as a regularization of the theory on a Euclidean spacetime $\mathbb{R}^D$. Unlike the examples presented in Chapter A, where the fields naturally have support on the vertices, the field $A = A_\mu \, \mathrm{d}x^\mu$ naturally lives on the trajectory $x \mapsto x + \mathrm{d}x^\mu$. On the lattice we will therefore place our degrees of freedom on the links of $\epsilon\mathbb{Z}^D$. More precisely, we will orient our links so that they go from x to $x + \epsilon e_\mu$. These finite-sized links x_μ support the Wilson lines $u(x_\mu)$, which we will take as the basic degrees of freedom in our theory.

Our starting point to the lattice action will be the infinitesimal Wilson line (2.19). In its current form, it yields trivial information about the gauge-invariant Wilson loop

$$w(x_{\mu\nu}) := \mathrm{tr} \, u(x_{\mu\nu}) = \mathrm{tr} \, 1 + \mathcal{O}(\epsilon^3), \tag{2.29}$$

since on semisimple Lie algebras the trace vanishes. Fortunately, we can use the group structure to extend this result to $\mathcal{O}(\epsilon^4)$ without much work. Indeed, for sufficiently small ϵ, we expect the path integral to be dominated by smooth configurations in which $u(x_{\mu\nu}) \in G$ is close to the identity. Thus, there is a Lie algebra element $X(x_{\mu\nu}) \in \mathfrak{g}$ for which

$$u(x_{\mu\nu}) = e^{X(x_{\mu\nu})}. \tag{2.30}$$

Thus, (2.19) implies that

$$X(x_{\mu\nu}) = -\epsilon^2 F_{\mu\nu}(x) + \mathcal{O}(\epsilon^3). \tag{2.31}$$

We thus can extrapolate a stronger expansion for the Wilson loop

$$\begin{aligned} w(x_{\mu\nu}) &= \operatorname{tr} 1 + \frac{1}{2}\operatorname{tr}(X(x_{\mu\nu})^2) + \mathcal{O}(\epsilon^6) \\ &= \operatorname{tr} 1 + \frac{\epsilon^4}{2}\operatorname{tr}(F_{\mu\nu}^2) + \mathcal{O}(\epsilon^5). \end{aligned} \tag{2.32}$$

This gauge invariant thus correlates directly to our continuum Yang-Mills action. We however should be careful to note that the $\mathcal{O}(\epsilon^5)$ terms could potentially introduce an imaginary part on our loops. Fortunately, since $\operatorname{tr}(F_{\mu\nu}^2) \in \mathbb{R}$ for our groups of interest, we also have

$$\operatorname{Re} w(x_{\mu\nu}) = \operatorname{tr} 1 + \frac{\epsilon^4}{2}\operatorname{tr}(F_{\mu\nu}^2) + \mathcal{O}(\epsilon^5). \tag{2.33}$$

We can thus build a real action

$$S = -\frac{\epsilon^{D-4}}{g^2}\sum_{x\in\mathbb{Z}^D}\sum_{\mu\neq\nu}\operatorname{Re} w(x_{\mu\nu}) = -\frac{2\epsilon^{D-4}}{g^2}\sum_{x\in\mathbb{Z}^D}\sum_{\mu>\nu}\operatorname{Re} w(x_{\mu\nu}), \tag{2.34}$$

which, up to an additive constant, coincides with the Yang-Mills action in the limit $\epsilon \to 0$. In here $x_{\mu\nu}$ is the square $x \mapsto x+\epsilon e_\mu \mapsto x+\epsilon e_\mu+\epsilon e_\nu \mapsto x+\epsilon e_\nu \mapsto x$, known as a plaquette. This is known as the Wilson action.

We finish this section with some notational comments. First, it is common for people not to drop the constant term, so that the action is often written in the form

$$S = \frac{2\epsilon^{D-4}}{g^2}\sum_{x\in\mathbb{Z}^D}\sum_{\mu>\nu}\big(\operatorname{tr} 1 - \operatorname{Re} w(x_{\mu\nu})\big). \tag{2.35}$$

We will not do this since, as we exemplify in the examples of Chapter A, an additive renormalization of the action is necessary to ensure that the vacuum has zero energy.

Second, people traditionally define g so that the trace is in the fundamental representation. For $\mathrm{SU}(N_c)$ one has $\operatorname{tr} 1 = N_c$ in it. In light of the statistical mechanical

interpretation, in which the action takes the interpretation of an energy divided by a temperature, people then replace g by $\beta := 2N_c\epsilon^{D-4}/g^2$ and write

$$S = \frac{\beta}{N_c}\sum_{x\in\mathbb{Z}^D}\sum_{\mu>\nu}\big(N_c - \operatorname{Re} w(x_{\mu\nu})\big). \tag{2.36}$$

We will not do this since on quantum computers the quantum mechanical interpretation is prevalent.

Finally, we note that for our unitary groups $u(x_{\mu\nu})^\dagger = u(x_{\nu\mu})$. Consequently, $w(x_{\mu\nu})^* = w(x_{\nu\mu})$. Thus, given

$$\operatorname{Re} w(x_{\mu\nu}) = \frac{1}{2}\big(w(x_{\mu\nu}) + w(x_{\mu\nu})^*\big), \tag{2.37}$$

we see we can write the action as a sum over all plaquettes, irrespective of their orientation

$$S = -\frac{\epsilon^{D-4}}{g^2}\sum_{x\in\mathbb{Z}^D}\sum_{\mu\neq\nu} w(x_{\mu\nu}), \tag{2.38}$$

In this form it is clear that the theory is invariant under changes of orientation. Picking an orientation is however useful for notational purposes. Moreover, once we include theta terms, this orientation invariance is lost.

2.1.2 Kogut-Susskind Hamiltonian

In order to construct our first Hamiltonian for this theory, we will follow the transfer matrix construction of the examples of Chapter A for the Wilson action [136]. In order to do so we need to begin by constructing the Hilbert space spanned by configurations at a given moment in time. Here we run into a first difficulty. Consider the Wilson line $u((0,\boldsymbol{x})_0)$. Should this be thought of as part of the configuration at t or at $t+\epsilon$? Fortunately there is a simple solution to this problem, which is to exploit gauge invariance to get rid of the Wilson lines $u(x_0)$ completely. Let us describe this procedure in detail since an analog of it will play an important role in the maximal tree construction of Section 2.2.2. Indeed, let us choose a gauge transformation that only acts non-trivially at $t = 0$, where it is given by $g(0,\boldsymbol{x}) = u((0,\boldsymbol{x})_0)$. This would map $u((0,\boldsymbol{x})_0) \mapsto 1$. Moreover, further gauge transformations won't disturb this as long as $g(0,\boldsymbol{x}) = g(\epsilon,\boldsymbol{x})$. We can then go on and consider the gauge transformation whose non-trivial elements are $g(0,\boldsymbol{x}) = g(\epsilon,\boldsymbol{x}) = u((\epsilon,\boldsymbol{x})_0)$. After this gauge transformation we now have $u((0,\boldsymbol{x})_0) = u((\epsilon,\boldsymbol{x})_0) = 1$. Iterating this procedure we can set $u(x_0) = 1$ everywhere in the lattice. This is known as the temporal gauge, for taking $\epsilon \to 0$, this effectively sets $A_0 = 0$.

As a brief intromission in our main line of discussion, let us note that there is an obstruction to doing this if there was a close loop along time. For example, suppose that our lattice had only two time slices and had temporal periodic boundary conditions

$(t, \boldsymbol{x}) \sim (t + 2\epsilon, \boldsymbol{x})$. Then, while the first gauge transformation we did would effectively set $u((0, \boldsymbol{x})_0) = 1$, the second one would set

$$\begin{aligned} u((\epsilon, \boldsymbol{x})_0) &\mapsto g(2\epsilon, \boldsymbol{x}) u((\epsilon, \boldsymbol{x})_0) g(\epsilon, \boldsymbol{x})^{-1} = g(0, \boldsymbol{x}) u((\epsilon, \boldsymbol{x})_0) g(\epsilon, \boldsymbol{x})^{-1} \\ &= u((\epsilon, \boldsymbol{x})_0). \end{aligned} \tag{2.39}$$

The reason for this obstruction is ultimately that the Wilson loop in the time direction is gauge invariant. Thus, the last link in the procedure carries the information of the loop. For the purposes of this dissertation, we will have finite time intervals without periodic boundary conditions, so that this will not be an issue. But it is an important consideration to have in mind in the constructions of Chapter 2.

Having solved this issue, we now for concreteness consider lattices of the form $\mathcal{M} = \underline{N_t}\epsilon \times \Sigma$, where

$$\underline{N_t}\epsilon := \{0, \epsilon, 2\epsilon, \dots, N_t\epsilon\} \quad \text{and} \quad \Sigma \in \left\{ \left(\underline{N_s} a\right)^d, a\mathbb{Z}^d \big/ L\mathbb{Z}^d \right\}. \tag{2.40}$$

This brings us to our next issue. We have now introduced lattices in which there are different temporal and spatial lattice spacings ϵ and a. We have done this since in the transfer matrix formalism we need to be able to take $\epsilon \to 0$ without taking $a \to 0$. We thus need to consider the modifications this would have on the Wilson action.

In order to do this, let us use Latin indices $i, j, k, \dots = 1, \dots, d$ to enumerate spatial coordinates. For spatial plaquettes Eqs. (2.19) and (2.33) remain intact with the replacement $\epsilon \mapsto a$. On the other hand, for temporal plaquettes we have

$$u(x_{0i}) = 1 - a\epsilon F_{0i}(x) + \mathcal{O}((a + \epsilon)^3), \tag{2.41}$$

Thus, the Wilson action becomes

$$S = -\frac{2a^{d-2}}{g_t^2 \epsilon} \sum_{x \in \underline{N_t - 1}\epsilon \times \Sigma} \sum_i \operatorname{Re} \operatorname{tr} u(x_{0i}) - \frac{2\epsilon a^{d-4}}{g_s^2} \sum_{x \in \underline{N_t - 1}\epsilon \times \Sigma} \sum_{i>j} \operatorname{Re} \operatorname{tr} u(x_{ij}). \tag{2.42}$$

In both sums each plaquette appears only with the displayed orientation: x_{0i} for temporal plaquettes and x_{ij}, with $i > j$, for spatial plaquettes. In what follows, $\mathcal{P}$ will denote the corresponding set of oriented spatial plaquettes. We have also introduced separate couplings g_t and g_s for the temporal and spatial plaquettes. While these should be the same when $\epsilon = a$ due to relativistic[2], in our anisotropic lattice this need not be the case. These play a role analogous to the one played by K_t and K_s in (A.166).

We are now ready to delve into the transfer matrix formalism. Let us take advantage of the things we learn through the examples of Chapter A to guide our calculation. First,

[2]In the Euclidean setting this corresponds to the group of spacetime rotations $O(D)$.

we note that, as we also do for the examples in Chapter A, our current action skips the spatial terms with $t = T$. This is so that the gluing axiom of path integrals is satisfied.

Second, a pattern arises after comparison with (A.106). Both that action and our current (2.42) have a term inversely proportional to ϵ and one proportional to ϵ. In the harmonic oscillator, the former arises from the kinetic part of the action, while the latter from the potential. In our present setting, the former will lead to the electric Hamiltonian, while the latter for the magnetic.

Third, the magnetic term is fully supported at a fixed time slice. As in Sections A.8.1 and A.9.1, the contributions of this term will be simple to quantize. The electric term, on the other hand, extends across time. In order to quantize it, we will employ two of the techniques we learn in those sections. We will first realize that this quantization problem reduces to the $D = 1$ case, as in the 2D Ising model we study in Section A.9. Then we will make use of the group structure to introduce electric operators, which play an analogous role to the momentum operators in the harmonic oscillator studied in Section A.8.1, in order to complete our quantization. The hardest part of this procedure will be to obtain the vacuum renormalization analogue to (A.122).

With a clear plan in mind, let us go ahead with our quantization procedure. We first recognize that configurations on Σ are given by functions u which assign to each link $\boldsymbol{x}_i$, starting at $\boldsymbol{x}$ and ending at $\boldsymbol{x} + e_i$, a group element $u(\boldsymbol{x}_i) \in G$. Denoting the space of links as E, we see that the Hilbert space is

$$\mathcal{H} = \mathrm{Span}\left\{ |u\rangle \mid u : E \to G \right\} \cong \otimes_{\boldsymbol{x}_i \in E} L^2(G). \tag{2.43}$$

Then we specialize to the infinitesimal $N_t = 1$ lattice. We intend to find a Hamiltonian H such that

$$\begin{aligned} &\langle u_f | e^{-\epsilon H} | u_i \rangle = \\ &e^{\frac{2a^{d-2}}{g_t^2 \epsilon} \sum_{\boldsymbol{x}_i \in E} \mathrm{Re}\,\mathrm{tr}(u_f(\boldsymbol{x}_i)^{-1} u_i(\boldsymbol{x}_i)) + \frac{2\epsilon a^{d-4}}{g_s^2} \sum_{\boldsymbol{x}_{ij} \in \mathcal{P}} \mathrm{Re}\, w_i(\boldsymbol{x}_{ij})}, \end{aligned} \tag{2.44}$$

Introducing the G-valued operators $U(\boldsymbol{x}_i)$, defined by

$$U(\boldsymbol{x}_i) \, |u\rangle = u(\boldsymbol{x}_i) \, |u\rangle \,, \tag{2.45}$$

and the Wilson-loop operators

$$W(\boldsymbol{x}_{ij}) \, |u\rangle = w(\boldsymbol{x}_{ij}) \, |u\rangle \,, \tag{2.46}$$

we define the operator H_0 via

$$e^{-\epsilon H} = e^{-\epsilon H_0} e^{\frac{2\epsilon a^{d-4}}{g_s^2} \sum_{\boldsymbol{x}_{ij} \in \mathcal{P}} \mathrm{Re}\, W(\boldsymbol{x}_{ij})}. \tag{2.47}$$

Then this operator satisfies

$$\langle u_f | e^{-\epsilon H_0} | u_i \rangle = e^{\frac{2a^{d-2}}{g_t^2 \epsilon} \sum_{\boldsymbol{x}_i \in E} \mathrm{Re}\,\mathrm{tr}(u_f(\boldsymbol{x}_i)^{-1} u_i(\boldsymbol{x}_i))}, \tag{2.48}$$

We can further define the operators $H_0(\boldsymbol{x}_i)$, localized on the link $\boldsymbol{x}_i$ and for which $H_0 = \sum_{\boldsymbol{x}_i \in E} H_0(\boldsymbol{x}_i)$. These then satisfy

$$\langle u_f | e^{-\epsilon H_0(\boldsymbol{x}_i)} | u_i \rangle = e^{\frac{2a^{d-2}}{g_t^2 \epsilon} \operatorname{Re} \operatorname{tr}(u_f(\boldsymbol{x}_i)^{-1} u_i(\boldsymbol{x}_i))}. \tag{2.49}$$

This leaves us with a remaining 1D calculation.

We thus shift our focus to the lattice with $N_t = 1$ and $\Sigma = \{0, 1\}$. The latter has a single link and thus we will drop the link index. The Hamiltonian in it should satisfy

$$\langle u_f | e^{-\epsilon H} | u_i \rangle = e^{\frac{2a^{d-2}}{g_t^2 \epsilon} \operatorname{Re} \operatorname{tr}(u_f^{-1} u_i)}, \tag{2.50}$$

where now $u_i, u_f \in G$. As in the examples presented in Chapter A, this requires a vacuum renormalization so that in the limit $\epsilon \to 0$ we recover the limit

$$\langle u_f | u_i \rangle = \delta(u_f, u_i). \tag{2.51}$$

To have the correct behavior for $u_f \neq u_i$ we introduce the constant that made the action positive definite, so that

$$\langle u_f | e^{-\epsilon H} | u_i \rangle = e^{\frac{2a^{d-2}}{g_t^2 \epsilon} (\operatorname{Re} \operatorname{tr}(u_f^{-1} u_i) - \operatorname{tr} 1)}. \tag{2.52}$$

Indeed, for all faithful unitary representations and $u \in G \setminus \{1\}$ we have

$$\operatorname{Re} \operatorname{tr} u < \operatorname{tr} 1, \tag{2.53}$$

as can be seen through the spectral structure of u. Thus, for $u_f \neq u_i$ we now have $\langle u_f | e^{-\epsilon H} | u_i \rangle \to 0$ as $\epsilon \to 0$.

Moreover, we also need to include a further vacuum renormalization so that

$$\int \mathrm{d} u_i \, \langle u_f | e^{-\epsilon H} | u_i \rangle \to 1 \tag{2.54}$$

Due to the invariance of the Haar measure we have

$$\begin{aligned} &\int \mathrm{d} u_i \, e^{\frac{2a^{d-2}}{g_t^2 \epsilon} (\operatorname{Re} \operatorname{tr}(u_f^{-1} u_i) - \operatorname{tr} 1)} = \\ &\int \mathrm{d} u \, e^{\frac{2a^{d-2}}{g_t^2 \epsilon} (\operatorname{Re} \operatorname{tr} u - \operatorname{tr} 1)} =: I\left(\frac{g_t^2 \epsilon}{2a^{d-2}} \right). \end{aligned} \tag{2.55}$$

Unlike the case of the harmonic oscillator, this integral has no general closed form. However, its ϵ dependence can be studied by noting that as $\epsilon \to 0$ this integral is dominated by the contributions near $u \sim 1$. Since the Lie algebra is the tangent space to G at 1, it yields

a natural coordinate system in which to evaluate this integral. There is a domain $D \subseteq \mathfrak{g}$, containing $0 \in \mathfrak{g}$ for which the exponential map is a diffeomorphism on a neighborhood of $1 \in G$. In fact, for the groups of interest in this dissertation, one can always choose D so that the image of this exponential is G up to a set of measure 0.

Let $X = X^a T_a \in \mathfrak{g}$ and $\mathrm{d}^{n:=\dim G} X = \mathrm{d}X^1 \cdots \mathrm{d}X^n$. Our goal is to express the Haar measure in terms of this form

$$\mathrm{d}u = \mathrm{d}^n X J(X), \tag{2.56}$$

with $u = e^X$. We can mirror the proof of existence and uniqueness of the Haar measure to do this [137]. Due to invariance of the Haar measure, we have

$$\begin{aligned} \mathrm{d}^n X J(X) = \mathrm{d}u = \mathrm{d}(gu) = \mathrm{d}^n(\ln(ge^X))J(\ln(ge^X)) \\ = \mathrm{d}^n X \det\left(\frac{\partial \ln(ge^X)}{\partial X}\right) J(\ln(ge^X)) \end{aligned} \tag{2.57}$$

Taking $g = e^{-X}$, we conclude that

$$J(X) = J(0) \det\left(\frac{\partial \ln(ge^X)}{\partial X}\right)\Bigg|_{g=e^{-X}}. \tag{2.58}$$

The coefficient $J(0)$ is fixed by the normalization $\int \mathrm{d}u = 1$. For our purposes, the remaining determinant only has to be computed to $\mathcal{O}(X^2)$. However, there is an elegant formula for this determinant to all orders in X, which we cannot avoid but derive.

Notice that the derivative in the determinant is the coefficient of the expansion to first order in δX of

$$\ln(e^{-X}e^{X+\delta X}). \tag{2.59}$$

There is a beautiful way to understand this exponential, which we adapt from [138]. The trick is to note that for any N we have

$$e^{X+\delta X} = (e^{X/N+\delta X/N})^N. \tag{2.60}$$

We can now expand each of the N terms to order $\mathcal{O}(\delta X)$

$$\begin{aligned} e^{X/N+\delta X/N} &= e^{X/N} + \frac{\partial e^{X/N+\delta X/N}}{\partial \delta X}\Bigg|_{\delta X=0} \delta X + \mathcal{O}(\delta X^2) \\ &= e^{X/N} + \frac{1}{N}\frac{\partial e^{X/N+\delta X}}{\partial \delta X}\Bigg|_{\delta X=0} \delta X + \mathcal{O}(\delta X^2), \end{aligned} \tag{2.61}$$

so that

$$\begin{aligned} e^{X+\delta X} &= e^X + \frac{1}{N}\sum_{n=0}^{N-1} e^{X(N-n-1)/N}\left.\frac{\partial e^{X/N+\delta X}}{\partial \delta X}\right|_{\delta X=0}\delta X e^{Xn/N} \\ &\quad + \mathcal{O}(\delta X^2) \\ &= e^X + e^{X(N-1)/N}\frac{1}{N}\sum_{n=0}^{N-1} e^{-nX/N}\left.\frac{\partial e^{X/N+\delta X}}{\partial \delta X}\right|_{\delta X=0}\delta X e^{nX/N} \\ &\quad + \mathcal{O}(\delta X^2) \\ &= e^X + e^{X(N-1)/N}\frac{1}{N}\sum_{n=0}^{N-1} e^{-n[X,\bullet]/N}\left(\left.\frac{\partial e^{X/N+\delta X}}{\partial \delta X}\right|_{\delta X=0}\delta X\right) \\ &\quad + \mathcal{O}(\delta X^2). \end{aligned} \tag{2.62}$$

The limit as $N \to \infty$ can now be taken, leading to

$$e^{X(N-1)/N} \to e^X, \tag{2.63}$$

$$\left.\frac{\partial e^{X/N+\delta X}}{\partial \delta X}\right|_{\delta X=0} \to 1, \tag{2.64}$$

and

$$\frac{1}{N}\sum_{n=0}^{N-1} e^{-n[X,\bullet]/N} = \frac{1}{N}\frac{1-e^{-[X,\bullet]}}{1-e^{-[X,\bullet]/N}} \to \frac{1-e^{-[X,\bullet]}}{[X,\bullet]}. \tag{2.65}$$

Therefore

$$\begin{aligned} \ln(e^{-X}e^{X+\delta X}) &= \ln\left(1+\frac{1-e^{-[X,\bullet]}}{[X,\bullet]}\delta X + \mathcal{O}(\delta X^2)\right) \\ &= \frac{1-e^{-[X,\bullet]}}{[X,\bullet]}\delta X + \mathcal{O}(\delta X^2). \end{aligned} \tag{2.66}$$

With this we now have a general formula for the Haar measure in terms of integration over the Lie algebra

$$\mathrm{d}u = \mathrm{d}^n X J(0)\det\left(\frac{1-e^{-[X,\bullet]}}{[X,\bullet]}\right) = \mathrm{d}^n X J(0)\det\left(\frac{2\sinh([X,\bullet]/2)}{[X,\bullet]}\right). \tag{2.67}$$

For the last form, we have used the fact that, for all unimodular groups, which is the case of our groups of interest, the trace in the adjoint representation of a Lie algebra element vanishes. This formula can be implemented, for example, by expressing the determinant in terms of the eigenvalues of $[X,\bullet]$.

For our purposes, however, we expand

$$\frac{2\sinh([X,\bullet]/2)}{[X,\bullet]} = 1 + \frac{1}{24}[X,\bullet]^2 + \mathcal{O}(X^4), \tag{2.68}$$

so that

$$\det\left(\frac{2\sinh([X,\bullet]/2)}{[X,\bullet]}\right) = 1 + \frac{1}{24}\operatorname{tr}([X,\bullet]^2) + \mathcal{O}(X^4). \tag{2.69}$$

In particular, we have

$$\mathrm{d}u = J(0)\,\mathrm{d}^n X(1 + \mathcal{O}(X^2)). \tag{2.70}$$

Thus

$$I(x) = \int \mathrm{d}u\, e^{(\operatorname{Re}\operatorname{tr} u - \operatorname{tr} 1)/x} = J(0)\int_D \mathrm{d}^n X\, e^{\frac{1}{2x}\operatorname{tr}(X^2)}(1 + \mathcal{O}(X^2)). \tag{2.71}$$

In terms of the inner product $\langle X, Y\rangle = -2\operatorname{tr}(XY)$ on $\mathfrak{g}$, it is clear that this is a Gaussian integral centered at $X = 0$. Thus, for small x, we can approximate it by integrating over all of $\mathfrak{g}$, so that

$$I(x) = J(0)\int \mathrm{d}^n X\, e^{-\frac{1}{4x}\langle X,X\rangle}(1 + \mathcal{O}(X^2)). \tag{2.72}$$

This is a path integral of a free matrix model over $\mathfrak{g}$ with a diagonal propagator $2x$. We thus obtain

$$I(x) = J(0)(4\pi x)^{n/2}(1 + \mathcal{O}(x)). \tag{2.73}$$

We conclude that the vacuum subtraction of the action must be such that

$$\langle u_f|e^{-\epsilon H}|u_i\rangle = \frac{1}{J(0)}\left(\frac{a^{d-2}}{2\pi g_t^2\epsilon}\right)^{n/2} e^{\frac{2a^{d-2}}{g_t^2\epsilon}(\operatorname{Re}\operatorname{tr}(u_f^{-1}u_i) - \operatorname{tr} 1)}. \tag{2.74}$$

The operator H can now be found using the group structure. Let $L(g)$ be the operator defined by

$$L(g)\,|u\rangle = |gu\rangle\,. \tag{2.75}$$

Much like in (A.126), we have

$$\langle u_f|\int \mathrm{d}g f(g)L(g)|u_i\rangle = f(u_f u_i^{-1}). \tag{2.76}$$

We thus have

$$e^{-\epsilon H} = \frac{1}{J(0)}\left(\frac{a^{d-2}}{2\pi g_t^2\epsilon}\right)^{n/2}\int \mathrm{d}g\, e^{\frac{2a^{d-2}}{g_t^2\epsilon}(\operatorname{Re}\operatorname{tr} g - \operatorname{tr} 1)}L(g). \tag{2.77}$$

We can evaluate this integral in the limit $\epsilon \to 0$ by again transforming it into an integral over the Lie algebra. For this we introduce the $\mathfrak{g}$-valued electric operators E, for which

$$e^{-i\langle E,X\rangle} = L(e^X). \tag{2.78}$$

In terms of $E_a = \langle E, T_a\rangle$, we have $\langle E, X\rangle = X^a E_a$. We can thus once again rewrite this as a Gaussian integral

$$e^{-\epsilon H} = \left(\frac{a^{d-2}}{2\pi g_t^2\epsilon}\right)^{n/2}\int \mathrm{d}^n X\, e^{-\frac{a^{d-2}}{2g_t^2\epsilon}X^a X^b\delta_{ab} - iX^a E_a}(1 + \mathcal{O}(X^2)). \tag{2.79}$$

Our earlier vacuum subtraction then cancels the normalization of this integral and the result is thus dominated by the classical saddle

$$\delta_{ab} X^b = -i \frac{g_t^2 \epsilon}{a^{d-2}} E_a, \tag{2.80}$$

so that

$$e^{-\epsilon H} = e^{-\frac{g_t^2 \epsilon}{2a^{d-2}} E_a E_b \delta^{ab}} (1 + \mathcal{O}(\epsilon)). \tag{2.81}$$

Alternatively, since $E = \delta^{ab} E_a T_b$, we can write this as

$$e^{-\epsilon H} = e^{-\frac{g_t^2 \epsilon}{2a^{d-2}} E^2} (1 + \mathcal{O}(\epsilon)), \tag{2.82}$$

where $E^2 = \langle E, E \rangle$.

With this we can now immediately solve for the Hamiltonian of the full theory, taking the limit $\epsilon \to 0$

$$H = \frac{g_t^2}{2a^{d-2}} \sum_{\boldsymbol{x}_i \in E} E(\boldsymbol{x}_i)^2 - \frac{2a^{d-4}}{g_s^2} \sum_{\boldsymbol{x}_{ij} \in \mathcal{P}} \operatorname{Re} W(\boldsymbol{x}_{ij}) \tag{2.83}$$

This is the Kogut-Susskind Hamiltonian, and will be the basis for the work we will do in this chapter. The first term of it is called the electric Hamiltonian H_E, while the second is the magnetic Hamiltonian H_B. More commonly, following the discussion in Section A.9.4, we will write this in terms of the dimensionless coupling

$$g^2 = \frac{g_t g_s}{a^{d-3}}, \tag{2.84}$$

and a temporal scale $\epsilon := a g_s / g_t$. This leaves us with the form

$$\epsilon H = \frac{g^2}{2} \sum_{\boldsymbol{x}_i \in E} E(\boldsymbol{x}_i)^2 - \frac{2}{g^2} \sum_{\boldsymbol{x}_{ij} \in \mathcal{P}} \operatorname{Re} W(\boldsymbol{x}_{ij}). \tag{2.85}$$

2.1.3 Magnetic Bases

The focus of this dissertation will be the cases $d = 1$ and $d = 2$. In those cases the naive $a \to 0$ limit in which we forget that g_t and g_s are functions of a, would suggest that $g^2 = a^{3-d} g_s g_t \to 0$. However, the real world corresponds to the situation $d = 3$. In it $g^2 = g_s g_t$ and its behavior in the limit $a \to 0$ is much more subtle. Fortunately, due to asymptotic freedom, it is also true that in that limit $g \to 0$ in the continuum limit. This is therefore the limit of focus on this dissertation.

Near the continuum, the magnetic part of the Hamiltonian dominates. It is thus sensible to implement the theory on quantum computers using an encoding that diagonalizes this

part of the Hamiltonian, so that its time-evolution can be performed simply and is less prone to errors. Fortunately, the field basis $|u\rangle$ already does this (2.46). This however comes with two fundamental difficulties.

The first is that we need an embedding of the Hilbert space of the theory into that of a quantum computer, in which states $|u\rangle$ are mapped to bit strings. In the case of a continuous group G, this is impossible, for the Hilbert space of Yang-Mills theory would be infinite-dimensional[3], while the Hilbert space of a digital quantum computer is finite-dimensional. Thus, this involves a choice of a finite-dimensional truncation $\mathfrak{H}$ of $L^2(G)$. This must be done so that the low-energy eigenstates of the theory are well-approximated by elements of $\mathfrak{H}$.

A natural avenue, in which field configurations can be mapped to bit strings, is to choose the truncation through a finite subgroup $D \subset G$ [89, 139–147]. In this case we can take $\mathfrak{H} = L^2(D)$, spanned by state $|u\rangle$ with $u \in D$. We remark that, $\mathfrak{H}$ is not a subspace of the untruncated Hilbert space $L^2(G)$. An advantage of this truncation is that it leaves us with a gauge theory based on the group D. A disadvantage is that, at small coupling, the magnetic Hamiltonian forces low energy states to have wave functions where the plaquette holonomies have $u \approx 1$. Since in a finite group the identity is isolated, there will be a minimum coupling in which states will freeze at $u = 1$ [148].

One might expect that this problem can be solved by choosing subgroups D that are denser near the identity than elsewhere in the group, in order to better resolve wave functions near $u \approx 1$. This is however impossible, since a group always acts on itself faithfully via multiplication. Thus, if one wants to have a better resolution of the weak-coupling states, one needs to consider discretizations D that are not subgroups. If done naively on G, this breaks directly the gauge structure of the theory [149].

It has thus been proposed to do this discretization only after fully gauge-fixing the theory [94, 98, 150–152]. This can be achieved through the maximal tree construction, which we will discuss in detail in the next section. In this way one obtains a magnetic truncation that is well-suited to describe low energy states near the continuum. But the price that one pays is rooted in the Aharonov-Bohm effect: Yang-Mills theory can be described in terms of gauge-invariant quantities, at the expense of losing manifest locality.

To better understand this point, let us restrict for the moment to a U(1) gauge theory, which we will consider classical. Consider a pair of quantum-mechanical infinitely heavy particles, with the same initial state $|\psi\rangle$, moving along a pair of trajectories $\mathcal{C}_1$ and $\mathcal{C}_2$ in spacetime. Then, as we showed in (2.4), the final states of these particles would be $u(\mathcal{C}_1)\,|\psi\rangle$ and $u(\mathcal{C}_2)\,|\psi\rangle$. In particular, we can then study the amplitude for the first particle to be found in the state of the second

$$\langle\psi|u(\mathcal{C}_2)^\dagger u(\mathcal{C}_1)|\psi\rangle = \langle\psi|w(\mathcal{C})|\psi\rangle\,, \tag{2.86}$$

[3]This is in stark contrast to, say, Chern-Simons theory, where this is not the case.

with $\mathcal{C}$ the trajectory that goes first through $\mathcal{C}_1$ and then backtracks through $\mathcal{C}_2$. The expression (2.9) yields a manifestly local formula for this probability. After all, it only involves knowledge of the field A on $\mathcal{C}$, which was the trajectory that our particles explored. However, A is redundant. We can find a gauge invariant expression by employing stokes theorem

$$w(\mathcal{C}) = e^{-\int_{\mathcal{C}} A} = e^{-\int_{\Sigma} F}, \tag{2.87}$$

where Σ is any surface bounded by $\mathcal{C}$ (assuming there is such a surface on which A is well-defined). This is now manifestly gauge invariant, but we have paid an important price. We know require knowledge of F on all of Σ, even though our particles only traversed its boundary. Therefore, it is manifestly non-local.

2.1.4 Electric Bases

Given the difficulties we have found in implementing a magnetic basis, it is useful to study bases in which the electric term of the Hamiltonian is diagonalized. Although it will be more difficult in them to reach their continuum limit, as we will see, they offer important simplifications for numerical analysis through quantum computers.

The key to diagonalize this part of the Hamiltonian is the Peter-Weyl theorem [153]. Recall that the Hilbert space on a link ℓ is $L^2(G)$ spanned by states $|u\rangle$ in which the Wilson line on the link is given by u. Let $\hat{G}$ be the set of all irreducible representations of G. The Peter-Weyl theorem states that

$$L^2(G) = \bigoplus_{R \in \hat{G}} R \otimes R^*. \tag{2.88}$$

The right-hand side is spanned by states of the form $|\psi\rangle \otimes \langle\phi|$, where $|\psi\rangle, |\phi\rangle \in R$. The identification in this theorem is obtained by declaring that amplitude for the Wilson line u in this state is

$$\langle u| \left(|\psi\rangle \otimes \langle\phi|\right) := \sqrt{\dim R}\, \langle\phi|u|\psi\rangle\,. \tag{2.89}$$

On the right-hand side, it is understood that u is in the representation R.

This suggests that we split the link ℓ into two halves, say a and b. The orientation of the link can be represented through an ordering of these half-edges, so that we can write $\ell = (b, a)$. Much like composition of Wilson lines, this should be read backwards, so that a is the starting half-edge and b is the finishing half-edge. This is shown in Fig. 2.1.

The Peter-Weyl theorem is implemented by assigning to each half-edge h the Hilbert space

$$\mathcal{H}(h) := \bigoplus_{R \in \hat{G}} R. \tag{2.90}$$

Then, on the link (b, a) we define the Hilbert space

$$\mathcal{H}(b, a) := \mathcal{H}(b) \otimes \mathcal{H}(a)^* \tag{2.91}$$

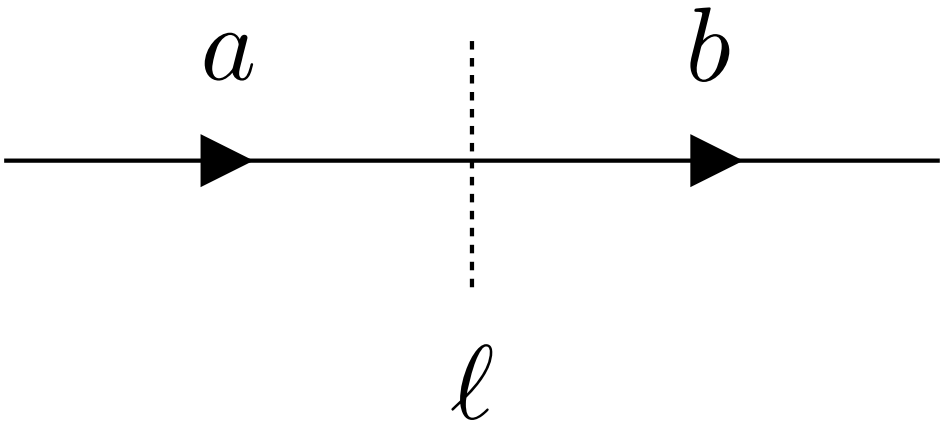


Figure 2.1: The oriented link $\ell = (b, a)$.

Note that this is not the original Hilbert space $L^2(G)$. Instead,

$$\mathcal{H}(b,a) = \bigoplus_{R_1,R_2\in\hat{G}} R_1 \otimes R_2^*. \tag{2.92}$$

The previous Hilbert space $L^2(G)$ however sits as a subspace of $\mathcal{H}(b,a)$ defined by the condition $R_1 = R_2$. This is known as the Abelian Gauss law.

To see why this diagonalizes the Hamiltonian, we further define electric operators $E(h)$ on each half-edge h. These generate the representation of G on $\mathcal{H}(h)$. Explicitly, for $\psi \in R \subset \mathcal{H}(h)$

$$e^{-i\langle E(h),X\rangle} |\psi\rangle = e^X |\psi\rangle , \tag{2.93}$$

where on the right-hand side e^X is understood to be in the representation R. The Peter-Weyl theorem establishes (2.88) as an equivalence of representations. In particular, if $\boldsymbol{x}_i = (b, a)$, then our electric operator $E(\boldsymbol{x}_i)$ appearing in (2.85) is precisely $E(b)$. On the other hand, $E(a)$ generates the transformations

$$e^{-i\langle E(a),X\rangle} |u\rangle = |u(e^{-X})\rangle , \tag{2.94}$$

on $\boldsymbol{x}_i$. For this reason $E(b)$ is often called the left electric field, while $E(a)$ is called the right electric field. Note that this might be confusing if you interpret this in view of Fig. 2.1. Thus, we will avoid this notation.

We now note that $E(h)^2$ is invariant. For this we recall that $-iE(h)$ is a representation of $\mathfrak{g}$, so that

$$[E_a(h), E_b(h)] = if^c{}_{ab} E_c(h), \tag{2.95}$$

in terms of the structure functions $[T_a, T_b] = f^c{}_{ab} T_c$. Moreover, invariance of our inner product $\langle \bullet, \bullet \rangle$ on $\mathfrak{g}$ implies that

$$0 = \langle [T_a, T_b], T_c\rangle + \langle T_b, [T_a, T_c]\rangle = f^d{}_{ab}\,\delta_{dc} + f^d{}_{ac}\,\delta_{bd}, \tag{2.96}$$

or after multiplying by $\delta^{cd}\delta^{bf}$

$$0 = f^{e}{}_{ab}\,\delta^{bf} + f^{f}{}_{ac}\,\delta^{cd}. \tag{2.97}$$

We can now compute

$$[E^2, E_a] = i\delta^{bc}(f^{d}{}_{ba}\,E_d E_c + f^{d}{}_{ca}\,E_b E_d). \tag{2.98}$$

Relabeling in the second term, this can be equivalently written as

$$[E^2, E_a] = i\delta^{bc} f^{d}{}_{ba}\,\{E_d, E_c\}. \tag{2.99}$$

We now take advantage of the symmetry of the anticommutator to set this to

$$[E^2, E_a] = \frac{i}{2}(\delta^{bc} f^{d}{}_{ba} + \delta^{bd} f^{c}{}_{ba})\{E_d, E_c\} = 0. \tag{2.100}$$

Since E^2 is invariant, Schur's lemma guarantees that in an irreducible representation R it is given by a number $C_2(R)$, so that for all $|\psi\rangle \in R$ we have

$$E^2\,|\psi\rangle = C_2(R)\,|\psi\rangle\,. \tag{2.101}$$

This is known as the quadratic Casimir of the representation. Note in particular that on a link $\ell = (b, a)$, the Abelian Gauss law guarantees that $E(b)^2 = E(a)^2$. Thus, either can be used in the electric part of (2.85). And they are both diagonal in this basis.

In the process of diagonalizing this sector of the Hamiltonian, we have enlarged the Hilbert space. While the original Hamiltonian (2.85) was only defined on the subspace that satisfied the Abelian Gauss law, it is instructive to try to extend it to the full Hilbert space we have now. There is of course no unique extension. For example, the electric part of the Hamiltonian associated to $\boldsymbol{x}_i = (b, a)$ could be extended to

$$E(a)^2, \quad E(b)^2, \quad \frac{1}{2}(E(a)^2 + E(b)^2), \quad \ldots\,. \tag{2.102}$$

For the purposes of this dissertation, we will choose one half-link $h(\boldsymbol{x}_i)$ for each link $\boldsymbol{x}_i$, and use its electric operator for the energy contribution of the whole link. This is certainly not the most democratic choice, but it will be useful for the formalism we will develop in this chapter.

Let us now focus on the form of the magnetic Hamiltonian. For this we need to understand the action of a Wilson line operator U on a link ℓ on a state of the form $|\psi_1\rangle \otimes \langle\phi_1|$ with $|\psi_1\rangle, |\phi_1\rangle \in R_1$

$$U(|\psi_1\rangle \otimes \langle\phi_1|) = \sqrt{\dim R_1}\int \mathrm{d}u\, u\,|u\rangle\,\langle\phi_1|u|\psi_1\rangle\,. \tag{2.103}$$

Given that U is a G-valued operator, we can instead consider its matrix elements $\langle\phi_2|U|\psi_2\rangle$ in an irreducible representation $|\psi_2\rangle, |\phi_2\rangle \in R_2$. These are defined by

$$\langle\phi_2|U|\psi_2\rangle\,|u\rangle = \langle\phi_2|u|\psi_2\rangle\,|u\rangle\,. \tag{2.104}$$

We thus want to understand the action

$$\langle\phi_2|U|\psi_2\rangle\,(|\psi_1\rangle\otimes\langle\phi_1|) = \sqrt{\dim R_1}\int \mathrm{d}u\;|u\rangle\,\langle\phi_2|u|\psi_2\rangle\,\langle\phi_1|u|\psi_1\rangle\,. \tag{2.105}$$

Finally, to remove reference to our defining magnetic variables, we compute the inner product against another vector $|\psi_3\rangle\otimes\langle\phi_3| \in R_3\otimes R_3^*$ in the electric basis

$$\begin{aligned}&(\langle\psi_3|\otimes|\phi_3\rangle)\,\langle\phi_2|U|\psi_2\rangle\,(|\psi_1\rangle\otimes\langle\phi_1|) = \\ &\sqrt{\dim R_1\dim R_3}\int \mathrm{d}u\;\langle\psi_3|u^\dagger|\phi_3\rangle\,\langle\phi_2|u|\psi_2\rangle\,\langle\phi_1|u|\psi_1\rangle\,.\end{aligned} \tag{2.106}$$

The resulting integral can be computed exactly by writing it in the form

$$\begin{aligned}&(\langle\psi_3|\otimes|\phi_3\rangle)\,\langle\phi_2|U|\psi_2\rangle\,(|\psi_1\rangle\otimes\langle\phi_1|) = \\ &\sqrt{\dim R_1\dim R_3}\,|\phi_3\rangle\otimes\langle\phi_2|\otimes\langle\phi_1|\,P_R\,\langle\psi_3|\otimes|\psi_2\rangle\otimes|\psi_1\rangle\,,\end{aligned} \tag{2.107}$$

for $R = R_3^*\otimes R_2\otimes R_1$ and

$$P_R = \int \mathrm{d}u\,R(u). \tag{2.108}$$

We will now show that P_R is the orthogonal projector onto the subspace of R invariant under the action of G.

The fact that the image of P_R is invariant under G is a consequence of the invariance of the Haar measure

$$R(g)P_R = \int \mathrm{d}u\,R(gu) = \int \mathrm{d}u\,R(u) = P_R. \tag{2.109}$$

Moreover, P_R leaves invariant states $|\psi\rangle \in R$ intact

$$P_R\,|\psi\rangle = \int \mathrm{d}u\,R(u)\,|\psi\rangle = \int \mathrm{d}u\;|\psi\rangle = |\psi\rangle\,. \tag{2.110}$$

We thus conclude that P_R is indeed a projector $P_R^2 = P_R$ onto the invariant subspace. Finally, orthogonality is another consequence of the invariance of the Haar measure and unitarity of the representation

$$P_R^\dagger = \int \mathrm{d}u\,R(u)^\dagger = \int \mathrm{d}u\,R(u^{-1}) = \int \mathrm{d}u\,R(u) = P_R. \tag{2.111}$$

In general, the image of P_R will be multidimensional. Given an orthogonal basis $|\alpha\rangle$ of this invariant subspace, we can write

$$P_R = \sum_\alpha |\alpha\rangle \langle\alpha| . \tag{2.112}$$

A method for building such a basis is to use Clebsch-Gordan theory. We can first decompose into irreducibles

$$R_2 \otimes R_1 = \bigoplus_{\tilde{R}\in\hat{G}} \bigoplus_\alpha \tilde{R}^\alpha, \tag{2.113}$$

where α labels the copy of $\tilde{R}$that appears within $R_2 \otimes R_1$. Let us denote by $P_{\tilde{R}^\alpha}$ the orthogonal projector from $R_2 \otimes R_1$ into the α-th copy of R. Then

$$R_3^* \otimes R_2 \otimes R_1 = \bigoplus_{\tilde{R}\in\hat{G}} \bigoplus_\alpha R_3^* \otimes \tilde{R}^\alpha. \tag{2.114}$$

An invariant vector in $R_3^* \otimes \tilde{R}$ would be the same as an invariant map between these irreducibles $\tilde{R}^* \to R_3^*$. By Schur's lemma, this is only possible if $\tilde{R} = R_3$, in which case such maps are all equal to the identity up to a constant. Thus, letting $|R_3, a\rangle$ be a basis for R_3, and $|R_3, a; \alpha\rangle$ be the associated basis for R_3^α we have the invariant vector

$$|\alpha\rangle = \frac{1}{\sqrt{\dim R_3}} \langle R_3, a| \otimes |R_3, a; \alpha\rangle , \tag{2.115}$$

where the normalization ensures that $|\alpha\rangle$ is normalized. In particular, for all $\langle\psi| \otimes |\phi\rangle \in R_3^* \otimes R_3^\alpha$, we have

$$\langle\alpha| (\langle\psi| \otimes |\phi\rangle) = \frac{1}{\sqrt{\dim R_3}} \langle\psi|\phi\rangle . \tag{2.116}$$

With this we have an explicit construction of a basis of the invariant subspace of R in terms of the appearances of R_3 in $R_2 \otimes R_1$.

By construction $|\alpha\rangle = 1_{R_3^*} \otimes P_{R_3^\alpha} |\alpha\rangle$. Therefore,

$$\langle\alpha| \langle\psi_3| \otimes |\psi_2\rangle \otimes |\psi_1\rangle = \frac{1}{\sqrt{\dim R_3}} \langle\psi_3| P_{R_3^\alpha} (|\psi_2\rangle \otimes |\psi_1\rangle). \tag{2.117}$$

We then obtain

$$\begin{aligned} &(\langle\psi_3| \otimes |\psi_3\rangle) \langle\phi_2|U|\psi_2\rangle (|\psi_1\rangle \otimes \langle\phi_1|) = \\ &\sqrt{\frac{\dim R_1}{\dim R_3}} \sum_\alpha \langle\phi_2| \otimes \langle\phi_1| P_{R_3^\alpha} |\phi_3\rangle \langle\psi_3| P_{R_3^\alpha} |\psi_2\rangle \otimes |\psi_1\rangle . \end{aligned} \tag{2.118}$$

While this formula defines the Wilson lines on the states that satisfy the Abelian Gauss law, it does not give an extension to states outside of it. Of course, such an extension would not be unique and can be chosen for the purposes of engineering simpler quantum circuits [93]. We give such an extension for the case of $G = \mathrm{SU}(2)$ theories in Section 2.4.3.

To exemplify this, let us pick an irreducible representation R_w for our Wilson line operators that has the special property that the decomposition of $R_w \otimes R$ into irreducibles does not have multiplicities. This is the case of the fundamental representation in all the groups $\mathrm{SU}(N_c)$. This does not pose a loss of generality for the action (2.25) since different representations are related by a rescaling of the coupling constant at leading order in the continuum limit. For each $\psi \in R_w$ we can define the operator $U(h)\,|\psi\rangle$ on $\mathcal{H}(h)$ given simply by

$$U(h)\,|\psi\rangle\,|\phi\rangle = \sum_{\tilde{R}} \left(\frac{\dim R}{\dim \tilde{R}}\right)^{1/4} P^{\tilde{R}}_{R_w \otimes R}\,|\psi\rangle \otimes |\phi\rangle\,, \tag{2.119}$$

for all $|\phi\rangle \in R \subseteq \mathcal{H}(h)$. In here $P^{\tilde{R}}_{R_w \otimes R}$ is the projector onto the irreducible component $\tilde{R}$ on $R_w \otimes R$. Let us denote the conjugate operator by $\langle\psi|\,U(h)^\dagger$. Further, let us introduce the projection $P(b,a)$ on $\mathcal{H}(b) \otimes \mathcal{H}(a)^*$ which projects onto the subspace satisfying the Abelian Gauss law. Then we can take

$$\langle\phi|U(b,a)|\psi\rangle = P(b,a)\,\langle\phi|U(a)^\dagger U(b)|\psi\rangle\,. \tag{2.120}$$

Such a projector is analogous to a syndrome measurement (and potentially correction) in a quantum error correcting code such as the 3-qubit bit flip code.

While it is difficult to achieve the continuum limit in this basis, it has the advantage that its states are described in terms of states in a representation R at each half-edge. These are discrete objects, whose mapping to qubits is simpler to study than those in the magnetic basis. In particular, truncation of the Hilbert space is naturally achieved by restricting to only a subset of the representations. These are usually chosen by their $C_2(R)$, which as we discussed will dictate their electric energy. As we tune to the continuum limit, we need to allow for more representations to appear, given the fact that the magnetic energy will dominate more and more. Moreover, unlike the magnetic truncations we mentioned before, the Hilbert space in these truncations naturally lies inside the full Hilbert space of the theory.

A final problem we would like to tackle is that the Hilbert space of the theory, as it stands, is very big, and most of it is unphysical. This was the situation in the magnetic bases as well, before we introduce the maximal tree construction. In fact, in this situation it is worse, since we have introduced a further Abelian Gauss law that has to be satisfied. Fortunately, there is a simple solution that makes it so that the Abelian Gauss law is the only constraint that has to be satisfied.

In order to see this, let us now consider a vertex p in our lattice with half-edges $h_1, \ldots, h_n$ attached to it. Let us denote by $|R, a\rangle$ a basis of the irreducible representation R. Then a

basis state on this vertex would be of the form

$$|R_1, a_1; \cdots; R_n, a_n\rangle = |R_1, a_1\rangle \otimes \cdots \otimes |R_n, a_n\rangle \,. \tag{2.121}$$

Under a gauge transformation g at our vertex, we would have

$$|R_1, a_1; \cdots; R_n, a_n\rangle \mapsto g\,|R_1, a_1\rangle \otimes \cdots \otimes g\,|R_n, a_n\rangle \,. \tag{2.122}$$

In particular, Gauss' law then demands that physical states are linear combinations of this basis that are invariant under such gauge transformations.

Alternatively, we can encode only a basis for the gauge invariant states in $R_1 \otimes \cdots \otimes R_n$. If we label these by an index Γ, we obtain a fully gauge invariant basis

$$|\Gamma; R_1, \ldots, R_n\rangle \,. \tag{2.123}$$

Enumerating such states is a classically tractable problem automatically solving the Gauss law through our splitting of links in terms of half-edges. The physical Hilbert space is then obtained by restricting combining these vertex states along the graph in a way that on each link the two representations appearing are conjugate to each other. For example, in SU(2), on a graph that is only trivalent, meaning that each vertex has only three half-edges attached to it, there are no multiplicities, so that states are completely determined by the placement of irreducibles along each half-link of the graph. As we will see in Section 2.3.1, gauge theories can always be placed on a trivalent graph without loss of generality.

2.2 Yang-Mills on General Graphs

Much like (2.27) makes sense on general manifolds with a metric, not only $\mathbb{R}^D$, we will now extend our lattice theory to general graphs. In order to do this, we will need to develop some common language that we can use to describe these structures.

2.2.1 Basics of Graph Theory

There exists several ways to formalize the notion of a graph and all of them are more or less equivalent to one another. Due to the advantages we wish to retain from the electric bases discussed in Section 2.1.4, we will use as a building block for our graphs the notion of a "half-edge." Fortunately, the same structure is also useful in the study of Feynman diagrams [154], where the notion of half-edge allows for a conceptually clear description of graph combinatorics.

A graph G consists of two sets, a set of half-edges H and a set of vertices V, along with an attaching map $\sigma : H \to H$ and an anchoring map $\pi : H \to V$. The latter assigns to each half-edge $h \in H$ the vertex $\pi(h) \in V$ to which it is anchored. The former attaches each

half-edge to a partner, so that $\{h, \sigma(h)\} \subseteq H$ is an edge. We thus assume that $\sigma(\sigma(h)) = h$, so that σ is an involution.

In the theory of Feynman diagrams, it is useful to allow for the possibility that $h = \sigma(h)$, so that h represents an external edge. However, for the applications in this dissertation it will not be necessary to entertain this possibility. We will thus demand that for all $h \in H$ we have $h \neq \sigma(h)$. The set of edges is thus

$$H\!/_{\sigma} = \{\, e = \{h, \sigma(h)\} \mid h \in H \,\}. \tag{2.124}$$

Note that edges, being sets of two elements, are unordered. Yang-Mills theory, being invariant under changes in orientation, can be written completely in terms of these. Nevertheless, it is notationally useful to introduce the concept of a link $\ell = (h, \sigma(h)) \in H \times H$, which is an ordered pair. As before, the orientation will be so that ℓ goes first through $\sigma(h)$ and then through h, so that links are left right to left. We will use the pullback notation $H \times_{\sigma} H$ for the set of all links. An orientation of the graph is a subset $\mathrm{L} \subseteq H \times_{\sigma} H$ of the set of all links, such that for each edge $\{h_1, h_2\}$ we have either $(h_1, h_2) \in \mathrm{L}$ or $(h_2, h_1) \in \mathrm{L}$.

It is notationally convenient to define the source and target maps

$$\begin{aligned} s : H \times_{\sigma} H &\to V \\ (h_1, h_2) &\mapsto \pi(h_2), \\ t : H \times_{\sigma} H &\to V \\ (h_1, h_2) &\mapsto \pi(h_1), \end{aligned} \tag{2.125}$$

which assign to each link the vertices where they start and end, respectively. With these we can now extend the notion of a link to that of a trajectory. A trajectory of length n is a map $\gamma : \{1, \ldots, n\} \to H \times_{\sigma} H$ which is continuous, in the sense that $t(\gamma(i)) = s(\gamma(i+1))$. We will denote the set of all such trajectories by T. The set of links can be identified with the set of trajectories of length $n = 1$. We can also extend the source and target maps by the equations $s(\gamma) = s(\gamma(1))$ and $t(\gamma) = t(\gamma(n))$.

The notion of a link and its extension to trajectories can be shifted to the notion of a corner and a corner trajectory. A corner is an ordered pair of half-edges $c = (h_1, h_2) \in H \times H$ which are anchored to the same vertex $\pi(h_1) = \pi(h_2)$. We will use a pullback notation $H \times_{\pi} H$ for the set of all corners as well. The source and target of such a corner $s, t : H \times_{\pi} H \to H$ are now half-edges, and are defined by $c = (t(c), s(c))$. A corner trajectory of length n is then a map $\gamma : \{1, \ldots, n\} \to H \times_{\pi} H$ for which $\sigma(t(\gamma(i))) = s(\gamma(i+1))$. We will denote the set of all such corner trajectories by C. As for links, the set of corners can be identified with that of corner trajectories of length $n = 1$. The source and target maps then extend via the equations $s(\gamma) = s(\gamma(1))$ and $t(\gamma) = t(\gamma(n))$.

Regardless of whether we are in the world of links or corners, we can invert orientation $(h_1, h_2)^{-1} := (h_2, h_1)$. This operation extends to their associated trajectories

$$\gamma^{-1}(i) := \gamma(n - i + 1)^{-1}. \tag{2.126}$$

We can also compose two trajectories γ_1 and γ_2 of lengths n and m, respectively, into a trajectory $\gamma = \gamma_1\gamma_2$ of length $n+m$. This will be defined whenever $t(\gamma_2) = s(\gamma_1)$ for link trajectories, or $\sigma(t(\gamma_2)) = s(\gamma_1)$ for corner trajectories. As always, this trajectory should be read right to left, so that

$$\gamma(i) = \begin{cases} \gamma_2(i), & i = 1, \dots, m \\ \gamma_1(i-m), & i = m+1, \dots, m+n. \end{cases} \tag{2.127}$$

In particular, trajectories can always be understood as the composition of their individual steps

$$\gamma = \gamma(n)\gamma(n-1)\cdots\gamma(1). \tag{2.128}$$

A link trajectory is said to be closed if $t(\gamma) = s(\gamma)$ and similarly a corner trajectory is said to be closed if $\sigma(t(\gamma)) = s(\gamma)$. Closed trajectories can be thought of as either link or corner trajectories. Indeed, if γ^c is a closed corner trajectory, we can define the closed link trajectory

$$\gamma^l(i) = (s(\gamma^c((i+1) \mod n)), t(\gamma^c(i))). \tag{2.129}$$

The latter is a closed link trajectory since

$$\begin{aligned} t(\gamma^l(i)) &= \pi(s(\gamma^c((i+1) \mod n))) = \pi(t(\gamma^c((i+1) \mod n))) \\ &= s(\gamma^l((i+1) \mod n)). \end{aligned} \tag{2.130}$$

Every non-trivial graph has a closed trajectory. Indeed, we can take a link ℓ and consider $\ell^{-1}\ell$. To remove this case, we introduce the notion of a reduced closed trajectory, which are ones for which

$$\gamma(i) \neq \gamma((i+1) \mod n)^{-1}. \tag{2.131}$$

Connected graphs that do not admit such reduced closed trajectories are called trees.

The last piece of technology we will need is that of a subgraph of G. This is a graph whose vertex set and set of half-edges is a subset of those of G, while the anchoring and attaching maps are the appropriate restrictions to these subsets. In particular, we will be interested in maximal trees. These are maximal subgraphs that are trees. They are maximal in the sense that adding any half-edge to them would result in there being a reduced closed trajectory.

2.2.2 Classical Aspects

The Yang-Mills field on a graph is an assignment u, of a Wilson line $u(\ell)$ to each link ℓ with the condition that $u(\ell^{-1}) = u(\ell)^{-1}$. Let us denote the set of possible configurations of this field by $\mathcal{E}$. Note that, the Wilson lines on a given edge are completely determined by

the Wilson line on one of its two possible orientations. Thus, given a choice of orientation L we have the isomorphism $\mathcal{E} \cong G^{\mathrm{L}}$. One can further define Wilson lines on trajectories

$$u(\gamma) = u(\gamma(n)) \cdots u(\gamma(2))u(\gamma(1)). \tag{2.132}$$

The group of gauge transformations is G^V. A gauge transformation $g \in \mathcal{G}$ acts on $u \in \mathcal{E}$ through

$$(gu)(\ell) = g(t(\ell))u(\ell)g(s(\ell))^{-1}, \tag{2.133}$$

which extends to trajectories through the replacement $\ell \mapsto \gamma$. This is the analog of (2.8). Two configurations in the same orbit, i.e. related by gauge transformations, should be considered completely equivalent, as on standard lattices. We will denote the set in which all configurations are considered equivalent up to gauge transformation by

$$\mathcal{E}/_{G^V}. \tag{2.134}$$

The main insight we will use is that, kinematically, two graphs lead to equivalent physics as long as this set is the same for the two.

We will now give a general coarse-graining procedure that will allow us to construct from one graph G another reduced graph $\mathrm{G}_{\mathrm{red}}$ which is kinematically equivalent to the first. The input to this construction is a set of trajectories T. Each $\gamma \in T$ will define a link in $\mathrm{G}_{\mathrm{red}}$ which we denote by the same symbol γ. Their half-edges, when thought of as part of $\mathrm{G}_{\mathrm{red}}$ will be denoted by

$$\gamma = (h_\gamma^{(t)}, h_\gamma^{(s)}). \tag{2.135}$$

The vertices of $\mathrm{G}_{\mathrm{red}}$ will be the set V_{red} of endpoints $s(\gamma)$ and $t(\gamma)$ of the trajectories $\gamma \in T$. And finally, the anchoring map is given by

$$\pi(h_\gamma^{(t)}) = t(\gamma), \quad \text{and} \quad \pi(h_\gamma^{(s)}) = s(\gamma), \tag{2.136}$$

while the attaching map is the involution satisfying

$$\sigma(h_\gamma^{(s)}) = h_\gamma^{(t)}. \tag{2.137}$$

Every configuration u on G induces a configuration u_{red} on $\mathrm{G}_{\mathrm{red}}$ by the realization that $u(\gamma)$ can be thought of as the Wilson line on the trajectory γ of G or on the link $u_{\mathrm{red}}(\gamma) = u(\gamma)$ carrying the same name on $\mathrm{G}_{\mathrm{red}}$. This yields a map $\mathcal{E} \to \mathcal{E}_{\mathrm{red}}$, the latter being the space of configurations on $\mathrm{G}_{\mathrm{red}}$. Similarly, each gauge transformation $g \in G^V$ induces a gauge transformation in $G^{V_{\mathrm{red}}}$ since $V_{\mathrm{red}} \subseteq V$. Due to the naturalness of this construction, the map $\mathcal{E} \to \mathcal{E}_{\mathrm{red}}$ is equivariant, so that it descends to a map

$$\mathcal{E}/_{G^V} \to \mathcal{E}_{\mathrm{red}}/_{G^{V_{\mathrm{red}}}} \tag{2.138}$$

We will now spell out two conditions that are sufficient to guarantee that this map determines an equivalence of the configurations up to gauge transformations, so that G and $\mathrm{G}_{\mathrm{red}}$ are kinematically equivalent.

The first condition that will be true in all of our examples is that the map $\mathcal{E} \to \mathcal{E}_{\mathrm{red}}$ is surjective. This guarantees that the resulting map (2.138) is as well. In most of our examples this will be true since for each trajectory $\gamma \in T$ there is a link ℓ traversed exactly once by γ that is not traversed by any other trajectory in T in any direction. This guarantees that each gauge configuration in $\mathrm{G}_{\mathrm{red}}$ can be interpreted as a gauge configuration in G. Indeed, consider a configuration u_{red} on $\mathrm{G}_{\mathrm{red}}$. This corresponds to a choice of Wilson lines $u_{\mathrm{red}}(\gamma)$ for each $\gamma \in T$. We would like to find a configuration u on all of G that gives rise to these Wilson lines. For this we can simply choose one of the links $\ell \in \mathrm{L}$ for each trajectory $\gamma \in T$, that is solely traversed by said trajectory, and set $u(\ell) = u_{\mathrm{red}}(\gamma)$, while keeping trivial Wilson lines on the remaining links. The constructed u is then compatible with our choice of Wilson lines $u(\gamma) = u_{\mathrm{red}}(\gamma)$.

Given the first condition, the second condition guaranteeing the injectiveness of (2.138) is that every pair of configurations $u_1, u_2 \in \mathcal{E}$ that map to the same reduced $u_{\mathrm{red}} \in \mathcal{E}_{\mathrm{red}}$ are related by a gauge transformation. This is generically harder to check. Our main tool in order to perform this check will be maximal tree gauge-fixing. Indeed, we will now show that given a tree T in G any configuration is equivalent to one in which all the Wilson lines along the tree are trivial.

The proof of this is a generalization of our discussion of the temporal gauge in Section 2.1.2, and was first explained to me by Irian D'Andrea. First, consider a trajectory γ in G that only goes through each vertex once. In order to set $u(\gamma(1))$ equal to the identity, consider a gauge transformation $g \in \mathcal{G}$ that is supported at $t(\gamma(1))$, meaning that $g(q) = 1$ whenever $q \neq t(\gamma(1))$. Let us take

$$g(t(\gamma(1))) = u(\gamma(1))^{-1}. \tag{2.139}$$

Then

$$(gu)(\gamma(1)) = 1. \tag{2.140}$$

Thus, we have succeeded in our goal. Now, suppose we have done the necessary gauge transformations to make u trivial on $\gamma(1)\gamma(2)\cdots\gamma(k)$. We can now make $u(\gamma(k+1))$ trivial by considering the gauge transformation $g \in \mathcal{G}$, supported on $t(\gamma(k+1))$, and given by

$$g(t(\gamma(k+1))) = u(\gamma(k+1))^{-1}. \tag{2.141}$$

Then

$$(gu)(\gamma(k+1)) = 1. \tag{2.142}$$

Notice that gu is still trivial on $\gamma(1)\cdots\gamma(k)$ since none of those links are anchored at $t(\gamma(k+1))$. Proceeding by induction, we conclude that there is an equivalent configuration

that is trivial on all of γ. The temporal gauge is the special case of this construction for a spacetime graph in which we consider purely temporal trajectories γ. Furthermore, we remark that in this construction all the gauge transformations along γ were used except for the one at $s(\gamma)$.

To see how this shows that on a tree T any configuration can be trivialized, let us first note that between any two vertices $p, q \in V$ there is a unique trajectory $\gamma_{q \leftarrow p}$ that goes from $p = s(\gamma)$ to $q = t(\gamma)$. Moreover, we note that there is a distinguished set of final points $p \in V$ characterized by the fact that only a single half-edge in the maximal tree is anchored at p. One then applies the construction above for all the trajectories $\gamma_{p \leftarrow \star}$.

2.2.3 Quantum Aspects and Symmetries

The space of configurations $\mathcal{E}$ can be naturally equipped with the measure

$$Du = \prod_{\ell \in \mathrm{L}} \mathrm{d}u. \tag{2.143}$$

Due to the invariance of the Haar measure under the group operations, this measure is independent of the choice of orientation L and is invariant under gauge transformations. The natural generalization of the Hilbert space of the theory to general graphs then $L^2(\mathcal{E}, Du) \equiv L^2(\mathcal{E})$. However, most of this Hilbert space is unphysical, and only the subspace $\mathcal{H} \subseteq L^2(\mathcal{E})$ of wave functions that are gauge invariant is physically relevant. Alternatively, this space can be thought of as

$$\mathcal{H} = L^2\Big(\mathcal{E}\big/_{G^V}\Big). \tag{2.144}$$

This shows that the kinematical equivalences discussed in the classical setting persist in the quantum one.

The loop operators between G and $\mathrm{G}_{\mathrm{red}}$ are related by the fact that for each $\gamma \in T$ one can interpret $U(\gamma)$ as a Wilson line operator in G

$$U(\gamma) = U(\gamma(n)) \cdots U(\gamma(1)), \tag{2.145}$$

or as a Wilson line operator on the link γ of $\mathrm{G}_{\mathrm{red}}$. Thus, the Wilson lines on trajectories of G that can be written as compositions of trajectories in T immediately descend into Wilson lines on $\mathrm{G}_{\mathrm{red}}$. The generalization of the electric operators to general graphs is more involved.

First pick a half-edge $h \in H$ and consider the action of $g \in G$ on $\mathcal{E}$ given by $u \mapsto \tilde{u}$, where $\tilde{u}$ assigns the same Wilson lines as u except for the edge $\{h, \sigma(h)\}$ in which

$$\tilde{u}(h, \sigma(h)) = g u(h, \sigma(h)). \tag{2.146}$$

We define the electric field $E(h)$ as the $\mathfrak{g}$-valued generator of this transformation

$$e^{-i\langle E(h),X\rangle}\,|u\rangle = |\tilde{u}\rangle\,, \tag{2.147}$$

This coincides with the link-based electric operators used in, e.g. (2.85), if we define

$$E(h,\sigma(h)) := E(h). \tag{2.148}$$

We would next like to understand the connection between the electric operators on G and on $\mathrm{G}_{\mathrm{red}}$. The key notion in order to do this will be that of parallel transport. Indeed, let us consider a half-edge $h \in H$ and a trajectory γ for which $s(\gamma) = \pi(h)$. Let us consider the transformation induced by a $g \in G$ on $\mathcal{E}$ that leaves intact all Wilson lines on all edges, except for

$$u(h,\sigma(h)) \mapsto u(\gamma^{-1})gu(\gamma)u(h,\sigma(h)). \tag{2.149}$$

This is the parallel transport of the action of G at h by the trajectory γ. The properties of this transformation are, in general, rather convoluted. Indeed, this need not be a group action. However, in the case that γ does not traverse h, we have that $u(\gamma) = \tilde{u}(\gamma)$, leading to simpler properties and, in particular, a left group action. We will restrict from now on to this case.

Let us take $g = e^X$ and denote the generator of this action by $\langle E(\gamma,h),X\rangle$. Note that this transformation equivalently maps

$$u(h,\sigma(h)) \mapsto e^{u(\gamma^{-1})Xu(\gamma)}u(h,\sigma(h)). \tag{2.150}$$

We thus have

$$e^{-i\langle E(\gamma,h),X\rangle}\,|u\rangle = e^{-i\langle E(h),u(\gamma^{-1})Xu(\gamma)\rangle}\,|u\rangle\,. \tag{2.151}$$

We thus conclude that

$$\langle E(\gamma,h),X\rangle\,|u\rangle = \langle E(h),u(\gamma^{-1})Xu(\gamma)\rangle\,|u\rangle\,, \tag{2.152}$$

or, in light of the invariance of the inner product on $\mathfrak{g}$

$$\langle E(\gamma,h),X\rangle\,|u\rangle = \langle u(\gamma)E(h)u(\gamma)^{-1},X\rangle\,|u\rangle\,, \tag{2.153}$$

This can be raised to an equivalence of $\mathfrak{g}$-valued operators

$$E(\gamma,h)\,|u\rangle = u(\gamma)E(h)u(\gamma^{-1})\,|u\rangle\,. \tag{2.154}$$

Finally, since $E(h)$ commutes with $U(\gamma)$ as operators, this can be lifted to an operator equation

$$E(\gamma,h) = U(\gamma)E(h)U(\gamma^{-1}). \tag{2.155}$$

The usefulness behind these operators is two-fold. First, invariance of the inner product on $\mathfrak{g}$ guarantees that

$$E(\gamma, h)^2 = E(h)^2. \tag{2.156}$$

Thus, in the Kogut-Susskind Hamiltonian (2.85), we can replace the electric operators by their parallel transports. Second, these parallel transports have a direct meaning on $\mathrm{G}_{\mathrm{red}}$. Indeed, assume we have a trajectory γ that goes through $(h, \sigma(h))$ once, so that it can be written as $\gamma = \gamma_2(h, \sigma(h))\gamma_1$ with γ_2 and γ_1 not overlapping with $(h, \sigma(h))$. We then have that $E(\gamma_2, h)$ generates the transformation

$$\begin{aligned} u(\gamma) &= u(\gamma_2)u(h, \sigma(h))u(\gamma_1) \\ &\mapsto u(\gamma_2)u(\gamma_2^{-1})gu(\gamma_2)u(h, \sigma(h))u(\gamma_1) = gu(\gamma). \end{aligned} \tag{2.157}$$

Thus, if $\gamma \in T$, the operator $E(\gamma_2, h)$ generates the same transformation on $u(\gamma)$ as $E(h_\gamma^{(t)})$.

Another fundamental example of parallel transports is in the relation between $E(h)$ and $E(\sigma(h))$. Indeed, the operator $E((\sigma(h), h), h)$ generates the transformation

$$u((h, \sigma(h))) \mapsto u((h, \sigma(h)))gu((\sigma(h), h))u((h, \sigma(h))) = u((h, \sigma(h)))g. \tag{2.158}$$

This is not a left action on $\mathcal{E}$. It is a right action, and is the one generated by $-E(\sigma(h))$. Given that $E(h)$ and $U(\sigma(h), h)$ do not commute, we cannot use (2.155). Nevertheless, (2.154) is still valid

$$-E(\sigma(h))\,|u\rangle = u((\sigma(h), h))E(h)u((h, \sigma(h)))\,|u\rangle\,. \tag{2.159}$$

This can be lifted to an operator equation by using the adjoint representation Ad of G on $\mathfrak{g}$, given by

$$\mathrm{Ad}(g)X = gXg^{-1}. \tag{2.160}$$

Then, on a basis of $\mathfrak{g}$ we have

$$-E^a(\sigma(h)) = E^b(h)\,\mathrm{Ad}(U(\sigma(h), h))^a{}_b. \tag{2.161}$$

2.3 Examples of Graph-Coarsening

2.3.1 Point-Splitting

As a first example of this technique, consider a section of a graph G with a vertex with $n-1$ links attached to it and a vertex with 3 links attached to it, as shown in Fig. 2.2a. Let us take as our set of trajectories $T = \{v_1 w, v_2 w\}$, so that coarse-graining leads to the graph $\mathrm{G}_{\mathrm{red}}$ found in Fig. 2.2b. Note that the resulting vertex now has a larger valency n.

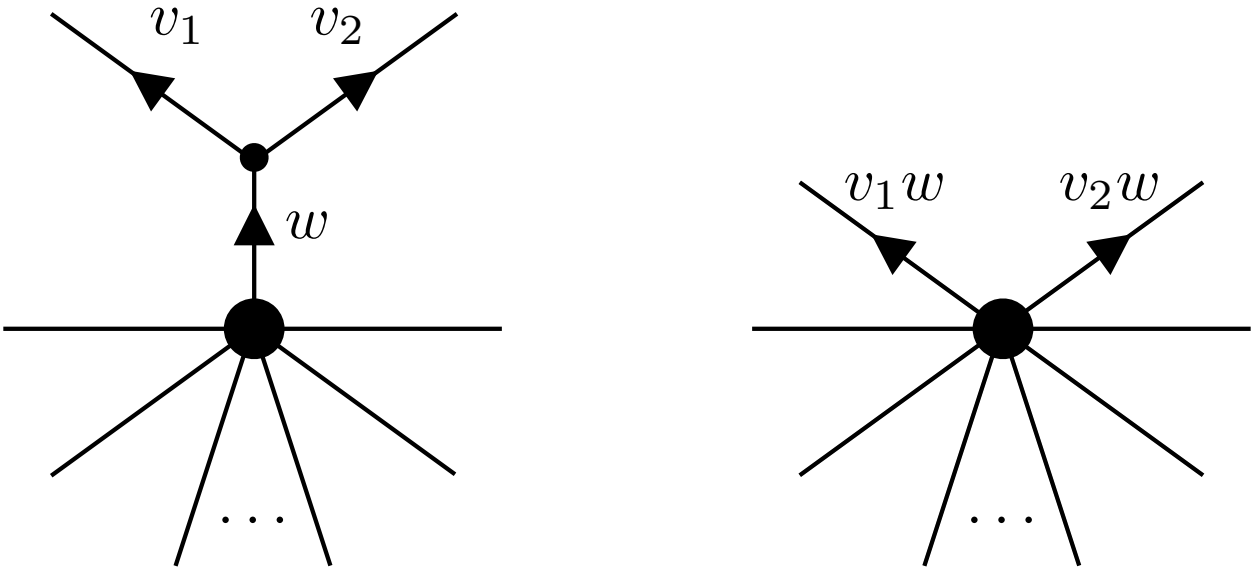


Figure 2.2: (b) shows a vertex in a graph G_{red} that has valency n. (a) shows the graph G obtained by point splitting G_{red}, which has now a vertex of valency $n-1$ and one of valency 3. From the point of view of this dissertation G_{red} is obtained from G using graph coarsening with the trajectories v_1w and v_2w.

The intuition for this is that the links $v_1 w$ and $v_2 w$ in $\mathrm{G}_{\mathrm{red}}$ are pinched at their source to create the link w in G. We will show that these two graphs lead to equivalent theories. In particular, this shows that one can always reduce the valency of vertices on a graph so that no vertex has a valency larger than 3. This is known as point-splitting.

The fact that these two graphs are equivalent is shown as follows. First, the map $\mathcal{E} \to \mathcal{E}_{\mathrm{red}}$ is surjective since v_1 is only traversed by $v_1 w$ and v_2 is only traversed by $v_2 w$. To show that it is injective, suppose that you have two configurations $u \in \mathcal{E}$ that maps to a given $u_{\mathrm{red}} \in \mathcal{E}_{\mathrm{red}}$. Then, consider the gauge transformation at $t(w) = s(v_1) = s(v_2) =: p$ given by

$$g(p) = u(w)^{-1}. \tag{2.162}$$

Then we have that $(gu)(w) = 1$ and furthermore

$$(gu)(v_1) = u(v_1) g(p)^{-1} = u(v_1) u(w) = u(v_1 w) = u_{\mathrm{red}}(v_1 w), \tag{2.163}$$

while

$$(gu)(v_2) = u(v_2) g(p)^{-1} = u(v_2) u(w) = u(v_2 w) = u_{\mathrm{red}}(v_2 w). \tag{2.164}$$

Thus, the configuration gu is completely determined by u_{red} and any configuration mapping to u_{red} will be gauge equivalent to this gu.

Having proven that the graph $\mathrm{G}_{\mathrm{red}}$ and its point-split version G lead to equivalent kinematics, we now show that the dynamics in $\mathrm{G}_{\mathrm{red}}$ can equivalently be expressed in terms of dynamics in G. The Wilson lines $U(v_1 w)$ and $U(v_2 w)$ on $\mathrm{G}_{\mathrm{red}}$ are immediately interpreted as Wilson lines on the trajectories $v_1 w$ and $v_2 w$ on G. On the other hand, the electric operators in the final half-edges of $v_1 w$ and $v_2 w$ in $\mathrm{G}_{\mathrm{red}}$ generate the same transformations on the trajectories $v_1 w$ and $v_2 w$ of G as the electric operators on the final half-edges of v_1 and v_2

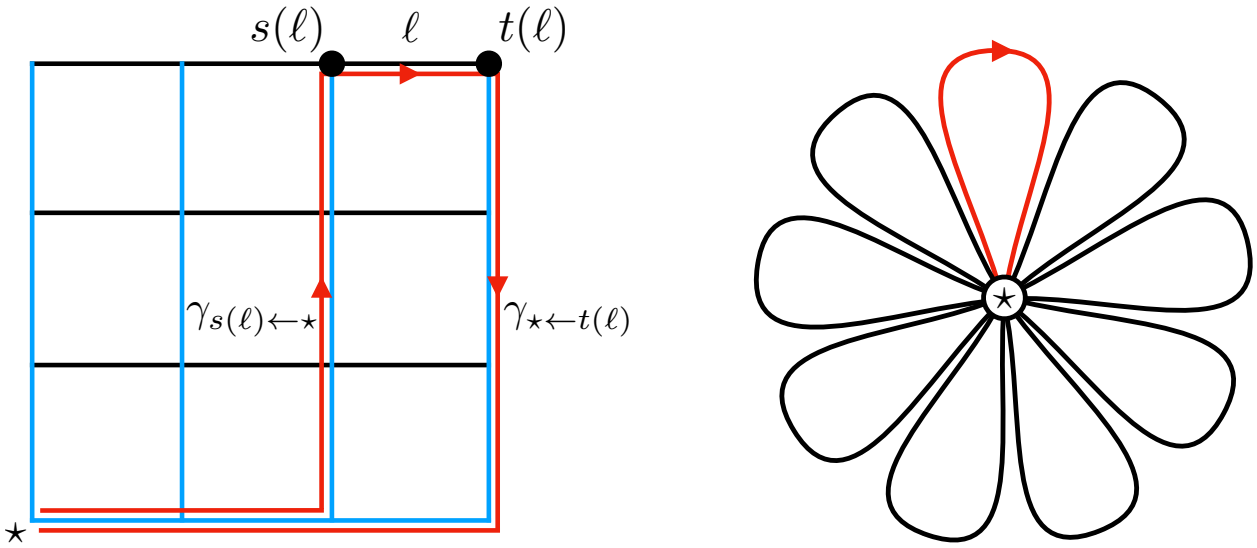
$$u(v_1) \mapsto g u(v_1) \quad \text{and} \quad u(v_2) \mapsto g u(v_2). \tag{2.165}$$

We thus have

$$E(v_1) = E(v_1 w) \quad \text{and} \quad E(v_2) = E(v_2 w), \tag{2.166}$$

where the operators on the left-hand side of the equality live in G while those on the right-hand side live in $\mathrm{G}_{\mathrm{red}}$. Finally, let us split into half-edges $v_1 = (a, b)$ and $v_2 = (c, d)$ on G, and $v_1 w = (a, bw)$ and $v_2 w = (c, dw)$ on $\mathrm{G}_{\mathrm{red}}$. We then have with the same notation

$$E(w^{-1}, b) = E(bw) \quad \text{and} \quad E(w^{-1}, d) = E(dw). \tag{2.167}$$



(a) (b)

Figure 2.3: (a) A maximal tree in a square lattice is shown in blue. We can find labelled one of the links ℓ that is not on the maximal tree, its source $s(\ell)$ and target $t(\ell)$ vertices, and a choice of root $\star$ for the maximal tree. The trajectory γ_ℓ is shown in red. It is explicitly shown in its decomposition $\gamma_{\star\leftarrow t(\ell)\ell\gamma_{s(\ell)\leftarrow\star}}$, with the factors separated by the vertices $s(\ell)$ and $t(\ell)$. (b) The flower obtained by coarse graining the square lattice through the trajectories obtained for each choice of ℓ not within the maximal tree.

2.3.2 Maximal-Tree Gauge Fixing

We now let G be a hypercubic lattice, with a maximal tree T on it and a choice of root vertex $\star$. An example for the case $d = 2$ is shown in Fig. 2.3a. For each link ℓ that is not within this maximal tree, consider the trajectory

$$\gamma_\ell = \gamma_{\star \leftarrow t(\ell)} \ell \gamma_{s(\ell) \leftarrow \star}, \tag{2.168}$$

shown in red in Fig. 2.3a. Let us set T to be the set of such trajectories, and coarse-grain along them. The resulting graph $\mathrm{G}_{\mathrm{red}}$ is shown in Fig. 2.3b, and we will refer to it as a flower.

Surjectivity of the map $\mathcal{E} \to \mathcal{E}_{\mathrm{red}}$ is immediate since for each γ_ℓ the link ℓ is not traversed by any other trajectory in T. In order to show injectivity, we recall that every gauge configuration is equivalent to one that is trivial along the maximal tree, as shown in Section 2.2.2. Furthermore, this can be done without applying a gauge transformation on the root $\star$, so that this procedure leaves invariant the Wilson lines on the trajectories of T, all of which start and at $\star$. In this gauge, we have

$$u(\ell) = u(\gamma_\ell) = u_{\mathrm{red}}(\gamma_\ell), \tag{2.169}$$

so that this configuration is completely determined by u_{red}. In particular, any gauge configuration that leads to the same u_{red} is gauge equivalent to u, completing our proof.

The Kogut-Susskind Hamiltonian (2.85) is defined on G. We will now show that all the operators involved in it can be cast as operators on the flower $\mathrm{G}_{\mathrm{red}}$. The Wilson lines are the easiest. Indeed, the Wilson loop on each plaquette can be cast as a Wilson loop of a composition of trajectories in T. For example, in $d = 2$, for the Wilson lines in the bottom row we simply have $W(\boldsymbol{x}_{12}) = W(\gamma^{-1}_{(\boldsymbol{x}+e_2)_1})$. For the remaining plaquettes we have

$$W(\boldsymbol{x}_{12}) = W(\gamma^{-1}_{(\boldsymbol{x}+e_2)_1} \gamma_{\boldsymbol{x}_1}). \tag{2.170}$$

An example of this trajectory is shown in Fig. 2.4. Note that, in Wilson loops, trajectories that are followed sequentially can be erased, showing why the resulting Wilson loop is equivalent to that of a plaquette.

We now turn to the electric part of the Hamiltonian. We first note that for each edge there is a half-edge h with the property that $\gamma_{\star \leftarrow \pi(h)}$ does not go through h. For the links in the maximal tree, this choice is unique, while for the links that aren't, either half-edge satisfies this property. Let us choose for each edge such a half-edge and denote the set of such half-edges by H_{T}. Note that the electric Hamiltonian can be written as

$$H_E = \frac{g^2}{2} \sum_{h \in H_{\mathrm{T}}} E(h)^2 = \frac{g^2}{2} \sum_{h \in H_{\mathrm{T}}} E(\gamma_{\star \leftarrow \pi(h)}, h)^2 \tag{2.171}$$

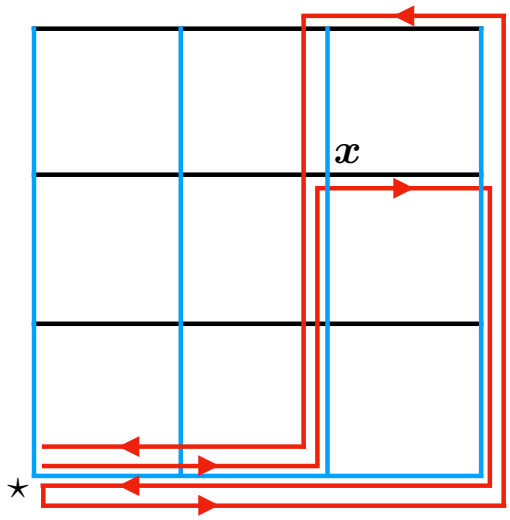


Figure 2.4: The trajectory $\gamma^{-1}_{(\boldsymbol{x}+e_2)_1}\gamma_{\boldsymbol{x}_1}$ is shown, showing that the Wilson loop on it is equivalent to that of the plaquette $\boldsymbol{x}_{12}$.

Fortunately, these parallel transports have a direct interpretation in terms of the flower $\mathrm{G}_{\mathrm{red}}$.

Let us consider a trajectory $\gamma \in T$ that goes through h in the forward direction only, meaning that it can be written as

$$\gamma = \gamma_{\star\leftarrow\pi(h)}(h, \sigma(h))(\cdots), \tag{2.172}$$

where $(\cdots)$ is a trajectory that does not overlap h. Then, the transformation generated by $E(\gamma_{\star\leftarrow\pi(h)}, h)$ on $u(\gamma)$ is the same as the transformation generated by $E(h^{(t)}_\gamma)$. On the other hand, if the trajectory goes through h in the backward direction only, meaning that it can be written as

$$\gamma = (\cdots)(\sigma(h), h)\gamma_{\pi(h)\leftarrow\star}, \tag{2.173}$$

then considering the trajectory γ^{-1} lands us in the same situation as the previous case. We thus conclude that $E(\gamma_{\star\leftarrow\pi(h)}, h)$ generates the same transformation as $E(h^{(s)}_\gamma)$.

The truly novel situation is when the overlap between h and γ happens at two points, one in the forward and one in the backward direction. Then it can be written in the form

$$\gamma = \gamma_{\star\leftarrow\pi(h)}(h, \sigma(h))(\cdots)(\sigma(h), h)\gamma_{\pi(h)\leftarrow\star}, \tag{2.174}$$

with $(\cdots)$ not overlapping with h. Under the transformation generated by $E(\gamma_{\star\leftarrow\pi(h)}, h)$

the Wilson line $u(\gamma)$ is transformed as

$$\begin{aligned} u(\gamma) \mapsto\, & u(\gamma_{\star\leftarrow\pi(h)})u(\gamma_{\pi(h)\leftarrow\star})gu(\gamma_{\star\leftarrow\pi(h)})u(h,\sigma(h))(\cdots) \\ & u(\sigma(h),h)u(\gamma_{\pi(h)\leftarrow\star})g^{-1}u(\gamma_{\star\leftarrow\pi(h)})u(\gamma_{\pi(h)\leftarrow\star}) \\ & = gu(\gamma)g^{-1}. \end{aligned} \tag{2.175}$$

This is the same transformation generated by $E(h_\gamma^{(t)}) + E(h_\gamma^{(s)})$.

Let us then denote by $T_{h\leftarrow}$ the set of trajectories that go through h in the forward direction, and $T_{\leftarrow h}$ the set of trajectories that go through h in the backward direction. We then have

$$E(\gamma_{\star\leftarrow\pi(h)}, h) = \sum_{\gamma\in T_{h\leftarrow}} E(h_\gamma^{(t)}) + \sum_{\gamma\in T_{\leftarrow h}} E(h_\gamma^{(s)}). \tag{2.176}$$

This completes the translation of (2.85) onto the flower

$$\epsilon H = \frac{g^2}{2}\sum_{h\in H_{\mathrm{T}}}\left(\sum_{\gamma\in T_{h\leftarrow}} E(h_\gamma^{(t)}) + \sum_{\gamma\in T_{\leftarrow h}} E(h_\gamma^{(s)})\right)^2 - \frac{2}{g^2}\sum_{\boldsymbol{x}_{ij}\in\mathcal{P}} \mathrm{Re}\, W(\boldsymbol{x}_{ij}), \tag{2.177}$$

where on the magnetic part $\boldsymbol{x}_{ij}$ should be interpreted as a trajectory on the flower that gives rise to the same Wilson loop as $\boldsymbol{x}_{ij}$.

2.3.3 Plaquette Flower

In $d = 2$, there is a slight modification that makes the magnetic term of (2.177) even simpler. If one uses the loops T' considered in [94] instead, the graph $\mathrm{G}'_{\mathrm{red}}$ is still given by a flower. But now to each plaquette $\boldsymbol{x}_{12}$ there is a single link in $\mathrm{G}'_{\mathrm{red}}$, which we will denote by $\boldsymbol{x}_{12}$ as well, that has the same Wilson loop. We show such a loop in Fig. 2.5. Furthermore, the translation of the electric Hamiltonian works in exactly the same manner, so that the complete Hamiltonian is still given by (2.177). Thus, we need only convince ourselves that in this construction the flower $\mathrm{G}'_{\mathrm{red}}$ is still kinematically equivalent to G.

In order to show surjectivity of the map $\mathcal{E} \to \mathcal{E}_{\mathrm{red}}$, we can no longer use the technique we have used so far. The issue is that for each loop in T we no longer have a link that is only traversed by it. Instead, to show the equivalence of the map (2.138), we will show that the plaquette flower $\mathrm{G}'_{\mathrm{red}}$ is equivalent to the flower $\mathrm{G}_{\mathrm{red}}$ we constructed in the previous section. But this is obvious once one notes that the Wilson line in Fig. 2.5 is precisely the Wilson line in Fig. 2.4, yielding a map $\mathcal{E}_{\mathrm{red}} \to \mathcal{E}'_{\mathrm{red}}$, where the latter is the set of configurations in the plaquette flower $\mathrm{G}'_{\mathrm{red}}$. The inverse of this map is shown in Fig. 2.6.

A key insight in [94] comes from the fact that at weak coupling the links should be dominated by Wilson lines near the identity. Then, expanding

$$U((h,\sigma(h))) = 1 + \mathcal{O}(g), \tag{2.178}$$

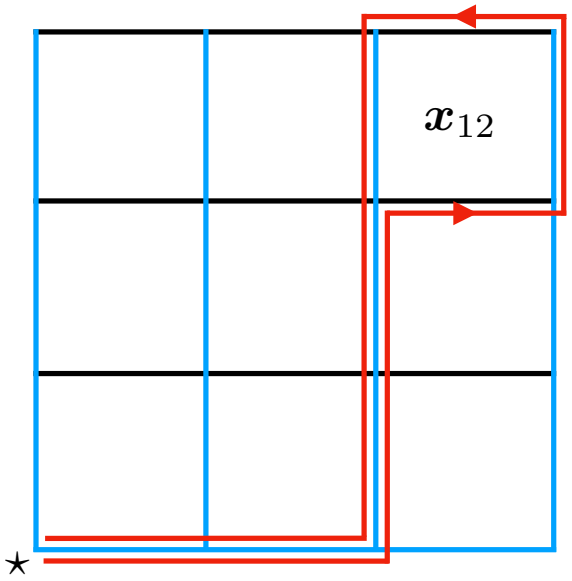


Figure 2.5: Generic loop in the construction leading to a flower whose links correspond to plaquettes.

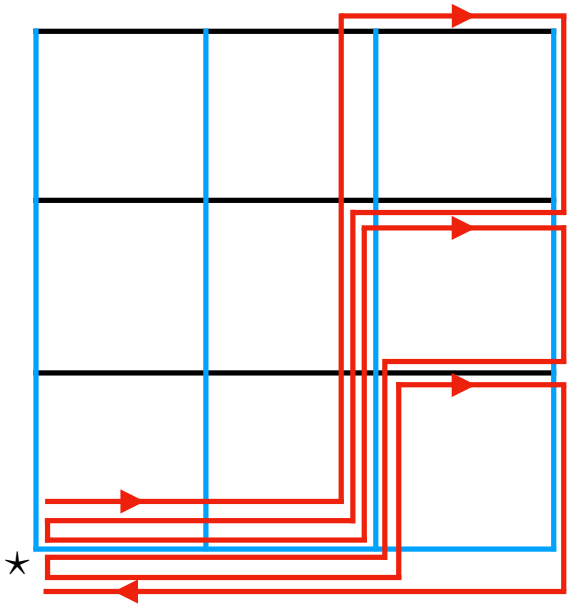


Figure 2.6: Trajectory built out of trajectories in T' with the same Wilson line as the trajectory shown in Fig. 2.3a.

one can, to lowest order in the coupling, set $E(\gamma) = E(h_\gamma^{(t)}) = -E(h_\gamma^{(s)})$ using (2.161). Thus, in a link based notation, the Hamiltonian (2.177) can be expanded as

$$\epsilon H = \frac{g^2}{2} \sum_{h \in H_{\mathrm{T}}} \left(\sum_{\gamma \in T_{h\leftarrow}} E(\gamma) - \sum_{\gamma \in T_{\leftarrow h}} E(\gamma) \right)^2 - \frac{2}{g^2} \sum_{\boldsymbol{x}_{12} \in \mathcal{P}} \mathrm{Re}\, W(\boldsymbol{x}_{12}) + \mathcal{O}(g^3). \tag{2.179}$$

In particular, trajectories γ that go through a link h in both the forward and backward direction no longer contribute. And for any given link $h \in H_T$, the only trajectories in T' that go through it only once are those associated to the plaquettes that h belongs to, each going in opposite directions. Thus, to lowest order in g, manifest locality of the theory is recovered.

Explicitly, this leaves us with the Hamiltonian

$$\epsilon H = \frac{g^2}{2} \sum_{\langle \boldsymbol{x}_{12}, \boldsymbol{y}_{12} \rangle} \left(E(\boldsymbol{x}_{12}) - E(\boldsymbol{y}_{12}) \right)^2 - \frac{2}{g^2} \sum_{\boldsymbol{x}_{ij} \in \mathcal{P}} \mathrm{Re}\, W(\boldsymbol{x}_{ij}) + \mathcal{O}(g^3). \tag{2.180}$$

The first sum goes over each pair of neighboring plaquettes, with the convention that each plaquette has exactly four neighbors. For plaquettes $\boldsymbol{x}_{12}$ at the boundary that do not actually have a neighboring $\boldsymbol{y}_{12}$ in one of the directions, we simply set $E(\boldsymbol{y}_{12}) = 0$. Alternatively, this Hamiltonian can be written as

$$\begin{aligned} \epsilon H = {} & 2g^2 \sum_{\boldsymbol{x}_{12} \in \mathcal{P}} E(\boldsymbol{x}_{12})^2 - g^2 \sum_{\langle \boldsymbol{x}_{12}, \boldsymbol{y}_{12} \rangle} \langle E(\boldsymbol{x}_{12}), E(\boldsymbol{y}_{12}) \rangle \\ & - \frac{2}{g^2} \sum_{\boldsymbol{x}_{12} \in \mathcal{P}} \mathrm{Re}\, W(\boldsymbol{x}_{12}) + \mathcal{O}(g^3), \end{aligned} \tag{2.181}$$

leading to a Hamiltonian of a G-spin model.

2.3.4 Branch

The main focus of this chapter will be in the graphs G like the one shown in figure Fig. 2.7. We will call these branches, and they were first considered in [94] through different methods. They are composed by P leaves, indexed $i = 1, \ldots, P$ from left to right. The structure of the i-th leaf is shown in Fig. 2.8. This graph has a unique maximal tree T. Given a choice of root $\star$, for each leaf i we consider a trajectory $\gamma_i = \gamma_{\star \leftarrow p_i} \ell_i \gamma_{p_i \leftarrow \star}$, where $\ell_i := (r_i, l_i)$. Denoting by T the set of all such trajectories, the resulting reduced graph $\mathrm{G}_{\mathrm{red}}$ is exactly a flower of P petals, as shown in Fig. 2.3b. Given that this is another maximal tree construction, the kinematic equivalence between the branch and the flower is established following the same line of argument.

One can consider this branch as a point-split version of the flower. The justification for it is that all of its vertices are, at most, 3-valent. As explained in Section 2.1.4, gauge

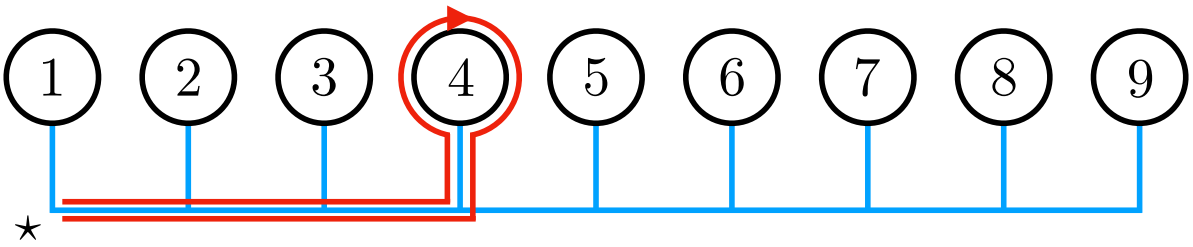


Figure 2.7: Branch G with $P = 9$ leaves. Its maximal tree highlighted in blue. In red is shown an example γ_4 of the trajectories in T for which the coarse-graining procedure leaves to a flower $\mathrm{G}_{\mathrm{red}}$ as the one shown in Fig. 2.3b.

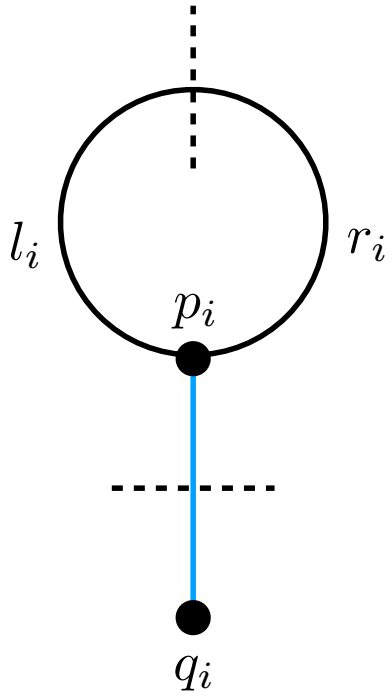


Figure 2.8: i-th leaf of a branch.

invariant states are built from invariants living inside the tensor product of the irreducibles at each half-edge attached to the vertex. Having smaller valency vertices, as opposed to the vertex of valency $2P$ in the flower, greatly simplifies the process of finding these invariants in electric bases.

Dynamically, we now need to translate the operators appearing in the Hamiltonian (2.177) to the operators available in the branch. This can be done both through the maximal tree flower discussed in Section 2.3.2, or through the plaquette flower discussed in Section 2.3.3. In the latter, the magnetic terms are all the Wilson loops on trajectories γ_i, which can be reduced to

$$W(\gamma_i) = W(\ell_i). \tag{2.182}$$

In the former, we have the additional complication of non-local magnetic terms which can be reduced to

$$W(\gamma_i^{-1}\gamma_j) = W(\gamma_{p_j \leftarrow p_i}\ell_i^{-1}\gamma_{p_i \leftarrow p_j}\ell_j) \tag{2.183}$$

An example of such a trajectory is shown in Fig. 2.9.

As for the electric operators, given that each γ_i bases through ℓ_i in the forward direction, and this is the only trajectory that overlaps with this half-edge, we immediately have

$$E(h^{(t)}_{\gamma_i}) = E(\gamma_{\star \leftarrow p_i}, r_i) \quad \text{and} \quad E(h^{(s)}_{\gamma_i}) = E(\gamma_{\star \leftarrow p_i}, l_i). \tag{2.184}$$

For the terms of the form $E(h^{(t)}_{\gamma_i})^2$ and $E(h^{(s)}_{\gamma_i})^2$ we can immediately replace them by their versions without parallel transport $E(r_i)^2$ and $E(l_i)^2$. The remaining terms will be of the form

$$\begin{aligned} &\langle E(\gamma_{\star \leftarrow p_i}, h_i), E(\gamma_{\star \leftarrow p_j}, h_j)\rangle \\ &= \langle U(\gamma_{\star \leftarrow p_i})E(h_i)U(\gamma_{p_i \leftarrow \star}), U(\gamma_{\star \leftarrow p_j})E(h_j)U(\gamma_{p_j \leftarrow \star})\rangle \,, \end{aligned} \tag{2.185}$$

where $h_i \in \{l_i, r_i\}$ and $h_j \in \{l_j, r_j\}$. Taking advantage of the invariance of the inner product, this can be reordered to

$$\begin{aligned} &\langle E(\gamma_{\star \leftarrow p_i}, h_i), E(\gamma_{\star \leftarrow p_j}, h_j)\rangle \\ &= \langle E(h_i), U(\gamma_{p_i \leftarrow p_j})E(h_j)U(\gamma_{p_j \leftarrow p_i})\rangle \,, \end{aligned} \tag{2.186}$$

Note that the resulting dynamics are independent of the choice of root $\star$ for the mapping to the flower. Moreover, for $d = 2$, in the plaquette flower interpretation, each leaf in the branch truly corresponds to a plaquette of the lattice. It can therefore be interpreted as a one-dimensional tensor network interweaving space, as shown in Fig. 2.10.

2.4 Loop-String-Hadron Formulation on General Graphs

The Loop-String-Hadron (LSH) formulation is a powerful way of constructing the invariant states (2.123), first developed for SU(2) in [95, 96], and currently in development for SU(3)

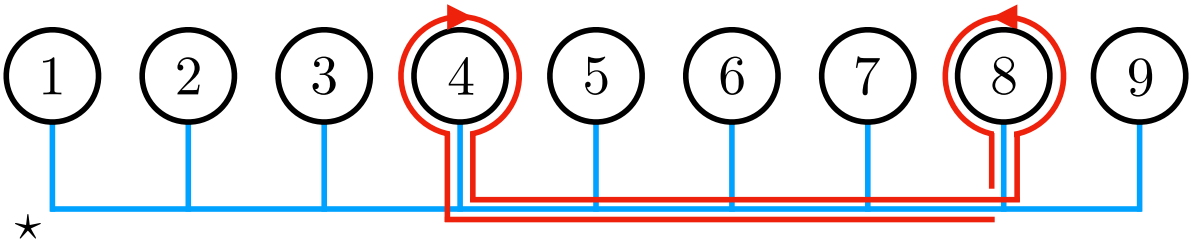


Figure 2.9: Trajectory $\gamma_{p_4 \leftarrow p_8} \ell_8^{-1} \gamma_{p_8 \leftarrow p_4} \ell_4$ carrying the same Wilson loop as $\gamma_8^{-1} \gamma_4$.

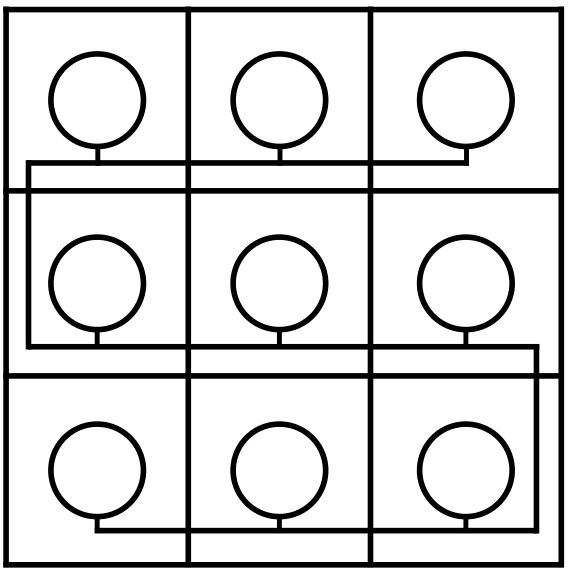


Figure 2.10: Embedding of a branch in a $d = 2$ lattice compatible with the plaquette flower construction.

[101, 102]. In this section we will explain it in the context of general graphs and for the group $G = \mathrm{SU}(2)$. Indeed, our ultimate goal will be, rather to apply it to hypercubic graphs, or their point-split versions as is most common in the literature, to apply it to branches. By applying the construction of an electric basis on a graph that is well-adapted to the study of small g physics, this builds a particularly exciting formulation for the study of weak coupling physics on digital quantum computers.

Before we start, we should however mention that the full importance of the LSH formulation is only realized in the presence of matter, in which string and hadron operators appear. Our main interest will however be on $G = \mathrm{SU}(2)$ Yang-Mills theory in the absence of matter. Most of the aspects of the LSH formulation that pertain the Yang-Mills sector were developed as part of prepotential formulation [155–158]. We will however continue referring to this as the LSH formulation since this terminology is more common nowadays.

2.4.1 Loop-String-Hadron on Half-Edges

We first restrict to a single half-edge h, which following Section 2.1.4 carries the Hilbert space

$$\mathcal{H} = \bigoplus_{j\in\mathbb{N}/2} V_j, \tag{2.187}$$

where $V_j = \mathrm{Span}\{\, |j,m\rangle \mid m = -j, \dots, j \,\}$ is the Hilbert space of spin j. The LSH formulation is based on the understanding of this space in terms of Schwinger bosons [159] a^A and $a^\dagger_A = (a^A)^\dagger$, with $A = 1, 2$. These satisfy the canonical commutation relations

$$[a^A, a^\dagger_B] = \delta^A_B. \tag{2.188}$$

With these we can build SU(2) generators

$$-\frac{i}{2}\langle E, \boldsymbol{\sigma}\rangle = \boldsymbol{E} = \frac{1}{2} a^\dagger_A \boldsymbol{\sigma}^A{}_B a^B, \tag{2.189}$$

where $\boldsymbol{\sigma} = (\sigma_x, \sigma_y, \sigma_z)$ is the vector of Pauli matrices. Indeed, these satisfy the commutation relations of $\mathfrak{su}(2)$

$$[E_a, E_b] = a^\dagger_A \left[\frac{1}{2}\sigma_a, \frac{1}{2}\sigma_b\right]^A_B a^B = i\epsilon_{ab}{}^c E_c. \tag{2.190}$$

Under these we have

$$[E_a, a^A] = -\frac{1}{2}\sigma^A{}_B a^B \quad \text{and} \quad [E_a, a^\dagger_A] = \frac{1}{2} a^\dagger_B \sigma^B{}_A. \tag{2.191}$$

We thus see that upper indices transform in the spin-$\frac{1}{2}$ representation, while the lower indices in its conjugate. By the completeness relation of the Pauli matrices, the $\mathfrak{su}(2)$-valued operator is given by

$$E = -\frac{i}{2}\boldsymbol{E}\cdot\boldsymbol{\sigma}. \tag{2.192}$$

The components of this operator can be computed by using the relation

$$\boldsymbol{\sigma}^A{}_B\cdot\boldsymbol{\sigma}^C{}_D = 2\delta^A_D\delta^C_B - \delta^A_B\delta^C_D. \tag{2.193}$$

We then have

$$\begin{aligned} E^A{}_B &= -\frac{i}{2}\frac{1}{2}a^\dagger_C a^D(2\delta^A_D\delta^C_B - \delta^A_B\delta^C_D) = -\frac{i}{2}a^\dagger_B a^A + \frac{i}{4}N\delta^A_B \\ &= -\frac{i}{2}a^A a^\dagger_B + \frac{i}{2}\Big(\frac{N}{2}+1\Big)\delta^A{}_B, \end{aligned} \tag{2.194}$$

in terms of the number operator

$$N = a^\dagger_A a^A. \tag{2.195}$$

This operator satisfies

$$E^2 = -2E^A{}_B E^B{}_A = \frac{N}{2}\Big(\frac{N}{2}+1\Big). \tag{2.196}$$

The number operator N is invariant under SU(2). Thus, the Hilbert space generated by the action of these bosons on the Schwinger vacuum $|0\rangle$, defined by $a^A|0\rangle = 0$, splits into subrepresentations with a well-defined number of bosons n. Such a subrepresentation has dimension $n+1$. Thus, one can guess it is the spin $j = n/2$ representation. Indeed, the identification

$$|j,m\rangle = \frac{(a^\dagger_1)^{j+m}(a^\dagger_2)^{j-m}}{\sqrt{(j+m)!(j-m)!}}|0\rangle, \tag{2.197}$$

expresses the (2.187) Hilbert space as the Hilbert space generated by these Schwinger bosons. This is seen by noting that

$$E_+ = a^\dagger_1 a^2, \quad E_- = a^\dagger_2 a^1, \quad \text{and} \quad E_3 = \frac{1}{2}(a^\dagger_1 a^1 - a^\dagger_2 a_2), \tag{2.198}$$

so that indeed

$$\begin{aligned} E_+|j,m\rangle &= \sqrt{(j+m+1)(j-m)}\,|j,m+1\rangle, \\ E_-|j,m\rangle &= \sqrt{(j+m)(j-m+1)}\,|j,m-1\rangle, \\ E_3|j,m\rangle &= m|j,m\rangle. \end{aligned} \tag{2.199}$$

The operator N therefore keeps track of which representation we are in.

On top of this, the Schwinger Boson Hilbert space also carries a U(1) representation

$$a^\dagger_A \mapsto e^{-i\theta} a^\dagger_A \quad \text{and} \quad a^A \mapsto e^{i\theta} a^A. \tag{2.200}$$

The number operator is also invariant under this action and thus, the Hilbert space splits into subrepresentations of U(1). Indeed, being mediated by the same operator N, this split coincides with that of SU(2), so that V_j transforms in the representation of charge $n = 2j$

$$|j, m\rangle \mapsto e^{-in\theta} |j, m\rangle . \tag{2.201}$$

The representations of SU(2) are self-dual. Indeed, we have the invariant tensor

$$\epsilon_{AB} = \begin{pmatrix} 0 & 1 \\ -1 & 0 \end{pmatrix}_{AB} \tag{2.202}$$

with which we lower indices

$$\psi_A := \epsilon_{AB} \psi^B, \tag{2.203}$$

transforming a spin-$\frac{1}{2}$ index into its dual. This is in light of the identity

$$\epsilon_{AB} \boldsymbol{\sigma}^B{}_C = -\boldsymbol{\sigma}^B{}_A \epsilon_{BC}. \tag{2.204}$$

Similarly, indices can be raised using the inverse $\epsilon^{AB} = -\epsilon_{AB}$. Since we are raising and lowering indices with an antisymmetric tensor, we need to fix a convention with which to contract upper and lower indices

$$\psi\phi := \psi_A \phi^A = \psi_A \epsilon^{AB} \phi_B. \tag{2.205}$$

In order to keep track simultaneously of the transformation properties under SU(2) and U(1) it is useful to pack into the same object all the creation and annihilation operators

$$A^\mu{}_A = \begin{cases} a^\dagger_A & \mu = +, \\ a_A & \mu = -, \end{cases} = \begin{pmatrix} a^\dagger_1 & a^\dagger_2 \\ a^2 & -a^1 \end{pmatrix}^\mu{}_A . \tag{2.206}$$

The index μ keeps track of the charge of the operator under U(1), while the placement of A keeps track of which representation of SU(2) we are in. More precisely, the U(1) representation is generated by the charge operator

$$Q^\mu{}_\nu = \begin{pmatrix} 1 & 0 \\ 0 & -1 \end{pmatrix}^\mu{}_\nu = \mu \delta^\mu_\nu. \tag{2.207}$$

Whenever $\mu = \nu$, these operators commute. More generally, we can write the commutation relations of this operator in the form

$$[A^\mu{}_A, A^\nu{}_B] = g^{\mu\nu} \epsilon_{AB}, \tag{2.208}$$

where

$$g^{\mu\nu} = \begin{pmatrix} 0 & 1 \\ 1 & 0 \end{pmatrix}^{\mu\nu}. \tag{2.209}$$

We will use this metric to raise and lower U(1) indices. Note that a μ in the lower index has the opposite meaning as in the upper index, as shown by the examples

$$Q_\mu{}^\nu = \begin{pmatrix} -1 & 0 \\ 0 & 1 \end{pmatrix}_\mu^{\ \nu} = -Q^\nu{}_\mu \quad \text{and} \quad A_\mu{}^A = \begin{pmatrix} a^1 & a^2 \\ -a_2^\dagger & a_1^\dagger \end{pmatrix}_\mu^{\ A}. \tag{2.210}$$

We can also define the conjugate operator

$$(A^\dagger)^A{}_\mu = (A^\mu{}_A)^\dagger = \begin{pmatrix} a^1 & a_2^\dagger \\ a^2 & -a_1^\dagger \end{pmatrix}_\mu^{\ A} = Q^\nu{}_\mu A_\nu{}^A. \tag{2.211}$$

This satisfies

$$[(A^\dagger)^A{}_\mu, A^\nu{}_B] = Q^\nu{}_\mu \delta_B^A \quad \text{and} \quad [(A^\dagger)^A{}_\mu, (A^\dagger)^B{}_\nu] = g_{\mu\nu}\epsilon^{AB} \tag{2.212}$$

In terms of it we have

$$(A^\dagger)^A{}_\mu A^\mu{}_B = (N+1)\delta_B^A. \tag{2.213}$$

This suggests the following definition for a Wilson line operator on a half-edge

$$U^\mu{}_A = A^\mu{}_A \frac{1}{\sqrt{N+1}}. \tag{2.214}$$

Then, defining $(U^\dagger)^A{}_\mu = (U^\mu{}_A)^\dagger$, we immediately have the unitarity condition

$$(U^\dagger)^A{}_\mu U^\mu{}_B = \delta_B^A. \tag{2.215}$$

On the other hand, we have

$$A^\mu{}_A (A^\dagger)^A{}_\nu = (N+1-Q)^\mu{}_\nu. \tag{2.216}$$

Therefore, we also obtain the unitarity condition

$$U^\mu{}_A (U^\dagger)^A{}_\nu = A^\mu{}_A \frac{1}{N+1} (A^\dagger)^A{}_\nu = \left(\frac{1}{N+1-Q}\right)_\rho^{\ \mu} A^\rho{}_A (A^\dagger)^A{}_\nu = \delta_\nu^\mu, \tag{2.217}$$

justifying our notation. In here we have used the identity

$$A^\mu{}_A f(N) = f(N-Q)^\mu{}_\nu A^\nu{}_A \tag{2.218}$$

Note that this identity is simple to implement since the operator Q is diagonal so that

$$f(N-Q)^\mu{}_\nu = f(N-\mu)\delta_\nu^\mu. \tag{2.219}$$

2.4.2 Loop-String-Hadron on Corners

Next, we consider a pair of half-edges h_1 and h_2 forming a corner at $p = \pi(h_1) = \pi(h_2)$. The Schwinger boson construction immediately yields operators on this corner that are invariant under gauge transformations

$$\begin{aligned}\mathcal{L}^{\mu}{}_{\nu}(h_1, h_2) &= A^{\mu}{}_{A}(h_1)(A^{\dagger})^{A}{}_{\nu}(h_2) \\ &= \begin{pmatrix} a_1^{\dagger}(h_1)a^1(h_2) + a_2^{\dagger}(h_1)a^2(h_2) & a_1^{\dagger}(h_1)a_2^{\dagger}(h_2) - a_2^{\dagger}(h_1)a_1^{\dagger}(h_2) \\ a^2(h_1)a^1(h_2) - a^1(h_1)a^2(h_2) & a^2(h_1)a_2^{\dagger}(h_2) + a^1(h_1)a_1^{\dagger}(h_2) \end{pmatrix}^{\mu}_{\ \nu}\end{aligned} \tag{2.220}$$

These operators coincide, up to a sign associated to the charge, with the ones found in [96], and up to a charge matrix with the ones in [100]. We will call them the LSH loop operators. And in the degenerate case we recover (2.216)

$$\mathcal{L}^{\mu}{}_{\nu}(h, h) = (N(h) + 1 - Q)^{\mu}{}_{\nu}. \tag{2.221}$$

Under a change of orientation we have

$$\mathcal{L}^{\mu}{}_{\nu}(h_1, h_2) = Q^{\mu}{}_{\sigma} Q^{\rho}{}_{\nu} \mathcal{L}_{\rho}{}^{\sigma}(h_2, h_1) = \mu\nu \mathcal{L}_{\nu}{}^{\mu}(h_2, h_1). \tag{2.222}$$

Moreover, if we assume $h_1 \neq h_2$, we have

$$[\mathcal{L}^{\mu}{}_{\nu}(h_1, h_2), \mathcal{L}^{\rho}{}_{\sigma}(h_2, h_1)] = Q^{\rho}{}_{\nu}(N(h_1) + 1)\delta^{\mu}_{\sigma} - Q^{\mu}{}_{\sigma}(N(h_2) + 1)\delta^{\rho}_{\nu}. \tag{2.223}$$

This determines the algebra of these operators on a single corner.

Now, let us consider a third half-edge h_3 at the same vertex $p = \pi(h_3)$, and assume all the half-edges h_1, h_2, and h_3, are different. Then we have the commutator

$$[\mathcal{L}^{\mu}{}_{\nu}(h_1, h_2), \mathcal{L}^{\rho}{}_{\sigma}(h_2, h_3)] = Q^{\rho}{}_{\nu} \mathcal{L}^{\mu}{}_{\sigma}(h_1, h_3). \tag{2.224}$$

This determines the algebra of these operators on an overlapping pair of corners.

Finally, we define the Wilson corners, as rescaled versions of these operators

$$\begin{aligned} U^{\mu}{}_{\nu}(h_1, h_2) &= U^{\mu}{}_{A}(h_1)(U^{\dagger})^{A}{}_{\nu}(h_2) \\ &= \frac{1}{\sqrt{N(h_2) + 1}} \mathcal{L}^{\mu}{}_{\nu}(h_1, h_2) \frac{1}{\sqrt{N(h_1) + 1}}. \end{aligned} \tag{2.225}$$

These are known as vertex factors in [96]. Note that, unlike link Wilson lines, these have U(1) indices instead of SU(2) symmetry. They are in particular automatically invariant under the action of SU(2) at p.

2.4.3 Loop-String-Hadron on Links

Now, we consider a link (h_1, h_2). We want to define a Wilson link operator $U^A{}_B$. If we do it through contraction of $(U^\dagger)^A{}_\mu(h_1)$ and $U^\nu{}_B(h_2)$, this will automatically transform in the correct SU(2) representation. However, direction contraction of the indices μ and ν would produce an operator preserving $N(h_1) + N(h_2)$. The Abelian Gauss law instead requires the $N(h_1) - N(h_2)$ is preserved, so that the resulting Wilson line preserves the condition $N(h_1) = N(h_2)$. We thus need to introduce an off-diagonal matrix $t^\mu{}_\nu(h_1, h_2)$ in order to have

$$U^A{}_B = (U^\dagger)^A{}_\mu(h_1) t^\mu{}_\nu U^\nu{}_B(h_2) \tag{2.226}$$

satisfy the Abelian Gauss law as well.

Before determining this matrix $t^\mu{}_\nu$, we note that any choice will lead to an operator $U^A{}_B$ in which all components automatically commute on the subspace that satisfies the Abelian Gauss law. This is most simply seen by separating the creation and annihilation parts of the Wilson line operator

$$\begin{aligned} U^{(+)A}{}_B &= (U^\dagger)^A{}_-(h_1) U^+{}_B(h_2), \\ U^{(-)A}{}_B &= (U^\dagger)^A{}_+(h_1) U^-{}_B(h_2), \end{aligned} \tag{2.227}$$

in terms of which we have

$$U^A{}_B = t^-{}_+ U^{(+)A}{}_B + t^+{}_- U^{(-)A}{}_B. \tag{2.228}$$

Therefore, we wish to show that

$$\begin{aligned} & U^A{}_B U^C{}_D - U^C{}_D U^A{}_B \\ &= (t^-{}_+)^2 \big(U^{(+)A}{}_B U^{(+)C}{}_D - U^{(+)C}{}_D U^{(+)A}{}_B \big) \\ &+ (t^+{}_-)^2 \big(U^{(-)A}{}_B U^{(-)C}{}_D - U^{(-)C}{}_D U^{(-)A}{}_B \big) \\ &+ t^+{}_- t^-{}_+ \big(U^{(+)A}{}_B U^{(-)C}{}_D - U^{(+)C}{}_D U^{(-)A}{}_B \big) \\ &+ t^+{}_- t^-{}_+ \big(U^{(-)A}{}_B U^{(+)C}{}_D - U^{(-)C}{}_D U^{(+)A}{}_B \big) \end{aligned} \tag{2.229}$$

vanishes.

Since this is to be true regardless of our choice of matrix $t^\mu{}_\nu$, we need to show that the terms proportional to $(t^-{}_+)^2$, $(t^+{}_-)^2$, and $t^+{}_- t^-{}_+$ vanish separately. The first two are the simplest since they are solely composed by creation or annihilation operators, without mixture. For example,

$$\begin{aligned} U^{(+)A}{}_B U^{(+)C}{}_D =& \frac{1}{\sqrt{N(h_1)+1}} (A^\dagger)^A{}_-(h_1) A^+{}_B(h_2) \frac{1}{\sqrt{N(h_2)+1}} \\ & \frac{1}{\sqrt{N(h_1)+1}} (A^\dagger)^C{}_-(h_1) A^+{}_D(h_2) \frac{1}{\sqrt{N(h_2)+1}}. \end{aligned} \tag{2.230}$$

When moving the block $(A^\dagger)^A{}_-(h_1)A^+{}_B(h_2)$ we must shift the intermediate $N(h_1) \mapsto N(h_1) - 1$ and $N(h_2) \mapsto N(h_2) - 1$. This block is then left multiplying the block $(A^\dagger)^C{}_-(h_1)A^+{}_D(h_2)$. The two blocks immediately commute since they are solely built out of creation operators. Finally, when moving the block $(A^\dagger)^C{}_-(h_1)A^+{}_D(h_2)$, the shifts in the number operators become undone. This shows that the term proportional to $(t^-{}_+)^2$ vanishes, and a similar argument does the same for the term proportional to $(t^+{}_-)^2$.

We thus now turn our attention to the terms proportional to $t^+{}_-t^-{}_+$. Our plan will be to compute simultaneously the third and fourth lines of (2.229) and show that they cancel each other. The terms in both of these lines have the form

$$\begin{aligned}
&U^{(\mu)A}{}_B U^{(\nu)C}{}_D - (A \leftrightarrow C, B \leftrightarrow D) = \\
&\frac{1}{\sqrt{N(h_1)+1}}(A^\dagger)^A{}_\nu(h_1)A^\mu{}_B(h_2)\frac{1}{\sqrt{N(h_2)+1}}\times \\
&\frac{1}{\sqrt{N(h_1)+1}}(A^\dagger)^C{}_\mu(h_1)A^\nu{}_D(h_2)\frac{1}{\sqrt{N(h_2)+1}}- \\
&(A \leftrightarrow C, B \leftrightarrow D) = \\
&\frac{1}{\sqrt{(N(h_1)+1)(N(h_2)+1-\mu)(N(h_1)+1+\nu)(N(h_2)+1)}}\times \\
&(A^\dagger)^A{}_\nu(h_1)(A^\dagger)^C{}_\mu(h_1)A^\mu{}_B(h_2)A^\nu{}_D(h_2)- \\
&(A \leftrightarrow C, B \leftrightarrow D),
\end{aligned} \tag{2.231}$$

with $\mu \neq \nu$. This double antisymmetrization can be made effective by noting that by virtue of the fact that the SU(2) indices only take two values, the antisymmetric part of any two index tensor is proportional to ϵ^{AB}. We therefore have the decompositions

$$(A^\dagger)^A{}_\nu(A^\dagger)^C{}_\mu = \frac{1}{2}(\epsilon^{AC}\mathcal{A}_{(\mu\nu)} + \mathcal{S}^{AC}_{(\mu\nu)}) \tag{2.232}$$

and

$$A^\mu{}_B A^\nu{}_D = \frac{1}{2}(\epsilon_{BD}\mathcal{A}^{(\mu\nu)} + \mathcal{S}^{(\mu\nu)}_{BD}), \tag{2.233}$$

uniquely determined by the requirement that $S^{AC}_{(\mu\nu)}$ and $S^{(\mu\nu)}_{BD}$ are symmetric under the exchanges $A \leftrightarrow C$ and $B \leftrightarrow D$, respectively. In terms of this decomposition we have

$$\begin{aligned}
&U^{(\mu)A}{}_B U^{(\nu)C}{}_D - (A \leftrightarrow C, B \leftrightarrow D) = \\
&\frac{1}{2\sqrt{(N(h_1)+1)(N(h_2)+1-\mu)(N(h_1)+1+\nu)(N(h_2)+1)}}\times \\
&\Big(\epsilon^{AC}\mathcal{A}_{(\mu\nu)}(h_1)\mathcal{S}^{(\mu\nu)}_{BD}(h_2) + \epsilon_{BD}\mathcal{S}^{AC}_{(\mu\nu)}(h_1)\mathcal{A}^{(\mu\nu)}(h_2)\Big).
\end{aligned} \tag{2.234}$$

We are left with the computation of these symmetric and antisymmetric tensors. Beginning with the antisymmetric

$$\begin{aligned}
\mathcal{A}_{(+-)} &= (A^\dagger)^2{}_-(A^\dagger)^1{}_+ - (A^\dagger)^1{}_-(A^\dagger)^2{}_+ = -N,\\
\mathcal{A}_{(-+)} &= (A^\dagger)^2{}_+(A^\dagger)^1{}_- - (A^\dagger)^1{}_+(A^\dagger)^2{}_- = N+2,\\
\mathcal{A}^{(+-)} &= A^+{}_1A^-{}_2 - A^+{}_2A^-{}_1 = -N,\\
\mathcal{A}^{(-+)} &= A^-{}_1A^+{}_2 - A^-{}_2A^+{}_1 = N+2.
\end{aligned} \tag{2.235}$$

This can be summarized to

$$\mathcal{A}^{(\mu\nu)} = \mathcal{A}_{(\mu\nu)} = \nu(N+1+\nu). \tag{2.236}$$

In particular, on the subspace that satisfies the Abelian Gauss law $N(h_1) = N(h_2)$, we conclude that

$$\begin{aligned}
&U^{(\mu)A}{}_B U^{(\nu)C}{}_D - (A \leftrightarrow C, B \leftrightarrow D) =\\
&\frac{\nu}{2\sqrt{(N(h_1)+1)(N(h_2)+1)}}\Big(\epsilon^{AC}\mathcal{S}^{(\mu\nu)}_{BD}(h_2) + \epsilon_{BD}\mathcal{S}^{AC}_{(\mu\nu)}(h_1)\Big).
\end{aligned} \tag{2.237}$$

The appearance of the prefactor ν clarifies the cancellation of the third and fourth lines of (2.229). The proof is therefore complete if we manage to show

$$S^{AB}_{(\mu\nu)} = S^{AB}_{(\nu\mu)} \quad \text{and} \quad S^{(\mu\nu)}_{AB} = S^{(\nu\mu)}_{AB}. \tag{2.238}$$

For example, we have

$$S^{(\mu\nu)}_{AB} = A^\mu{}_A A^\nu{}_B + A^\mu{}_B A^\nu{}_A = g^{\mu\nu}\epsilon_{AB} + g^{\mu\nu}\epsilon_{BA} + S^{(\nu\mu)}_{AB} = S^{(\nu\mu)}_{AB}. \tag{2.239}$$

This thus completes our proof that $U^A{}_B U^C{}_D = U^C{}_D U^A{}_B$.

With this in hand, we now determine the matrix $t^\mu{}_\nu$. Since the components of $U^A{}_B$ commute, they are simultaneously diagonalizable, so that it has the potential of forming an SU(2)-valued operator. If we want this to be the case, we must ensure that the eigenstates $|u\rangle$ have eigenvalues $u \in \mathrm{SU}(2)$. The SU(2) conditions can thus be requested at the operator level. We thus first introduce

$$(U^\dagger)^A{}_B = (U^B{}_A)^\dagger = (U^\dagger)^A{}_\mu(h_2)(t^\dagger)^\mu{}_\nu U^\nu{}_B(h_1), \quad (t^\dagger)^\mu{}_\nu := (t^\nu{}_\mu)^*, \tag{2.240}$$

and start by demanding the unitarity condition

$$\delta^A{}_C = (U^\dagger)^A{}_B U^B{}_C = U^A{}_B (U^\dagger)^B{}_C. \tag{2.241}$$

In light of Eqs. (2.215) and (2.217), this is guaranteed if we demand that $t^\mu{}_\nu$ is unitary.

Second, we demand that the matrix $U^A{}_B$ has unit determinant as an SU(2) matrix

$$1 = U^1{}_1 U^2{}_2 - U^1{}_2 U^2{}_1 = -\frac{1}{2}\epsilon_{AB}\epsilon^{CD}U^A{}_C U^B{}_D = -\frac{1}{2}U^A{}_C U_A{}^C. \tag{2.242}$$

We can put this expression into a normal ordering

$$\begin{aligned} &U^A{}_C U_A{}^C = \\ &\frac{t^\mu{}_\nu t^\rho{}_\sigma}{\sqrt{(N(h_1)+1)(N(h_2)+1-\nu)(N(h_1)+1+\mu)(N(h_2)+1-\sigma-\nu)}} \\ &\times (A^\dagger)^A{}_\mu(h_1)(A^\dagger)_{A\rho}(h_1)A^\nu{}_C(h_2)A^{\sigma C}(h_2). \end{aligned} \tag{2.243}$$

This is simplified by using (2.216) to show the identities

$$(A^\dagger)^A{}_\mu(A^\dagger)_{A\rho} = Q_{\mu\rho}(N+1-\rho) \quad \text{and} \quad A^\nu{}_C A^{\sigma C} = Q^{\nu\sigma}(N+1-\nu). \tag{2.244}$$

Therefore, we conclude that

$$\begin{aligned} &U^A{}_C U_A{}^C = t^\mu{}_\nu t^\rho{}_\sigma Q_{\mu\rho}Q^{\nu\sigma} \\ &\frac{(N(h_1)+1-\rho)(N(h_2)+1-\nu)}{\sqrt{(N(h_1)+1)(N(h_2)+1-\nu)(N(h_1)+1+\mu)(N(h_2)+1-\sigma-\nu)}}. \end{aligned} \tag{2.245}$$

The matrices $Q_{\mu\rho}$ and $Q^{\nu\sigma}$ are antisymmetric, so that only contractions in which $\mu = -\rho$ and $\nu = -\sigma$ survive. We can thus safely set

$$U^A{}_C U_A{}^C = t^\mu{}_\nu t^\rho{}_\sigma Q_{\mu\rho}Q^{\nu\sigma}\sqrt{\frac{(N(h_1)+1+\mu)(N(h_2)+1-\nu)}{(N(h_1)+1)(N(h_2)+1)}}. \tag{2.246}$$

Similarly, since $t^\mu{}_\nu$ is off-diagonal, we can further set $\nu = -\mu$ and reduce this to

$$U^A{}_C U_A{}^C = t^\mu{}_\nu t^\rho{}_\sigma Q_{\mu\rho}Q^{\nu\sigma}\frac{N+1+\mu}{N+1}, \tag{2.247}$$

on the sector satisfying the Abelian Gauss law $N(h_1) = N(h_2) = N$. Carrying out the contraction we realize that

$$U^A{}_C U_A{}^C = t^-{}_+ t^+{}_-\left(\frac{N}{N+1} + \frac{N+2}{N+1}\right) = -2\det t. \tag{2.248}$$

We thus conclude that the condition that $U^A{}_B$ is SU(2)-valued in the sector that satisfies the Abelian Gauss law is satisfied if $t^\mu{}_\nu$ is itself a unitary matrix of unit determinant. Off-diagonal matrices satisfying this condition are all of the form

$$t^\mu{}_\nu = \begin{pmatrix} 0 & e^{i\theta} \\ -e^{-i\theta} & 0 \end{pmatrix}^\mu{}_\nu. \tag{2.249}$$

To be explicit about the orientation of the link, let us include it in the notation, so that the link objects we have built carry the indicator (h_1, h_2). This includes $t^{\mu}{}_{\nu}(h_1, h_2)$. Indeed, if we want to impose $(U^{\dagger})^{A}{}_{B}(h_1, h_2) = U^{A}{}_{B}(h_2, h_1)$, (2.240) shows that we must have

$$t^{\mu}{}_{\nu}(h_2, h_1) = (t^{\nu}{}_{\mu}(h_1, h_2))^* = \begin{pmatrix} 0 & -e^{i\theta(h_1,h_2)} \\ e^{-i\theta(h_1,h_2)} & 0 \end{pmatrix}^{\mu}{}_{\nu} = -t^{\mu}{}_{\nu}(h_1, h_2). \tag{2.250}$$

Fortunately we were unable to completely restrict the form of $t^{\mu}{}_{\nu}$. Indeed, we need to make different choices for each orientation of the link. Given an orientation of the graph, we will choose

$$t^{\mu}{}_{\nu}(\ell) = \begin{pmatrix} 0 & 1 \\ -1 & 0 \end{pmatrix}^{\mu}{}_{\nu}, \tag{2.251}$$

for positively oriented links ℓ. Ultimately, the need for a choice of this orientation comes from the fact that to identify the Hilbert space on a link with $L^2(\mathrm{SU}(2))$, we need to decide which link is going to the dual representation in (2.88).

2.4.4 Loop-String-Hadron on Trajectories

In order to describe dynamics in the LSH formulation, we need to further consider Wilson lines on trajectories

$$U(\gamma)^{A}{}_{B} = U(\gamma(n))^{A}{}_{C_{n-1}} \cdots U(\gamma(2))^{C_2}{}_{C_1} U(\gamma(1))^{C_1}{}_{B} \tag{2.252}$$

In particular, for closed trajectories, as required in the magnetic part of the Hamiltonian, we can define the Wilson line operator

$$W(\gamma) = U(\gamma)^{A}{}_{A}. \tag{2.253}$$

The starting point $\gamma(1)$ of the trajectory is immaterial since all components of Wilson line operators commute.

Alternatively, for a corner trajectory Γ, set $\Gamma(i) = (h_1(i), h_2(i))$. We can then define the Wilson line operator

$$\begin{aligned} U(\Gamma)^{\mu}{}_{\nu} = U(\Gamma(n))^{\mu}{}_{\nu_n} \cdots t^{\nu_3}{}_{\mu_2}(h_2(3), h_1(2)) U(\Gamma(2))^{\mu_2}{}_{\nu_2} \\ \times t^{\nu_2}{}_{\mu_1}(h_2(2), h_1(1)) U(\Gamma(1))^{\mu_1}{}_{\nu}. \end{aligned} \tag{2.254}$$

The advantage of working with these is that they immediately have a representation in terms of LSH operators (2.225). The disadvantage is that the components of Wilson corners do not generally commute, so that care must be place in the ordering of these operators.

To understand the connection between these, consider a trajectory γ. Set $\gamma(i) = (h_2(i), h_1(i))$ throughout the trajectory $i = 1, \dots, n$. Consider the smaller corner trajectory given by

$$\Gamma(i) = (h_1(i+1), h_2(i)), \quad i = 1, \dots, n-1 \tag{2.255}$$

We then have

$$U(\gamma)^A{}_B = (U^\dagger)^A{}_\mu(h_2(n))t^\mu{}_\nu(\gamma(n))U^\nu{}_\rho(\Gamma)t^\rho{}_\sigma(\gamma(1))U^\sigma{}_B(h_1(1)). \tag{2.256}$$

This yields an expression for arbitrary Wilson lines that is mostly written in terms of LSH operators. Fortunately, in the two cases of importance for the construction of the Hamiltonian, we can find expressions that are fully in terms of the LSH operators.

Focusing first on the magnetic Hamiltonian, consider a closed trajectory γ. The Wilson line is then

$$W(\gamma) = (U^\dagger)^A{}_\mu(h_2(n))t^\mu{}_\nu(\gamma(n))U^\nu{}_\rho(\Gamma)t^\rho{}_\sigma(\gamma(1))U^\sigma{}_A(h_1(1)). \tag{2.257}$$

Now, assume that Γ does not go through $h_1(1)$. As far as the Wilson line is concerned, the starting point of γ is immaterial, and in all cases of interest in this dissertation, one can always choose the starting point so that this is the case. Thus, we can commute the operator at $h_1(1)$ to the tail of the Wilson line. Thus, we have

$$W(\gamma) = U(\gamma^c)^\sigma{}_\rho t^\rho{}_\sigma(\gamma(1)) =: W(\gamma_c), \tag{2.258}$$

where

$$\gamma^c = (h_1(1), h_2(n))\Gamma \tag{2.259}$$

is simply the trajectory γ understood as a corner trajectory. This allows us to build the magnetic Hamiltonian solely in terms of LSH operators.

Turning now our attention to the electric Hamiltonian, let us consider a pair of half-edges h_1 and h_2 with a trajectory γ which does not overlap either of these half-edges and which has $s(\gamma) = \pi(h_2)$ and $t(\gamma) = \pi(h_1)$. Our goal is then to understand inner products $\langle E(h_1), U(\gamma)E(h_2)U(\gamma^{-1})\rangle$ completely in terms of LSH operators.

This is another trace calculation

$$\begin{aligned}\langle E(h_1), U(\gamma)E(h_2)U(\gamma^{-1})\rangle &= -2\,\mathrm{tr}(E(h_1)U(\gamma)E(h_2)U(\gamma^{-1})) \\ &= -2E^A{}_B(h_1)U^B{}_C(\gamma)E^C{}_D(h_2)U^D{}_A(\gamma^{-1}).\end{aligned} \tag{2.260}$$

Expanding using the first line of (2.194) for the electric operator at h_1 and the second line

for h_2, this takes the form

$$\begin{aligned}
&\langle E(h_1), U(\gamma)E(h_2)U(\gamma^{-1})\rangle = \\
&\frac{1}{2}a^\dagger_B(h_1)a^A(h_1)U^B{}_C(\gamma)a^C(h_2)a^\dagger_D(h_2)U^D{}_A(\gamma^{-1}) \\
&-\frac{N(h_1)}{4}U^B{}_C(\gamma)a^C(h_2)a^\dagger_D(h_2)U^D{}_B(\gamma^{-1}) \\
&-\frac{1}{2}a^\dagger_B(h_1)a^A(h_1)U^B{}_C(\gamma)\left(\frac{N(h_2)}{2}+1\right)U^C{}_A(\gamma^{-1}) \\
&+\frac{N(h_1)}{4}U^B{}_C(\gamma)\left(\frac{N(h_2)}{2}+1\right)U^C{}_B(\gamma^{-1})
\end{aligned} \tag{2.261}$$

The third and fourth line of this expansion vanish. Indeed, γ has no overlapping support with h_1 and h_2, so that in the fourth line we can use $U^B{}_C(\gamma)U^C{}_B(\gamma^{-1}) = \delta^B_B = 2$, yielding the contribution

$$\frac{N(h_1)}{2}\left(\frac{N(h_2)}{2}+1\right). \tag{2.262}$$

Similarly, in the third line we can use $U^B{}_C(\gamma)U^C{}_A(\gamma^{-1}) = \delta^B_A$, so that we obtain the contribution

$$-\frac{N(h_1)}{2}\left(\frac{N(h_2)}{2}+1\right), \tag{2.263}$$

cancelling the previous contribution. Finally, in the second line we can use the fact that Wilson line operators commute to use $U^D{}_B(\gamma^{-1})U^B{}_C(\gamma) = \delta^D_C$, leaving us with

$$-\frac{N(h_1)}{4}(N(h_2)+2). \tag{2.264}$$

Our final task is then to compute in terms of LSH operators the first line of

$$\begin{aligned}
&\langle E(h_1), U(\gamma)E(h_2)U(\gamma^{-1})\rangle = \\
&\frac{1}{2}a^\dagger_B(h_1)a^A(h_1)U^B{}_C(\gamma)a^C(h_2)a^\dagger_D(h_2)U^D{}_A(\gamma^{-1}) - \frac{N(h_1)}{4}(N(h_2)+2).
\end{aligned} \tag{2.265}$$

We once again use the fact that γ does not overlap h_1 to reorder

$$\begin{aligned}
&a^\dagger_B(h_1)a^A(h_1)U^B{}_C(\gamma)a^C(h_2)a^\dagger_D(h_2)U^D{}_A(\gamma^{-1}) = \\
&a^\dagger_B(h_1)U^B{}_C(\gamma)a^C(h_2)a^\dagger_D(h_2)U^D{}_A(\gamma^{-1})a^A(h_1).
\end{aligned} \tag{2.266}$$

We now use the replacements

$$\begin{aligned}
a^\dagger_A &= A^+{}_A = U^+{}_A\sqrt{N+1}, \\
a^A &= (A^\dagger)^A{}_+ = \sqrt{N+1}(U^\dagger)^A{}_+,
\end{aligned} \tag{2.267}$$

to write this as

$$\begin{aligned} &a^\dagger_B(h_1)a^A(h_1)U^B{}_C(\gamma)a^C(h_2)a^\dagger_D(h_2)U^D{}_A(\gamma^{-1}) = \\ &U^+{}_B(h_1)\sqrt{N(h_1)+1}U^B{}_C(\gamma)\sqrt{N(h_2)+1}(U^\dagger)^C{}_+(h_2) \\ &\times U^+{}_D(h_2)\sqrt{N(h_2)+1}U^D{}_A(\gamma^{-1})\sqrt{N(h_1)+1}(U^\dagger)^A{}_+(h_1). \end{aligned} \tag{2.268}$$

After normal ordering by putting the creation operators to the right, this becomes

$$\begin{aligned} &a^\dagger_B(h_1)a^A(h_1)U^B{}_C(\gamma)a^C(h_2)a^\dagger_D(h_2)U^D{}_A(\gamma^{-1}) = N(h_1)(N(h_2)+1) \\ &\times U^+{}_B(h_1)U^B{}_C(\gamma)(U^\dagger)^C{}_+(h_2)U^+{}_D(h_2)U^D{}_A(\gamma^{-1})(U^\dagger)^A{}_+(h_1). \end{aligned} \tag{2.269}$$

Finally, this last product of Wilson operators can be understood as a Wilson line on a corner trajectory Γ

$$\begin{aligned} &a^\dagger_B(h_1)a^A(h_1)U^B{}_C(\gamma)a^C(h_2)a^\dagger_D(h_2)U^D{}_A(\gamma^{-1}) = N(h_1)(N(h_2)+1) \\ &\times U^+{}_+(\Gamma)U^+{}_+(\Gamma^{-1}). \end{aligned} \tag{2.270}$$

This corner trajectory has the form $\Gamma(i) = (h_1(i), h_2(i-1))$, for $i = 1, \dots, n+1$, in terms of $\gamma(i) = (h_2(i), h_1(i))$ with the understanding that $h_2(0) = h_2$ and $h_1(n+1) = h_1$.

Putting these results together, we conclude that

$$\begin{aligned} \langle E(h_1), U(\gamma)E(h_2)U(\gamma^{-1})\rangle = &\frac{N(h_1)}{2}(N(h_2)+1)U^+{}_+(\Gamma)U^+{}_+(\Gamma^{-1}) \\ &- \frac{N(h_1)}{4}(N(h_2)+2). \end{aligned} \tag{2.271}$$

One might be worried that these operators can potentially not satisfy the Abelian Gauss law on h_1 and h_2 since there are potentially no operators acting on $\sigma(h_1)$ and $\sigma(h_2)$. Fortunately, while $U^+{}_+(\Gamma)$ creates a flux of electric energy on h_1, the operator $U^+{}_+(\Gamma^{-1})$ annihilates a flux on h_1. A similar phenomenon happens for h_2. Thus, not only is the Abelian Gauss law conserved, but these operators also do not affect the number of electric fluxes through h_1 and h_2. With these we will now be able to express the dynamics of our theory fully in terms of LSH operators.

2.4.5 Loop-String-Hadron on Vertices

We now discuss the construction of states in the LSH formalism. As discussed in Section 2.1.4, in electric formulations these are built out of gauge invariant states on the vertices. We thus now focus on a single vertex p with n half-edges $h_1, \dots, h_n$ attached to it. We can thus build our gauge invariant states through the application of gauge invariant creation operators, which are given by $\mathcal{L}^{++}$ on the electric vacuum $|0\rangle$ which is annihilated by the Schwinger annihilation operators.

This construction yields all gauge-invariant states. The problem however is that, they will in general not be orthogonal to one another, due to Mandelstam constraints. This has been one of the major difficulties in extending the LSH formalism to SU(3) [101]. However, in SU(2), there is a simple solution to this problem since a triple tensor product of irreducible representations can only have at most one invariant. We thus now restrict to vertices with $n \leq 3$. The point-splitting procedure studied in Section 2.3.1 shows that one can always find an equivalent graph in which this is always the case.

For definiteness, we choose an ordering of the corners (h_1, h_2), (h_2, h_3) and (h_3, h_1) at this vertex. In order to simplify the notation, we will replace the arguments (h_i, h_j) in our operators by subindices ij. For example, we write

$$\mathcal{L}_{ij}^{\mu\nu} := \mathcal{L}^{\mu\nu}(h_i, h_j), \quad n_{ij} := n(h_i, h_j), \quad N_i := N(h_i). \tag{2.272}$$

Then the states at this vertex are given by the number of excitations n_{ij} at each of these corners

$$|n_{12}, n_{23}, n_{31}\rangle \propto (\mathcal{L}_{12}^{++})^{n_{12}} (\mathcal{L}_{23}^{++})^{n_{23}} (\mathcal{L}_{31}^{++})^{n_{31}} |0\rangle . \tag{2.273}$$

In order to compute the normalization of these states, we note that

$$(\mathcal{L}_{12}^{++})^\dagger = \mathcal{L}_{21}^{--}. \tag{2.274}$$

We thus need to study the expectation

$$\begin{aligned} C(n_{12}, n_{23}, n_{31}) = \langle 0| (\mathcal{L}_{13}^{--})^{n_{31}} (\mathcal{L}_{32}^{--})^{n_{23}} (\mathcal{L}_{21}^{--})^{n_{12}} \\ (\mathcal{L}_{12}^{++})^{n_{12}} (\mathcal{L}_{23}^{++})^{n_{23}} (\mathcal{L}_{31}^{++})^{n_{31}} |0\rangle . \end{aligned} \tag{2.275}$$

This expectation is most easily studied by computing the state

$$\begin{aligned} &\mathcal{L}_{21}^{--} (\mathcal{L}_{12}^{++})^{n_{12}} (\mathcal{L}_{23}^{++})^{n_{23}} (\mathcal{L}_{31}^{++})^{n_{31}} |0\rangle = \\ &[\mathcal{L}_{21}^{--}, (\mathcal{L}_{12}^{++})^{n_{12}} (\mathcal{L}_{23}^{++})^{n_{23}} (\mathcal{L}_{31}^{++})^{n_{31}}] |0\rangle . \end{aligned} \tag{2.276}$$

The commutator can be split into three summands

$$\begin{aligned} &[\mathcal{L}_{21}^{--}, (\mathcal{L}_{12}^{++})^{n_{12}} (\mathcal{L}_{23}^{++})^{n_{23}} (\mathcal{L}_{31}^{++})^{n_{31}}] = \\ &[\mathcal{L}_{21}^{--}, (\mathcal{L}_{12}^{++})^{n_{12}}] (\mathcal{L}_{23}^{++})^{n_{23}} (\mathcal{L}_{31}^{++})^{n_{31}} + \\ &(\mathcal{L}_{12}^{++})^{n_{12}} [\mathcal{L}_{21}^{--}, (\mathcal{L}_{23}^{++})^{n_{23}}] (\mathcal{L}_{31}^{++})^{n_{31}} + \\ &(\mathcal{L}_{12}^{++})^{n_{12}} (\mathcal{L}_{23}^{++})^{n_{23}} [\mathcal{L}_{21}^{--}, (\mathcal{L}_{31}^{++})^{n_{31}}] \end{aligned} \tag{2.277}$$

The action of the third on the vacuum immediately vanishes since it contains an annihilation operator on h_2.

The second term also vanishes on the vacuum, but this is harder to see. For this we need the commutator

$$[\mathcal{L}_{21}^{--}, \mathcal{L}_{23}^{++}] = -\mathcal{L}_{13}^{-+}. \tag{2.278}$$

This operator commutes with $\mathcal{L}_{23}^{++}$, so that

$$[\mathcal{L}_{21}^{--}, (\mathcal{L}_{23}^{++})^{n_{23}}] = -n_{23}(\mathcal{L}_{23}^{++})^{n_{23}-1}\mathcal{L}_{13}^{-+}. \tag{2.279}$$

We now claim that

$$\mathcal{L}_{13}^{-+}(\mathcal{L}_{31}^{++})^{n_{31}}\,|0\rangle = 0 \tag{2.280}$$

Indeed, this is a state whose excitations are 0 on h_2, n_{31} on h_3 and $n_{31}-1$ on h_1. It is impossible to build a state like the form (2.273).

With these simplifications we conclude that

$$\begin{aligned}&\mathcal{L}_{21}^{--}(\mathcal{L}_{12}^{++})^{n_{12}}(\mathcal{L}_{23}^{++})^{n_{23}}(\mathcal{L}_{31}^{++})^{n_{31}}\,|0\rangle = \\ &[\mathcal{L}_{21}^{--}, (\mathcal{L}_{12}^{++})^{n_{12}}](\mathcal{L}_{23}^{++})^{n_{23}}(\mathcal{L}_{31}^{++})^{n_{31}}\,|0\rangle\end{aligned} \tag{2.281}$$

We now use the commutator

$$[\mathcal{L}_{21}^{--}, \mathcal{L}_{12}^{++}] = N_1 + N_2 + 2. \tag{2.282}$$

Accordingly,

$$\begin{aligned}[\mathcal{L}_{21}^{--}, (\mathcal{L}_{12}^{++})^{n_{12}}] =&(\mathcal{L}_{12}^{++})^{n_{12}-1}\sum_{m=0}^{n_{12}-1}(N_1+N_2+2+2m)\\ &= (\mathcal{L}_{12}^{++})^{n_{12}-1}n_{12}(N_1+N_2+1+n_{12})\end{aligned} \tag{2.283}$$

We thus conclude that

$$\begin{aligned}&\mathcal{L}_{21}^{--}(\mathcal{L}_{12}^{++})^{n_{12}}(\mathcal{L}_{23}^{++})^{n_{23}}(\mathcal{L}_{31}^{++})^{n_{31}}\,|0\rangle\\ &= (\mathcal{L}_{12}^{++})^{n_{12}-1}(\mathcal{L}_{23}^{++})^{n_{23}}(\mathcal{L}_{31}^{++})^{n_{31}}n_{12}(n_{12}+n_{23}+n_{31}+1)\,|0\rangle\,.\end{aligned} \tag{2.284}$$

This result sets up a recursion relation

$$C(n_{12}, n_{23}, n_{31}) = n_{12}(n_{12}+n_{23}+n_{31}+1)C(n_{12}-1, n_{23}, n_{31}) \tag{2.285}$$

This can be iterated to reduce the general normalization to that of a state with $n_{12} = 0$

$$C(n_{12}, n_{23}, n_{31}) = n_{12}!\frac{(n_{12}+n_{23}+n_{31}+1)!}{(n_{23}+n_{31}+1)!}C(0, n_{23}, n_{31}). \tag{2.286}$$

Repeating this reduction on n_{23} and n_{31}

$$C(n_{12}, n_{23}, n_{31}) = n_{12}!n_{23}!n_{31}!(n_{12}+n_{23}+n_{31}+1)!. \tag{2.287}$$

We thus define our LSH states as

$$|n_{12}, n_{23}, n_{31}\rangle = \frac{(\mathcal{L}_{12}^{++})^{n_{12}} (\mathcal{L}_{23}^{++})^{n_{23}} (\mathcal{L}_{31}^{++})^{n_{31}} |0\rangle}{\sqrt{n_{12}! n_{23}! n_{31}! (n_{12} + n_{23} + n_{31} + 1)!}}. \tag{2.288}$$

We finish by clarifying the action of the LSH operators on these states. Note that

$$\mathcal{L}_{12}^{++} |n_{12}, n_{23}, n_{31}\rangle = \sqrt{(n_{12} + 1)(n_{12} + n_{23} + n_{31} + 2)}\, |n_{12} + 1, n_{23}, n_{31}\rangle . \tag{2.289}$$

Let us then define the operators

$$N_{12} = \frac{1}{2}(N_1 + N_2 - N_3) \quad \text{and} \quad N_{123} = N_{12} + N_{23} + N_{31} + 1, \tag{2.290}$$

with N_{23} and N_{31} defined by analogy with N_{12}. Then we find a polar decomposition

$$\mathcal{L}_{12}^{++} = \sqrt{N_{12} N_{123}} \Lambda_{12}^{+}, \tag{2.291}$$

where

$$\Lambda_{12}^{+} |n_{12}, n_{23}, n_{31}\rangle = |n_{12} + 1, n_{23}, n_{31}\rangle . \tag{2.292}$$

Polar decompositions of $\mathcal{L}_{23}^{++}$ and $\mathcal{L}_{31}^{++}$ are constructed similarly. For the annihilation operators we have

$$\mathcal{L}_{21}^{--} = \sqrt{(N_{12} + 1)(N_{123} + 1)} \Lambda_{21}^{-}, \tag{2.293}$$

with

$$\Lambda_{21}^{-} |n_{12}, n_{23}, n_{31}\rangle = |n_{12} - 1, n_{23}, n_{31}\rangle , \tag{2.294}$$

and annihilating the state if $n_{12} = 0$. The corresponding polar decompositions of $\mathcal{L}_{32}^{--}$ and $\mathcal{L}_{13}^{--}$ are built by analogy. For mixed operators we use the commutation relations

$$[\mathcal{L}_{12}^{++}, \mathcal{L}_{23}^{--}] = -\mathcal{L}_{13}^{+-} \quad \text{and} \quad [\mathcal{L}_{12}^{--}, \mathcal{L}_{23}^{++}] = \mathcal{L}_{13}^{-+}, \tag{2.295}$$

which, in conjunction with

$$\mathcal{L}_{12}^{\mu\nu} = -\mu\nu \mathcal{L}_{21}^{\nu\mu}, \tag{2.296}$$

lead to

$$\begin{aligned} \mathcal{L}_{13}^{-+} &= -\sqrt{(N_{12} + 1) N_{23}} \Lambda_{21}^{-} \Lambda_{23}^{+} = \mathcal{L}_{31}^{+-}, \\ \mathcal{L}_{13}^{+-} &= -\sqrt{N_{12} (N_{23} + 1)} \Lambda_{12}^{+} \Lambda_{32}^{-} = \mathcal{L}_{31}^{-+}. \end{aligned} \tag{2.297}$$

The cyclic combinations are built accordingly.

At this stage, the LSH workflow is complete. Pick an orientation of the vertices, in order to define the states (2.288). Then one knows the action of the LSH loop operators (2.220) through their polar decompositions. After choosing an orientation for the links, the Hamiltonian is fully expressed in terms of corner Wilson lines through Eqs. (2.258) and (2.271), which are themselves expressed in terms of LSH loop operators (2.225). The required number operators in this construction are given by

$$N_1 = N_{12} + N_{31}, \tag{2.298}$$

and their cyclic permutations.

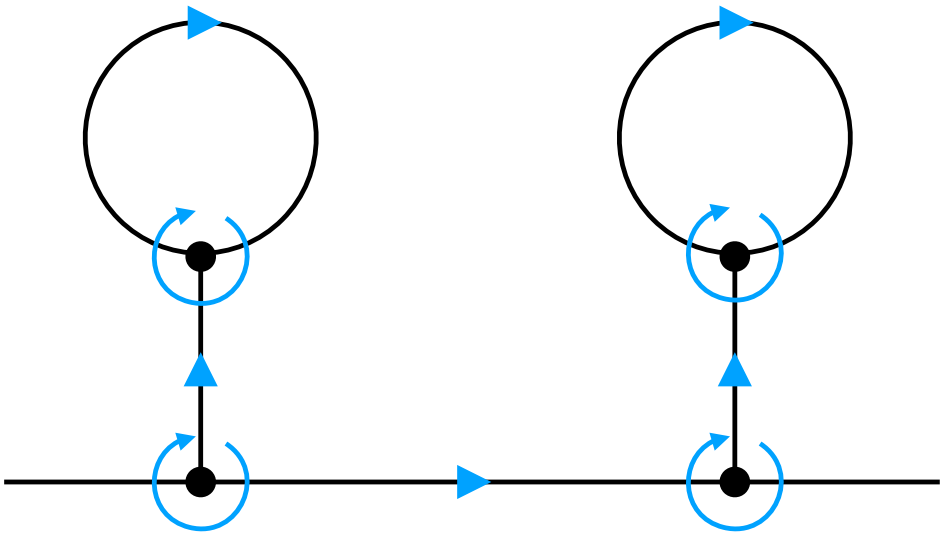


Figure 2.11: The orientation on a pair of leaves in a branch is shown. The arrows on each link determine our convention for their orientation, so that loops are oriented clockwise, horizontal links from left to right and vertical links from bottom to top. Additional guiding arrows show the orientation of each vertex, so that their half-edges are oriented clockwise.

2.5 Loop-String-Hadron on Branches

2.5.1 States on the Branch

Having developed the LSH formulation, we are now ready to apply it to our branches Fig. 2.7. Our orientation conventions for the graph are shown in Fig. 2.11. The corresponding corners with this orientation are labelled in Fig. 2.11.

The simplicity of a branch allows us to immediately solve the Abelian Gauss law. In terms of occupation numbers, our states must satisfy

$$\begin{aligned} n(u_i) &= n(v_i), \\ n(l_i) + n(r_i) &= n(u_i) + n(v_i), \\ n(r_i) + n(d_i) &= n(l_{i+1}) + n(d_{i+1}), \end{aligned} \tag{2.299}$$

with $n(l_1) = n(d_1) = n(r_P) = n(d_P) = 0$. Therefore, the quantum numbers $n(d_i)$ and $n(u_i) = n(v_i)$ are completely determined in terms of the quantum numbers $n(l_i)$, $n(r_i)$ and $n(n_i)$. The quantum number $n(l_P)$ is also completely determined. We thus obtain a

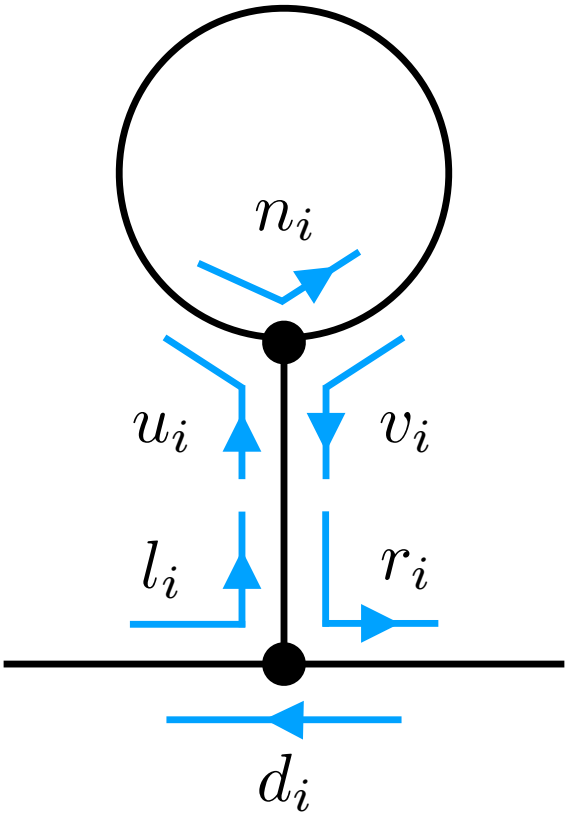


Figure 2.12: Labeling of the corners on the i-th leaf compatible with the vertex orientation choices in Fig. 2.11.

non-redundant basis for the theory of the form

$$\begin{aligned}|n\rangle &\equiv |n(n_1), n(r_1); n(n_2), n(l_2), n(r_2); \cdots; n(n_P)\rangle \\ &:= \prod_{i=1}^{P} \Lambda^+(n_i)^{n(n_i)} \Lambda^+(u_i)^{n(u_i)} \Lambda^+(v_i)^{n(v_i)} \Lambda^+(l_i)^{n(l_i)} \Lambda^+(r_i)^{n(r_i)} \Lambda^+(d_i)^{n(d_i)} \, |0\rangle \, .\end{aligned} \tag{2.300}$$

The constraints in these quantum numbers are that $n(l_i) + n(r_i)$ must be even and none of the $n(d_i)$ can be negative. The first constraint is easily solved in terms of integers a_i and b_i, as well as a bit $\epsilon_i \in \{0, 1\}$, by setting

$$n(l_i) = 2a_i + \epsilon_i \quad \text{and} \quad n(r_i) = 2b_i + \epsilon_i. \tag{2.301}$$

The remaining constraint is solved by demanding that

$$\begin{aligned}n(r_1) \geq \max\{&n(l_2), n(l_2) - n(r_2) + n(l_3), \\ &n(l_2) - n(r_2) + n(l_3) - n(r_3) + n(l_4), \cdots\},\end{aligned} \tag{2.302}$$

so that

$$\begin{aligned}n(d_2) &= n(r_1) - n(l_2) \geq 0, \\ n(d_3) &= n(r_2) - n(l_3) + n(r_1) - n(l_2) \geq 0, \\ n(d_4) &= n(r_3) - n(l_4) + n(r_2) - n(l_3) + n(r_1) - n(l_2) \geq 0, \\ &\vdots\end{aligned} \tag{2.303}$$

Alternatively, the constraints can be made fully local by defining

$$\begin{aligned}2L_i &:= n(u_i) + n(v_i) = n(l_i) + n(r_i), \\ 2L_{1\cdots i} &:= n(r_i) + n(d_i) = n(l_{i+1}) + n(d_{i+1}),\end{aligned} \tag{2.304}$$

which count the total electric flux at each edge, as shown in Fig. 2.13. Then one can solve for $n(u_i) = n(v_i) = L_i$ and

$$\begin{aligned}n(l_i) &= L_i + L_{1\cdots i-1} - L_{1\cdots i}, \\ n(r_i) &= L_i - L_{1\cdots i-1} + L_{1\cdots i}, \\ n(d_i) &= -L_i + L_{1\cdots i-1} + L_{1\cdots i}.\end{aligned} \tag{2.305}$$

Demanding that these occupation numbers are nonnegative, we conclude that

$$|L_i - L_{1\cdots i-1}| \leq L_{1\cdots i} \leq L_i + L_{1\cdots i-1}. \tag{2.306}$$

These are of course the conditions for an angular momentum $L_{1\cdots i}$ to be built by coupling a system of angular momentum $L_{1\cdots i-1}$ and one of angular momentum L_i.

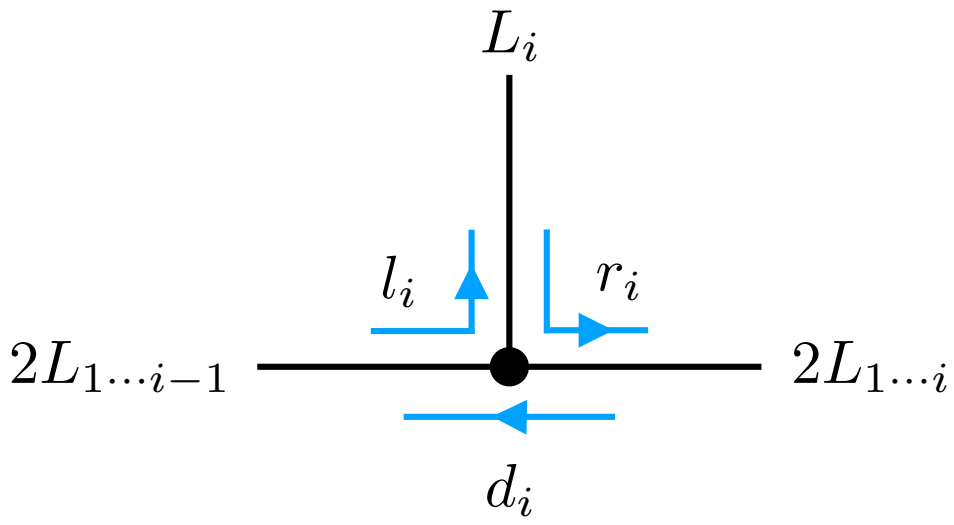


Figure 2.13: Spin labels counting the number of fluxes through each edge (2.304).

2.5.2 Magnetic Hamiltonian

We now turn to the construction of the Hamiltonian. We will restrict at this stage to the Hamiltonian coming from the plaquette flower Section 2.3.3, which leads to an ultralocal magnetic Hamiltonian and a simple weak-coupling limit. Thus, in this setting, the magnetic Hamiltonian is

$$\epsilon H_B = -\frac{2}{g^2}\sum_{i=1}^{P} \operatorname{Re} W(n_i). \tag{2.307}$$

For explicit calculations, it is useful to label the half-edges of the graph. We will choose the conventions shown in Fig. 2.14. For example, the corners in Fig. 2.12 correspond to

$$\begin{aligned} n_i &= (b_i, a_i), \\ u_i &= (a_i, f_i), \\ v_i &= (f_i, b_i), \\ l_i &= (g_i, x_i), \\ r_i &= (y_i, g_i), \\ d_i &= (x_i, y_i). \end{aligned} \tag{2.308}$$

Using this notation,

$$W(n_i) = U^{\mu}{}_{\nu}(n_i) t^{\nu}{}_{\mu}(a_i, b_i). \tag{2.309}$$

Since the link (a_i, b_i) is in the wrong orientation according to Fig. 2.11, we can flip the orientation

$$W(n_i) = -U^{\mu}{}_{\nu}(n_i) t^{\nu}{}_{\mu}(n_i). \tag{2.310}$$

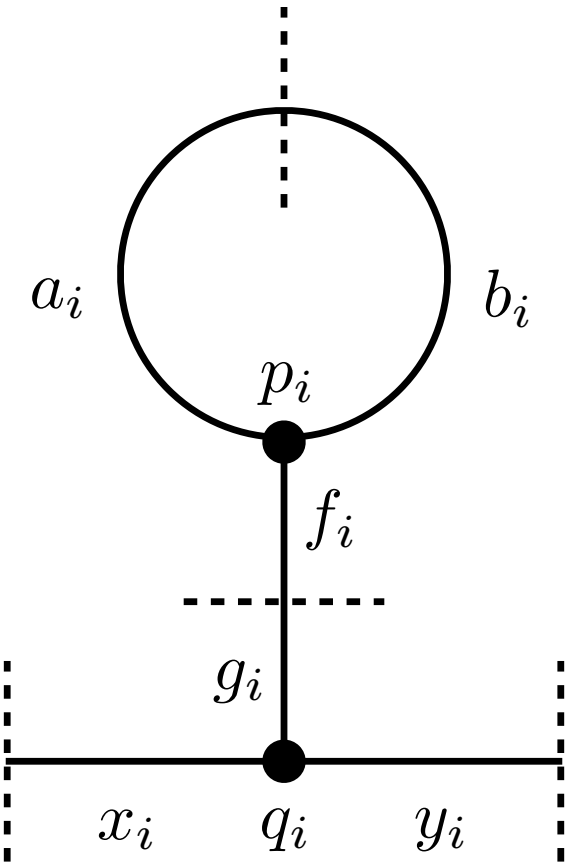


Figure 2.14: Labelling convention for the branch half-edges.

Next we use (2.225), to set

$$W(n_i) = -\frac{1}{\sqrt{N(a_i)+1}}\mathcal{L}^{\mu}{}_{\nu}(n_i)\frac{1}{\sqrt{N(b_i)+1}}t^{\nu}{}_{\mu}(n_i). \tag{2.311}$$

Now we can use (2.251) and (2.209) to write this as

$$\begin{aligned} W(n_i) = &-\frac{1}{\sqrt{N(a_i)+1}}\mathcal{L}^{--}(n_i)\frac{1}{\sqrt{N(b_i)+1}} \\ &+ \frac{1}{\sqrt{N(a_i)+1}}\mathcal{L}^{++}(n_i)\frac{1}{\sqrt{N(b_i)+1}}. \end{aligned} \tag{2.312}$$

Using (2.296), this becomes

$$\begin{aligned} W(n_i) = &\frac{1}{\sqrt{N(a_i)+1}}\mathcal{L}^{--}(n_i^{-1})\frac{1}{\sqrt{N(b_i)+1}} \\ &+ \frac{1}{\sqrt{N(a_i)+1}}\mathcal{L}^{++}(n_i)\frac{1}{\sqrt{N(b_i)+1}}. \end{aligned} \tag{2.313}$$

In terms of Eqs. (2.291) and (2.293), we are left with

$$\begin{aligned} W(n_i) = &\sqrt{\frac{(N(n_i)+1)(N(f_i,b_i,a_i)+1)}{N(a_i)+1}}\Lambda^{-}(n_i^{-1})\frac{1}{\sqrt{N(b_i)+1}} \\ &+ \sqrt{\frac{N(n_i)N(f_i,b_i,a_i)}{N(a_i)+1}}\Lambda^{+}(n_i)\frac{1}{\sqrt{N(b_i)+1}}. \end{aligned} \tag{2.314}$$

This expression can be normal ordered to

$$\begin{aligned} W(n_i) = &\sqrt{\frac{(N(n_i)+1)(N(f_i,b_i,a_i)+1)}{(N(a_i)+1)(N(b_i)+2)}}\Lambda^{-}(n_i^{-1}) \\ &+ \sqrt{\frac{N(n_i)N(f_i,b_i,a_i)}{(N(a_i)+1)N(b_i)}}\Lambda^{+}(n_i). \end{aligned} \tag{2.315}$$

Expanding into corner number operators[4],

$$N(a_i) = N(b_i) = L_i + N(n_i) \quad \text{and} \quad N(f_i,b_i,a_i) = N(n_i) + 2L_i + 1 \tag{2.316}$$

[4]We allow ourselves the abuse of notation of using the same notation L_i for the operator and for its eigenvalues

we have the final expression

$$W(n_i) = \sqrt{\frac{(N(n_i)+1)(N(n_i)+2L_i+2)}{(N(n_i)+L_i+1)(N(n_i)+L_i+2)}}\Lambda^-(n_i^{-1}) + \sqrt{\frac{N(n_i)(N(n_i)+2L_i+1)}{(N(n_i)+L_i+1)(N(n_i)+L_i)}}\Lambda^+(n_i) = \mathrm{Re}\, W(n_i). \tag{2.317}$$

This expression shows that the magnetic Hamiltonian drives excitations of electric flux concentrated solely on individual leaves. This is why we call this magnetic Hamiltonian ultralocal in this formulation.

2.5.3 Ultralocal Electric Hamiltonian

We now turn to the ultralocal pieces of the electric Hamiltonian. The Casimir operators are given by (2.196)

$$E(a_i)^2 = E(b_i)^2 = \frac{N(n_i)+L_i}{2}\left(\frac{N(n_i)+L_i}{2}+1\right). \tag{2.318}$$

Moreover, we can also examine the inner product $\langle E(b_i), E(a_i)\rangle$ as an application of (2.271) to the trajectory $\Gamma = n_i$.

For this we expand

$$U^+{}_+(n_i) = \frac{1}{\sqrt{N(a_i)+1}}\mathcal{L}^{+-}(n_i)\frac{1}{\sqrt{N(b_i)+1}}. \tag{2.319}$$

With our current ordering

$$\mathcal{L}^{+-}(n_i) = -\sqrt{(N(u_i)+1)N(v_i)}\Lambda^-(u_i^{-1})\Lambda^+(v_i). \tag{2.320}$$

Therefore, after normal ordering

$$U^+{}_+(n_i) = -\sqrt{\frac{(N(u_i)+1)N(v_i)}{(N(a_i)+1)N(b_i)}}\Lambda^-(u_i^{-1})\Lambda^+(v_i). \tag{2.321}$$

A similar calculation has to be done for

$$U^+{}_+(n_i^{-1}) = \frac{1}{\sqrt{N(b_i)+1}}\mathcal{L}^{+-}(n_i^{-1})\frac{1}{\sqrt{N(a_i)+1}}. \tag{2.322}$$

Given the change in orientation, we now have

$$\mathcal{L}^{+-}(n_i^{-1}) = -\sqrt{N(u_i)(N(v_i)+1)}\Lambda^+(u_i)\Lambda^-(v_i^{-1}). \tag{2.323}$$

Thus, after normal ordering

$$U^+{}_+(n_i^{-1}) = -\sqrt{\frac{N(u_i)(N(v_i)+1)}{(N(b_i)+1)N(a_i)}}\Lambda^+(u_i)\Lambda^-(v_i^{-1}). \tag{2.324}$$

We now turn to the product,

$$U^+{}_+(n_i)U^+{}_+(n_i^{-1}) = \frac{(N(u_i)+1)N(v_i)}{(N(a_i)+1)N(b_i)}\Lambda^-(u_i^{-1})\Lambda^+(u_i)\Lambda^+(v_i)\Lambda^-(v_i^{-1}). \tag{2.325}$$

While $\Lambda^-(u_i^{-1})\Lambda^+(u_i) = 1$, we cannot say the same of $\Lambda^+(v_i)\Lambda^-(v_i^{-1})$. Indeed, this term annihilates the electric vacuum. Therefore,

$$\Lambda^+(v_i)\Lambda^-(v_i^{-1}) = 1 - \delta_{N(v_i),0}. \tag{2.326}$$

We would thus have

$$U^+{}_+(n_i)U^+{}_+(n_i^{-1}) = \frac{(N(u_i)+1)N(v_i)}{(N(a_i)+1)N(b_i)}(1-\delta_{N(v_i),0}). \tag{2.327}$$

Fortunately, the numerator vanishes on states with $N(v_i) = 0$. We can therefore forget about this subtlety for the moment.

Reexpressing these in terms of corner number operators, we have

$$U^+{}_+(n_i)U^+{}_+(n_i^{-1}) = \frac{(L_i+1)L_i}{(N(n_i)+L_i+1)(N(n_i)+L_i)}. \tag{2.328}$$

Therefore

$$\langle E(b_i), E(a_i)\rangle = \frac{L_i}{2}(L_i+1) - \frac{N(n_i)+L_i}{2}\left(\frac{N(n_i)+L_i}{2}+1\right). \tag{2.329}$$

The inner product in the opposite order is the same.

We can now test the assertion that at weak coupling one can, to lowest order, set $E(a_i) = -E(b_i)$. Our calculations show that

$$(E(b_i)+E(a_i))^2 = L_i(L_i+1). \tag{2.330}$$

Therefore, the weak coupling limit leading to the Hamiltonian (2.181) is deeply connected to low truncations in L_i.

2.5.4 Comments on Nearest Neighbor Interactions

As a final example of the structure of the Hamiltonian in this formulation, let us consider the inner products $\langle E(a_i), E(a_{i+1})\rangle$ and $\langle E(a_i), E(b_{i+1})\rangle$. In here, and from now on, we will assume the parallel transport is implicit in these inner products.

To compute $\langle E(a_i), E(a_{i+1})\rangle$ we need to study the Wilson line on the corner trajectory $\Gamma = (a_i, f_i)(g_i, y_i)(x_{i+1}, g_{i+1})(f_{i+1}, a_{i+1})$. This would require three contractions of Wilson operators, leading to $2^3 = 8$ terms. After multiplication against the Wilson line on the inverse trajectory, this would lead to 64 terms, which is already a difficult computation to keep track off by hand. For this reason, these calculations are most efficiently done using symbolic computing programs. Code to do this is found in [135].

After doing this, one sees the result reduces to $3^3 = 27$ terms, distinguished by their ladder operator structure. By studying the ladder operator structure of these operators, we see that they correspond to transitions in which

$$\Delta L_{1\cdots i-1} = \Delta L_{1\cdots i+1} = 0, \quad \Delta n_i = -\Delta L_i, \quad \text{and} \quad \Delta n_{i+1} = -\Delta L_{i+1} \tag{2.331}$$

Each term is completely classified by the triple of transitions $(\Delta L_i, \Delta L_{1\cdots i}, \Delta L_{i+1})$, each of which can be 0 or ± 1. Once we take into account Hermitian adjoint $1 \leftrightarrow -1$ and parity $\Delta L_i \leftrightarrow \Delta L_{i+1}$, only 10 of these are independent.

From this inner product, we can also recover the other four inner products involving this same two leaves. Indeed, replacing $a_i \mapsto b_i$ multiplies each transition by $(-1)^{\Delta L_i}$. Similarly, replacing $a_{i+1} \mapsto b_{i+1}$ multiplies each transition by $(-1)^{\Delta L_{i+1}}$.

These calculations are shown in the code found in [135].

2.5.5 Examples

One Plaquette

The one plaquette system can be understood through a branch with $P = 1$ and $L_1 = 0$. The associated flower has a single petal, whose associated loop goes through each edge once. With these realizations we conclude that

$$\epsilon H = g^2 N\Big(\frac{N}{2} + 1\Big) - \frac{2}{g^2}(\Lambda^- + \Lambda^+), \tag{2.332}$$

suppressing the single corner labels since all operators are evaluated at n_1.

At strong coupling, we can disregard the magnetic Hamiltonian, leading to a diagonal Hamiltonian

$$\epsilon H = g^2 \sum_{n=0}^{\infty} n\Big(\frac{n}{2} + 1\Big) |n\rangle\langle n| \,. \tag{2.333}$$

At weak coupling on the other hand, we can discard the electric contribution, so that the Hamiltonian is

$$\epsilon H = -\frac{2}{g^2}\sum_{n=0}^{\infty}(|n\rangle\langle n+1| + |n+1\rangle\langle n|). \tag{2.334}$$

It is interesting to note that this Hamiltonian is related to a quantum random walk in the space of electric fluxes. Indeed, on a $d = 1$ lattice of spacing a, a random walk of a particle of unit mass has a kinetic term

$$-\sum_x \frac{|x\rangle\langle x+a| + |x\rangle\langle x-a| - 2\,|x\rangle\langle x|}{2a^2}. \tag{2.335}$$

Therefore, setting the lattice spacing $a = g/2$ and $x = na$, we conclude that this is a random walk for a particle on a half-line $x \geq 0$, interacting with the potential of a slightly displaced harmonic oscillator

$$V(X) = \sum_{n=0}^{\infty}\left(g^2 n\Big(\frac{n}{2}+1\Big) - \frac{4}{g^2}\right)|n\rangle\langle n| = 2(X+a)^2 - 2a^2 - 1/a^2. \tag{2.336}$$

In the limit $g \to 0$, which coincides with the continuum limit of this theory, the potential coincides exactly with that of the harmonic oscillator with frequency $\omega = 2$. The hard wall condition at $x = 0$ selects the antisymmetric states of that theory, so that the remaining energy levels are

$$\epsilon E_k - \epsilon E_0 = \omega\left(2k+1+\frac{1}{2}\right) - \frac{3}{2}\omega = 4k. \tag{2.337}$$

The resulting spectrum of the theory is shown in Fig. 2.15

Two Plaquettes

Let us now mover over to a system with two plaquettes. The set of half-edges H_T is denoted in Fig. 2.16a. The non-empty sets determining the electric Hamiltonian are

$$\begin{aligned}
&T_{\leftarrow h_1} = \{(b_1, a_1)\}, && \\
&T_{\leftarrow h_2} = \{(b_2, a_2)\}, && T_{h_2\leftarrow} = \{(b_1, a_1)\}, \\
& && T_{h_3\leftarrow} = \{(b_2, a_2)\}, \\
&T_{\leftarrow h_4} = \{(b_2, a_2)\}, && T_{h_4\leftarrow} = \{(b_1, a_1), (b_2, a_2)\}, \\
& && T_{h_5\leftarrow} = \{(b_2, a_2)\}, \\
& && T_{h_6\leftarrow} = \{(b_1, a_1)\}, \\
& && T_{h_7\leftarrow} = \{(b_2, a_2)\}.
\end{aligned} \tag{2.338}$$

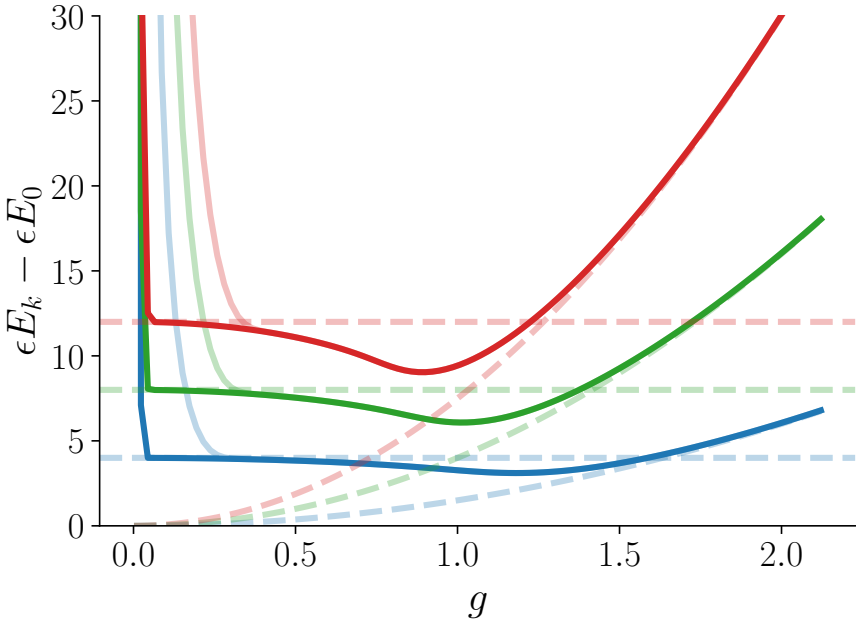


Figure 2.15: Energy levels measured with respect to the ground state are shown in solid lines. The one with transparency corresponds to a truncation into the Hilbert space with a maximum $n = 2^4$. The one without has a maximum $n = 2^7$. Dashed lines correspond to the exact solutions at $g = 0$ and at strong coupling.

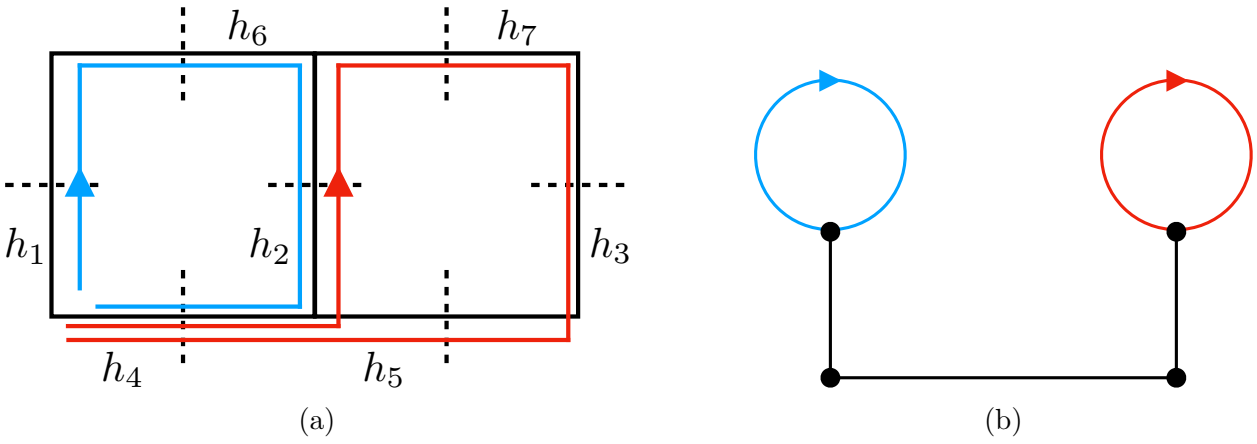


Figure 2.16: (a) A two-plaquette chain with a choice of half-edges H_T with the maximal tree compatible with Fig. 2.3a. The trajectories in T are shown in blue and red colors. (b) A $P = 2$ branch, whose loops are color coded to indicate correspondence to those on (a).

The electric Hamiltonian is thus obtained by the sum

$$\begin{aligned}
&E(a_1)^2 + (E(a_2) + E(b_1))^2 + E(b_2)^2 + (E(a_2) + E(b_1) + E(b_2))^2 \\
&+ E(b_2)^2 + E(b_1)^2 + E(b_2)^2 \\
&= 4E(a_1)^2 + 6E(a_2)^2 \\
&\quad + 4\langle E(a_2), E(b_1)\rangle + 2\langle E(a_2), E(b_2)\rangle + 2\langle E(b_1), E(b_2)\rangle .
\end{aligned} \tag{2.339}$$

Now, note that Fig. 2.16b is effectively the graph considered in Section 2.5.4 with the condition $L_{1\cdots i-1} = L_{1\cdots i+1} = 0$. The triangle conditions then demand that

$$L_i = L_{1\cdots i} = L_{i+1} \equiv L. \tag{2.340}$$

It is therefore useful to define

$$\Lambda^+(L) = \Lambda^+(r_i)\Lambda^+(l_{i+1})\Lambda^+(v_{i+1})\Lambda^+(u_{i+1})\Lambda^+(l_{i+1})\Lambda^+(r_i)\Lambda^+(v_i)\Lambda^+(u_i). \tag{2.341}$$

One of the inner product is then given by

$$\begin{aligned}
&\langle E(b_1), E(b_2)\rangle = \\
&-\frac{L}{4}\sqrt{\frac{(N(n_1)+1)(N(n_1)+2L+1)(N(n_2)+1)(N(n_2)+2L+1)}{4L^2-1}} \\
&\quad \times \Lambda^+(L)\Lambda^-(n_1^{-1})\Lambda^-(n_2^{-1}) + \text{h.c.} - \frac{L}{4}(L+1).
\end{aligned} \tag{2.342}$$

The other inner product $\langle E(b_1), E(a_2)\rangle$ is identical but carries the opposite sign on the terms that have a non-trivial ladder operator structure.

With these results, the full Hamiltonian takes the following form

$$\begin{aligned}
&\epsilon H = g^2(N(n_1)+L)\left(\frac{N(n_1)+L}{2}+1\right) \\
&+ g^2(N(n_2)+L)\left(\frac{N(n_2)+L}{2}+1\right) - \frac{g^2}{4}L(L+1) \\
&- \frac{2}{g^2}\sqrt{\frac{N(n_1)(N(n_1)+2L+1)}{(N(n1)+L+1)(N(n_1)+L)}}\Lambda^+(n_1) + \text{h.c.} \\
&- \frac{2}{g^2}\sqrt{\frac{N(n_2)(N(n_2)+2L+1)}{(N(n2)+L+1)(N(n_2)+L)}}\Lambda^+(n_2) + \text{h.c.} \\
&+ \frac{g^2 L}{4}\sqrt{\frac{(N(n_1)+1)(N(n_1)+2L+1)(N(n_2)+1)(N(n_2)+2L+1)}{4L^2-1}} \\
&\times \Lambda^+(L)\Lambda^-(n_1^{-1})\Lambda^-(n_2^{-1}) + \text{h.c.}.
\end{aligned} \tag{2.343}$$

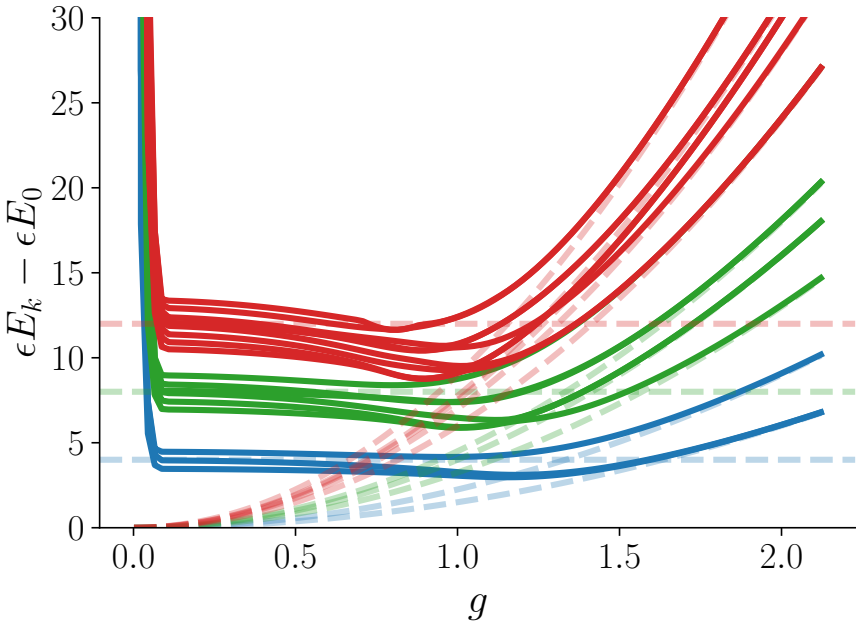


Figure 2.17: Spectrum for the two plaquette system. Dashed lines correspond to both the $g \to 0$ limit and the leading order strong-coupling expansion. Colors were chosen arbitrarily to gather states with a similar behavior at small g. These were obtained using sparse matrices. The truncation was chosen so that $N(n_i) \leq 2^6$ and $L \leq 3$.

At $g = 0$, the theory should decouple into a pair of independent plaquettes, so that the energy levels should take the form

$$\epsilon E_k - \epsilon E_0 = 4k \tag{2.344}$$

In the strong coupling limit, we could have instead worked directly on an electric basis. We can identify $j_1 = (N(n_1) + L)/2$ and $j_2 = (N(n_2) + L)/2$ to be the representations going through the three links each plaquette has that is not shared with the other. Then the third link can have flux $|j_1 - j_2| \leq j \leq j_1 + j_2$. The energy of such a state is then

$$\frac{g^2}{2}(3j_1(j_1+1) + 3j_2(j_2+1) + j(j+1)). \tag{2.345}$$

The low-lying spectrum for this theory is shown in Fig. 2.17. It seems to agree qualitatively with the one shown in [160].

Chapter 3

Scattering in Finite Volumes

3.1 The S-matrix

In a relativistic theory, the Hilbert space $\mathcal{H}$ carries a representation of the Poincaré group[1], which includes the translations generated by the momentum operators $P_\mu = (H, -\boldsymbol{P})$. These play a distinguished role, since they commute with one another $[P_\mu, P_\nu] = 0$ and thus can be simultaneously diagonalized. Therefore, the whole Hilbert space can be spanned by states with definite energy E and momentum $\boldsymbol{P}$. These operators are however not Lorentz invariant, and thus fail to commute with the Lorentz group. On the other hand, the Lorentz invariant combination $P^2 = P^\mu P_\mu$ is, and thus its eigenspaces form representations of the Poincaré group. The momentum $\boldsymbol{P}$ of a state can be used to boost it into a frame in which it has zero momentum, known as its center-of-momentum (CM) frame. It is thus clear that P^2 corresponds to the energy-squared of the state in this frame.

Let us now describe the structure of the spectrum of P^2 for the theories that will be considered in this dissertation. Its lowest eigenvalue is 0 and its eigenspace is spanned by a single vector, the vacuum $|\Omega\rangle$. The Poincaré group acts trivially on this space. Next we will have an isolated eigenvalue $m^2 > 0$. This corresponds to the space of states of the lightest stable particle of the theory, and $m > 0$ corresponds to its mass. This mass gap between the vacuum and the lightest particles will be crucial to our analysis. For example, in a model of QCD in which isospin symmetry is exact, having up and down quarks with the same mass, this would be the space of states of the pions π. In all the examples that will be considered in this theory, the representation of the Lorentz group will be that of a scalar particle. The study of these states will be the goal of Section 3.2.

The continuous spectrum will start at $(2m)^2$, known as the two-particle threshold, which has states with enough energy to contain two of the lightest particles. This sector

[1] or more precisely, its fundamental cover

contains states of the form $|\boldsymbol{p}_1, \boldsymbol{p}_2\rangle_{\text{in/out}}$, with momenta $\boldsymbol{P} = \boldsymbol{p}_1 + \boldsymbol{p}_2$ and energy

$$E = \sqrt{m^2 + \boldsymbol{p}_1^2} + \sqrt{m^2 + \boldsymbol{p}_2^2}. \tag{3.1}$$

These correspond to states with two of the lightest particles being infinitely far away from one another in the distant past (in) or future (out), so that they are non-interacting. In the CM these particles would have momenta $\boldsymbol{p}_*$ for which

$$s := P^2 = 4(m^2 + \boldsymbol{p}_*^2), \tag{3.2}$$

explaining the continuity of the spectrum in this sector. Similarly, new thresholds open at $(3m)^2$, $(4m)^2$, and so on, corresponding to multiparticle states. The construction of associated multiparticle states is similar.

In generic theories, one can have other stable particles corresponding to isolated eigenvalues in $(m^2, (2m)^2)$. For example, if there is a stable composite particle of mass M consisting of two of the lightest particles, its states will have eigenvalue $M^2 < (2m)^2$, with the binding energy equal to $2m - M$. One can even have stable particles above the $(2m)^2$ threshold. An example would be the proton, which has a mass of ~ 938MeV, to be compared against the pion mass $m_\pi \sim 135$MeV. However, in these cases one can often split the spectrum of P^2 into subrepresentations of other commuting symmetry groups, so as to have this situation disappear. In our running example, the proton has spin 1/2, while the pions are scalar. Thus, when looking at the scalar sector of the theory, the protons disappear. On the other hand, when looking at the spin 1/2 sector, the protons are the lightest particle. Otherwise, would-be-stable particles above multiparticle thresholds tend to decay into lighter components. They instead become resonances corresponding to short-lived particles and the would-be-eigenvalues on the real line "move to the complex plane." None of the examples discussed in this dissertation will present any of these complications.

The basic goal of scattering theory is to study the S matrix. This is an operator defined on the Fock space of single particle states

$$\langle \boldsymbol{q}_1 \cdots \boldsymbol{q}_n | S | \boldsymbol{p}_1 \cdots \boldsymbol{p}_m \rangle := {}_{\text{out}}\langle \boldsymbol{q}_1 \cdots \boldsymbol{q}_n | \boldsymbol{p}_1 \cdots \boldsymbol{p}_m \rangle_{\text{in}}. \tag{3.3}$$

It yields the probability amplitude for a state with stable particles of momenta $\boldsymbol{p}_1, \cdots, \boldsymbol{p}_m$ in the infinite past to evolve to a state with particles of momenta $\boldsymbol{q}_1, \cdots, \boldsymbol{q}_n$ in the infinite future. We will have two basic tools in order to do this calculation. One will be to describe the in and out states through the action of local operators on the vacuum. This will lead us to the LSZ reduction formula of Section 3.4, which we will obtain following the Haag-Ruelle approach [161, 162], closely following [163]. The other will be the analytic constraints imposed on the S-matrix by the basic principles of relativistic symmetry.

3.2 Single-Particle States

States with definite momentum are delocalized. It is thus difficult to make sense of having multiple particles with definite momentum that are separated enough so as to have negligible interactions. It will thus be useful to consider wavepackets in the one particle sector. We thus start by considering linear combinations

$$|\psi\rangle = \int \mathrm{d}\mu(p)\, \psi(\boldsymbol{p})\, |\boldsymbol{p}\rangle \tag{3.4}$$

of the one particle state $|\boldsymbol{p}\rangle$ which satisfy

$$\boldsymbol{P}\,|\boldsymbol{p}\rangle = \boldsymbol{p}\,|\boldsymbol{p}\rangle \quad \text{and} \quad H\,|\boldsymbol{p}\rangle = E_{\boldsymbol{p}}\,|\boldsymbol{p}\rangle\,, \quad E_{\boldsymbol{p}} := \sqrt{m^2+\boldsymbol{p}^2}. \tag{3.5}$$

It is useful to use the relativistic invariant measure to construct this linear combination, which up to a constant is uniquely determined to be

$$\mathrm{d}\mu(p) := \đ^D p\, 2\pi\delta(p^2-m^2)\Theta(p^0) = \frac{\đ^d \boldsymbol{p}}{2E_{\boldsymbol{p}}}, \quad \đ^n := \frac{\mathrm{d}^n}{(2\pi)^n}. \tag{3.6}$$

We further choose the normalization

$$\langle \boldsymbol{p}|\boldsymbol{q}\rangle = 2E_{\boldsymbol{p}}(2\pi)^d\delta(\boldsymbol{p}-\boldsymbol{q}), \tag{3.7}$$

so that the resolution of the identity reads

$$\int \frac{\đ^d \boldsymbol{p}}{2E_{\boldsymbol{p}}}\; |\boldsymbol{p}\rangle\langle\boldsymbol{p}| = 1, \tag{3.8}$$

and we have $\psi(\boldsymbol{p}) = \langle \boldsymbol{p}|\psi\rangle$.

We can also construct a position wavefunction for such a state

$$\psi(x) = \int \mathrm{d}\mu(p)\, e^{-ip\cdot x}\psi(\boldsymbol{p}). \tag{3.9}$$

It satisfies the Klein-Gordon equation

$$(\Box + m^2)\psi = 0 \tag{3.10}$$

on account of μ having support on the hyperboloid $p^2 = m^2$.

The space of solutions to the Klein-Gordon equation is quite special. On account of it being cut by the equations of motion of an action

$$S(\bar\psi,\psi) = -\int \mathrm{d}^D x\, \bar\psi(\Box + m^2)\psi, \tag{3.11}$$

it can be thought of as a phase space. Accordingly, it has a symplectic structure, which we proceed to construct. The variation of the action takes the form

$$\delta S = \int \mathrm{d}^D x \, \delta\bar{\psi}(\cdots) + \int \mathrm{d}^D x \, (\cdots)\delta\psi - \int \mathrm{d}^D x \, \partial_\mu(\bar{\psi}\partial^\mu \delta\psi - \partial_\mu \bar{\psi}\delta\psi), \tag{3.12}$$

where the terms $(\cdots)$ vanish on the solutions to the Klein-Gordon equation. Thus, restricting to solutions that vanish at spatial infinity, we conclude that

$$\delta S = -\left[\int \mathrm{d}^d \boldsymbol{x} \left(\bar{\psi}\frac{\partial \delta\psi}{\partial t} - \frac{\partial \bar{\psi}}{\partial t}\delta\psi\right)\right]_{t=0}^{T}, \tag{3.13}$$

computing the action on a spacetime with a finite time interval $[0, T] \times \mathbb{R}^d$. In particular, taking another variation δ, the fact that $\delta^2 = 0$ shows that the symplectic form

$$\omega(\delta\bar{\psi}, \delta\psi) = \int \mathrm{d}^d \boldsymbol{x} \left(\delta\bar{\psi}\frac{\partial \delta\psi}{\partial t} - \frac{\partial \delta\bar{\psi}}{\partial t}\delta\psi\right), \tag{3.14}$$

on the space of solutions of the Klein-Gordon equation is time independent.

We finish this section noting that we chose a non-symmetric form of the Klein-Gordon action. Indeed, the asymmetry is controlled by the total derivative

$$S(\psi, \phi) - S(\phi, \psi) = \int \mathrm{d}^D x \, \partial_\mu(\phi\partial_\mu\psi - \partial_\mu\phi\psi). \tag{3.15}$$

In particular, if ψ is a solution to the equations of motion that vanishes at spatial infinity

$$S(\psi, \phi) = [\omega(\phi, \psi)]_{t=-\infty}^{\infty} \tag{3.16}$$

3.3 Exciting Single-Particle States

Local operators $\mathcal{O}(x)$ satisfy

$$e^{iP\cdot a}\mathcal{O}(x)e^{-iP\cdot a} = \mathcal{O}(x + a). \tag{3.17}$$

Throughout this dissertation we will use the notation $|\mathcal{O}\rangle = \mathcal{O}\,|\Omega\rangle$, commonly found in discussion of the GNS representation of an operator algebra [130]. Translation invariance of the vacuum then guarantees that

$$\langle P|\mathcal{O}(x)\rangle = e^{iP\cdot x}\,\langle P|\mathcal{O}(0)\rangle\,, \tag{3.18}$$

for states $|P\rangle$ with momentum P. In particular, $\langle\Omega|\mathcal{O}(x)\rangle = \langle\Omega|\mathcal{O}(0)\rangle$ is a constant. Furthermore, restricting to scalar operators as appropriate to the study of scalar single-particle operators in the following, Lorentz invariance further guarantees that $\langle p|\mathcal{O}(0)\rangle$ is Lorentz invariant.

Let us now consider a single particle state $|\psi\rangle$ defined in (3.4). Let us assume that the constant $\langle \boldsymbol{p}|\mathcal{O}^\dagger(0)\rangle \neq 0$. Through the redefinition

$$\mathcal{O}^\dagger(x) \mapsto \frac{1}{\langle \boldsymbol{p}|\mathcal{O}^\dagger(0)\rangle}(\mathcal{O}^\dagger(x) - \langle\Omega|\mathcal{O}^\dagger(0)\rangle), \tag{3.19}$$

we can assume without loss of generality that $\langle \boldsymbol{p}|\mathcal{O}^\dagger(0)\rangle = 1$ and $\langle\Omega|\mathcal{O}^\dagger(0)\rangle = 0$. We will now show that the state $|i\omega(\mathcal{O}^\dagger,\psi)\rangle$, which can be thought of as a smearing of the operator $\mathcal{O}^\dagger$ by a solution of the Klein-Gordon equation, coincides with $|\psi\rangle$ in the infinite past and future. This is done by studying the overlap of this state with the arbitrary definite-momentum states $|P = (E, \boldsymbol{P})\rangle$.

We first note that

$$\omega(\mathcal{O}^\dagger,\psi) = \int \mathrm{d}\mu(p) \int \mathrm{d}^d\boldsymbol{x}\, e^{-ip\cdot x}\left(\mathcal{O}^\dagger(-iE_{\boldsymbol{p}})\psi(\boldsymbol{p}) - \frac{\partial\mathcal{O}^\dagger}{\partial t}\psi(\boldsymbol{p})\right). \tag{3.20}$$

Furthermore, given (3.18), we have

$$\left\langle P\left|\frac{\partial\mathcal{O}^\dagger(x)}{\partial t}\right.\right\rangle = iE\,\langle P|\mathcal{O}^\dagger(x)\rangle\,. \tag{3.21}$$

We thus conclude that

$$\langle P|\omega(\mathcal{O}^\dagger,\psi)\rangle = -i\int \mathrm{d}\mu(p) \int \mathrm{d}^d\boldsymbol{x}\, e^{-i(p-P)\cdot x}\psi(\boldsymbol{p})(E_{\boldsymbol{p}} + E)\,\langle P|\mathcal{O}^\dagger(0)\rangle\,. \tag{3.22}$$

The integral over $\boldsymbol{x}$ then sets $\boldsymbol{p} = \boldsymbol{P}$, leaving us with

$$\langle P|\omega(\mathcal{O}^\dagger,\psi)\rangle = -ie^{-i(E_{\boldsymbol{P}}-E)t}\psi(\boldsymbol{P})\frac{E_{\boldsymbol{P}} + E}{2E_{\boldsymbol{P}}}\,\langle P|\mathcal{O}^\dagger(0)\rangle\,. \tag{3.23}$$

A trivial consequence of this calculation is that

$$\langle\Omega|\omega(\mathcal{O}^\dagger,\psi)\rangle = 0 = \langle\Omega|\psi\rangle\,. \tag{3.24}$$

A less trivial consequence is that

$$\langle \boldsymbol{p}|i\omega(\mathcal{O}^\dagger,\psi)\rangle = \psi(\boldsymbol{p}) = \langle \boldsymbol{p}|\psi\rangle\,. \tag{3.25}$$

Now, the crucial fact is that for multiparticle states we have

$$E^2 = P^2 + \boldsymbol{P}^2 > (2m)^2 + \boldsymbol{P}^2 = 3m^2 + E_{\boldsymbol{P}}^2 > E_{\boldsymbol{P}}^2, \tag{3.26}$$

which is where our assumption of a finite mass gap $m \neq 0$ is key. In particular, for those states the oscillations $e^{-i(E_{\boldsymbol{P}}-E)t}$ will annihilate the remaining inner products in the infinite past and future[2]. We thus conclude that

$$\lim_{t\to\pm\infty} \langle \Psi | i\omega(\mathcal{O}^\dagger, \psi)\rangle = \langle \Psi|\psi\rangle\,, \tag{3.27}$$

for generic states $|\Psi\rangle$ in the Hilbert space of our QFT.

We conclude that, in the limits $t \to \pm\infty$, the operator $i\omega(\mathcal{O}^\dagger, \psi)$ acts as a creation operator of a one-particle state $|\psi\rangle$. One would expect then that its adjoint $-i\omega(\mathcal{O}, \overline{\psi})$ would act as an annihilation operator. Indeed, conjugating the spatial wave function in the derivation of (3.23), would have led to

$$\langle P|\omega(\mathcal{O}, \overline{\psi})\rangle = ie^{i(E_{\boldsymbol{P}}+E)t}\bar{\psi}(\boldsymbol{P})\frac{E_{\boldsymbol{P}}-E}{2E_{\boldsymbol{P}}}\langle P|\mathcal{O}(0)\rangle\,. \tag{3.28}$$

In this case, the positivity of energy guarantees that, regardless of $|P\rangle$, the phase does not vanish. Therefore, we conclude that

$$\lim_{t\to\pm\infty} \langle \Psi| - i\omega(\mathcal{O}, \bar{\psi})\rangle = 0, \tag{3.29}$$

as expected.

3.4 LSZ Reduction Formula

We are now ready to derive the LSZ reduction formula. Our starting point will be the time-ordered correlators

$$\langle \Omega \,|\, \mathcal{T}\mathcal{O}(x_1)\cdots\mathcal{O}(x_n)\mathcal{O}^\dagger(y_1)\cdots\mathcal{O}^\dagger(y_m)\,|\,\Omega\rangle\,. \tag{3.30}$$

These can be computed in perturbation theory through Feynman diagrams[3]. Our objective is thus to extract from these the S-matrix.

In order to do this, we first consider (3.16) with

$$\phi(x) := \langle \Omega \,|\, \mathcal{T}A\mathcal{O}^\dagger(x)\,|\,\Omega\rangle\,. \tag{3.31}$$

In here A is an arbitrary operator that has no support at $t = x^0$. Then

$$i\int \mathrm{d}^D x\, \psi(-\Box - m^2)\phi = iS(\psi,\phi) = [i\omega(\phi,\psi)]_{t=-\infty}^{\infty}. \tag{3.32}$$

[2]This is true after smearing the states with wavefunctions that have support above the two-particle threshold

[3]Our diagrams lack disconnected tadpoles, on account of our condition $\langle\Omega|\mathcal{O}|\Omega\rangle = 0$, as well as vacuum components, for we assume $\langle\Omega|\Omega\rangle = 1$.

Since ϕ is linear in $\mathcal{O}^\dagger$ and the support of A is disjoint from the time slice at x^0, we conclude that

$$i \int \mathrm{d}^D x \, \psi(-\Box - m^2) \, \langle \Omega | \mathcal{T} A \mathcal{O}^\dagger(x) | \Omega \rangle = \langle \Omega \, | \, \mathcal{T} A [i\omega(\mathcal{O}^\dagger, \psi)]_{t=-\infty}^{\infty} \, | \, \Omega \rangle \, . \tag{3.33}$$

This is known as the LSZ reduction of the operator $\mathcal{O}^\dagger$, which replaces it in time-ordered vacuum correlation functions, by the differences of its associated out creation operator and in creation operator.

We can perform LSZ reduction iteratively on each of the operators appearing in (3.30). We then obtain

$$\begin{aligned} & i^{m+n} \int \prod_{i=1}^{n} \mathrm{d}^D x_i \, \bar{\phi}_i(x_i)(\Box_{x_i} + m^2) \prod_{j=1}^{m} \mathrm{d}^D y_j \, \psi_j(y_j)(\Box_{y_j} + m^2) \\ & \langle \Omega | \mathcal{T} \mathcal{O}(x_1) \cdots \mathcal{O}(x_n) \mathcal{O}^\dagger(y_1) \cdots \mathcal{O}^\dagger(y_m) | \Omega \rangle = \\ & \left\langle \Omega \right| \mathcal{T} \prod_{i=1}^{n} [-i\omega(\mathcal{O}, \bar{\phi}_i)]_{x_i^0=-\infty}^{\infty} \prod_{j=1}^{m} [i\omega(\mathcal{O}^\dagger, \psi_j)]_{y_j^0=\infty}^{-\infty} \left| \Omega \right\rangle \end{aligned} \tag{3.34}$$

The left-hand side of this equation, while long in position space, reduces to a simple prescription in momentum space. Taking the solutions of the Klein-Gordon equation ϕ_i and ψ_j to be plane waves, which would then have to be on-shell, the Klein-Gordon operators reduce to the pole piece of the propagators $p^2 - m^2$ in the external legs. In other words, this left-hand side computes the residue of (3.30) as the external legs of our Feynman diagrams go on-shell.

Our final goal will then be to show that

$$\begin{aligned} & \left\langle \Omega \right| \mathcal{T} \prod_{i=1}^{n} [-i\omega(\mathcal{O}, \bar{\phi}_i)]_{x_i^0=-\infty}^{\infty} \prod_{j=1}^{m} [i\omega(\mathcal{O}^\dagger, \psi_j)]_{y_j^0=\infty}^{-\infty} \left| \Omega \right\rangle \\ & = \langle \phi_1, \ldots, \phi_n | S | \psi_1, \ldots, \psi_m \rangle, \end{aligned} \tag{3.35}$$

Our main assumption in order to do this is to extend (3.27) to

$$\lim_{t \to \pm\infty} \langle \Psi | i\omega(\mathcal{O}^\dagger, \psi_1) \cdots i\omega(\mathcal{O}^\dagger, \psi_n) \rangle = \langle \Psi | \psi_1, \ldots, \psi_n \rangle_{\text{out/in}} \, . \tag{3.36}$$

We will assert this is the case as long as the velocity supports of all the Klein-Gordon solutions considered are different. This ensures that in the infinite past and future these wave packets will be infinitely far away from one another.

There are 2^{n+m} terms appearing in the left-hand side of (3.35). In each of these are $n+m$ limits, one for each of the time variables that will be considered. The order in which these limits are taken is immaterial to the full expression. But once it has been separated

into the sum of these 2^{n+m} terms, care must be taken to take the limits in the same order for each of the 2^{n+m} terms. For definiteness, let us assume that the y limits are taken first, in any order. Due to time ordering, the $y_j^0 \to \infty$ terms will vanish since they will annihilate $\langle\Omega|$. Therefore

$$\begin{aligned}&\left\langle \Omega \left| \mathcal{T} \prod_{i=1}^{n} [-i\omega(\mathcal{O}, \bar{\phi}_i)]_{x_i^0=-\infty}^{\infty} \prod_{j=1}^{m} [i\omega(\mathcal{O}^\dagger, \psi_j)]_{y_j^0=\infty}^{-\infty} \right| \Omega \right\rangle \\ &= \left\langle \Omega \left| \mathcal{T} \prod_{i=1}^{n} [-i\omega(\mathcal{O}, \bar{\phi}_i)]_{x_i^0=-\infty}^{\infty} \right| \psi_1, \dots, \psi_m \right\rangle_{\text{in}}\end{aligned} \tag{3.37}$$

The evaluation of the remaining limits is more delicate. Let us consider the $i = n$ limit next.

$$\begin{aligned}&\left\langle \Omega \left| \mathcal{T} \prod_{i=1}^{n} [-i\omega(\mathcal{O}, \bar{\phi}_i)]_{x_i^0=-\infty}^{\infty} \prod_{j=1}^{m} [i\omega(\mathcal{O}^\dagger, \psi_j)]_{y_j^0=\infty}^{-\infty} \right| \Omega \right\rangle \\ &= \left\langle \phi_n \left| \mathcal{T} \prod_{i=1}^{n-1} [-i\omega(\mathcal{O}, \bar{\phi}_i)]_{x_i^0=-\infty}^{\infty} \right| \psi_1, \dots, \psi_m \right\rangle_{\text{in}} \\ &- \left\langle \Omega \left| \mathcal{T} \prod_{i=1}^{n-1} [-i\omega(\mathcal{O}, \bar{\phi}_i)]_{x_i^0=-\infty}^{\infty} (-i\omega(\mathcal{O}, \bar{\phi}_n))_{x_n^0=-\infty} \right| \psi_1, \dots, \psi_m \right\rangle_{\text{in}}\end{aligned} \tag{3.38}$$

If $\bar{\phi}_n$ has a velocity support that does not overlap with all the initial wave packets ψ_i, as $t \to -\infty$ they will have no spatial overlap. Thus, based on (3.29), we will assume that $-i\omega(\mathcal{O}, \bar{\phi}_n)_{x_n^0=-\infty}$ also annihilates the state $|\psi_1, \dots, \psi_m\rangle_{\text{in}}$. In particular, the second term vanishes. Continuing along these lines, we conclude that as long as all the momenta involved in the scattering process are different, we have (3.35).

3.5 $2 \to 2$ Scattering

We now specialize to the case in which we have two particles in the initial and final state. For this case, in [163] a more detailed derivation is presented which, although assumes that all the momenta within the initial state are different from each other, and the same for the final state, does not require the assumption that the momenta in the final state are all different from the one in the initial state. For this, we specialize our previous relation to

$n, m = 2$

$$\begin{aligned}
&\left\langle \Omega \left| \mathcal{T} \prod_{i=1}^{2} [-i\omega(\mathcal{O}, \bar{\phi}_i)]_{x_i^0=-\infty}^{\infty} \prod_{j=1}^{2} [i\omega(\mathcal{O}^\dagger, \psi_j)]_{y_j^0=\infty}^{-\infty} \right| \Omega \right\rangle \\
&= \left\langle \phi_2 \left| [-i\omega(\mathcal{O}, \bar{\phi}_1)]_{x_1^0=-\infty}^{\infty} \right| \psi_1, \psi_2 \right\rangle_{\text{in}} \\
&\quad - \left\langle \Omega \left| \mathcal{T} [-i\omega(\mathcal{O}, \bar{\phi}_1)]_{x_1^0=-\infty}^{\infty} (-i\omega(\mathcal{O}, \bar{\phi}_2))_{x_2^0=-\infty} \right| \psi_1, \psi_2 \right\rangle_{\text{in}}
\end{aligned} \tag{3.39}$$

We now take our final limit

$$\begin{aligned}
&\left\langle \Omega \left| \mathcal{T} \prod_{i=1}^{2} [-i\omega(\mathcal{O}, \bar{\phi}_i)]_{x_i^0=-\infty}^{\infty} \prod_{j=1}^{2} [i\omega(\mathcal{O}^\dagger, \psi_j)]_{y_j^0=\infty}^{-\infty} \right| \Omega \right\rangle \\
&= {}_{\text{out}}\langle \phi_1, \phi_2 | \psi_1, \psi_2 \rangle_{\text{in}} - \left\langle \phi_2 \left| (-i\omega(\mathcal{O}, \bar{\phi}_1))_{x_1^0=-\infty} \right| \psi_1, \psi_2 \right\rangle_{\text{in}} \\
&\quad - \left\langle \phi_1 \left| -i\omega(\mathcal{O}, \bar{\phi}_2)_{x_2^0=-\infty} \right| \psi_1, \psi_2 \right\rangle_{\text{in}} \\
&\quad + \left\langle \Omega \left| (-i\omega(\mathcal{O}, \bar{\phi}_1))_{x_1^0=-\infty} (-i\omega(\mathcal{O}, \bar{\phi}_2))_{x_2^0=-\infty} \right| \psi_1, \psi_2 \right\rangle_{\text{in}}
\end{aligned} \tag{3.40}$$

The fourth term creates a single particle state in the bra, so that it cancels the third term. On the other hand, the second creates an in state

$${}_{\text{in}}\langle \phi_1, \phi_2 | \psi_1, \psi_2 \rangle_{\text{in}} = \langle \phi_1, \phi_2 | \psi_1, \psi_2 \rangle \,. \tag{3.41}$$

We thus conclude that we have

$$\begin{aligned}
&\left\langle \Omega \left| \mathcal{T} \prod_{i=1}^{2} [-i\omega(\mathcal{O}, \bar{\phi}_i)]_{x_i^0=-\infty}^{\infty} \prod_{j=1}^{2} [i\omega(\mathcal{O}^\dagger, \psi_j)]_{y_j^0=\infty}^{-\infty} \right| \Omega \right\rangle \\
&= \langle \phi_1, \phi_2 | S - 1 | \psi_1, \psi_2 \rangle
\end{aligned} \tag{3.42}$$

It is then clear that the LSZ reduction formula does not resolve the S-matrix, but rather the T-matrix defined by

$$S = 1 + iT. \tag{3.43}$$

Let us further take the limit in which the initial and final states have definite momentum. Single particle states $|\boldsymbol{p}\rangle$ have momentum space wavefunctions

$$\psi(\boldsymbol{q}) = (2\pi)^d 2E_{\boldsymbol{p}} \delta(\boldsymbol{p} - \boldsymbol{q}). \tag{3.44}$$

Then the corresponding position wavefunctions will be

$$\psi(x) = e^{-ip\cdot x}, \tag{3.45}$$

with $p^0 = E_{\boldsymbol{p}}$. The LSZ formula for these states then reduces to

$$\begin{aligned} &i^4 \int \prod_{i=1}^{2} \mathrm{d}^D x_i \, e^{iq_i\cdot x_i} (\Box_{x_i} + m^2) \prod_{j=1}^{2} \mathrm{d}^D y_j \, e^{-ip_j\cdot y_i} (\Box_{y_j} + m^2) \\ &\langle \Omega \,|\, \mathcal{T}\mathcal{O}(x_1)\mathcal{O}(x_2)\mathcal{O}^\dagger(y_1)\mathcal{O}^\dagger(y_2) \,|\, \Omega\rangle = i \,\langle q_1, q_2|T|p_1, p_2\rangle \,. \end{aligned} \tag{3.46}$$

Assuming the correlator involved decays sufficiently fast at infinity, we can integrate by parts to rewrite it in the form

$$\begin{aligned} &\prod_{i=1}^{2} \left(\frac{q_i^2 - m^2}{i} \right) \prod_{j=1}^{2} \left(\frac{p_j^2 - m^2}{i} \right) \\ &\int \prod_{i=1}^{2} \mathrm{d}^D x_i \, e^{iq_i\cdot x_i} \prod_{j=1}^{2} \mathrm{d}^D y_j \, e^{-ip_i\cdot y_i} \,\langle \Omega \,|\, \mathcal{T}\mathcal{O}(x_1)\mathcal{O}(x_2)\mathcal{O}^\dagger(y_1)\mathcal{O}^\dagger(y_2) \,|\, \Omega\rangle \\ &= i \,\langle q_1, q_2|T|p_1, p_2\rangle \,. \end{aligned} \tag{3.47}$$

Let us define

$$\mathcal{O}^\dagger(p) := \int \mathrm{d}^D x \, e^{-ip\cdot x} \mathcal{O}^\dagger(x) \quad \text{and} \quad \mathcal{O}(p) = (\mathcal{O}^\dagger(p))^\dagger. \tag{3.48}$$

These are chosen so that the operator $\mathcal{O}^\dagger(p)$ carries momentum p

$$\begin{aligned} [P_\mu, \mathcal{O}^\dagger(p)] &= \frac{1}{i} \frac{\partial}{\partial \epsilon^\mu} (e^{iP\cdot\epsilon} \mathcal{O}^\dagger(p) e^{-iP\cdot\epsilon})_{\epsilon=0} \\ &= \frac{1}{i} \frac{\partial}{\partial \epsilon^\mu}\bigg|_{\epsilon=0} \int \mathrm{d}^D x \, e^{-ip\cdot x} \mathcal{O}^\dagger(x+\epsilon) \\ &= \frac{1}{i} \frac{\partial}{\partial \epsilon^\mu}\bigg|_{\epsilon=0} \int \mathrm{d}^D x \, e^{-ip\cdot(x-\epsilon)} \mathcal{O}^\dagger(x) = p_\mu \mathcal{O}^\dagger(p), \end{aligned} \tag{3.49}$$

and $\mathcal{O}(p)$ carries momentum $-p$. Similarly, define $\langle A\rangle := \langle \Omega|\mathcal{T}A|\Omega\rangle$. We thus conclude that

$$\begin{aligned} &\prod_{i=1}^{2} \left(\frac{q_i^2 - m^2}{i} \right) \prod_{j=1}^{2} \left(\frac{p_j^2 - m^2}{i} \right) \langle \mathcal{O}(q_1)\mathcal{O}(q_2)\mathcal{O}^\dagger(p_1)\mathcal{O}^\dagger(p_2)\rangle \\ &= i \,\langle q_1, q_2|T|p_1, p_2\rangle \,. \end{aligned} \tag{3.50}$$

Given an action principle, the correlator in the left hand side can be expressed as a sum of Feynman diagrams. These have a single-valent vertex for each operator insertion in the correlator, as well as an arbitrary number of vertices coming from the action. Assuming the Feynman diagrams are expanded around the free action containing the physical mass

of the particles, the legs joining the operators insertions to the rest of the diagram are going to contribute the propagators

$$\prod_{i=1}^{2}\left(\frac{i}{q_i^2-m^2}\right)\prod_{j=1}^{2}\left(\frac{i}{p_j^2-m^2}\right). \tag{3.51}$$

Thus, the LSZ formula tells us that in order to extract the matrix elements of iT, we need to take these Feynman diagrams and erase the contribution from these legs. In other words, they have to be amputated.

We note that the argument above is not quite true for diagrams in which there is no scattering. Those diagrams instead only have two propagators, so that in the LSZ formula, they will go to 0 on-shell. Thus, we can consider only diagrams in which there is non-trivial scattering. Moreover, the condition $\langle\Omega|\Omega\rangle = 1$ guarantees we need not consider vacuum bubble components in our diagrams. Finally, the condition $\langle\mathcal{O}^\dagger\rangle = 0$, guarantees we don't have to consider tad poles attached to one of our operator insertions. We thus conclude that we need only consider connected Feynman diagrams.

For a translation invariant theory, we have

$$\langle\mathcal{O}(x_1)\mathcal{O}(x_2)\mathcal{O}^\dagger(y_1)\mathcal{O}^\dagger(y_2)\rangle = \langle\mathcal{O}(x_1-y_2)\mathcal{O}(x_2-y_2)\mathcal{O}^\dagger(y_1-y_2)\mathcal{O}^\dagger(0)\rangle. \tag{3.52}$$

In taking the Fourier transform, we can then do displacements $x \mapsto x - y_2$ in all variables of integration other than y_2. This trivializes the integral over y_2, which then yields an overall momentum conserving delta function

$$\langle\mathcal{O}(q_1)\mathcal{O}(q_2)\mathcal{O}^\dagger(p_1)\mathcal{O}^\dagger(p_2)\rangle \propto (2\pi)^D\delta(p_1+p_2-q_1-q_2). \tag{3.53}$$

In terms of Feynman diagrams, all the vertices in the theory will contain momentum conserving delta functions, and all momenta other than the ones attached to the external legs will be integrated over. We can use these delta functions to reduce the number of momentum integrals to integrals over a set of loop momenta. In doing so, there will be single momentum conserving overall delta function left. The usual Feynman rules in momentum space found in text books, compute Feynman diagrams without this momentum conserving delta function. Thus, defining

$$(2\pi)^D\delta(p_1+p_2-q_1-q_2)i\mathcal{M}(s,t) = \langle q_1,q_2|iT|p_1,p_2\rangle\,, \tag{3.54}$$

we conclude that the scattering amplitude $i\mathcal{M}$ is computed by the sum of all momentum-conserving, amputated, and connected $2\to 2$ Feynman diagrams. Due to Lorentz invariance, it only depends on the invariants we can form out of the four momenta involved in the process (restricted by momentum conservation)

$$s = (p_1+p_2)^2 \quad \text{and} \quad t = (p_1-q_1)^2 \tag{3.55}$$

3.6 Real-Time Estimators for Scattering Observables

To date, most applications of the LSZ formula rely on perturbative explorations of time ordered correlators (3.30) through Feynman diagrams. With the development of quantum technology, the possibility to estimate these in a nonperturbative way is opening up. The question we will answer in the remainder of this dissertation is whether these estimators can be used to obtain nonperturbative information on scattering amplitudes. Our answer is positive, and unlike the methodologies we have available through the information we have access to in classical computers, valid for general processes.

There are many potential challenges to the use of estimators of time-ordered correlators for the extraction of scattering amplitudes. The most obvious is, well, extracting the correlators themselves. The development of formulations such as the one presented in Chapter 2, along with further experimental and algorithmic advances are crucial for this. Throughout the rest of this dissertation we will assume this problem has been solved, so that estimators of time-ordered correlators can be produced with high accuracy.

Another potential issue is that of the lattice itself. In order to obtain results that accurately reflect the theory of interest, we need to ensure that we can study small lattice spacings. This is however just a specific example of a potential difficulty in the extraction of correlators. We will thus follow suit and assume that this can also be overcome and that correlators can be extracted at small lattice spacings.

If we believe that traditional Lattice QCD is a good guiding principle for the development of Lattice QCD, there is however a fundamental obstruction to the extraction of scattering amplitudes. Without overcoming it, the quantum Lattice QCD program is doomed to fail. This is the one of finite-volume effects. The theory of scattering heavily relies on the notion of asymptotic states discussed in Section 3.2. Such states in general do not exist in a finite volume.

The past years have seen impressive demonstrations of direct simulations of scattering processes in $d = 1$ quantum field theories. These can be done in large enough lattices in which one can safely assume that the incoming and outgoing particles are non-interacting. In other words, they are asymptotic scattering states. This, however, will likely not be the case in $d = 3$. The characteristic spatial length L of modern Lattice QCD calculations is of the order of $m_\pi L \sim 4$, with m_π the mass of a pion. Given that $1/m_\pi$ is the length scale of the strong interaction mediated by the pion, we see that in general these boxes are not big enough to admit several non-interacting particles in them. It is therefore crucial that we understand the finite-volume effects involved in our estimators and how they will introduce errors in our determinations of scattering amplitudes through them.

3.6.1 Spectral Structure of Estimators

In order to understand these finite-volume effects better, let us explore the spectral structure of the time-ordered correlators (3.30), mirroring the techniques used in Section A.6. For simplicity, let us consider a $2 \to 2$ scattering process, in which one of the initial and one of the outgoing particles has already undergone LSZ reduction

$$C(t, \boldsymbol{x}) = \langle \boldsymbol{p}_f | \mathcal{T} \mathcal{O}(t, \boldsymbol{x}) \mathcal{O}^\dagger(0) | \boldsymbol{p}_i \rangle \,. \tag{3.56}$$

A classical result [32] is that the finite-volume effects on single-particle states of a gapped theory are always exponentially suppressed. Thus, depending on algorithmic details, it might be more useful to consider correlators of this form, rather than the vacuum correlators in (3.30).

In any case, introducing the spectral decomposition of the Hamiltonian in the finite-volume, which as discussed in Section A.6 should be discrete, this correlator can be written in the form

$$C(t, \boldsymbol{x}) = \begin{cases} \sum_n e^{-it(E_n - E_{\boldsymbol{p}_f})} \langle \boldsymbol{p}_f | \mathcal{O}(\boldsymbol{x}) | n \rangle \langle n | \mathcal{O}^\dagger(0) | \boldsymbol{p}_i \rangle & t > 0, \\ \sum_n e^{-it(E_{\boldsymbol{p}_i} - E_n)} \langle \boldsymbol{p}_f | \mathcal{O}^\dagger(0) | n \rangle \langle n | \mathcal{O}(\boldsymbol{x}) | \boldsymbol{p}_i \rangle & t < 0. \end{cases} \tag{3.57}$$

The Fourier transform of this into energy space then yields

$$\begin{aligned} C(\omega, \boldsymbol{x}) &= \int \mathrm{d}t \, e^{-i\omega t - \varepsilon |t|} C(t, \boldsymbol{x}) \\ &= i \sum_n \left(\frac{\langle \boldsymbol{p}_f | \mathcal{O}(\boldsymbol{x}) | n \rangle \langle n | \mathcal{O}^\dagger(0) | \boldsymbol{p}_i \rangle}{E_{\boldsymbol{p}_f} - E_n - \omega + i\varepsilon} - \frac{\langle \boldsymbol{p}_f | \mathcal{O}^\dagger(0) | n \rangle \langle n | \mathcal{O}(\boldsymbol{x}) | \boldsymbol{p}_i \rangle}{E_n - E_{\boldsymbol{p}_i} - \omega - i\varepsilon} \right). \end{aligned} \tag{3.58}$$

This function is therefore a sum of poles at the finite-volume energies $\omega = E_{\boldsymbol{p}_f} - E_n$ or $\omega = E_n - E_{\boldsymbol{p}_i}$.

As $L \to \infty$, the finite-volume energy levels should condense, giving way to the continuum of states discussed in Section 3.1. Accordingly, in the infinite-volume limit the poles of $C(\omega)$ should condense into more complicated complex structures, such as branch cuts. In order to have a better feeling of this, let us introduce a toy model for this pole condensation phenomena.

Consider the function $f(z) = z^{-1/2}$ with its branch cut extended along the non-negative real axis $[0, \infty)$. This function is analytic away from this branch cut, so that the trajectory $\mathcal{C}$ in Fig. 3.1 can be deformed to an infinitesimal loop around any $z \in \mathbb{C} \setminus [0, \infty)$. This allows us to conclude that

$$f(z) = \frac{1}{2\pi i} \int_{\mathcal{C}} \mathrm{d}w \, \frac{f(w)}{w - z}. \tag{3.59}$$

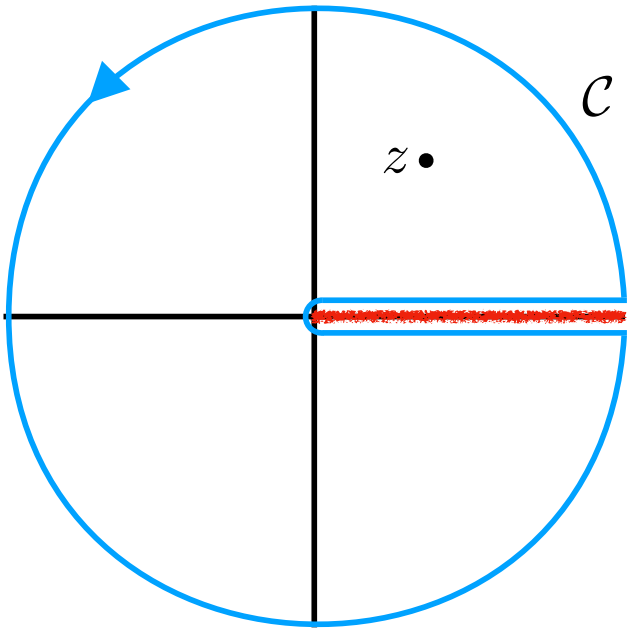


Figure 3.1: Example of a trajectory $\mathcal{C}$ that can be smoothly deformed to an infinitesimal loop around z without going through the positive real line.

Since f vanishes at infinity, we can omit the circular piece of the contour, restricting our attention to the pieces above and below $[0, \infty)$. Given that

$$f(w - i\epsilon) = -f(w + i\epsilon), \tag{3.60}$$

we conclude that for $z \in \mathbb{C} \setminus [0, \infty)$ we have

$$f(z) = \frac{1}{i\pi} \int_0^\infty \mathrm{d}x \, \frac{1}{\sqrt{x}(x - z)}. \tag{3.61}$$

In order to avoid the singularity at $x = 0$, let us recast this integral in terms of a variable $k = \sqrt{x}$, so that

$$f(z) = \frac{2}{i\pi} \int_0^\infty \mathrm{d}k \, \frac{1}{k^2 - z} = \frac{1}{i\pi} \int_{-\infty}^\infty \mathrm{d}k \, \frac{1}{k^2 - z} \tag{3.62}$$

Let us now consider a small Δk and a big integer N. We can define the estimator

$$f_{\Delta k}(z) := \frac{\Delta k}{i\pi} \sum_{n=-\infty}^{\infty} \frac{1}{(n\Delta k)^2 - z}, \tag{3.63}$$

which is simply the Riemann approximation to the integral expression for $f(z)$. Using exercise 3, one can show this has an analytic solution

$$f_{\Delta k}(z) = \frac{i}{\sqrt{z}} \cot\left(\frac{\pi\sqrt{z}}{\Delta k}\right) \tag{3.64}$$

Away from the branch cut, this Riemann approximation converges exponentially fast to the correct result, with a rate determined by the distance from the branch cut

$$f_{\Delta k}(z) - f(z) = \frac{2}{\sqrt{z}} \frac{e^{\frac{i2\pi\sqrt{z}}{\Delta k}}}{1 - e^{\frac{i2\pi\sqrt{z}}{\Delta k}}} = \mathcal{O}\Big(e^{-\frac{2\pi}{\Delta k}\,\mathrm{Im}\,\sqrt{z}}\Big) \tag{3.65}$$

At the branch cut, however, the estimator $f_{\Delta k}$ disagrees harshly with f. Rather than having a branch cut, it has poles at $z = (n\Delta k)^2$. However, as $\Delta k \to 0$, we should recover our original function f, thus yielding a toy model for the $L \to \infty$ limit.

3.6.2 The Proposal

Our toy model teaches us an important lesson. Given the difference between the analytic structures of correlation functions in finite and infinite volumes, one should not attempt to relate the two at real energies. Instead, one should attempt to relate them, at energies with a small imaginary part. Indeed, if this lands us in a regime of analyticity of these correlators, we can expect the finite-volume correlators to be good estimators for the infinite-volume ones. And if the region that we land in is not too far from the real axis, we expect the infinite-volume result to be itself close to the one at real energies. We can therefore apply the LSZ formalism to these amplitudes. This embodies the Real-Time Estimators for Scattering Observables (RESOs) proposal [83]. Quantum technologies are crucial to it, for they yield a general path towards the computation of the finite-volume real-time correlators. The energies in these can be shifted to the complex plane by taking a finite ϵ in (3.58).

In the following, we will show that indeed our intuition is correct. More precisely, we will prove, to all orders in perturbation theory, that the finite-volume effects on time-ordered correlators are indeed exponentially suppressed in the volume. The rate of this suppression is however controlled by the parameter ϵ in charge of displacing the energy into the complex plane. Thus, the larger the volume, the closer to real energies we can get. Since the estimated correlators are close to the infinite-volume ones, we expect LSZ reduction to allow us to extract generic scattering amplitudes. This has been explored numerically in [82].

The RESOs proposal also suggests a general technique for further reduction of finite-volume effects. The idea is to take advantage that a finite volume breaks invariance under Lorentz boosts, given that these mix space and time. Thus, in the finite-volume world,

even if we consider two kinematics which would be approximately related to each other by Lorentz transformations in an infinite volume, their corresponding finite-volume correlators need not be the same. Our same analysis in all orders perturbation theory will show that averaging over these kinematics reduces the finite-volume effects.

3.6.3 Finite-volume Effects on Feynman Diagrams

For the proof of RESOs, let us consider an arbitrary Feynman Diagram. We will restrict to scalar field theories for the moment. We will show that the result for these theories extends to general theories. Let us label the internal momenta by $k = (k^i)_{i=1}^{N_P}$ and the external momenta by $P = (P^A)_{A=1}^{N_E}$, so that our diagram has N_P internal legs and $N_E + 1$ external ones. We will further make a choice of independent loop momenta $\ell = (\ell^a)_{a=1}^{N_L}$, with N_L the number of loops. Accordingly, the internal momenta can be written as a linear combination of the external and loop momenta

$$k^i = f^i{}_a \, \ell^a + F^i{}_A \, P^A. \tag{3.66}$$

Introducing the notation

$$D(k^i) = \frac{i}{(k^i)^2 - m^2 + i\epsilon}, \tag{3.67}$$

we have that a generic Feynman diagram can be written as

$$iI = i^{N_V} \int \text{đ}^{N_L D}\ell \prod_{i=1}^{N_P} D(k^i). \tag{3.68}$$

In here $N_V = N_P - N_L + 1$ is the number of vertices and the integration measure is

$$\text{đ}^{N_L D}\ell := \prod_{a=1}^{N_L} \text{đ}^D \ell^a. \tag{3.69}$$

The parameter ϵ pushes the finite-volume energy levels into the complex plane. While not exactly the same as the regulator ε, used before, it plays an analogous role.

On a finite volume, the same contribution to the correlation function is obtained by replacing the integral over loop momenta for a sum over the allowed momenta. We will consider a hypercubic space with periodic boundary conditions

$$\Sigma = \mathbb{R}^d \diagup L\mathbb{Z}^d, \tag{3.70}$$

so that L^d is the volume of space. Thefore the allowed momenta is

$$\tilde{\Sigma} = \frac{2\pi}{L}\mathbb{Z}^d, \tag{3.71}$$

The Feynman diagram in the finite volume is then

$$iI_L = \frac{i^{N_V}}{L^{N_L d}} \int \prod_{a=1}^{N_L} \mathrm{đ}^{N_L}(\ell^a)^0 \sum_{\ell \in \tilde{\Sigma}^{N_L}} \prod_{i=1}^{N_P} D(k^i). \tag{3.72}$$

Alternatively, we can use the Poisson summation formula to write this in the form

$$iI_L = \sum_{\boldsymbol{n} \in \mathbb{Z}^{N_L d}} iI_{\boldsymbol{n}}, \tag{3.73}$$

with

$$iI_{\boldsymbol{n}} = i^{N_V} \int \mathrm{đ}^{N_L D} \ell \, e^{iLn_a \cdot \ell^a} \prod_{i=1}^{N_P} D(k^i). \tag{3.74}$$

In here $n = (n_a)_{a=1}^{N_L}$ is a choice of spatial vector $n_a = (0, \boldsymbol{n}_a)$ for each loop. In particular, the $\boldsymbol{n}^a = 0$ case corresponds to the infinite volume integral. Therefore, our task will be to compute the finite-volume effects $I_{\boldsymbol{n}}$ for $\boldsymbol{n} \neq 0$.

In order to do this, we employ Feynman parametrization, which allows us to write

$$\prod_{i=1}^{N_P} D(k^i) = (N_P - 1)! \int_{[0,1]^{N_P}} \mathrm{d}^{N_P} u \, \delta\left(1 - \sum_{i=1}^{N_P} u^i\right) \mathcal{D}^{N_P}, \tag{3.75}$$

with

$$i\mathcal{D}^{-1} = \sum_{i=1}^{N_P} u^i i D(k^i)^{-1}. \tag{3.76}$$

The latter is a quadratic form in the loop momenta

$$i\mathcal{D}^{-1} = g_{ab} \ell^a \cdot \ell^b + 2p_a \cdot \ell^a - \Delta + g^{ab} p_a \cdot p_b, \tag{3.77}$$

where

$$\begin{aligned} g_{ab} &= \sum_{i=1}^{N_P} u^i f^i{}_a f^i{}_b, \\ p_a &= \sum_{i=1}^{N_P} u^i f^i{}_a F^i{}_A P^A, \\ \Delta - g^{ab} p_a \cdot p_b &= -\sum_{i=1}^{N_P} u^i F^i{}_A F^i{}_B P^A \cdot P^B + m^2 - i\epsilon. \end{aligned} \tag{3.78}$$

When $u^i > 0$, the matrix g_{ab} determines a metric on loop space. Indeed, if there was a non-trivial v^a for which $f^i_a v^a = 0$, the shift $\ell^a \mapsto \ell^a + v^a$ would leave the internal momenta k^i invariant and the decomposition (3.66) would not be unique. Thus, we can define g^{ab}

to be its inverse. We will use these to raise and lower loop indices. This then also defines Δ if we take g^{ab} to be the inverse to g_{ab}.

Shifting $\ell^a \mapsto \ell^a + p^a$, this can be written simply as

$$i\mathcal{D}^{-1} = g_{ab}\ell^a \cdot \ell^b - \Delta. \tag{3.79}$$

The full finite-volume difference becomes

$$iI_{\boldsymbol{n}} = (N_P - 1)! \int_{[0,1]^{N_P}} \mathrm{d}^{N_P} u \, \delta\left(1 - \sum_{i=1}^{N_P} u^i\right) e^{-iLn_a \cdot p^a} iJ_{\boldsymbol{n}}, \tag{3.80}$$

with

$$iJ_{\boldsymbol{n}} := i^{N_V} \int \mathrm{đ}^{N_L D}\ell \, e^{iLn_a \cdot \ell^a} \mathcal{D}^{N_P}. \tag{3.81}$$

We will show that the factor of $e^{-iLn_a \cdot p^a}$ is responsible for reducing finite-volume effects, while the factor $iJ_{\boldsymbol{n}}$ is the exponentially suppressed factor.

Focusing first on the boost averaging, let us track down the Lorentz breaking artifacts. Let us start by discussing how the infinite-volume diagram (3.68) is indeed Lorentz invariant. This diagram depends on the external momenta via Lorentz invariant combinations

$$P^A \cdot P^B \quad \text{and} \quad P^A \cdot \ell^a. \tag{3.82}$$

Under a Lorentz transformation $P^A \mapsto \Lambda P^A$, the first is invariant, while the second is not. We can however perform the same transformation on the loop momenta $\ell^a \mapsto \Lambda \ell^A$, so that now the whole integrand is invariant. The integral remains invariant since the measure $\mathrm{đ}^D \ell^a$ is invariant under this transformation.

This same line of reasoning could be applied to (3.74). But in the last step, we now also alter the exponent $n_a \cdot \ell^a \mapsto n_a \cdot \Lambda \ell^a = \Lambda^{-1} n_a \cdot \ell^a$. Since the sum over $\boldsymbol{n}$ is not invariant under this transformation, the finite-volume diagrams are not Lorentz invariant, as expected. The power of Feynman parametrization (3.80), however, is that all the dependence on the external momenta of $iJ_{\boldsymbol{n}}$ is now contained in the scalars $P^A \cdot P^B$ in Δ. Therefore, it is manifestly Lorentz invariant, with no need to perform Lorentz transformations on the shifted loop momenta ℓ^a. The Lorentz breaking term has been isolated out of the loop integrals, to $e^{-iLn_a \cdot p^a} \mapsto e^{-iLn_a \cdot \Lambda p^a}$. Therefore, if we average over different Lorentz transformations,

$$\langle iI_{\boldsymbol{n}} \rangle = (N_P - 1)! \int_{[0,1]^{N_P}} \mathrm{d}^{N_P} u \, \delta\left(1 - \sum_{i=1}^{N_P} u^i\right) \langle e^{-iLn_a \cdot p^a} \rangle \, iJ_{\boldsymbol{n}}. \tag{3.83}$$

In general

$$| \langle e^{-iLn_a \cdot p^a} \rangle | \leq 1, \tag{3.84}$$

so the cancellations in these phases gives rise to a suppression of the finite-volume effects.

Before moving on, it should be noted that in practice this boost averaging, cannot be done by directly applying Lorentz transformations. Indeed, given some kinematics P^A that are accessible in the finite volume, the kinematics ΛP^A will in general not be accessible. Instead, we must do a binning in the Lorentz invariants, that is wide enough so that we have several P^A whose invariants lie in these bins. If the bins are too wide, however, the results might become worse, simply because the amplitude we are ultimately interested in might vary too much within the bin. To our knowledge, this has to be studied on a case by case basis through numerical methods. Examples of this are given in [82].

We now turn to the exponential suppression of $J_{\boldsymbol{n}}$. Since this factor is Lorentz invariant, the standard methods for manipulation of Feynman diagrams give a closed formula for it. First, let us introduce a basis of loop space e^a_α that diagonalizes the metric $g_{ab}e^a_\alpha e^b_\beta = \delta_{\alpha\beta}$, i.e. a vielbein. In this basis the loop momenta has components $\ell^a = q^\alpha e^a_\alpha$, and we can write

$$iJ_{\boldsymbol{n}} = i^{N_V}\int \text{đ}^{N_L D}q\, g^{-D/2}e^{iLn_\alpha\cdot q^\alpha}\mathcal{D}^{N_P}, \tag{3.85}$$

with $g = \det g_{\bullet\bullet}$ and $n_\alpha = n_a e^a_\alpha$. The integrand is particularly simple in this basis

$$i\mathcal{D}^{-1} = q^2 - \Delta, \tag{3.86}$$

with $q^2 = \delta_{\alpha\beta}q^\alpha\cdot q^\beta$. In particular, under the Wick rotation $e^{i\theta}(q^\alpha)^0$, where $\theta\in[0,\pi/2]$, we have

$$\text{Im}(i\mathcal{D}^{-1}) = \sin(2\theta)\delta_{\alpha\beta}(q^\alpha)^0(q^\beta)^0 + \epsilon \geq \epsilon > 0. \tag{3.87}$$

Thus, Wick rotation avoids all potential poles and we can set

$$J_{\boldsymbol{n}} = \int \text{đ}^{N_L D}q\, g^{-D/2}e^{iLn_\alpha\cdot q^\alpha}\mathcal{D}_E^{N_P}, \tag{3.88}$$

where all inner products in this expression are now Euclidean and

$$\mathcal{D}_E^{-1} = q^2 + \Delta. \tag{3.89}$$

The next step is to apply Schwinger parametrization, with which we set

$$\mathcal{D}_E^{N_P} = \frac{1}{(N_P-1)!}\int_0^\infty \text{d}s\, s^{N_P-1}e^{-s(q^2+\Delta)}. \tag{3.90}$$

The integration over the loop momenta then becomes Gaussian

$$\int \text{đ}^{N_L D}q e^{-s(q^2+\Delta)-iLn_\alpha\cdot q^\alpha} = (4\pi s)^{-N_L D/2}e^{-\frac{L^2n^2}{4s}-s\Delta}, \tag{3.91}$$

with $n^2 = \delta_{\alpha\beta} n^\alpha \cdot n^\beta = g_{ab} n^a \cdot n^b$. Furthermore, the remaining integral over s can be done exactly in terms of modified Bessel functions of the second kind

$$\int_0^\infty \mathrm{d}s\, s^{-\nu/2-1} e^{-\frac{L^2 n^2}{4s} - s\Delta} = 2\left(\frac{2\sqrt{\Delta}}{L\|n\|}\right)^{\nu/2} K_{\nu/2}(L\|n\|\sqrt{\Delta}), \tag{3.92}$$

with $\|n\| = \sqrt{n^2}$ and $\nu = N_L D - 2N_P$ the dimension of the diagram. We thus conclude that

$$J_{\boldsymbol{n}} = \frac{2}{(4\pi)^{N_L D/2}(N_P - 1)! g^{D/2}} \left(\frac{2\sqrt{\Delta}}{L\|n\|}\right)^{\nu/2} K_{\nu/2}(L\|n\|\sqrt{\Delta}). \tag{3.93}$$

This closed formula now allows us to study the large L asymptotics of this the finite-volume effects

$$|K_{\nu/2}(L\|n\|\sqrt{\Delta})| \sim \sqrt{\frac{\pi}{2L\|n\||\sqrt{\Delta}|}} e^{-L\|n\| \operatorname{Re}\sqrt{\Delta}}. \tag{3.94}$$

Since for bigger $\|n\|$ the less suppression of $I_{\boldsymbol{n}}$ is bigger, restricting to smaller $\boldsymbol{n}$ case yields the dominant suppression structure. This completes our proof of exponential suppression for scalar theories. It immediately extends to general theories with more general propagators by taking derivatives with respect to n_a in (3.74).

Note that, since $\operatorname{Im}\Delta = -\epsilon < 0$, we have

$$\operatorname{Re}\sqrt{\Delta} \approx \begin{cases} \sqrt{|\Delta|}, & \operatorname{Re}\Delta > 0 \\ \frac{\epsilon}{2\sqrt{|\Delta|}}, & \operatorname{Re}\Delta < 0. \end{cases} \tag{3.95}$$

Whenever $\operatorname{Re}\Delta > 0$ throughout the u integration, the rate of this suppression is dominated by the kinematics one is interested in. However, in kinematic regimes in which $\operatorname{Re}\Delta < 0$, the rate is controlled by $\epsilon/\sqrt{|\Delta|}$. Therefore, suppression of finite volume effects requires one to have $L\epsilon$ to be much bigger than the energy scales involved in the process.

On top of the exponential suppression, there are also power law components to the finite-volume effects

$$J_{\boldsymbol{n}} \sim L^{-(\nu+1)/2}. \tag{3.96}$$

In particular, as D increases, the finite-volume effects are suppressed. The same is true as the number of loops increases, hinting that this result might hold at a nonperturbative level. On the other hand, as the number of propagators increases, which is usually the case as the external kinematics becomes more complex, the finite-volume effects are enhanced. This is at the root of the difficulty behind finding a general prescription for the study of generic reactions in traditional Lattice QCD.

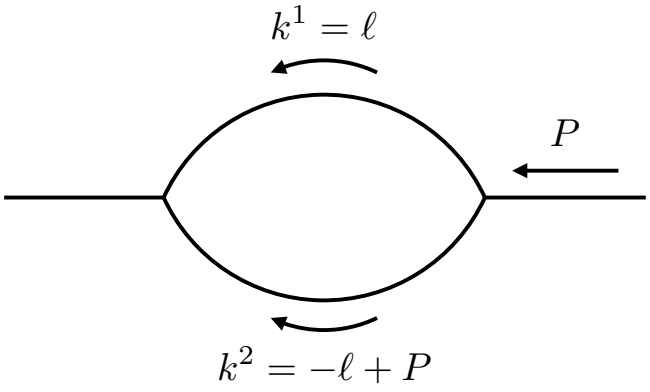


Figure 3.2: Bubble diagram.

3.6.4 Bubble Diagrams

As an example of these techniques, let us consider the bubble diagram Fig. 3.2. For this diagram we have $N_L = 1$, $N_P = 2$, $N_E = 1$, and $\nu = D - 4$. The reconstruction of the propagators is done through the matrices

$$f^i_{\ a} = \begin{pmatrix} 1 \\ -1 \end{pmatrix}^i_{\ a} \quad \text{and} \quad F^i_{\ A} = \begin{pmatrix} 0 \\ 1 \end{pmatrix}. \tag{3.97}$$

These lead to a trivial metric

$$g_{ab} = \left(u^1 + u^2 = 1\right)_{ab}, \tag{3.98}$$

and the rescaled momenta

$$p_a = \left(-u^2 P\right)_a. \tag{3.99}$$

The energy scale is given by

$$\Delta = -u^2(1-u^2)P^2 + m^2 - i\epsilon, \tag{3.100}$$

whose real part is bounded as

$$-\frac{1}{4}P^2 + m^2 \leq \mathrm{Re}\,\Delta \leq m^2, \tag{3.101}$$

for timelike P. In particular, we see that the transition of the regimes of finite-volume suppression is precisely when the CM energy $E^* = \sqrt{P^2} > 2m$, which is when the intermediate particles in the diagram can go on-shell. This is always the case for incoming two-particle states, leading to the famous finite-volume power law effects in these diagrams at the basis of Lüscher's method [35, 40]. On the other hand, when this diagram appears as a correction to the mass and wavefunction renormalizations of a single-particle operator, $P^2 \sim m^2$ and finite-volume effects are suppressed [32].

The finite-volume effects are finally given by

$$I_{\boldsymbol{n}} = \frac{2}{(4\pi)^{D/2}} \left(\frac{2}{L\|\boldsymbol{n}\|} \right)^{\frac{D-4}{2}} \int_0^1 \mathrm{d}u \, e^{-iuL\boldsymbol{n}\cdot\boldsymbol{P}} \Delta^{\frac{D-4}{4}} K_{\frac{D-4}{2}}(L\|\boldsymbol{n}\|\sqrt{\Delta}), \tag{3.102}$$

where we have replaced $u^2 \mapsto u$. The regime change across $E^\star = 2m$ is shown in Figs. 3.3 and 3.4. We can also show numerically the effects of boost averaging through the following thought experiment. Assume the incoming momentum $P = (E, \boldsymbol{P})$ is that of a two particle state

$$\begin{aligned} E &= \sqrt{m^2 + \boldsymbol{p}_1^2} + \sqrt{m^2 + \boldsymbol{p}_2^2}, \\ \boldsymbol{P} &= \boldsymbol{p}_1 + \boldsymbol{p}_2. \end{aligned} \tag{3.103}$$

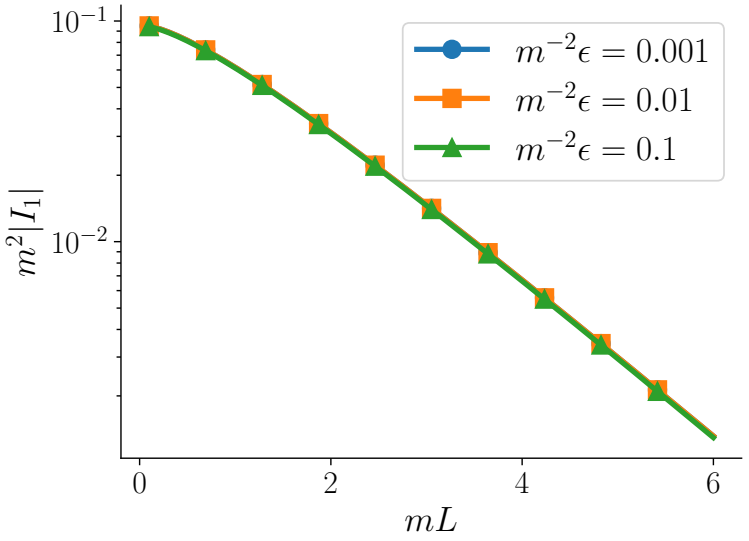
Furthermore, assume that scattering is happening on a lattice with lattice spacing a, so that the number of accessible single-particle momenta is L/a. Of course, in practice, only a subset of this momenta can be resolved in numerical calculations. We can then search for all accessible kinematics $\boldsymbol{p}_1$ and $\boldsymbol{p}_2$ on this lattice such that P^2 is within a target s up to some tolerance. Averaging over these kinematics, lowers the finite-volume error as shown in Fig. 3.5.

3.6.5 Applications to Traditional Lattice QCD

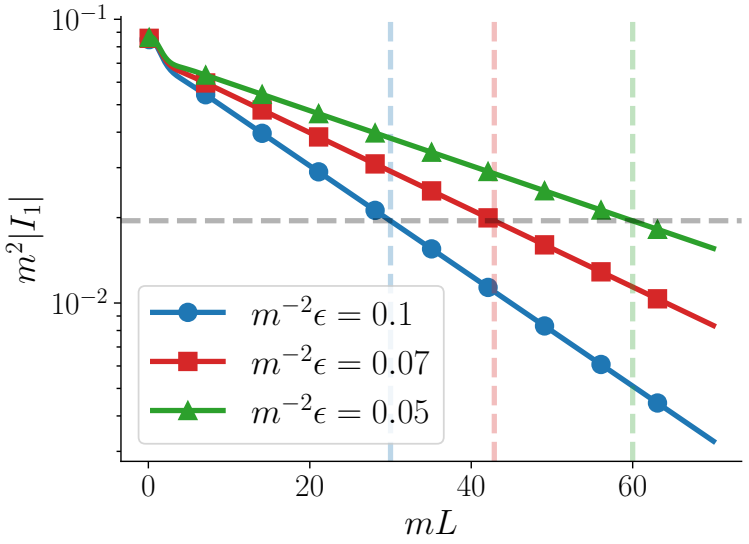
In traditional Lattice QCD, mappings between Euclidean observables and scattering amplitudes often require the calculation of the finite-volume effects of Feynman diagrams like the ones we are considering at $\epsilon = 0$. In here, the universal exponential suppression at the heart of quantum applications is non-existent, leading instead to polynomial errors in certain kinematic regimes. To finish this dissertation, we will provide evidence that our results can be used to furnish closed formulas that can be used to do these calculations up to corrections that are exponentially suppressed in the kinematics.

Let us restrict to the bubble diagram, whose finite-volume effects are (3.102). First, let us make the change of variables $v = u - \frac{1}{2}$ so that

$$\Delta = sv^2 - \|\boldsymbol{p}^\star\|^2 - i\epsilon, \tag{3.104}$$

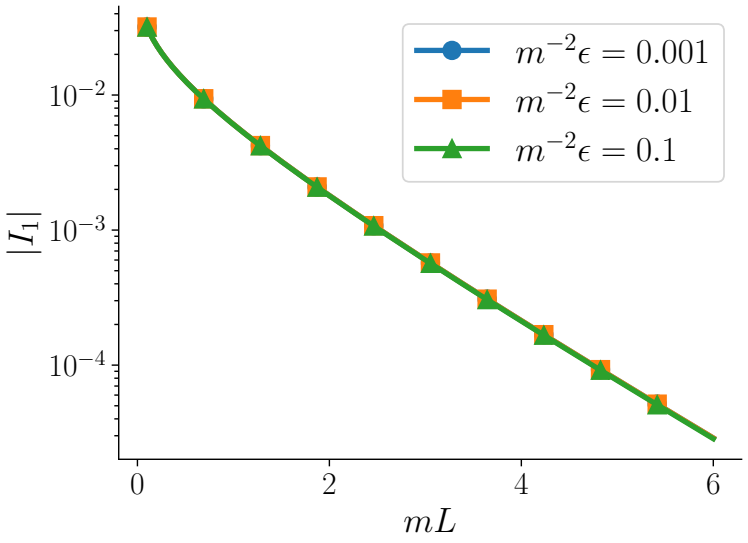


(a)

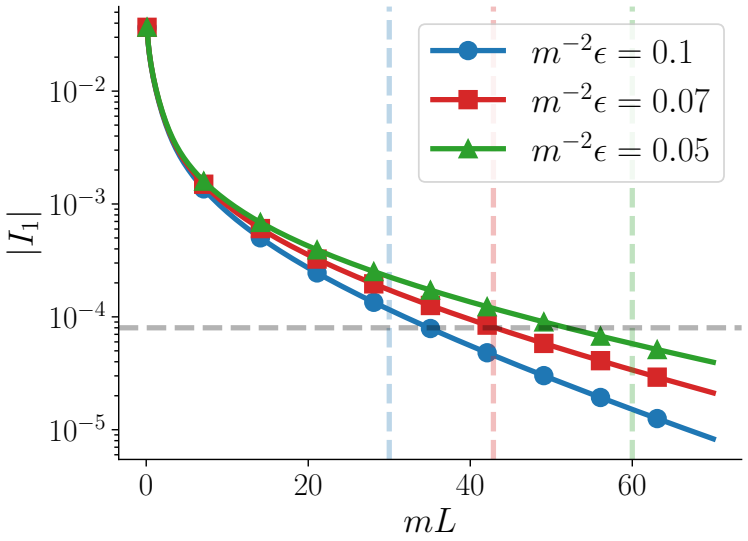


(b)

Figure 3.3: Finite-Volume effects for the bubble diagram in Fig. 3.2 in $D = 2$ with $\boldsymbol{n} = 1$. Calculations were done in the CM frame. (a) was done below the two particle threshold $E^* = m < 2m$. The overlapping lines show that the suppression of finite-volume effects is independent of ϵ. (b) was done above the two particle threshold $E^* = 3m > 2m$. Vertical dashed lines correspond to $\epsilon L/E^* = 1$, which marks the transition in which the exponential suppression starts becoming considerable. The Horizontal dashed line is a visual aid.



(a)



(b)

Figure 3.4: $D = 4$ correspondence to Fig. 3.3 with $\|\boldsymbol{n}\| = 1$. Note that the suppression at large L is enhanced by comparison with the $D = 2$ case due to the power law effects.

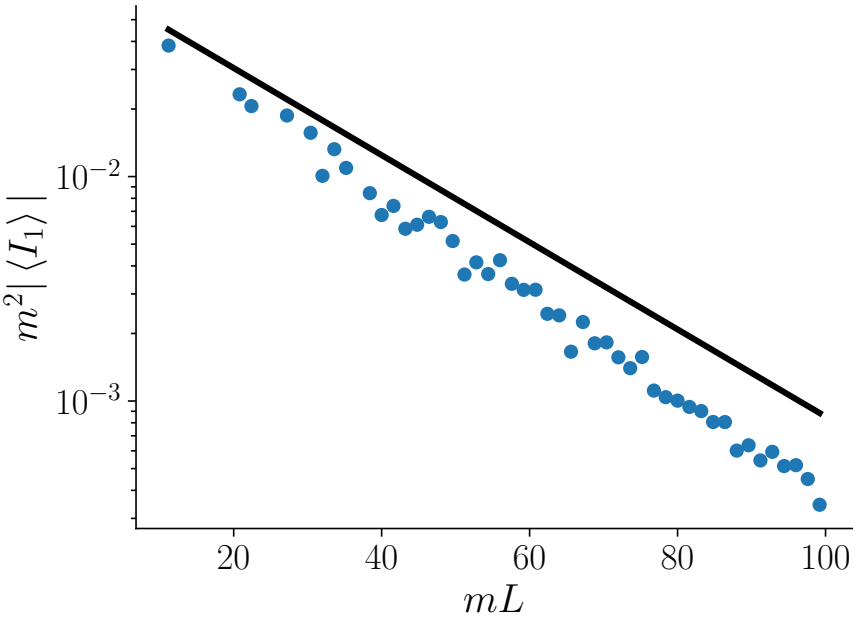


Figure 3.5: Finite-volume effects for the bubble diagram in $D = 2$. Black line shows the results in the CM frame for $E_0^* = \sqrt{s_0} = 3m$. Blue dots correspond to averaging over all kinematics of a two-particle state in which none of the particles have momentum higher than $\frac{\pi}{8a}$ and where their corresponding s is within 1% of s_0. The lattice spacing is taken to be $ma = 0.1$

in terms of the momentum of a particle in the CM frame of a two particle state with momentum P,

$$\|\boldsymbol{p}^\star\|^2 = \frac{s}{4} - m^2, \tag{3.105}$$

In here $s = (E^\star)^2 = P^2$. Then we have

$$\begin{aligned} I_{\boldsymbol{n}} &= \frac{2}{(4\pi)^{D/2}} \left(\frac{2}{L\|\boldsymbol{n}\|}\right)^{\frac{D-4}{2}} e^{iL\boldsymbol{n}\cdot\boldsymbol{P}/2} \times \\ &\quad \int_{-\frac{1}{2}}^{\frac{1}{2}} \mathrm{d}v\, e^{ivL\boldsymbol{n}\cdot\boldsymbol{P}} \Delta^{\frac{D-4}{4}} K_{\frac{D-4}{2}}(L\|\boldsymbol{n}\|\sqrt{\Delta}) \\ &= \frac{4}{(4\pi)^{D/2}} \left(\frac{2}{L\|\boldsymbol{n}\|}\right)^{\frac{D-4}{2}} e^{iL\boldsymbol{n}\cdot\boldsymbol{P}/2} \times \\ &\quad \int_{0}^{\frac{1}{2}} \mathrm{d}v\, \cos(vL\boldsymbol{n}\cdot\boldsymbol{P}) \Delta^{\frac{D-4}{4}} K_{\frac{D-4}{2}}(L\|\boldsymbol{n}\|\sqrt{\Delta}) \end{aligned} \tag{3.106}$$

We can now ask, what would happen if we extended the integration range to $v \in \mathbb{R}$. The error in the integral would be

$$\int_{\frac{1}{2}}^{\infty} \mathrm{d}v\, \cos(vL\boldsymbol{n}\cdot\boldsymbol{P}) \Delta^{\frac{D-4}{4}} K_{\frac{D-4}{2}}(L\|\boldsymbol{n}\|\sqrt{\Delta}). \tag{3.107}$$

In this region Δ goes from $m^2 - i\epsilon$ to $\infty - i\epsilon$. Then the asymptotics of the modified Bessel function of the second kind, shows that this integral is of order $e^{-mL\|n\|}$. Thus, if we content ourselves with giving a closed formula up to corrections suppressed by the kinematics, we have

$$\begin{aligned} I_{\boldsymbol{n}} &= \frac{4}{(4\pi)^{D/2}} \left(\frac{2}{L\|\boldsymbol{n}\|}\right)^{\frac{D-4}{2}} e^{iL\boldsymbol{n}\cdot\boldsymbol{P}/2} \times \\ &\quad \int_{0}^{\infty} \mathrm{d}v\, \cos(vL\boldsymbol{n}\cdot\boldsymbol{P}) \Delta^{\frac{D-4}{4}} K_{\frac{D-4}{2}}(L\|\boldsymbol{n}\|\sqrt{\Delta}). \end{aligned} \tag{3.108}$$

It turns out that this integral has a closed form [164], which we repeat here for convenience of the reader

$$\begin{aligned} &\int_0^\infty \mathrm{d}t\, t^{s+1} J_s(\rho t)(t^2+\xi^2)^{-\nu/2} K_\nu(a\sqrt{t^2+\xi^2}) = \\ &\frac{\rho^s}{a^\nu}\left(\frac{\sqrt{a^2+\rho^2}}{\xi}\right)^{\nu-s-1} K_{\nu-s-1}(\xi\sqrt{a^2+\rho^2}). \end{aligned} \tag{3.109}$$

In particular, if we take $s \mapsto -1/2$, the Bessel function of the first kind satisfies

$$\sqrt{t} J_{-1/2}(\rho t) = \sqrt{\frac{2}{\pi\rho}} \cos(\rho t). \tag{3.110}$$

Moreover, we have $K_\nu = K_{-\nu}$. Thus, we can employ the corollary

$$\begin{aligned} &\int_0^\infty \mathrm{d}t \, \cos(\rho t)(t^2+\xi^2)^{\nu/2} K_\nu(a\sqrt{t^2+\xi^2}) = \\ &\sqrt{\frac{\pi}{2}} a^\nu \left(\frac{\xi}{\sqrt{a^2+\rho^2}} \right)^{\nu+1/2} K_{\nu+1/2}(\xi\sqrt{a^2+\rho^2}). \end{aligned} \tag{3.111}$$

We now take

$$\begin{aligned} t &\mapsto v \\ \nu &\mapsto \frac{D-4}{2} \\ \rho &\mapsto L\boldsymbol{n}\cdot\boldsymbol{P} \\ \xi^2 &\mapsto -\frac{\|\boldsymbol{p}^\star\|^2 + i\epsilon}{s} \\ a &\mapsto L\|n\|E^\star. \end{aligned} \tag{3.112}$$

The formula assumes that we define ξ to have a positive real part. Therefore, taking $\epsilon \to 0^+$, we have

$$\xi \mapsto -i\|\boldsymbol{p}^\star\|/E^\star. \tag{3.113}$$

With this we have

$$\begin{aligned} t^2+\xi^2 &\mapsto \frac{\Delta}{s}, \\ \rho t &\mapsto vL\boldsymbol{n}\cdot\boldsymbol{P}, \\ a\sqrt{t^2+\xi^2} &\mapsto L\|n\|\sqrt{\Delta}, \\ a^2+\rho^2 &\mapsto L^2\|n\|^2 s + L^2(\boldsymbol{n}\cdot\boldsymbol{P})^2 =: sL^2\|\Lambda\boldsymbol{n}\|^2 \\ \nu+\frac{1}{2} &\mapsto \frac{D-3}{2}. \end{aligned} \tag{3.114}$$

In here we have defined the length scale

$$\|\Lambda\boldsymbol{n}\| = \sqrt{\|\boldsymbol{n}\|^2 + \frac{(\boldsymbol{n}\cdot\boldsymbol{P})^2}{s}}, \tag{3.115}$$

which is simply the length of the vector $\boldsymbol{n}$ in the reference frame obtained through a boost Λ into the CM frame. These conventions set

$$\begin{aligned} &s^{\frac{4-D}{4}} \int_0^\infty \mathrm{d}v\, \cos(vL\boldsymbol{n}\cdot\boldsymbol{P})\Delta^{\frac{D-4}{4}} K_{\frac{D-4}{2}}(L\|\boldsymbol{n}\|\sqrt{\Delta}) = \\ &\sqrt{\frac{\pi}{2}}(L\|\boldsymbol{n}\|E^*)^{\frac{D-4}{2}}\left(\frac{-i\|\boldsymbol{p}^\star\|}{sL\|\Lambda\boldsymbol{n}\|}\right)^{\frac{D-3}{2}} K_{\frac{D-3}{2}}(-iL\|\boldsymbol{p}^\star\|\|\Lambda\boldsymbol{n}\|). \end{aligned} \tag{3.116}$$

Plugging this into the finite-volume errors we conclude that

$$\begin{aligned} I_{\boldsymbol{n}} &= \frac{e^{iL\boldsymbol{n}\cdot\boldsymbol{P}/2}}{2(2\pi)^{\frac{D-1}{2}}\sqrt{s}}\left(\frac{-i\|\boldsymbol{p}^\star\|}{L\|\Lambda\boldsymbol{n}\|}\right)^{\frac{D-3}{2}} K_{\frac{D-3}{2}}(-iL\|\boldsymbol{p}^\star\|\|\Lambda\boldsymbol{n}\|) \\ &= \left\{\begin{array}{ll} \frac{i}{4E^\star\|\boldsymbol{p}^\star\|} & D=2 \\ \frac{1}{8\pi E^\star L\|\Lambda\boldsymbol{n}\|} & D=4 \end{array}\right\} e^{iL\|\boldsymbol{p}^\star\|\|\Lambda\boldsymbol{n}\|+iL\boldsymbol{n}\cdot\boldsymbol{P}/2}, \end{aligned} \tag{3.117}$$

up to exponentially suppressed corrections. Note that the first phase is always a sign since $\boldsymbol{P} = \frac{2\pi}{L}\boldsymbol{d}$, and thus

$$e^{iL\boldsymbol{n}\cdot\boldsymbol{P}/2} = (-1)^{\boldsymbol{n}\cdot\boldsymbol{d}}. \tag{3.118}$$

We have included the specific cases in $D=2$ and $D=4$ which agree with the results in the literature [40, 80, 165].

This shows evidence that Eqs. (3.80) and (3.93) can be used as the basis for the general exploration of finite-volume effects in the limit $\epsilon \to 0^+$ as well, which is the limit of interest to many applications in traditional Lattice QCD. It should however be noted that the associated sums obtained from Poisson summation are in general divergent for $\epsilon = 0$. Thus, naively, the $\epsilon \to 0^+$ limit has to be obtained through an extrapolation procedure.

An exciting alternative can be seen by studying the $D=2$ bubble diagram in closer detail. In here, $\|\Lambda\boldsymbol{n}\| = \gamma\|\boldsymbol{n}\|$, where $\gamma = E/E^*$. Thus, we are left with a geometric sum

$$\begin{aligned} I_L &= \frac{i}{4E^\star\|\boldsymbol{p}^\star\|}\sum_{\boldsymbol{n}\neq 0} e^{iL\gamma\|\boldsymbol{p}^*\|\|\boldsymbol{n}\|}(-1)^{\boldsymbol{n}\cdot\boldsymbol{d}} \\ &= \frac{i}{2E^*\|\boldsymbol{p}^*\|}\sum_{\boldsymbol{n}=1}^{\infty} e^{iL\gamma\|\boldsymbol{p}^*\|\|\boldsymbol{n}\|}(-1)^{\|\boldsymbol{n}\|\boldsymbol{d}} = \frac{i}{2E^\star\|\boldsymbol{p}^\star\|}\frac{1}{(-1)^{\boldsymbol{d}}e^{-iL\gamma\|\boldsymbol{p}^\star\|}-1}. \end{aligned} \tag{3.119}$$

In here we have used the result

$$\sum_{n=0}^{\infty} x^n = \frac{1}{1-x}, \tag{3.120}$$

which is valid only when $|x|<1$. In here however used it for a phase $|x|=1$. If we had maintained ϵ, the phase would have been multiplied by a dampening factor, required to guarantee convergence of this sum. Thus, our result holds. It however does beg whether

there is a procedure that can be generalized in order to resum the divergent $\epsilon = 0$ series and obtain the correct answer directly. This is particularly exciting since, it is often the case, that divergent series converge faster than convergent ones!

Let us mention one potential solution, namely that of Padé resummation. At its heart is the realization that the convergence rate of Taylor series is affected by the requirement that these series must converge on disks. Indeed, the sum $1 + x + x^2 + \cdots$ cannot converge for $|x| > 1$ since at $x = 1$ its analytic continuation $1/(1 - x)$ has a pole. But what if we attempted to approximate a Taylor series by, say, a continued fraction

$$a_0 + a_1 x + a_2 x^2 + \cdots = b_0 + \frac{c_0 x}{b_1 + \frac{c_1 x}{b_2 + \cdots}}, \tag{3.121}$$

Well, for the series $1 + x + x^2 + \cdots$, the continued fraction approximation would be exact after the first step and would converge everywhere except at $x = 1$. After all, $1/(1 - x)$ is a continued fraction!

Any truncation of a continued fraction is a ratio of polynomials. Thus, Padé summation of a potentially divergent series $a_0 + a_1 + \cdots$ builds a matrix whose (L, M) entry is a ratio

$$\frac{A_0 + A_1 x + \cdots + A_L x^L}{1 + B_1 x + \cdots + B_M x^M}, \tag{3.122}$$

defined so that its first $L+M+1$ Taylor coefficients coincide with those of $a_0+a_1 x+a_2 x^2+\cdots$. The Padé approximation is then obtained by taking $x = 1$ and L and M large. As we already saw, for the bubble diagram in $D = 2$, Padé summation converges immediately. In order to give evidence that these resummation techniques warrant further study for the general study of finite-volume effects, in Fig. 3.6 we show the results of applying Padé resummation to a series in $D = 4$ whose terms have been organized by the norm of their associated $\boldsymbol{n}$.

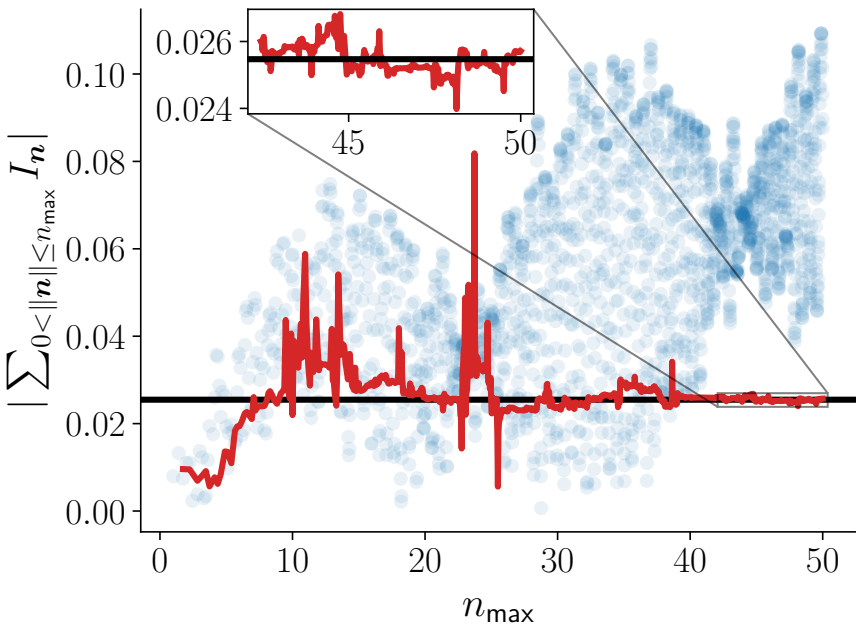


Figure 3.6: Approximations to I_L for the bubble diagram Fig. 3.2 at $D = 4$. Calculations were done in the CM frame with $E^\star = 3m$ and $\epsilon = 0$. Blue dots correspond to the naive results, which lead to a divergent series. The red line corresponds to the diagonal elements of the Padé table where the terms have been organized by $\|\boldsymbol{n}\|$. The black horizontal line corresponds to the result through an implementation of the more traditional methods [53].

Chapter 4

Conclusions and the Path Forward

This dissertation has, both, shown advances towards a formulation of QCD amenable to quantum computation in Chapter 2, and towards a general methodology for the study of arbitrary hadronic reaction in Chapter 3. In the former, a fully gauge-fixed formulation has been developed for SU(2) Yang-Mills theory. Accordingly, errors characteristic of the NISQ device era will not have the opportunity of drifting states into an unphysical sector. Furthermore, by employing the LSH construction, the basis used in this formulation is discrete and well suited to organize truncations that are able to increasingly access the weak-coupling limit of the theory. In the latter, the RESOs proposal has been shown at all orders in perturbation theory to always have exponentially suppressed finite-volume corrections in the presence of a non-zero regulator. This gives important evidence towards the claim that it is able to explore general kinematics and particle multiplicities, which makes RESOs unique amongst numerical nonperturbative studies of hadronic reactions.

The goal of realizing hadronic reactions that are beyond the scope of those already achieved on traditional LQCD is still far from reach. However, complementary paths forward are clear. On the one hand, research should focus on implementing RESOs for $D = 1 + 1$ quantum field theories. These are an important stepping stone, for even in this case there is no known generic method to extract general amplitudes from LQCD-like calculations. Furthermore, quantum computers are already able to perform calculations in these settings that can perform initial RESOs calculations. These are however likely to remain noisy throughout the NISQ era. Fortunately, a diverse class of integrable $1 + 1$ theories exist for which scattering amplitudes can be computed exactly and can be used for comparison with the device results. Moreover, tensor network calculations are often very successful in $D = 1 + 1$, so that classical calculations can be performed parallelly. While this does show that $D = 1 + 1$ is unlikely to be enough to show true quantum advantage, tensor networks will still be a useful benchmark for non-integrable theories of the future capabilities of quantum computers.

On the other hand, simultaneous efforts must be made towards a full formulation of

QCD with dynamical fermions in $D = 1 + 3$. It is not clear to us at this point whether the formulation presented in this thesis will be able to efficiently accommodate fermions in the theory. Similarly, it is not clear what the consequences of non-locality in $D = 1 + 3$ will be, since the reduction to a G-spin model only holds in $D = 1 + 2$. However, the most immediate path forward is the study of whether the weak-coupling limit in $D = 1 + 2$ of the spin model is actually able to correctly describe the continuum limit of the theory.

Appendix A

Introduction to Lattice Quantum Field Theories

Lagrangian and Hamiltonian mechanics play a complementary role in the analytical description of mechanics. They are not two different formulations of the same theory. Instead, they form a unified framework necessary for the complete description of mechanical systems. Restricting ourselves to only one part of said framework will inevitably lead to an incomplete understanding of the system in question [166]. A similar thing can be said of the path integral and operator perspectives towards quantum mechanics. A complete understanding of quantum theories requires one to be able to simultaneously think in both languages. This chapter aims to describe this synergy, first in abstract terms, inspired by the Atiyah-Segal axioms [167] for topological field theories, and later with explicit examples.

These two perspectives are not exclusive to quantum theories. Indeed, classical statistical mechanics can also be formulated using both path integrals and operators. This sets up a useful connection between quantum mechanics and classical statistical mechanics. Intuitively, this is obtained by replacing the quantum fluctuations in the former by the thermal fluctuations of the latter. This is at the heart of the methodologies used to explore quantum field theories with classical computers. Throughout this dissertation we will attempt to emphasize this duality, often jumping between quantum and thermal interpretations to obtain a clearer picture of the systems we will study.

For no reason other than the personal preference of the author, we have decided to start from the path integral perspective. Whenever one does so, the interconnection between path integrals and operators is known as the transfer matrix formalism, particularly in statistical mechanics. While contrary to the historical development of the subject, we hope that this might offer a fresh perspective to readers who are not already experts in the field.

A.1 Path Integrals

Throughout this dissertation, the description of our theories will always begin with three ingredients. The first will be a spacetime $\mathcal{M}$. It will generically be some smooth manifold, perhaps equipped with a Lorentzian or Euclidean metric. Or it could also be a graph, acting as a discrete approximation of the above. Some examples we will discuss throughout this dissertation are:

1. Our physical target will be the study of quantum field theories on Minkowski spacetime $\mathbb{R}^{1,3}$ with the metric $\mathrm{d}s^2 = \mathrm{d}t^2 - \mathrm{d}\boldsymbol{x}^2$.

2. We will often restrict to simpler toy models in spacetimes $\mathbb{R}^{1,d}$ with spatial dimensions $d = 1, 2$. These will be useful testing grounds for new ideas, as well as interesting laboratories for the development of intuition.

3. Due to the memory restrictions associated with any computing device, we will often have to deal with finite-volume versions of these spacetimes $\mathbb{R} \times \Sigma$, where, instead of $\Sigma = \mathbb{R}^d$, we will often have to consider a box $\Sigma = [0, L]^d$. Attempting to maintain translation invariance, we will also consider boxes with periodic boundary conditions leading to tori $\Sigma = T^d = (S^1)^d$.

4. Often in physics we are interested in predicting phenomena at time $t = T$ from initial data at time $t = 0$. In these cases, we will be interested in spacetimes of the form $[0, T] \times \Sigma$, which have initial $\Sigma_i = \{0\} \times \Sigma$ and final $\Sigma_f = \{T\} \times \Sigma$ time slices. A more generic curved spacetime of this form is shown in Fig. A.1.

5. The connection with thermal physics is obtained by instead considering spacetimes $\mathcal{M}$ with a Euclidean metric, such as $\mathbb{R} \times \Sigma$ with the metric $\mathrm{d}s^2 = \mathrm{d}t^2 + \mathrm{d}\boldsymbol{x}^2$. While such $\mathcal{M}$ can hardly be called spacetimes, in the context of quantum statistical mechanics, the coordinate t is often called Euclidean or imaginary time. In this interpretation it is often even useful to consider periodic imaginary times $\mathcal{M} = S^1 \times \Sigma$, as we will see below.

6. In classical statistical physics, the interpretation of $\mathcal{M}$ is not that of a spacetime, but rather the geometry of some physical object, such as a ferromagnetic material. We stress that in this interpretation an $\mathcal{M}$ of the form $[0, T] \times \Sigma$ does not describe the time evolution of anything. It instead describes a cylinder with cross-section Σ. In this setting time doesn't play a role because, rather than keeping track of the intricate thermal fluctuations of the system across time, we aim to describe its states as probabilistic ensembles. This is a good approximation when the system is in thermal equilibrium.

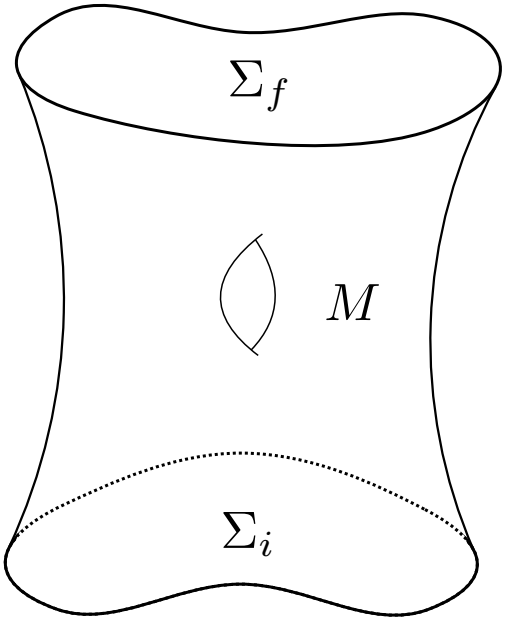


Figure A.1: A generic spacetime $\mathcal{M}$ is shown which is bounded by an initial time slice Σ_i and a final time slice Σ_f.

7. Due partly to the memory restrictions mentioned above, but mostly due to the inherent difficulties we will find in trying to make sense of the naive picture we will set up in the remainder of this section, in lattice quantum field theory we often replace the continuous examples above by discrete versions in terms of graphs.

The second ingredient will be a space of fields $\mathcal{E}(\mathcal{M})$. In all the examples considered in this work (except, due to topological subtleties associated with gauge invariance, Yang-Mills theory in the continuum), this is some subset of functions on $\mathcal{M}$. These functions can take values on some finite set (e.g. the Ising model), on the real line (which we would call a scalar field), on $\mathbb{R}^n$ (which we would call the linear sigma model), or more general objects (such as the manifolds that appear in non-linear sigma model or the groups and Lie algebras that appear in gauge theories). In this section we will denote general elements of $\mathcal{E}(\mathcal{M})$ by ϕ. If spacetime has boundaries, such as Σ_i and Σ_f in Fig. A.1, appropriate boundary conditions have to be imposed on $\mathcal{E}(\mathcal{M})$. Initial and final boundary conditions play a distinguished role, and for the rest of this section they will be denoted respectively by φ_i and φ_f. In this dissertation, the boundary conditions will be of Dirichlet kind, [1] so that for all $\phi \in \mathcal{E}(\mathcal{M})$ we have $\phi(x) = \varphi_i(x)$ and $\phi(y) = \varphi_f(y)$ for all $x \in \Sigma_i$ and $y \in \Sigma_f$.

[1] However, we warn the reader that these boundary conditions can be of a different nature for more general theories, necessary to ensure that stationary-action principle is well posed.

The third is a measure $\mathcal{D}\phi\, e^{-S}$ on $\mathcal{E}(\mathcal{M})$. This defines an integration theory on $\mathcal{E}(\mathcal{M})$, so that for certain functions O on $\mathcal{E}(\mathcal{M})$ we can define

$$\int_{\mathcal{E}(\mathcal{M})} \mathcal{D}\phi\, e^{-S(\phi)} O(\phi). \tag{A.1}$$

These are known as path integrals (or functional integrals to avoid confusion with the concept of line integrals in vector calculus). The name is due to their quantum mechanical interpretation. The field $\phi(t, \boldsymbol{x})$ describes the trajectory in time t of a field in space $\boldsymbol{x}$. This path integral corresponds to a sum over all such trajectories, or paths [168].

The notation $\mathcal{D}\phi\, e^{-S}$ comes from an intuitive separation of this measure into two components. One corresponds to a "uniform" integration measure $\mathcal{D}\phi$ on the space of fields $\mathcal{E}(\mathcal{M})$, which is, roughly speaking

$$\mathcal{D}\phi = \prod_{x \in \mathcal{M}} \mathrm{d}\phi(x), \tag{A.2}$$

in terms of some measure $\mathrm{d}\phi(x)$ of the space in which the field takes values. The second is the action S. This is a function on [2] $\mathcal{E}(\mathcal{M})$. To first approximation, $I = iS$ corresponds to the usual action in the quantum mechanical interpretation, which can often be interpreted as an integral over time of a kinetic minus a potential energy. There, I is real, so that S is purely imaginary. In the quantum statistical interpretation, after going to imaginary time S becomes real, and it is often equal to an integral over time of the sum of the kinetic and potential energies. In the classical statistical field theory, S itself acquires the interpretation of the energy of the system divided by its temperature.

A.2 Time Evolution Operator

Consider a spatial slice Σ on the spacetime $\mathcal{M}$, as shown in Fig. A.2. The boundaries Σ_i and Σ_f are other examples of such spatial slices. In the quantum mechanical interpretation, associated to such a spatial slice there is a Hilbert space $\mathcal{H}(\Sigma)$ of states of the theory at that instant of time. For the purposes of this dissertation, [3] given a configuration φ of the field on Σ, there is a corresponding state $|\varphi\rangle \in \mathcal{H}(\Sigma)$ which is, with complete certainty, in that configuration. In fact, the Hilbert space will be spanned by such states, so that every $|\psi\rangle \in \mathcal{H}(\Sigma)$ can be written as

$$|\psi\rangle = \int D\varphi\ |\varphi\rangle \langle\varphi|\psi\rangle\,, \tag{A.3}$$

[2] For non-compact $\mathcal{M}$, generically this function is not well-defined on all of $\mathcal{E}(\mathcal{M})$, but only on a subset of functions that vanish sufficiently fast. But this will not be a main concern for us in this dissertation. See [169] for a discussion on this point.

[3] A more formal treatment requires the machinery of geometric quantization.

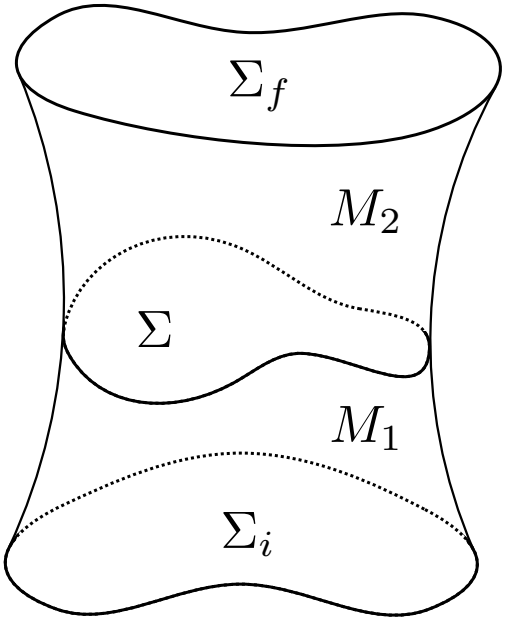


Figure A.2: A spacetime with an incoming boundary Σ_i, an outgoing boundary Σ_f, and a spatial slice Σ.

in terms of some integration measure[4] $D\varphi$ for the space of field configurations on Σ.

The wave function $\langle\varphi|\psi\rangle$ corresponds to the probability amplitude for the field to be found in configuration φ upon measurement. The introduction of a measure $D\varphi$ yields an inner product on $\mathcal{H}(\Sigma)$ with which we can construct bras in the dual space and for which we have a resolution of the identity

$$1 = \int D\varphi \; |\varphi\rangle\langle\varphi| \,. \tag{A.4}$$

Thus, we can interpret $\mathcal{H}(\Sigma)$ as the space of functions on the space of fields on Σ that are square integrable with respect to $D\varphi$.

The path integral (A.1) defines the time evolution operator $U(\mathcal{M}) : \mathcal{H}(\Sigma_i) \to \mathcal{H}(\Sigma_f)$ through its matrix elements

$$\langle\varphi_f|U(\mathcal{M})|\varphi_i\rangle := \int_{\mathcal{E}(\mathcal{M})} \mathcal{D}\phi \, e^{-S(\phi)}. \tag{A.5}$$

The name comes from its quantum mechanical interpretation. In that setting, $U(\mathcal{M})$ is an operator which identifies the Hilbert spaces $\mathcal{H}(\Sigma_i)$ and $\mathcal{H}(\Sigma_f)$ with one another. The

[4]We will use D to denote integration measure on the space of field configurations on a spatial slice, while $\mathcal{D}$ will be reserved for measures on the space of field configurations on spacetime, as in (A.1).

state $U(\mathcal{M})\,|\varphi_i\rangle$ should be interpreted as the state at $\mathcal{H}(\Sigma_f)$ obtained by preparing $|\varphi_i\rangle$ at Σ_i and letting it evolve along spacetime $\mathcal{M}$. The matrix element (A.5) then corresponds to the amplitude for the state $|\varphi_i\rangle$ at Σ_i to be measured in state $|\varphi_f\rangle$ at Σ_f.

Let us consider a splitting of $\mathcal{M}$ into two spacetimes $\mathcal{M}_1$ and $\mathcal{M}_2$ with the common boundary Σ, as shown in Fig. A.2. Time-evolution operators will satisfy the property that $U(\mathcal{M}) = U(\mathcal{M}_2)U(\mathcal{M}_1)$, corresponding to the fact that full time evolution by $\mathcal{M}$ can be obtained by first evolving along $\mathcal{M}_1$ and the along $\mathcal{M}_2$. This yields a pasting formula for path integrals

$$\begin{aligned}
&\int_{\mathcal{E}(\mathcal{M})} \mathcal{D}\phi\, e^{-S_{\mathcal{M}}(\phi)} = \langle\varphi_f|U(\mathcal{M})|\varphi_i\rangle = \langle\varphi_f|U(\mathcal{M}_2)U(\mathcal{M}_1)|\varphi_i\rangle \\
&= \int D\varphi\ \langle\varphi_f|U(\mathcal{M}_2)|\varphi\rangle\,\langle\varphi|U(\mathcal{M}_1)|\varphi_i\rangle \\
&= \int D\varphi \int_{\mathcal{E}(\mathcal{M}_2)} \mathcal{D}\phi_2\, e^{-S_{\mathcal{M}_2}(\phi_2)} \int_{\mathcal{E}(\mathcal{M}_1)} \mathcal{D}\phi_1\, e^{-S_{\mathcal{M}_1}(\phi_1)}.
\end{aligned} \tag{A.6}$$

In here we have included a subindex in the action to clarify over which spacetimes it should be computed. It should also be understood that the fields on $\mathcal{E}(\mathcal{M}_2)$ ($\mathcal{E}(\mathcal{M}_1)$) have initial (final) boundary conditions on Σ corresponding to φ. Another important property these operators will satisfy is that, for spacetimes with no temporal extent there cannot be any time evolution, so that the time-evolution operator reduces to the identity operator $U(\mathcal{M}) = 1$.

For Lorentzian cylindrical spacetimes $\mathcal{M} = [0,T]\times\Sigma$, like the one shown in Fig. A.3a, in a setting with time-translation symmetry, this operator can be written in the form $U(\mathcal{M}) = e^{-iTH}$ for a Hermitian operator H on $\mathcal{H}(\Sigma)$ known as the Hamiltonian. This is equivalent to saying that states evolve under Schrödinger's equation

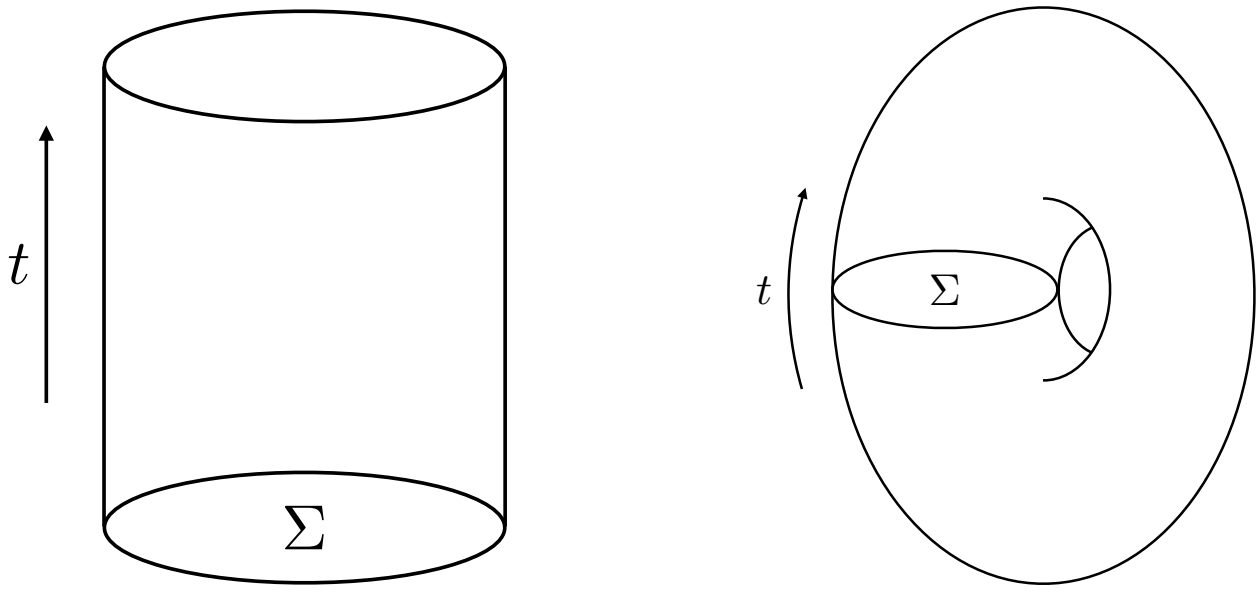
$$i\frac{\mathrm{d}\,|\psi\rangle}{\mathrm{d}t} = H\,|\psi\rangle\,. \tag{A.7}$$

This yields an explicit formula for the matrix elements of the Hamiltonian

$$\langle\varphi_f|H|\varphi_i\rangle = i\,\frac{\mathrm{d}}{\mathrm{d}T}\bigg|_{T=0} \langle\varphi_f|U(\mathcal{M})|\varphi_i\rangle\,. \tag{A.8}$$

The fact that this formula only depends on spacetimes with an infinitesimally small T will be a big simplification in our computations of Hamiltonians.

In the Euclidean context, achieved by the replacement $t \to -it$, known as Wick rotation, this operator instead takes the form $U(\mathcal{M}) = e^{-TH}$. The axiomatics of these theories are studied in [30], with a particular focus on lattice gauge theories in [170]. This corresponds to the unnormalized density matrix for a state at thermal equilibrium with



(a) (b)

Figure A.3: Subfigure (a) corresponds to a spacetime of the form $\mathcal{M} = [0, T] \times \Sigma$. The time coordinate has the range $0 \leq t \leq T$. Subfigure (b) corresponds to a spacetime of the form $\mathcal{M} = S^1 \times \Sigma$, with a circle of circumference T. In this case the time coordinate has the identification $t \sim t + T$.

temperature $1/T$. It is important to note that, regardless of whether one is in the Euclidean or Lorentzian context, the Hamiltonian operator is the same. Therefore, both are important tools in the study of the Hamiltonian of a quantum field theory. For example, in Euclidean LQCD, we will strive to take T as large as possible to obtain cold systems which have a high probability to be in their vacuum state.

In the Euclidean setting we will often take time to be periodic, leading to spacetimes of the form shown in Fig. A.3b. This can be thought of as identifying $\{0\} \times \Sigma$ and $\{T\} \times \Sigma$ and imposing periodic boundary conditions on our fields. This is equivalent to having identical initial and final boundary conditions $\varphi_i = \varphi_f = \varphi$ and summing over all such possibilities φ. The corresponding path integral then computes the trace[5]

$$U(S^1 \times \Sigma) = \int D\varphi \, \langle \varphi | U([0,T] \times \Sigma) | \varphi \rangle = \operatorname{tr} U([0,T] \times \Sigma). \tag{A.9}$$

This can be thought of as an expression of the pasting property (A.6). This is the normalization $\operatorname{tr} e^{-TH}$ of the Gibbs state, which is why these path integrals are also often called partition functions

$$Z = U(S^1 \times \Sigma) \tag{A.10}$$

For $\mathcal{M}$ in which S is real, in the classical statistical interpretation $e^{-S(\phi)}$ corresponds to a Boltzmann weight. It characterizes the relative probability for the system to be in configuration the configuration ϕ. The actual probability requires a normalization factor $e^{-S(\phi)}/Z$, where

$$Z = \int \mathcal{D}\phi \, e^{-S(\phi)}. \tag{A.11}$$

This is the partition function of statistical mechanics.

Observe that when $\mathcal{M} = S^1 \times \Sigma$ and is Euclidean, the partition functions of the classical and quantum statistical interpretations coincide. However, their interpretation is rather different, as exemplified by the quantity corresponding to temperature in both formulations. While in the quantum interpretation the role of temperature was played by the inverse of the temporal extent, in the classical setting, the role of temperature is instead played by the introduction of a constant $\hbar$ and the rescaling of the energy $S \to S/\hbar$. In quantum mechanics $\hbar$ is instead Planck's constant, which characterizes quantum mechanical fluctuations. This is at the heart of the reason why Euclidean LQCD works on classical computers – in the transition from quantum to classical pictures, quantum mechanical fluctuations are replaced by classical, albeit thermal, ones. And in that setting these path integrals correspond to the normalization of these Boltzmann factors. Thus, we are entitled to call all path integrals partition functions. In this setting, the operators $U(\mathcal{M})$ are usually called transfer matrices.

[5]At the beginning of this section we claimed that $U(\mathcal{M})$ can always be interpreted as an operator. However, whenever $\mathcal{M}$ lacks initial and final boundaries, such as in this case, $U(\mathcal{M})$ is a number. This can be reconciled by setting the Hilbert space of an empty slice to $\mathcal{H}(\varnothing) = \mathbb{C}$.

A.3 Path Integral Quantization

We now consider functions O on $\mathcal{E}(\mathcal{M})$ that only depend on the germ of the field at a slice Σ. This means that O can be computed only having knowledge of the configuration of the field on an infinitesimal neighborhood of Σ. Such functions are often called operators. Indeed, they can be interpreted as operators on $\mathcal{H}(\Sigma)$ defined by the property that, on spacetimes like the one in Fig. A.2 one has

$$\langle\varphi_f|U(\mathcal{M}_2)OU(\mathcal{M}_1)|\varphi_i\rangle = \int_{\mathcal{E}(\mathcal{M})} \mathcal{D}\phi\, e^{-S(\phi)}O(\phi). \tag{A.12}$$

Alternatively, defining the Heisenberg picture operator $O_\Sigma := U(\mathcal{M}_1)^{-1}OU(\mathcal{M}_1)$ acting on $\mathcal{H}(\Sigma_i)$, we can write

$$\langle\varphi_f|U(\mathcal{M})O_\Sigma|\varphi_i\rangle = \int_{\mathcal{E}(\mathcal{M})} \mathcal{D}\phi\, e^{-S(\phi)}O(\phi). \tag{A.13}$$

We stress that the definition of O_Σ depends on an implicit understanding of the spacetime $\mathcal{M}_1$ bounded by Σ_i and Σ. In particular, it depends on Σ_i. In fact, often we will use the same symbol O_Σ to denote operators defined with respect to different spacetime slices Σ_i. When confusion can arise, these can be inferred from the $\mathcal{H}(\Sigma_i)$ on which this operator is acting.

Given that time-evolution operators reduce to the identity as the temporal extent goes to zero, this yields an analog of (A.8) for the calculation of the matrix elements of O in terms of path integrals

$$\langle\varphi_f|O|\varphi_i\rangle = \lim_{T\to 0}\langle\varphi_f|U([T/2,T]\times\Sigma)OU([0,T/2]\times\Sigma)|\varphi_i\rangle\,. \tag{A.14}$$

The procedure of identifying functions on $\mathcal{E}(\mathcal{M})$ with operators on a Hilbert space is usually called quantization.

For operators that only depend on the field configuration at Σ we can consider a simpler prescription. Consider the spacetime $\mathcal{M} = [0,T]\times\Sigma$ and place the operator O at $t = 0$. Then

$$\begin{aligned}\langle\varphi_f|U(\mathcal{M})O|\varphi_i\rangle &= \int_{\mathcal{E}(\mathcal{M})} \mathcal{D}\phi\, e^{-S(\phi)}O(\phi) = O(\varphi_i)\int_{\mathcal{E}(\mathcal{M})}\mathcal{D}\phi\, e^{-S(\phi)}\\ &= O(\varphi_i)\,\langle\varphi_f|U(\mathcal{M})|\varphi_i\rangle\,.\end{aligned} \tag{A.15}$$

Taking the limit as $T\to 0$ we conclude that $O\,|\varphi\rangle = O(\varphi)\,|\varphi\rangle$ for these operators.

We can consider path integrals with more than one operator insertion. Let us consider two operators A and B on Σ_1 and Σ_2, respectively, in the spacetime shown in Fig. A.4.

Letting $\mathcal{M}_1$ and $\mathcal{M}_2$ be the portions of spacetime between Σ_i and Σ, and between Σ and Σ_f, respectively, we have a splitting of the path integral of the form

$$\begin{aligned}&\int_{\mathcal{E}(\mathcal{M})} \mathcal{D}\phi\, e^{-S(\phi)} B(\phi) A(\phi) \\ &= \int D\varphi \int_{\mathcal{E}(\mathcal{M}_2)} \mathcal{D}\phi_2\, e^{-S_{\mathcal{M}_2}(\phi_2)} B(\phi_2) \int_{\mathcal{E}(\mathcal{M}_1)} \mathcal{D}\phi_1\, e^{-S_{\mathcal{M}_1}(\phi_1)} A(\phi_1).\end{aligned} \tag{A.16}$$

The right-hand side of this equality corresponds to the matrix element[6].

$$\begin{aligned}&\int D\varphi\ \langle\varphi_f|U(\mathcal{M}_2)B_{\Sigma_2}|\varphi\rangle\,\langle\varphi|U(\mathcal{M}_1)A_{\Sigma_1}|\varphi_i\rangle \\ &= \langle\varphi_f|U(\mathcal{M}_2)B_{\Sigma_2}U(\mathcal{M}_1)A_{\Sigma_1}|\varphi_i\rangle = \langle\varphi_f|U(\mathcal{M})B_{\Sigma_2}A_{\Sigma_1}|\varphi_i\rangle\,.\end{aligned} \tag{A.17}$$

If, instead, Σ_1 was to the future of Σ_2, we would have obtained $\langle\varphi_f|U(\mathcal{M})A_{\Sigma_1}B_{\Sigma_2}|\varphi_i\rangle$. Thus, it is generically useful to introduce the time ordering operator defined by

$$T(B_{\Sigma_2}A_{\Sigma_1}) = \begin{cases} B_{\Sigma_2}A_{\Sigma_1}, & \text{if } \Sigma_2 \text{ is to the future of } \Sigma_1, \\ A_{\Sigma_1}B_{\Sigma_2}, & \text{if } \Sigma_1 \text{ is to the future of } \Sigma_2, \end{cases} \tag{A.18}$$

in terms of which we have

$$\int_{\mathcal{E}(\mathcal{M})} \mathcal{D}\phi\, e^{-S(\phi)} B(\phi) A(\phi) = \langle\varphi_f|U(\mathcal{M})T(B_{\Sigma_2}A_{\Sigma_1})|\varphi_i\rangle\,. \tag{A.19}$$

Taking the temporal extent of $\mathcal{M}$ to 0 yields a path integral formulation for computing the product of the operators AB and BA, depending on the temporal ordering of Σ_1 and Σ_2.

In statistical mechanics these path integrals have a natural interpretation. In the quantum one, the state of the system at temperature $1/T$ is given by $\rho = U([0,T]\times\Sigma)/U(S^1\times\Sigma) = e^{-TH}/U(S^1\times\Sigma)$. The expectation value of an operator O in this state is

$$\begin{aligned}\langle O\rangle &:= \mathrm{tr}(\rho O) = \frac{\mathrm{tr}(U([0,T]\times\Sigma)O)}{U(S^1\times\Sigma)} \\ &= \frac{1}{U(S^1\times\Sigma)}\int D\varphi\ \langle\varphi|U([0,T]\times\Sigma)O|\varphi\rangle\,.\end{aligned} \tag{A.20}$$

Much like in the discussion leading to (A.9), the remaining matrix element in the numerator can be reinterpreted as a path integral on a spacetime with periodic time

$$\langle O\rangle = \frac{1}{U(S^1\times\Sigma)}\int_{\mathcal{E}(S^1\times\Sigma)} \mathcal{D}\phi\, e^{-S(\phi)} O(\phi). \tag{A.21}$$

[6]Note that in this equation B_{Σ_2} is used to denote two different operators, one of which acts on $\mathcal{H}(\Sigma)$ and the other on $\mathcal{H}(\Sigma_i)$.

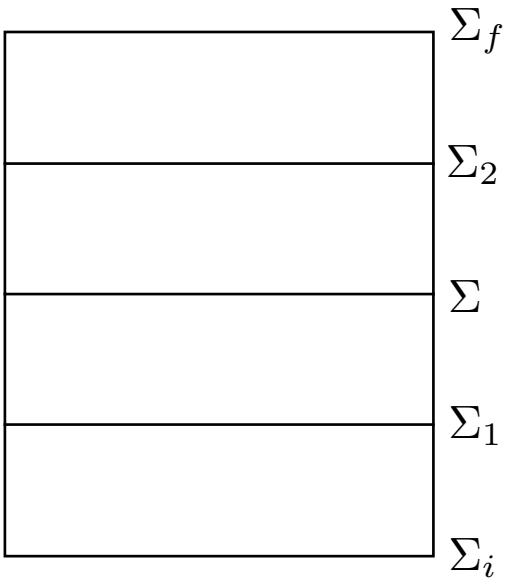


Figure A.4: A spacetime with spatial slices Σ_i, Σ_1, Σ, Σ_2 and Σ_f, in that temporal order.

In classical statistical mechanics, regardless of the structure of $\mathcal{M}$, expectation values are taken with respect to the probability measure $\mathcal{D}\phi e^{-S}/Z$, leading to

$$\langle O\rangle = \frac{1}{Z}\int_{\mathcal{E}(\mathcal{M})} \mathcal{D}\phi\, e^{-S(\phi)}O(\phi). \tag{A.22}$$

Observe that in both the quantum and statistical interpretations the formulae for expectation values are identical. However, one must keep in mind their differences. For example, reintroducing $\hbar$ which in the classical interpretation corresponds to temperature, the expectation value of the energy can be written in terms of derivatives with respect to the temperature

$$\langle S\rangle = \frac{1}{Z}\int_{\mathcal{E}(\mathcal{M})} \mathcal{D}\phi\, e^{-S(\phi)/\hbar}S(\phi) = -\frac{1}{Z}\frac{\mathrm{d}Z}{\mathrm{d}\hbar^{-1}} = -\frac{\mathrm{d}\ln Z}{\mathrm{d}\hbar^{-1}} \tag{A.23}$$

On the other hand, in the quantum interpretation, the roles of temperature and energy are played by different quantities, so that the expectation value of the energy is instead

$$\langle H\rangle = \frac{1}{Z}\operatorname{tr}(e^{-TH}H) = -\frac{1}{Z}\frac{\mathrm{d}Z}{\mathrm{d}T} = -\frac{\mathrm{d}\ln Z}{\mathrm{d}T}, \quad Z = U(S^1\times\Sigma). \tag{A.24}$$

A.4 Comments on Renormalization

Observe that the product AB at the end of the discussion of the previous section is not the product of A and B as functions on $\mathcal{E}(\mathcal{M})$, which trivially commutes. Instead, this is a product of operators, which in general does not commute. This will be reflected as a discontinuity of the path integral as Σ_1 and Σ_2 are moved towards one another. In particular, path integrals of overlapping operators is in general ill-defined. This leads us to the theory of renormalization.

To exemplify this, let us consider a theory in which $\mathcal{E}(\phi)$ consists of scalar fields. Then, operators like $\phi(x)^4$ are ill-defined. Instead, we must introduce a regularization scheme in which our calculations will succeed. However, this often requires the introduction of a regulator ϵ, which is an arbitrary unphysical quantity on which our calculations will depend. In the lattice, this regulator is the spacing in between the lattice points. In the continuum, one often performs calculations in $D = 4 - 2\epsilon$ dimensions. The theory of renormalization allows us to remove this regulator through the choice of a renormalization scheme μ. This instructs us to replace the operators like $\phi(x)^4$ by renormalized operators $:\phi(x)^4:$, which depend on μ, and which lead to well-defined calculations even as the regulator is removed.

Renormalization is, in fact, not only necessary when considering operator insertions in the path integral. For example, when performing perturbative calculations with an action of the form

$$S(\phi) = S_0(\phi) + \frac{\lambda}{4!}\int \mathrm{d}^4x\, \phi^4, \quad S_0(\phi) = \frac{1}{2}\int \mathrm{d}^4x\, \big((\partial_\mu\phi)^2 + m^2\phi^2\big), \tag{A.25}$$

one needs to perform manipulations of the form

$$e^{-S(\phi)} = e^{-S_0(\phi)}\left(1 - \frac{\lambda}{4!}\int \mathrm{d}^4x\, \phi^4 + \cdots\right). \tag{A.26}$$

These bring down terms from the action as operator insertions. Thus, the action itself has to be renormalized. In practice, the theory of renormalization of the action is sufficient to make QFT well-defined, for one can always invert this process and think of operator insertions as infinitesimal deformations of the action

$$e^{-S(\phi)}O(\phi) = -\left.\frac{\mathrm{d}}{\mathrm{d}J}\right|_{J=0} e^{-S_O(\phi)}, \quad S_O(\phi) := S(\phi) + JO(\phi). \tag{A.27}$$

The specifics of different renormalization schemes are best presented in the context of specific examples. We will therefore avoid an in-depth discussion at this stage. However, we finalize this section by showing a glaring contradiction one obtains by using the formalism above without keeping these subtleties in mind. While we have realized that operators of

the form $\phi(x)^4$ have to be ill-defined without regularization, our discussion above gave an immediate formula

$$\phi(x)^4 \left|\varphi\right\rangle = \varphi(x)^4 \left|\varphi\right\rangle, \tag{A.28}$$

for states $\left|\varphi\right\rangle \in \mathcal{H}(\Sigma)$ with $x \in \Sigma$. Our only way out is to conclude that our Hilbert space $\mathcal{H}(\Sigma)$, itself, requires regularization and renormalization. To the best of our knowledge a satisfactory general theory of the construction of these spaces is still lacking. Of particular difficulty is the problem of constructing measures $D\varphi$. On the other hand, the theory of renormalization of full path integrals, which amounts to the problem of construction of the measure $\mathcal{D}\phi$, or more precisely $\mathcal{D}\phi\, e^{-S}$ is at a much more mature stage, although a full nonperturbative definition is still lacking. Fortunately for us, on the lattice all of these objects are well-defined, and the problem of a rigorous definition of these measures consists of taming the limit as our lattice spacing goes to zero. Whoever manages to do this will have solved one of the Clay Mathematics Institute Millennium Prize Problems and will be one million US dollars richer. If you do this, please let me know before you publish. I would love to share the prize with you.

A.5 Schwinger-Dyson Equations

We now turn to more practical matters regarding methods of calculation of the path integral. Arguably, one of the most important methods is the Schwinger-Dyson equations, which play the role of the equations of motion of quantum theories. Our discussion is heavily influenced by [171].

To discuss the Schwinger-Dyson equations, we will assume that $\mathcal{E}(\mathcal{M})$ is finite-dimensional. In lattice theories this is the norm. In all our examples (and in the case in which $\mathcal{E}(\mathcal{M})$ is a vector space), there is an additional group structure which selects a Haar measure $\mathcal{D}\phi$ unique up to an overall normalization. Our main interest in this section will be in the calculation of integrals of the form

$$\langle O\rangle := \frac{1}{Z}\int_{\mathcal{E}(\mathcal{M})} \mathcal{D}\phi\, e^{-S(\phi)} O(\phi), \quad Z := \int_{\mathcal{E}(\mathcal{M})} \mathcal{D}\phi\, e^{-S(\phi)}, \tag{A.29}$$

which are independent of this normalization [132]. We will further assume that S grows sufficiently fast so that boundary contributions vanish and this integral is convergent.

Consider coordinates $\phi = (\phi^1, \ldots, \phi^{n:=\dim \mathcal{E}(\mathcal{M})})$ on $\mathcal{E}(\mathcal{M})$, in terms of which there is a normalization of the measure for which we can locally write

$$\mathcal{D}\phi = \prod_{i=1}^{n} \mathrm{d}\phi^i. \tag{A.30}$$

The Schwinger-Dyson equations stem from the assumption that the boundary contribution vanishes in

$$0 = \int_{\mathcal{E}(\mathcal{M})} \mathcal{D}\phi \, \frac{\partial}{\partial \phi^i}(e^{-S(\phi)}O). \tag{A.31}$$

The product rule then implies the Schwinger-Dyson equation

$$\left\langle \frac{\partial O}{\partial \phi^i} \right\rangle = \left\langle \frac{\partial S}{\partial \phi^i} O \right\rangle . \tag{A.32}$$

In order to interpret this equation we note that the principle of stationary action dictates that the classical equations of motion, the Euler-Lagrange equations, are $\frac{\partial}{\partial \phi^i} S = 0$. The Schwinger-Dyson equation states that this equation remains true in correlation functions in which there is no other observable O which depends on ϕ^i. For example, if the index i corresponds to position, it says that the equations of motion at i remain true as long as there are no other operators that depend on the field at that point. Moreover, it gives a precise determination of how these equations break in the presence of overlapping operators.

In the particular case that S is a quadratic function[7] $S(\phi) = \frac{1}{2}\phi^i A_{ij} \phi^j$, with A symmetric, we have

$$\left\langle \frac{\partial O}{\partial \phi^i} \right\rangle = A_{ij} \left\langle \phi^j O \right\rangle . \tag{A.33}$$

This is the case for free theories. Our decay assumptions imply that A is positive-definite and, therefore, invertible. Thus, introducing its inverse P, for which $P^{ij} A_{jk} = \delta^i_k$, we conclude that

$$\left\langle \phi^i O \right\rangle = P^{ij} \left\langle \frac{\partial O}{\partial \phi^j} \right\rangle . \tag{A.34}$$

Observe that P^{ij} is simply the solution to the equations of motion for the action $S(\phi) - \phi^j$, which is why this is called the propagator.

A particular example is

$$\left\langle \phi^i \phi^j \right\rangle = P^{ij}. \tag{A.35}$$

In general, we obtain Wick's theorem

$$\left\langle \phi^{i_1} \cdots \phi^{i_n} \right\rangle = \sum_{r=2}^{n} P^{i_1 i_r} \left\langle \widehat{\phi^{i_1}} \cdots \widehat{\phi^{i_r}} \cdots \phi^{i_n} \right\rangle , \tag{A.36}$$

where on the right-hand side we omit both ϕ^{i_1} and ϕ^{i_r} from the expectation value.

[7] We will employ the Einstein summation convention for contracting upper and lower indices

A.6 Spectrum in a Euclidean Finite Volume

Let us now consider Euclidean spacetimes[8] with the structure $\mathcal{M} = [0,T] \times \Sigma$ or $\mathcal{M} = S^1 \times \Sigma$. In particular, we have a well-defined Hamiltonian H independent of time for which $U([0,T] \times \Sigma) = e^{-TH}$ and $U(S^1 \times \Sigma) = \mathrm{tr}(e^{-TH})$. We further assume that Σ is a space with a finite volume and that the theory has a mass gap. In this case it is expected that under quite general conditions the spectrum of the theory will be discrete. We will now explore how to reconstruct the energy levels and the associated wave functions of this theory. Rather than attempting to directly diagonalize H, which for most theories would be computationally impossible, we will focus on methodologies relying on the path integral.

Let us assume the Hamiltonian is shifted so that its lowest energy level is at $E_0 = 0$, corresponding to a vacuum state $|0\rangle$. The remaining energy levels will be organized in the form $E_1 \leq E_2 \leq E_3 \leq \cdots$, corresponding to the states $|1\rangle$, $|2\rangle$, ... The spectral theorem guarantees that there is a resolution of the identity of the form

$$1 = \sum_n |n\rangle\langle n| \,. \tag{A.37}$$

Inserting this resolution of the identity on the partition function of the theory, we obtain

$$\langle \varphi_f | U([0,T] \times \Sigma) | \varphi_i \rangle = \sum_n e^{-TE_n} \langle \varphi_f | n \rangle \langle n | \varphi_i \rangle \,. \tag{A.38}$$

This then allows us to solve for the energy levels. By studying the dependence on T, one can extract the energy levels E_n and the coefficients $\langle \varphi_f | n \rangle \langle n | \varphi_i \rangle$. Then, by studying the dependence on φ_f and φ_i of this coefficient, one can recover the associated wave function $\langle \varphi | n \rangle$.

In practice, numerical calculations of this partition function are very difficult. This is especially true considering the large set of possible boundary conditions one would have to consider. If one instead considers a single choice of boundary conditions, the structure of the wave functions would be lost. For example, computing traces in the basis of states with definite energy, we obtain

$$U(S^1 \times \Sigma) = \sum_n e^{-TE_n} . \tag{A.39}$$

In traditional Lattice QCD, it is much simpler to compute correlation functions of operators. These are statistical averages that can be implemented using Monte Carlo techniques. As an example, consider a pair of operators O_i and O_f, localized at $t = 0$ and

[8] Similar statements can be made in Lorentzian spacetime

t, respectively, on $S^1 \times \Sigma$. Then

$$\begin{aligned}\langle O_f(t) O_i^*(0)\rangle &= \frac{\mathrm{tr}(e^{-(T-t)H} O_f e^{-tH} O_i^\dagger)}{\mathrm{tr}(e^{-TH})} \\ &= \sum_{n,m} \frac{e^{-(T-t)E_m - tE_n}}{\mathrm{tr}(e^{-TH})} \langle m|O_f|n\rangle \langle n|O_i^\dagger|m\rangle \,.\end{aligned} \tag{A.40}$$

This is particularly transparent in the case $T \to \infty$. Recalling that in the quantum statistical interpretation $1/T$ plays the role of temperature, this corresponds to the cold limit in which only the vacuum state, which we assume to be unique, contributes

$$\langle O\rangle \to \langle 0|O|0\rangle \,. \tag{A.41}$$

We thus conclude that in this limit

$$\langle O_f(t) O_i^*(0)\rangle = \sum_n e^{-tE_n} \langle 0|O_f|n\rangle \langle n|O_i^\dagger|0\rangle \,. \tag{A.42}$$

Our explorations in traditional Lattice QCD will be mostly concerned with this last kind of calculation. By judiciously choosing our operators O in these correlation functions, we will be able to select states $|n\rangle$ with $\langle n|O^\dagger|0\rangle \neq 0$. Due to the rapid decay of exponentials, it will be simpler to study those states with small E_n.

We will also be interested in the extraction of transition matrix elements $\langle n|J|m\rangle$ for more generic states than the vacuum. This can be done by considering three-point functions in the $T \to \infty$ limit

$$\langle O_f(t) J(t_0) O_i^*(0)\rangle = \sum_{n,m} e^{-E_n(t-t_0) - E_m t_0} \langle 0|O_f|n\rangle \langle n|J|m\rangle \langle m|O_i^\dagger|0\rangle \,, \tag{A.43}$$

with $0 < t_0 < t$. When supplemented by the knowledge coming from the correlators $\langle O_f(t) O_i^*(0)\rangle$, this allows us to extract our desired matrix elements.

A.7 1D Ising Model

We start by considering what is arguably the simplest model in which we can put to practice the preceding formalism: the one-dimensional Ising model. I once asked professor Davide Gaiotto at the Perimeter Institute what was the best way to truly learn what quantum field theory was. He said to study the Ising model, and that everything in quantum field theory can be learned from it.

This model happens on one dimensional lattices $\mathcal{M}$. We will think of this as a discrete set of points labelled by t and spaced by ϵ, leading to the lattice $\mathcal{M} = \epsilon\mathbb{Z}$. In fact, to make our action well-defined we will restrict to lattices $\mathcal{M} = \{0, \epsilon, \cdots, N_t\epsilon\} =: \underline{N_t}\epsilon$, corresponding

to time evolution by a time $T = \epsilon N_t$, or to the periodic version $\mathcal{M} = {}^{\epsilon\mathbb{Z}}\!/_{T\mathbb{Z}}$, where $t \sim t+T$. In either case, $N_t \in \mathbb{N}^+$ corresponds to the number of links in the lattice.

The fields in this theory are functions ϕ on $\mathcal{M}$ for which $\phi(t) = \pm 1$. When $\mathcal{M} = \underline{N_t}\epsilon$, the space of fields $\mathcal{E}(\mathcal{M})$ is supplemented by boundary conditions $\phi(0) = \varphi_i$ and $\phi(T) = \overline{\varphi_f}$. The space of fields $\mathcal{E}(\mathcal{M})$ is finite, with

$$|\mathcal{E}(\underline{N_t}\epsilon)| = 2^{N_t - 1} \quad \text{and} \quad \left|\mathcal{E}\left({}^{\epsilon\mathbb{Z}}\!/_{T\mathbb{Z}}\right)\right| = 2^{N_t}. \tag{A.44}$$

Therefore, there is a very natural measure $\mathcal{D}\varphi$, namely, the counting measure! This measure is defined by

$$\int_{\mathcal{E}(\mathcal{M})} \mathcal{D}\phi\, O(\phi) := \sum_{\phi \in \mathcal{E}(\mathcal{M})} O(\phi). \tag{A.45}$$

The action of this theory is given by

$$S(\phi) = -K \sum_{n=0}^{N_t - 1} \phi(n\epsilon)\phi((n+1)\epsilon), \tag{A.46}$$

defined by some dimensionless constant K.

A.7.1 Classical Statistical Mechanical Interpretation

The first interpretation we will give is the one from classical statistical mechanics, to which this model owes its name. In it the spacetime $\mathcal{M}$ should instead be viewed as containing no time at all. Instead, the lattice can be viewed as an array of atoms, with the coordinate t parametrizing their position along the array. In this simplistic model, the spin of the atoms is constrained to point along a single axis and to have a fixed magnitude. Thus, $\phi(t)$ characterizes the spin of the atom at position t. We remark that, albeit the concept of spin is usually treated quantum mechanically, in this interpretation it is a classical variable. Therefore, in all states of this spin chain, the spin of an atom is known with complete certainty, and superpositions of different spin configurations of the chain are not allowed.

In this context, the action $S(\phi)$ corresponds to the energy of the system, when measured in units of the temperature. This is why the constant K is dimensionless. Given that, the higher the energy, the smaller the probability e^{-S} of the configuration, for $K > 0$ this system favors spins that are aligned, and the chain is ferromagnetic. More precisely, a pair of neighboring sites that are aligned contributes $-K$ to the energy, while a pair of anti-aligned sites contributes K to the energy. In fact, this suggests a simple solution for the partition function of this model, known as the low-temperature expansion, to which we now turn.

First, let us consider the lattice $\mathcal{M} = \underline{N_t}\epsilon$. The dual lattice to this is the lattices of the links between the spins $\tilde{\mathcal{M}} = \{\epsilon, \cdots, N_t\epsilon\}$, coordinatized by e. Thus, the link (also known

as edge, explaining our notation) e joins the spins at $t = e - \epsilon$ and $t = e$. We now define a field Φ on $\tilde{\mathcal{M}}$, taking values in the set $\{0, 1\}$. A $\Phi(e) = 1$ indicates that the spins at each end of e are anti-aligned. At low temperature, the system will prefer to be in its lowest energy states. Thus, most spins are aligned, so that $\Phi(e) = 1$ corresponds to a wall in between domains of aligned spins. Correspondingly, $\Phi(e) = 0$ corresponds to the absence of a domain wall. The space of fields $\tilde{\mathcal{E}}(\tilde{\mathcal{M}})$ corresponds to all possible configurations Φ of domain walls. Unlike $\mathcal{E}(\mathcal{M})$, this space does not need boundary conditions. Instead, if $\varphi_i = \varphi_f$, the fields in $\tilde{\mathcal{E}}(\tilde{\mathcal{M}})$ are restricted to have only an even number of domain walls. If $\varphi_i = -\varphi_f$, we must instead have an odd number of them. Once this has been agreed on, the fields in $\mathcal{E}(\mathcal{M})$ and $\tilde{\mathcal{E}}(\tilde{\mathcal{M}})$ are in one-to-one correspondence with each other.

In the absence of domain walls, all spins are aligned, and the energy is $S = -N_t K$. Each domain wall contributes $2K$ to the energy so that

$$S(\Phi) = -N_t K + 2K \sum_{n=1}^{N_t} \Phi(n\epsilon) = -\sum_{n=1}^{N_t} \left(K - 2K\Phi(n\epsilon)\right). \tag{A.47}$$

In this reinterpretation of the field the system is almost not interacting, for each link has its own separate contribution to the energy. This is reflected by the fact that the Boltzmann weights factorize as a product over individual Boltzmann weights

$$e^{-S(\Phi)} = \prod_{e=1}^{N_t} e^{K - 2K\Phi(e)}. \tag{A.48}$$

However, there is still a lingering interaction, due to the global constraint of having an even or odd number of domain walls. This means that

$$\sum_{\Phi \in \tilde{\mathcal{E}}(\tilde{\mathcal{M}})} \neq \sum_{\Phi} := \sum_{\Phi(1)=0}^{1} \cdots \sum_{\Phi(N_t)=0}^{1}. \tag{A.49}$$

Let us first solve this in the case where $\varphi_i = \varphi_f$, meaning that the fields in $\tilde{\mathcal{E}}(\tilde{\mathcal{M}})$ have an even number of domain walls. A nice trick we can use is to note that

$$\sum_{\Phi \in \tilde{\mathcal{E}}(\tilde{\mathcal{M}})} e^{-S(\Phi)} = \frac{1}{2}\left(\sum_{\Phi} e^{-S(\Phi)} + \sum_{\Phi} (-1)^{\sum_{e=1}^{N_t} \Phi(e)} e^{-S(\Phi)} \right). \tag{A.50}$$

In here the contributions corresponding to fields Φ with an odd number of domain walls contribute with opposite signs, so that they cancel out. Now, both sums correspond to partition functions of completely uninteracting theories, so that they factor as product over the partition functions over a single link

$$\sum_{\Phi(e)=0}^{1} e^{K - 2K\Phi(e)} = 2\cosh(K) \quad \text{and} \quad \sum_{\Phi(e)=0}^{1} (-1)^{\Phi(e)} e^{K - 2K\Phi(e)} = 2\sinh(K). \tag{A.51}$$

Indeed, we have

$$\sum_{\Phi} e^{-S(\Phi)} = \prod_{e=1}^{N_t} \sum_{\Phi(e)=0}^{1} e^{K-2K\Phi(e)} = (2\cosh(K))^{N_t}, \tag{A.52}$$

and

$$\sum_{\Phi} (-1)^{\sum_{e=1}^{N_t} \Phi(e)} e^{-S(\Phi)} = \prod_{e=1}^{N_t} \sum_{\Phi(e)=0}^{1} (-1)^{\Phi(e)} e^{K-2K\Phi(e)} = (2\sinh(K))^{N_t}. \tag{A.53}$$

The case with $\varphi_i \neq \varphi_f$, corresponding to an odd number of domain walls can be similarly treated by replacing the + sign in (A.50) by a − sign. We thus conclude that

$$Z = \begin{cases} \frac{(2\cosh(K))^{N_t} + (2\sinh(K))^{N_t}}{2}, & \varphi_i = \varphi_f, \\ \frac{(2\cosh(K))^{N_t} - (2\sinh(K))^{N_t}}{2}, & \varphi_i \neq \varphi_f. \end{cases} \tag{A.54}$$

Now, let $\mathcal{M} = {}^{\epsilon\mathbb{Z}}\!/_{T\mathbb{Z}}$. The dual lattice can still be thought of as the same $\tilde{\mathcal{M}} = \{\epsilon, \cdots, N_t\epsilon\}$ with the same space of fields, with the constraint that the number of domain walls now has to be even. However, now every field configuration Φ now corresponds to two fields ϕ and $-\phi$, related to one another by flipping all the spins. The energy $S(\phi)$ is unchanged by this symmetry, so that all we need to do is multiply our partition function of domain walls by two

$$Z = (2\cosh(K))^{N_t} + (2\sinh(K))^{N_t}. \tag{A.55}$$

While this is the standard interpretation given to the Ising model, the range of applicability of this model is extremely wide. For example, one can think of it as a model of a fluid near its liquid-vapor transition. In here $\phi(t) = \pm 1$ corresponds to the presence or absence of a fluid molecule at site t. In this interpretation $K > 0$ yields the intermolecular forces that make the fluid want to coalesce into a liquid phase. Or alternatively, we can use this as a model in sociology where $\phi(t) = \pm 1$ corresponds to the political alignment of the individual t and $K > 0$ to the value people give to agreeing with their neighbors. More importantly for us, will be the quantum field-theoretic interpretation we will discuss next.

A.7.2 Hamiltonian

Spatial slices in this theory correspond to single points $\Sigma = \{t\}$. The field configurations on such slices simply correspond to values $\varphi = \pm 1$. Much like before, the counting measure provides a natural measure $D\varphi$ on this space

$$\int D\varphi\, f(\varphi) = \sum_{\varphi=\pm 1} f(\varphi) = f(1) + f(-1). \tag{A.56}$$

The Hilbert space of this theory is therefore a complex two-dimensional vector space $\mathcal{H} = \text{Span}\{|+1\rangle, |-1\rangle\} \cong \mathbb{C}^2$, with an inner product defined by

$$\langle 1|1\rangle = \langle -1|-1\rangle = 1 \quad \text{and} \quad \langle +1|-1\rangle = \langle -1|+1\rangle = 0. \tag{A.57}$$

There is a standard interpretation for such systems. Namely, this is precisely the Hilbert space of a quantum spin-$\frac{1}{2}$ particle. It is important to remember the differences between the quantum and classical interpretations. While in the classical one, there was a chain of spins, all existing simultaneously, in the quantum pictures there is a single spin. The lattice in the latter corresponds to the time evolution of this single particle. Furthermore, in the quantum picture, general states do not have a well-defined orientation for the spin, as it will be generically a superposition

$$|\psi\rangle = a\,|+1\rangle + b\,|-1\rangle\,. \tag{A.58}$$

In fact, in the quantum interpretation the spin is truly three-dimensional and not constrained to point along a single axis. The states $|\pm 1\rangle$ do not correspond to a spin pointing along, say, the x-axis. They instead correspond to a spin whose component along the x-axis is well-defined. However, we can have states with well-defined spins along the z-axis instead

$$|g\rangle := \frac{|+1\rangle + |-1\rangle}{\sqrt{2}} \quad \text{and} \quad |e\rangle := \frac{|+1\rangle - |-1\rangle}{\sqrt{2}}. \tag{A.59}$$

The Euclidean time-evolution operator of this theory is

$$\langle \varphi_f | U(\underline{N_t}\epsilon) | \varphi_i \rangle = \sum_{\phi \in \mathcal{E}(\underline{N_t}\epsilon)} e^{-S(\phi)}. \tag{A.60}$$

We need to check that these path integrals can be pasted together so that this operator is well-defined. For this it suffices to consider what happens when we split $\underline{N_t}\epsilon$ into $\underline{N_t - 1}\epsilon$ and the points $\{(N_t-1)\epsilon, N_t\epsilon\}$. We only need to note that

$$\begin{aligned} e^{-S_{\underline{N_t}\epsilon}(\phi)} &= e^{K\sum_{n=0}^{N_t-2}\phi(n\epsilon)\phi((n+1)\epsilon) + K\phi((N_t-1)\epsilon)\phi(N_t\epsilon)} \\ &= e^{K\sum_{n=0}^{N_t-2}\phi(n\epsilon)\phi((n+1)\epsilon)} e^{K\phi((N_t-1)\epsilon)\phi(N_t\epsilon)} \\ &= e^{-S_{\underline{N_t-1}\epsilon}(\phi)} e^{-S_{\{(N_t-1)\epsilon, N_t\epsilon\}}(\phi)}, \end{aligned} \tag{A.61}$$

and that sums over $\mathcal{E}(\underline{N_t}\epsilon)$ can be split as

$$\sum_{\substack{\phi \in \mathcal{E}(\underline{N_t}\epsilon) \\ \phi(0)=\varphi_i \\ \phi(N_t\epsilon)=\varphi_f}} = \sum_{\varphi \in \{\pm 1\}} \sum_{\substack{\phi \in \mathcal{E}(\underline{N_t-1}\epsilon) \\ \phi(0)=\varphi_i \\ \phi((N_t-1)\epsilon)=\varphi}} \sum_{\substack{\phi \in \mathcal{E}(\{(N_t-1)\epsilon, N_t\epsilon\}) \\ \phi((N_t-1)\epsilon)=\varphi \\ \phi(N_t\epsilon)=\varphi_f}}. \tag{A.62}$$

Putting these two results together we conclude that

$$\langle\varphi_f|U(\underline{N_t}\epsilon)|\varphi_i\rangle = \sum_{\varphi=\pm 1} \langle\varphi_f|U(\{(N_t-1)\epsilon, N_t\epsilon\})|\varphi\rangle \langle\varphi|U(\underline{N_t-1}\epsilon)|\varphi_i\rangle\,, \tag{A.63}$$

or, using the resolution of the identity,

$$U(\underline{N_t}\epsilon) = U(\{(N_t-1)\epsilon, N_t\epsilon\})U(\underline{N_t-1}\epsilon). \tag{A.64}$$

To construct the Hamiltonian, we need only consider an infinitesimally small lattice, which in this context corresponds to two points $\mathcal{M} = \{0, \epsilon\}$. Then

$$\langle\varphi_f|U(\{0,\epsilon\})|\varphi_i\rangle = e^{K\varphi_f\varphi_i}. \tag{A.65}$$

This operator is diagonalized by the states with a well-defined z-component, on which

$$U(\{0,\epsilon\})\,|g\rangle = 2\cosh(K)\,|g\rangle \quad \text{and} \quad U(\{0,\epsilon\})\,|e\rangle = 2\sinh(K)\,|e\rangle\,. \tag{A.66}$$

With these,

$$U(\{0,\epsilon\}) = 2\cosh(K)\,|g\rangle\langle g| + 2\sinh(K)\,|e\rangle\langle e|\,. \tag{A.67}$$

Taking powers of this operator, we can immediately compute the partition function of this theory for larger lattices

$$U(\underline{N_t}\epsilon) = (2\cosh(K))^{N_t}\,|g\rangle\langle g| + (2\sinh(K))^{N_t}\,|e\rangle\langle e|\,. \tag{A.68}$$

Taking the trace of this operator, for example, leads us immediately to (A.55).

Interpreting this lattice as Euclidean, so that $U(\{0,\epsilon\}) = e^{-\epsilon H}$, we can take the logarithm of this equation and find that

$$\epsilon H = -\ln(2\cosh(K))\,|g\rangle\langle g| - \ln(2\sinh(K))\,|e\rangle\langle e|\,, \tag{A.69}$$

meaning that

$$\epsilon H\,|g\rangle = -\ln(2\cosh(K))\,|g\rangle \quad \text{and} \quad \epsilon H\,|e\rangle = -\ln(2\sinh(K))\,|e\rangle\,. \tag{A.70}$$

Observe that the resulting operator is Hermitian only in the ferromagnetic case. In this case, the ground state is $|g\rangle$ and the excited state is $|e\rangle$, which explains the notation.

Up to an overall shift in the energy, all Hamiltonians of such a two-level system can be interpreted as the interaction with a magnetic field. The fact that the eigenstates of the Hamiltonian have a well-defined z-component shows that this magnetic field points along the z-axis. Although it has been instructive to consider this interpretation for its relation to the classical statistical one, from now on we will prefer an interpretation that is closer to quantum field theory. In particular, we will interpret the state $|g\rangle$ to be the vacuum

of this $1+0$-dimensional universe. It corresponds to an absence of particles. Its energy $\epsilon E_0 = -\ln(2\cosh(K))$ is unobservable in this theory. The state $|e\rangle$ then corresponds to the existence of a single particle. Since space in this model is a point, the particle lies stationary without any motion. Its energy in a relativistic interpretation, when measured with respect to the energy of the vacuum, solely comes from its mass m

$$H|e\rangle = (E_0 + m)|e\rangle . \tag{A.71}$$

It is given by

$$\epsilon m := \ln(2\cosh(K)) - \ln(2\sinh(K)) = \ln(\coth(K)). \tag{A.72}$$

Since there are no further excited states, we conclude that at most one particle can exist. In this sense, this system can be interpreted as fermionic.

A.7.3 Renormalization

The only parameter present in the theory (A.46) is the dimensionless K. Once a K has been chosen, all the predictions of the theory will be dimensionless functions of K, such as (A.72). Obtaining dimensionful predictions requires experimental input. For example, if an experimentalist was to measure the mass m, we could use said measurement to find our lattice spacing

$$\epsilon = \frac{\epsilon m}{m}. \tag{A.73}$$

A different choice of K, would then lead to a different value of ϵm. But, rather than thinking of this as a description of a different physical system, we could think of this as a description of the same system of mass m, but with a different ϵ. There is thus a functional dependence between K and ϵ. Understanding this functional dependence is crucial to take the continuum limit $\epsilon \to 0$, which will allow us to construct e^{-tH} for arbitrary t. The associated change in the action is precisely the renormalization anticipated in Section A.4.

A first hint of how to do this comes from our transfer matrix expression (A.65). The left-hand side of that equation becomes $\delta_{\varphi_i \varphi_f}$ as $\epsilon \to 0$. For $\varphi_i \neq \varphi_f$, this vanishes, while the right-hand side of the equation is e^{-K}. Thus, we must have $K \to \infty$ as $\epsilon \to 0^+$. On the other hand, for $\varphi_i = \varphi_f$, the left-hand side becomes 1, while the right-hand side is $e^K \to \infty$. We have thus reached a contradiction!

The origin of this contradiction comes from the fact that, with our current conventions, the combination

$$\epsilon E_0 \to -K \to -\infty, \quad \epsilon \to 0^+. \tag{A.74}$$

But, as we mentioned before, the energy of the vacuum is unobservable. Corresponding to this, is the fact that we can add a constant term to the action S without modifying the expectation values of the classical statistical theory. Indeed, under a shift $S \mapsto S + N_t s$,

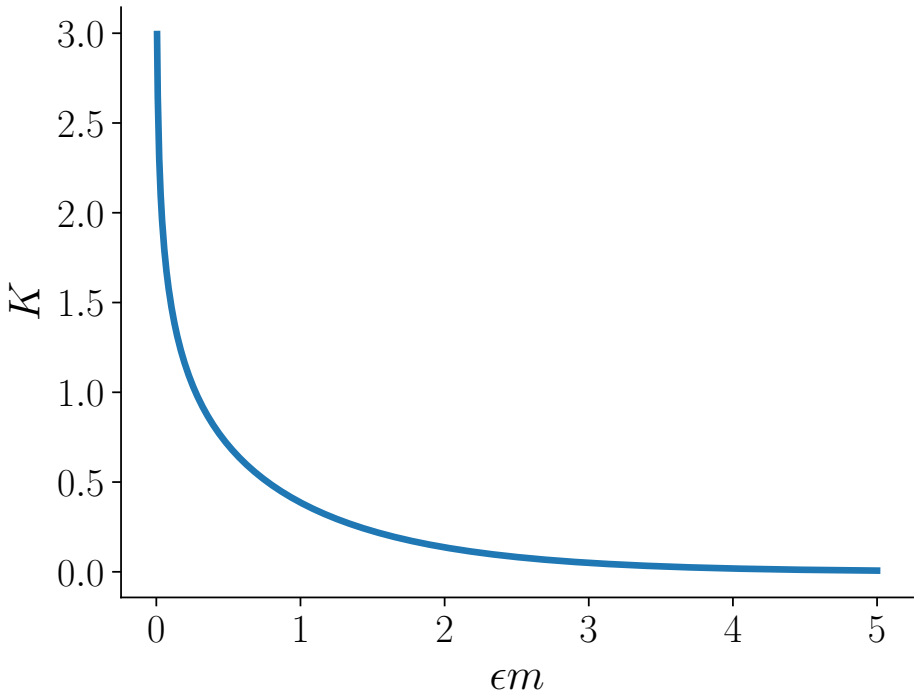


Figure A.5: Renormalization (A.76) of the coupling of the 1D Ising model as a function of the lattice spacing ϵ.

we obtain a corresponding shift of the Hamiltonian of $\epsilon H \mapsto \epsilon H + s$. We thus need to choose an s for which $s \to \infty$ as $\epsilon \to 0^+$. More precisely, in this limit we must have

$$e^{-K-s} \to 0 \quad \text{and} \quad e^{K-s} \to 1, \tag{A.75}$$

so that s has to be chosen so that $s \to K$. This is called a vacuum counterterm. Non-constant counterterms are also needed in more complicated theories and specifying the construction of these is necessary to fully specify a theory.

Having realized the need for a vacuum counterterm, we can now implement our renormalization scheme by inverting (A.72) to set the bare coupling K to be equal to

$$K = \operatorname{arccoth}(e^{\epsilon m}) = -\frac{1}{2}\ln\Big(\frac{\epsilon m}{2}\Big) + \mathcal{O}(\epsilon^2). \tag{A.76}$$

In particular, $K \to \infty$ as $\epsilon \to 0^+$, as required. This is shown in Fig. A.5. From now on, we can make our predictions dimensionful by using this formula to replace the parameter K by m.

We now turn to the determination of s. At this stage it is useful to introduce the number operator N given by

$$N\left|g\right\rangle = 0 \quad \text{and} \quad N\left|e\right\rangle = \left|e\right\rangle. \tag{A.77}$$

in terms of which we can write

$$H = -s/\epsilon + mN, \quad s := \ln(2\cosh(K)). \tag{A.78}$$

With this choice of s, the vacuum counterterm $S \to S + N_t s$ modifies our Hamiltonian to $H \mapsto H + s/\epsilon = mN$, so that the energy of the vacuum is now 0. Rather than replacing K by m using (A.76), for theoretical calculations it is often simpler to directly work with the renormalized form of the Hamiltonian $H = mN$.

A.7.4 Operators

With our choice of Hilbert space, there is a natural operator

$$\phi\left|\varphi\right\rangle = \varphi\left|\varphi\right\rangle, \tag{A.79}$$

which in the spin-$\frac{1}{2}$ interpretation measures the spin along the x-axis. Alternatively, we can introduce the operator that measures the spin along the z-axis

$$\pi\left|g\right\rangle = \left|g\right\rangle \quad \text{and} \quad \pi\left|e\right\rangle = -\left|e\right\rangle, \tag{A.80}$$

in terms of which

$$N = \frac{1-\pi}{2} \tag{A.81}$$

and

$$H = -\frac{m}{2}\pi + \frac{m}{2}. \tag{A.82}$$

In our quantum field theory, the interpretation of this operator stems from the fact that

$$\pi\left|\varphi\right\rangle = \left|-\varphi\right\rangle. \tag{A.83}$$

It is therefore the symmetry operator corresponding to the $\mathbb{Z}_2$ action reflecting the spin along the x-axis. It is a unitary operator satisfying $\pi^2 = 1$ and $\pi\phi\pi = -\phi$. The fact that this implements a symmetry of the theory is given by the fact that $\pi H \pi = H$.

In general, operators O for which $\pi O \pi = O$ are called even, while operators for which $\pi O \pi = -O$ are called odd. This property is multiplicative, the product of operators with the same parity is even, while products with different parity are odd. The space of all operators splits into a direct sum of the operators of these two types, as shown by the decomposition

$$O = \frac{O + \pi O \pi}{2} + \frac{O - \pi O \pi}{2}. \tag{A.84}$$

Thus, without loss of generality, we can restrict to calculations for operators that are either even or odd.

This greatly simplifies the algebra in our calculations, for even operators are diagonal in the basis of states with definite energy, while odd operators are off-diagonal in this basis. This is a consequence of the relations

$$\langle g|O|e\rangle = -\langle g|\pi O\pi|e\rangle = -\langle g|O|e\rangle\,, \tag{A.85}$$

for even operators, and

$$\langle g|O|g\rangle = -\langle g|\pi O\pi|g\rangle = -\langle g|O|g\rangle\,, \tag{A.86}$$

which remain the same under the exchange $|g\rangle \leftrightarrow |e\rangle$. In particular, for periodic lattices odd operators always lead to vanishing traces. We further have

$$\langle \varphi_f|O|\varphi_i\rangle = \pm\langle \varphi_f|\pi O\pi|\varphi_i\rangle = \pm\langle -\varphi_f|O|-\varphi_i\rangle\,, \tag{A.87}$$

with the $+$ sign for even operators and the $-$ sign for odd ones. Thus, without loss of generality, we will from now on restrict our calculations to boundary conditions where $\varphi_i = 1$. For such operators, we have

$$\langle \pm 1|O|1\rangle = \frac{\langle g|O|g\rangle \pm \langle e|O|e\rangle}{2}, \tag{A.88}$$

in the even case, while we have

$$\langle \pm 1|O|1\rangle = \frac{\langle g|O|e\rangle \pm \langle e|O|g\rangle}{2} \tag{A.89}$$

in the odd one.

The primary example of an even operator is the time evolution operator $U([0,t])$. This property can be written as

$$\pi U([0,t]) = U([0,t])\pi. \tag{A.90}$$

This shows that π is a topological operator – it can be moved across time without changing results of calculations, as long as it doesn't cross any ϕ operators.

A.7.5 Correlation Functions

Making use of the $\mathbb{Z}_2$ symmetry, we can now trivially compute correlation functions in this theory. We will do this in the renormalized theory with Hamiltonian $H = Nm$. Since the time-evolution operator is even, for an open time interval

$$\langle \pm 1|U([0,T])|1\rangle = \frac{1 \pm e^{-Tm}}{2}. \tag{A.91}$$

On the other hand, matrix elements of ϕ can be computed noting that it is odd

$$\langle \pm 1|U([t,T])\phi U([0,t])|1\rangle = \frac{e^{-tm} \pm e^{-(T-t)m}}{2} \tag{A.92}$$

The quotient then yields the one-point function of this theory

$$\langle \phi(t)\rangle = \frac{e^{-tm} \pm e^{-(T-t)m}}{1 \pm e^{-Tm}}. \tag{A.93}$$

By the same token, this one point function vanishes on periodic times.

As we will explain in the next section, on an open interval $\langle \phi(t_2)\phi(t_1)\rangle$ is only a function of $t_2 - t_1$. This can be checked through an explicit calculation in the quantum theory. We stress that this is not a consequence of translational symmetry, for the boundary conditions do not respect it. Instead, it is connected to the fact that we are working in one dimensions, and there is only one path joining t_1 and t_2 along the interval. In any case, using this we have

$$\langle \phi(t_2)\phi(t_1)\rangle = \langle \phi(t_2 - t_1)\phi(0)\rangle = \langle \phi(t_2 - t_1)\rangle \,. \tag{A.94}$$

On the other hand, for a periodic time, the two-point function does not vanish. In fact, for even operators O expectation values on periodic times coincide with expectation values on open time intervals with $\varphi_i = \varphi_f = 1$

$$\frac{\operatorname{tr} O}{\operatorname{tr} U([0,T])} = \frac{\langle 1|O|1\rangle}{\langle 1|U([0,T])|1\rangle}. \tag{A.95}$$

While this result was obtained in the continuum, since we have the exact relationship between m and K, it can equally be used on discrete lattices. Indeed, if one is interested in computing $\phi(n\epsilon)$ for a lattice with N_t links and a coupling K, one can use (A.93) using $tm = n\epsilon m$ and $Tm = N_t \epsilon m$, with ϵm given by (A.72). This is exemplified in Fig. A.6.

A.7.6 First quantization

In our interpretation in terms of quantum fields the partition function is a sum over all possible field configurations. The notion of a particle only appeared once we studied the spectrum of the Hamiltonian. This is however not the only useful notion of particle in physics. For example, in QCD, quarks and gluons fail to appear in the spectrum of the Hamiltonian due to confinement. Instead, quarks and gluons appear as a way to interpret the partition function in terms of trajectories of these particles. This is known as first-quantization and is intimately related to the perturbation theory through Feynman diagrams. In the context of the 1D Ising model, it corresponds to the high-temperature expansion, to which we now turn.

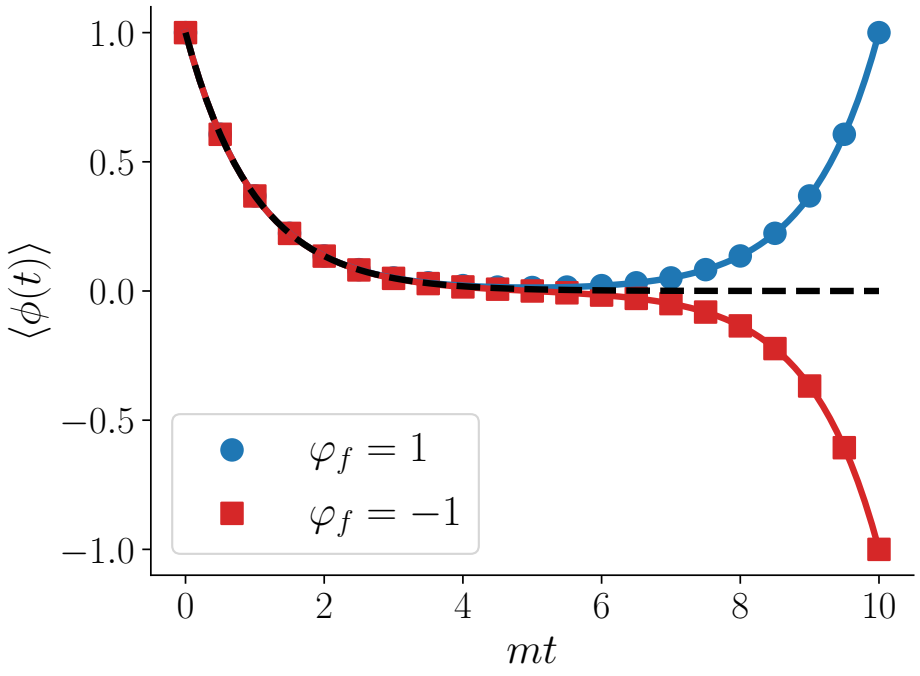


Figure A.6: One point function for the 1D Ising model on a time interval with $mT = 10$ and $\varphi_i = 1$. In solid the continuum result is shown. Scattered points correspond to an Ising chain with $N_t = 20$ links. This corresponds to $K \approx 0.7$. In dashed lines is the result with $T \to \infty$. Letting $t = t_2 - t_1$, these also correspond to $\langle\phi(t_2)\phi(t_1)\rangle$ on this open interval. The $\varphi_f = 1$ curve also yields $\langle\phi(t_2)\phi(t_1)\rangle$ for periodic times.

At high-temperature, K is small and we are therefore inclined to expand e^{-S} in terms of powers of K. However, recalling that $\varphi(t)\varphi(t+\epsilon) \in \{\pm 1\}$, we can perform the manipulation

$$\begin{aligned} e^{K\phi(t)\phi(t+\epsilon)} &= \cosh(K) + \phi(t)\phi(t+\epsilon)\sinh(K) \\ &= \cosh(K)(1 + \phi(t)\phi(t+\epsilon)\tanh(K)). \end{aligned} \tag{A.96}$$

Given that for small K we have $\tanh(K) \approx K + \mathcal{O}(K^3)$, we will instead use $\tanh(K)$ as an expansion parameter.

Let us start focusing on a periodic lattice $\mathcal{M} = \epsilon\mathbb{Z}/L\mathbb{Z}$. In terms of this expansion, the partition function can be written as

$$\begin{aligned} \mathrm{tr}(U(\mathcal{M})) &= \sum_{\phi\in\mathcal{E}(\mathcal{M})} e^{-S(\phi)} = \sum_{\phi\in\mathcal{E}(\mathcal{M})} \prod_{n=0}^{N_t-1} e^{K\phi(n\epsilon)\phi((n+1)\epsilon) - \ln(2\cosh(K))} \\ &= \frac{1}{2^{N_t}} \sum_{\phi\in\mathcal{E}(\mathcal{M})} \prod_{n=0}^{N_t-1} (1 + \phi(n\epsilon)\phi((n+1)\epsilon)\tanh(K)) \end{aligned} \tag{A.97}$$

recalling the extra constant terms we have added to the action to ensure that the vacuum energy vanishes. A generic term in this product can be specified by an unoriented trajectory γ in $\mathcal{M}$ that cannot backtrack. If the trajectory goes through the link joining t and $t+\epsilon$, the term $\phi(t)\phi(t+\epsilon)\tanh(K)$ is chosen. Otherwise, the term 1 is chosen. Then the partition function takes the form

$$\mathrm{tr}(U(\mathcal{M})) = \sum_{\gamma} e^{-S(\gamma)}, \tag{A.98}$$

in terms of a new action, defined for trajectories on $\mathcal{M}$ rather than fields, given by

$$e^{-S(\gamma)} := \frac{1}{2^{N_t}} \sum_{\phi\in\mathcal{E}(\mathcal{M})} \prod_{n=0}^{N_t-1} (\phi(n\epsilon)\phi((n+1)\epsilon)\tanh(K))^{\gamma(n)}. \tag{A.99}$$

In here, $\gamma(n) \in \{0,1\}$ is the number of times γ goes through the link joining $n\epsilon$ and $(n+1)\epsilon$.

To simplify this action, we begin by considering a trajectory for which there is an $n\epsilon \in \mathcal{M}$ for which $\gamma(n-1) = 0$ but $\gamma(n) = 1$. Then in $e^{-S(\gamma)}$, $\phi(n\epsilon)$ appears only once, so that it can be written in the form

$$e^{-S(\gamma)} = \frac{1}{2^{N_t}} \sum_{\phi\in\mathcal{E}(\mathcal{M})} \phi(n\epsilon)(\cdots), \tag{A.100}$$

where $(\cdots)$ does not depend on $\phi(n\epsilon)$. Then the contributions with $\phi(n\epsilon) = 1$ will cancel those of $\phi(n\epsilon) = -1$. The same is of course true if $\gamma(n-1) = 1$ and $\gamma(n) = 0$. We conclude that trajectories with a finite action must have each $\phi(t)$ appearing twice. In this simple geometry, there are only two possible trajectories then. On the one hand, we

have the empty trajectory, which has length 0 and has an action with $e^{-S(\gamma)} = 1$. On the other, we have the trajectory that goes through all links, which has length T and an action $e^{-S(\gamma)} = \tanh(K)^{N_t}$. We conclude that the action for the allowed trajectories is

$$S(\gamma) = ms(\gamma), \tag{A.101}$$

where s is the duration of the trajectory γ.

This action is precisely the action of a relativistic particle of mass m in a Euclidean spacetime. In there γ is the worldline of the particle and $s(\gamma)$ is its proper time, which simplify to our variables for a $D = 1$ spacetime. This gives us yet another avenue towards finding the particle nature of this theory, as well as its mass. It also gives us a new way of computing the partition function, which in our present conventions is thus given by

$$\mathrm{tr}(U(\mathcal{M})) = 1 + e^{-mT}. \tag{A.102}$$

This can be extended to the calculation of correlation functions. For example, on $\mathcal{M} = N_t\epsilon$, there are two trajectories that contribute to $\langle\phi(t_2)\phi(t_1)\rangle$. Let us assume that $t_1 \leq t_2$. There is the one that goes from t_1 to t_2, which has length $t = t_2 - t_1$. The other goes from 0 to t_1 and from t_2 to T, which has length $t_1 + T - t_2 = T - t$. In particular, their durations only depend on t, which explains why this correlation function only depends on t.

A.7.7 Quantum Implementation

We now turn to real time, where our objective is to compute matrix elements with the time evolution operator e^{-iHt}. The Hilbert space of this system is naturally already the same as that of a quantum computer with a single qubit, with the identifications $|1\rangle \mapsto |0\rangle$ and $|-1\rangle \mapsto |1\rangle$ between the physical and logical states. In particular, the Hilbert space already has finite-dimension and there is no need to further restrict it. Furthermore, the time evolution operator is directly implementable in terms of native gates, for under this dictionary $\pi \mapsto X$ and the time evolution operator is simply

$$U(T) = e^{-iTH} = R_X(-mT), \tag{A.103}$$

up to a constant phase. In here we use the standard `qiskit` notation $R_X(\theta) = e^{-iX\theta/2}$.

The simplest calculation one can do is to initialize a single qubit in state $|0\rangle$ and evolve it by time T into $U(T)|0\rangle$. Measurement of the resulting state then yields 0 with probability

$$|\langle 1|U(T)|1\rangle|^2 = \cos(mT/2)^2, \tag{A.104}$$

and 1 with the complementary probability. The results of this simple experiment are found in Fig. A.7.

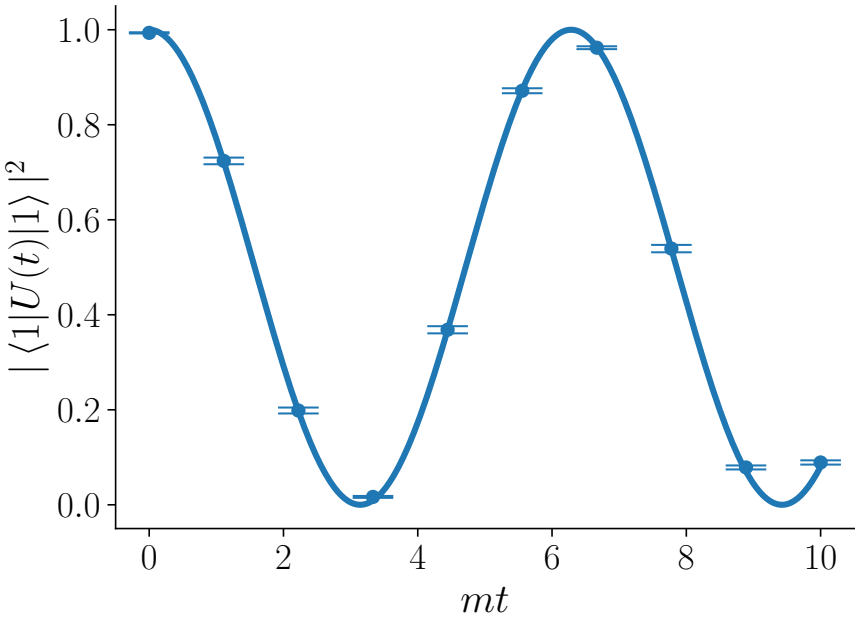


Figure A.7: Transition probability $|\langle 1|U(t)|1\rangle|^2$ in the 1D Ising model. The data were run on `ibm_marrakesh`, with 4096 shots used for each point.

A.8 Harmonic Oscillator

People often say that an education in physics consists in learning to solve the harmonic oscillator in increasingly complicated ways.

We will stay within the realm of one dimensional quantum field theories. However, in this case, we will start with a continuous theory on an interval $\mathcal{M} = [0, T]$ or on a circle $\mathcal{M} = S^1$, both parametrized by a variable t ranging between 0 and T. The field will be a function $\phi : \mathcal{M} \to \mathbb{R}$ and the action will be

$$S(\phi) = \int_{\mathcal{M}} \mathrm{d}t \left(\frac{1}{2} \dot{\phi}^2 + \frac{1}{2} m_0^2 \phi^2 \right), \tag{A.105}$$

which depends on a single parameter m_0 with units of energy. The field ϕ is dimensionful and has mass units $-1/2$.

Under the replacements $\phi \mapsto x$ and $m_0 \mapsto \omega$, the reader will recognize this as the action of a Harmonic oscillator with trajectory $x(t)$ and of unit mass. Observe that in this interpretation m_0 is not the mass of the oscillator, but rather its frequency. We will however prefer a QFT interpretation, much like the one we used in the 1D Ising model. Indeed, we will see that this field theory gives rise to a particle of mass m_0. However, unlike in the Ising model, this particle is a boson. In particular, there will be an infinite number of states, corresponding to excitations with many such particles.

Alternatively, we can also interpret this as a classical statistical theory. This is most simply done after discretizing the above action to spacetimes $\mathcal{M} = \underline{N_t}\epsilon$ or $\mathcal{M} = {}^{\epsilon\mathbb{Z}}\!/_{T\mathbb{Z}}$. We will choose the discretization

$$S(\phi) = \sum_{n=0}^{N_t - 1} \epsilon \left[\frac{1}{2} \left(\frac{\phi(n\epsilon + \epsilon) - \phi(n\epsilon)}{\epsilon} \right)^2 + \frac{1}{2} m_0^2 \phi(n\epsilon)^2 \right]. \tag{A.106}$$

Note that, the term $\frac{1}{2} m_0^2 \phi(T)^2$ does not appear in this version of the action (although it will in the alternative action we will later consider (A.135)). We do this so that the pasting condition of path integrals is satisfied with this action.

Note that, if we were to add the additional constraint that $\phi(t) = \pm\sqrt{K\epsilon}$, for some constant K, then this action reduces to (A.46), up to an additive constant. We can therefore think of this as a generalization of the Ising model without constraints. In particular, we can think of $\mathcal{M}$ as a chain of spins, whose magnetic moment is unconstrained and determined by ϕ. The kinetic term in the action here ensures that there is an energy cost for there being differences between $\phi(t)$ and $\phi(t + \epsilon)$. The potential term ensures that there is an energy cost for $\phi(t)$ being away from 0.

In order to define path integrals

$$\int \mathcal{D}\phi \, e^{-S(\phi)}, \tag{A.107}$$

we need to establish a measure on the space of fields. For $\mathcal{M} = {}^{\epsilon\mathbb{Z}}\!/_{T\mathbb{Z}}$, time translation invariance suggests that we take as a measure

$$\mathcal{D}\phi = \prod_{n=0}^{N_t-1} \mathrm{d}\phi(n\epsilon). \tag{A.108}$$

However, given that the corresponding path integral has to correspond to $\mathrm{tr}\, U(\mathcal{M})$, which is dimensionless, this cannot be correct. More importantly, there is no clear generalization of this to the continuum limit. Nevertheless, for the purposes of studies of correlation functions on the lattice, this measure will be sufficient. Indeed, as we will see, the required corrections come in the form of normalization constants which cancel in the quotients required to compute expectation values.

Exercise 1

1. Let $\mathcal{M} = {}^{\epsilon\mathbb{Z}}\!/_{T\mathbb{Z}}$ and consider the vector space of fields $\mathcal{E}(\mathcal{M}) = \{\phi : \mathcal{M} \to \mathbb{R}\}$. Define on it the inner product

$$\langle \phi_1, \phi_2 \rangle = \epsilon \sum_{t\in\mathcal{M}} \phi_1(t)\phi_2(t). \tag{A.109}$$

   Show that the action (A.106) can be rewritten as $\frac{1}{2}\langle \phi, Q\phi \rangle$, where $Q : \mathcal{E}(\mathcal{M}) \to \mathcal{E}(\mathcal{M})$ is the linear operator $Q := -\Delta + m_0^2$, with

$$(\Delta\phi)(t) := \frac{\phi(t+\epsilon) - 2\phi(t) + \phi(t-\epsilon)}{\epsilon^2}. \tag{A.110}$$

2. Let $\mathcal{M} = S^1$ and $\mathcal{E}(\mathcal{M}) = C^\infty(\mathcal{M})$. Consider the inner product

$$\langle \phi_1, \phi_2 \rangle = \int_{\mathcal{M}} \mathrm{d}t\, \phi_1(t)\phi_2(t). \tag{A.111}$$

   Show instead that the action (A.105) can be rewritten as $\frac{1}{2}\langle \phi, Q\phi \rangle$, with $Q = -\Delta + m_0^2$. In here Δ is the Laplacian $\Delta = \frac{\mathrm{d}^2}{\mathrm{d}t^2}$. Hint: Use integration by parts.

3. Let $\mathcal{M} = [0, T]$ and $\mathcal{E}(\mathcal{M}) = \{\, \phi \in C^\infty(\mathcal{M}) \mid \phi(0) = \varphi_i \quad \text{and} \quad \phi(T) = \varphi_f \,\}$.

   (a) Why is $\mathcal{E}(\mathcal{M})$ not a vector space?

   (b) Consider a $\phi_c \in \mathcal{E}(\mathcal{M})$. Show that $\mathcal{E}(\mathcal{M}) = \phi_c + \mathcal{F}(\mathcal{M})$, where $\mathcal{F}(\mathcal{M})$ is the vector space

$$\mathcal{F}(\mathcal{M}) = \{\, \phi \in C^\infty(\mathcal{M}) \mid \phi(0) = \phi(T) = 0 \,\}. \tag{A.112}$$

Hint: In other words, this exercise is asking you to show that for every element $\phi \in \mathcal{E}(\mathcal{M})$ there exists a $\tilde{\phi} \in \mathcal{F}(\mathcal{M})$ such that $\phi = \phi_c + \tilde{\phi}$. This exercise shows that $\mathcal{E}(\mathcal{M})$ is an affine space modelled on $\mathcal{F}(\mathcal{M})$. This latter vector space is called the space of quantum fluctuations.

(c) Show that

$$S(\phi) = \frac{1}{2}\int_{\mathcal{M}} \mathrm{d}t\, \phi(-\Delta + m_0^2)\phi + \left[\phi\dot{\phi}\right]_{t=0}^{T}. \tag{A.113}$$

Using this show that a solution $\phi_c \in \mathcal{E}(\mathcal{M})$ of the equations of motion must have an action equal to

$$S(\phi_c) = \varphi_f \dot{\phi}_c(T) - \varphi_i \dot{\phi}_c(0). \tag{A.114}$$

(d) Equip $\mathcal{F}(\mathcal{M})$ with the inner product defined by (A.111). Let $\phi_c \in \mathcal{E}(\mathcal{M})$ be a solution of the equations of motion and $\tilde{\phi} \in \mathcal{F}(\mathcal{M})$. Show that

$$S(\phi_c + \tilde{\phi}) = S(\phi_c) + \frac{1}{2}\langle \tilde{\phi}, Q\tilde{\phi}\rangle\,, \quad Q \coloneqq -\Delta + m_0^2. \tag{A.115}$$

A.8.1 Hamiltonian

As a further application of the transfer matrix formalism, let us see how the Hamiltonian of the Harmonic oscillator arises from the lattice action (A.106). At a fixed t, a configuration is determined by the value of the field $\varphi \in \mathbb{R}$ at this moment in time. The Hilbert space is then spanned by states which have a definite field configuration $|\varphi\rangle$

$$\mathcal{H} = \mathrm{Span}\,\{\,|\varphi\rangle \mid \varphi \in \mathbb{R}\,\} \cong L^2(\mathbb{R}) \tag{A.116}$$

This basis has an inner product

$$\langle \varphi_f | \varphi_i \rangle = \delta(\varphi_f - \varphi_i). \tag{A.117}$$

Much like we did in Section A.7.2, we can find the Hamiltonian by studying a lattice with a single link $\mathcal{M} = \{0, \epsilon\}$. The partition function is then trivial in this case and we are left with the problem of finding a Hamiltonian H acting on this space for which

$$\langle \varphi_f | e^{-\epsilon H} | \varphi_i \rangle = e^{-\epsilon\left[\frac{1}{2}\left(\frac{\varphi_f - \varphi_i}{\epsilon}\right)^2 + \frac{1}{2}m_0^2\varphi_i^2\right]} \tag{A.118}$$

Since we are mostly interested in the continuum limit, we immediately note that, much like in Section A.7.3, we will need to include an additive counterterm to ensure that the energy of the ground state is well-defined. Associated to this is the fact that the left-hand

side of (A.118) has the $\epsilon \to 0$ limit of $\delta(\varphi_f - \varphi_i)$. Fortunately, for $\varphi_f \neq \varphi_i$, we already have that the right-hand side vanishes in this limit. For $\varphi_f = \varphi_i$, the limit of the right-hand side is however equal to one. Thus, we need to add a term to the action which makes this diverge.

A simple way to find such a term is to compute the integral

$$\int \mathrm{d}\varphi_f \, e^{-\epsilon\left[\frac{1}{2}\left(\frac{\varphi_f-\varphi_i}{\epsilon}\right)^2+\frac{1}{2}m_0^2\varphi_i^2\right]} = \sqrt{2\pi\epsilon}e^{-\epsilon\frac{1}{2}m_0^2\varphi_i^2}. \tag{A.119}$$

We can then add to the action the counterterm $N_t \ln(2\pi\epsilon)/2$ to ensure that one obtains the correct normalization as $\epsilon \to 0$. We then need to find a Hamiltonian for which

$$\langle\varphi_f|e^{-\epsilon H}|\varphi_i\rangle = \frac{1}{\sqrt{2\pi\epsilon}}e^{-\epsilon\left[\frac{1}{2}\left(\frac{\varphi_f-\varphi_i}{\epsilon}\right)^2+\frac{1}{2}m_0^2\varphi_i^2\right]} \tag{A.120}$$

We first quantize the field, so that

$$\phi\,|\varphi\rangle = \varphi\,|\varphi\rangle\,. \tag{A.121}$$

Then, if we write $e^{-\epsilon H} = e^{-\epsilon H_0}e^{-\epsilon\frac{1}{2}m_0^2\phi^2}$, we conclude that H_0 must satisfy

$$\langle\varphi_f|e^{-\epsilon H_0}|\varphi_i\rangle = \frac{1}{\sqrt{2\pi\epsilon}}e^{-\frac{(\varphi_f-\varphi_i)^2}{2\epsilon}}. \tag{A.122}$$

This is in particular the Hamiltonian for a theory with $m_0 = 0$.

To find this Hamiltonian we introduce the translation operator $T(a)$

$$T(a)\,|\varphi\rangle = |\varphi + a\rangle\,, \tag{A.123}$$

which is unitary. Expanding in a Taylor series, we see that

$$\langle\varphi|T(a)|\psi\rangle = \langle\varphi - a|\psi\rangle = e^{-a\frac{\mathrm{d}}{\mathrm{d}\varphi}}\,\langle\varphi|\psi\rangle\,. \tag{A.124}$$

Therefore, we can write $T(a) = e^{-ia\pi}$ in terms of the operator π defined by

$$\langle\varphi|\pi|\psi\rangle = -i\frac{\mathrm{d}}{\mathrm{d}\varphi}\,\langle\varphi|\psi\rangle\,. \tag{A.125}$$

This operator is useful because we have

$$\langle\varphi_f|\int \mathrm{d}\varphi\, f(\varphi)T(\varphi)|\varphi_i\rangle = f(\varphi_f - \varphi_i). \tag{A.126}$$

We then conclude that

$$e^{-\epsilon H_0} = \frac{1}{\sqrt{2\pi\epsilon}}\int \mathrm{d}\varphi\, e^{-\frac{\varphi^2}{2\epsilon}}T(\varphi). \tag{A.127}$$

This Gaussian integral can be computed immediately, so that

$$H_0 = \frac{\pi^2}{2}. \tag{A.128}$$

We conclude that

$$e^{-\epsilon H} = e^{-\epsilon\pi^2/2} e^{-\epsilon m_0^2 \phi^2/2}. \tag{A.129}$$

So far, this has been exact, regardless of the value of ϵ. In particular, the Hamiltonian we have obtained is not Hermitian, since this equation is not. However, if we take infinitesimally small ϵ, we can combine these exponentials, without having to account for π and ϕ not commuting with one another. We conclude that

$$H = \frac{\pi^2}{2} + \frac{1}{2} m_0^2 \phi^2. \tag{A.130}$$

This coincides with the Hamiltonian of the harmonic oscillator. In particular, we see that the spectrum consists of a tower of states $|n\rangle$, for $n = 0, 1, 2, ...$, and energies $E_n = nm_0$ measured with respect to the vacuum. This corresponds to states of n bosons, each contributing an energy equal to their mass m_0.

A.8.2 Renormalization

Although we have convinced ourselves that this theory does describe the physics of a single boson of mass m_0, it would still be interesting to solve for the Hamiltonian of a theory with a non-zero ϵ. At the end of the day, lattice theories will always have this. In order to do this, let us go back to the calculation of the Hamiltonian defined by (A.129). In general, we could expand this in orders of ϵ to compute H in perturbation theory. However, this system is simple enough that we can compute H exactly.

In order to do this we note that the Baker-Campbell-Hausdorff formula guarantees that H can be written as a linear combination of the operators in the Lie algebra generated by π^2 and ϕ^2. So we begin by characterizing this Lie algebra. Using that $[\phi, \pi] = i$, we find that

$$[\phi^2, \pi^2] = 2i\{\phi, \pi\}, \quad \{\phi, \pi\} = \phi\pi + \pi\phi. \tag{A.131}$$

Furthermore,

$$[\phi^2, \{\phi, \pi\}] \propto \phi^2 \quad \text{and} \quad [\pi^2, \{\phi, \pi\}] \propto \pi^2. \tag{A.132}$$

Thus, we see that ϕ^2, π^2 and $\{\phi, \pi\}$ form a basis of this Lie algebra. The Hamiltonian has to be a linear combination of these three operators.

This linear combination can be computed in any faithful representation of the Lie algebra. In particular, it is easier to work in the finite-dimensional representation obtained

by the adjoint action of the algebra on the space generated by the operators ϕ and π themselves. Indeed, we can compute

$$\begin{aligned} e^{-\epsilon\pi^2/2}\phi e^{\epsilon\pi^2/2} = e^{-\epsilon[\pi^2,\cdot]/2}\phi = \phi + i\epsilon\pi \quad \text{and} \quad e^{-\epsilon\pi^2/2}\pi e^{\epsilon\pi^2/2} = \pi, \\ e^{-\epsilon m_0^2\phi^2/2}\pi e^{\epsilon m_0^2\phi^2/2} = \pi - i\epsilon m_0^2\phi \quad \text{and} \quad e^{-\epsilon m_0^2\phi^2/2}\phi e^{\epsilon m_0^2\phi^2/2} = \phi. \end{aligned} \tag{A.133}$$

This yields

$$e^{-\epsilon H}\phi e^{\epsilon H} = \phi + i\epsilon\pi \quad \text{and} \quad e^{-\epsilon H}\pi e^{\epsilon H} = (1+\epsilon^2 m_0^2)\pi - i\epsilon m_0^2\phi. \tag{A.134}$$

The logarithm can now be computed by diagonalizing this action. However, the fact that our target Hamiltonian is not Hermitian makes this cumbersome. Therefore, we now switch to an alternative to the discretization (A.106)

$$S(\phi) = \sum_{n=0}^{N_t-1} \epsilon \left[\frac{1}{2}\left(\frac{\phi(n\epsilon+\epsilon) - \phi(n\epsilon)}{\epsilon} \right)^2 + \frac{1}{4} m_0^2 (\phi(n\epsilon)^2 + \phi((n+1)\epsilon)^2) \right]. \tag{A.135}$$

This action coincides with our previous one in the case of periodic times. But on open intervals, while (A.106) was asymmetric in the roles of $\phi(0)$ and $\phi(T)$, this action now treats them equally. With it, the transfer matrix would instead be

$$e^{-\epsilon H} = e^{-\epsilon m_0^2\phi^2/4} e^{-\epsilon\pi^2/2} e^{-\epsilon m_0^2\phi^2/4}, \tag{A.136}$$

which does lead to a Hermitian Hamiltonian.

With this new transfer matrix, we can recompute its adjoint action

$$\begin{aligned} e^{-\epsilon H}\phi e^{\epsilon H} &= (1+\epsilon^2 m_0^2/2)\phi + i\epsilon\pi \\ e^{-\epsilon H}\pi e^{\epsilon H} &= (1+\epsilon^2 m_0^2/2)\pi - i\epsilon m_0^2(1+\epsilon^2 m_0^2/4)\phi. \end{aligned} \tag{A.137}$$

In the (ϕ, π) basis, this has the matrix representation

$$\begin{pmatrix} 1+\epsilon^2 m_0^2/2 & -i\epsilon m_0^2(1+\epsilon^2 m_0^2/4) \\ i\epsilon & 1+\epsilon^2 m_0^2/2 \end{pmatrix}, \tag{A.138}$$

which is a 2×2 matrix with unit determinant. Accordingly its eigenvalues are reciprocals, and thus can be written in the form $e^{\pm\epsilon m}$, in terms of a new energy scale m. We can solve for this energy scale by computing the trace of this matrix

$$2\cosh(\epsilon m) = 2 + \epsilon^2 m_0^2. \tag{A.139}$$

This matrix representation is thus

$$\begin{pmatrix} \cosh(\epsilon m) & -i\sinh(\epsilon m)^2/\epsilon \\ i\epsilon & \cosh(\epsilon m) \end{pmatrix}. \tag{A.140}$$

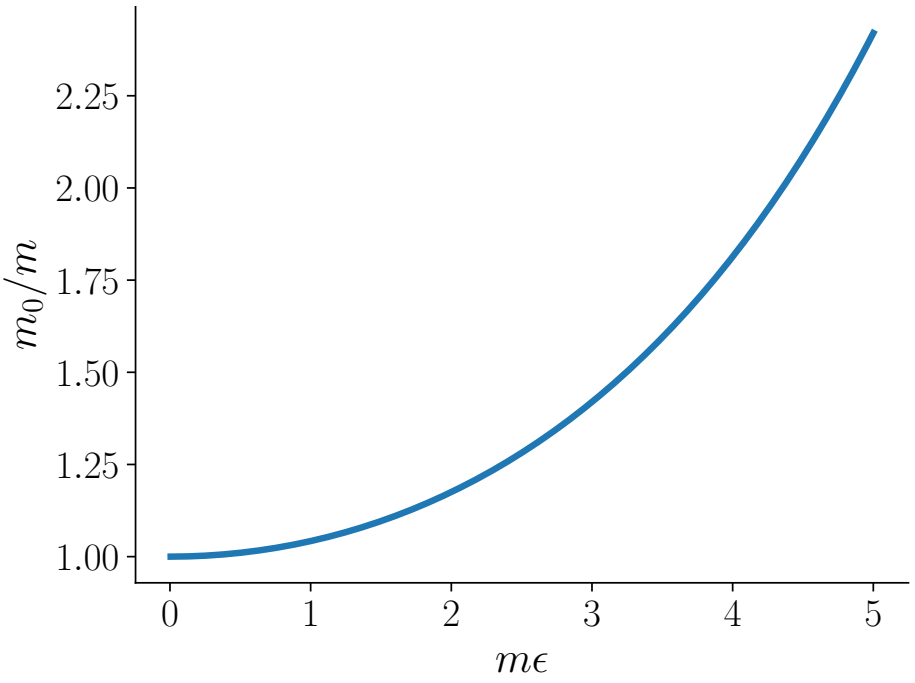


Figure A.8: Mass renormalization (A.139) for the harmonic oscillator.

We then conclude that the eigenspaces associated to $e^{\pm\epsilon m}$ are

$$\mathcal{O}^{\pm} = \sinh(\epsilon m)\phi \pm i\epsilon\pi. \tag{A.141}$$

In particular,

$$[H, \mathcal{O}^{\pm}] = \mp m\mathcal{O}^{\pm}. \tag{A.142}$$

We thus see that $a = \mathcal{O}^{+}$ and $a^{\dagger} = \mathcal{O}^{-}$ are operators of annihilation and creation, respectively, creating particles of mass m.

We thus conjecture that the theory with $\epsilon \neq 0$ is equivalent to the theory in the continuum limit, but with particles of mass m instead of m_0. The two of course agree when $\epsilon \to 0$. The dependence of the bare parameter m_0 on ϵ is given in (A.139) and shown in Fig. A.8.

To make this conjecture precise, we recall that the Baker-Campbell-Hausdorff formula and the Hermitian property demands that H is a real linear combination of ϕ^2, π^2 and $\{\phi, \pi\}$. Then (A.142) implies that

$$[H, \phi] = \frac{-i\epsilon m}{\sinh(\epsilon m)^2}\pi \quad \text{and} \quad [H, \pi] = \frac{im}{\epsilon}\sinh(\epsilon m)^2\phi. \tag{A.143}$$

Since

$$[\{\phi,\pi\},\phi]\propto\phi,\quad [\{\phi,\pi\},\pi]\propto\pi,\quad \frac{1}{2}[\pi^2,\phi]=-i\pi\quad\text{and}\quad \frac{1}{2}[\phi^2,\pi]=i\phi, \tag{A.144}$$

We conclude that

$$H=\frac{1}{2}\frac{\epsilon m}{\sinh(\epsilon m)}\pi^2+\frac{1}{2}\frac{m\sinh(\epsilon m)}{\epsilon}\phi^2. \tag{A.145}$$

This confirms as expected that for $\epsilon\neq 0$ the theory is still that of a Harmonic oscillator. In fact, to put it in a form that is simpler to contrast with (A.130), we can introduce renormalized operators

$$\Pi=\sqrt{\frac{\epsilon m}{\sinh(\epsilon m)}}\pi\quad\text{and}\quad \Phi=\sqrt{\frac{\sinh(\epsilon m)}{\epsilon m}}\phi, \tag{A.146}$$

which maintain the canonical commutation relations $[\Phi,\Pi]=i$, and in terms of which

$$H=\frac{1}{2}\Pi^2+\frac{1}{2}m^2\Phi^2. \tag{A.147}$$

This makes it evident that the mass of this theory is indeed m. The multiplicative renormalization in (A.146) is called wavefunction renormalization.

Exercise 2

Construct the effective non-hermitian Hamiltonian coming from the non-symmetric action (A.106). This is the Hamiltonian that satisfies (A.129) exactly.

A.8.3 Operators

Following Section A.3, the operator ϕ quantized directly according to $\phi\,|\varphi\rangle=\varphi\,|\varphi\rangle$. However, the quantization of the operator $\dot{\phi}$, given that it contains derivatives, is more involved. In this section we will show that $\pi=i\dot{\phi}$. Note the extra factor of i due to the fact that we are in Euclidean time.

In order to extract the quantization, we will first consider the difference operator $(\phi(\epsilon)-\phi(0))/\epsilon$, on a lattice $\{0,\epsilon\}$ with action (A.106). Then the path integral with this operator insertion is

$$\begin{aligned}\frac{1}{\sqrt{2\pi\epsilon}}e^{-\frac{(\varphi_f-\varphi_i)^2}{2\epsilon}-\epsilon\frac{\varphi_i^2}{2}}\frac{\varphi_f-\varphi_i}{\epsilon}&=-\frac{\mathrm{d}}{\mathrm{d}\varphi_f}\frac{1}{\sqrt{2\pi\epsilon}}e^{-\frac{(\varphi_f-\varphi_i)^2}{2\epsilon}-\epsilon\frac{\varphi_i^2}{2}}\\&=-\frac{\mathrm{d}}{\mathrm{d}\varphi_f}\langle\varphi_f|e^{-\epsilon H}|\varphi_i\rangle\,,\end{aligned} \tag{A.148}$$

which for sufficiently small ϵ should be equal to the path integral in the continuum with this operator insertion. However, the latter corresponds to $\langle\varphi_f|e^{-\epsilon H}\dot{\phi}|\varphi_i\rangle$. Thus, taking the $\epsilon \to 0$ limit, we conclude that

$$\langle\varphi_f|\dot{\phi}|\varphi_i\rangle = -\frac{\mathrm{d}}{\mathrm{d}\varphi_f}\langle\varphi_f|\varphi_i\rangle\,. \tag{A.149}$$

Comparison with (A.125) then yields $\pi = i\dot{\phi}$, as desired.

A.8.4 Correlation Functions

We now consider the computation of the two point function $\langle\phi(t)\phi(0)\rangle$ on a periodic time $\mathcal{M} = S^1$ of circumference T. Following Section A.5, we know that this correlation function satisfies the equations of motion of the action $S(\phi) - \phi(0)$, whose variation is

$$\delta S - \delta\phi(0) = \int \mathrm{d}t\,\big(-\ddot{\phi} + m^2\phi - \delta(t)\big)\delta\phi. \tag{A.150}$$

All boundary contributions vanish due to the periodic boundary conditions. We conclude that

$$\ddot{f} - m^2 f = -\delta(t), \tag{A.151}$$

with $f(t) = \langle\phi(t)\phi(0)\rangle$.

These equations are easily solved. For this we will take as coordinates of the circle $t \in [0, T)$. For $t \neq 0$, the solution is a linear combination of the functions $e^{\pm mt}$. Periodic boundary conditions then enforce that $f(t) \propto e^{mt} + e^{m(T-t)}$. The constant of proportionality is then fixed by integrating the equation of motion around $t = 0$, which demands that

$$\dot{f}(0) - \dot{f}(T) = -1. \tag{A.152}$$

We conclude that

$$\langle\phi(t)\phi(0)\rangle = \frac{\cosh\big(m\big(\frac{T}{2} - t\big)\big)}{2m\sinh\big(\frac{mT}{2}\big)}. \tag{A.153}$$

The discussion in Section A.8.2 shows that this immediately generalizes to the lattice $\mathcal{M} = {}^{\epsilon\mathbb{Z}}\!/_{T\mathbb{Z}}$ by using renormalized quantities

$$\langle\Phi(t)\Phi(0)\rangle = \frac{\cosh\big(m\big(\frac{T}{2} - t\big)\big)}{2m\sinh\big(\frac{mT}{2}\big)}. \tag{A.154}$$

Moreover, we can consider the thermodynamic limit $T \to \infty$, where the two point function becomes

$$\langle\Phi(t)\Phi(0)\rangle = \frac{e^{-mt}}{2m}. \tag{A.155}$$

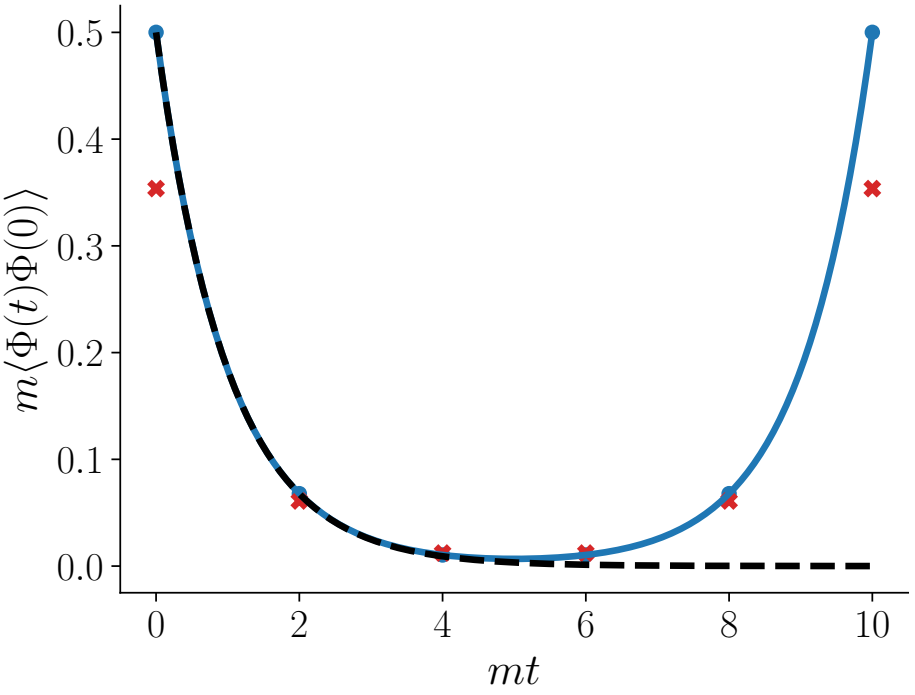


Figure A.9: Two-point function for the harmonic oscillator on a periodic time with $mT = 10$. In solid the continuum result is shown. Scattered points correspond to a chain with $N_t = 5$ links. In dashed lines is the result with $T \to \infty$. In crossed markers, we show the naive unrenormalized propagator $m_0 \langle\phi(t)\phi(0)\rangle$ on the chain, had we taken instead $m_0 T = 10$, showing the importance of renormalization in comparing lattice and physical results.

These are shown in Fig. A.9.

It is important to remark that (A.155) is only valid for $t > 0$, since it was obtained from a solution in which t was restricted to $[0, T]$. Its extension to $\mathbb{R}$ is given by time reversal symmetry

$$\langle \Phi(t)\Phi(0)\rangle = \frac{e^{-m|t|}}{2m}. \tag{A.156}$$

This is a solution to the sourced equations of motion on $\mathbb{R}$. However, it is not unique, for we can always add a solution to the homogeneous equation of motion. It is however unique in that the field does not diverge as $t \to \pm\infty$. These boundary conditions are the ones selected by taking the infinite-volume limit from periodic boundary conditions.

As an illustration of the interplay between the path integral and operator formalisms, note that by differentiation we can compute

$$\begin{aligned} \langle \pi(t)\phi(0)\rangle = i\frac{\mathrm{d}}{\mathrm{d}t}\langle \phi(t)\phi(0)\rangle = -\frac{i}{2}e^{-m|t|}(2\Theta(t)-1), \\ \Theta(t) := \begin{cases} 1 & t > 0 \\ 0 & t < 0 \end{cases} \end{aligned} \tag{A.157}$$

where for simplicity we decided to work on $\mathcal{M} = \mathbb{R}$. We conclude that

$$\langle [\pi(0), \phi(0)]\rangle = \lim_{\epsilon\to 0^+}(\langle \pi(\epsilon)\phi(0)\rangle - \langle \pi(-\epsilon)\phi(0)\rangle) = -i, \tag{A.158}$$

as is consistent with the canonical commutation relations.

Exercise 3

1. Starting from either (A.106) or (A.135) on $\mathcal{M} = {}^{\epsilon\mathbb{Z}}\!/_{T\mathbb{Z}}$, show that

$$\delta S = \sum_{t\in\mathcal{M}} \epsilon\Big[-\frac{1}{\epsilon^2}(\phi(t+\epsilon)+\phi(t-\epsilon)-2\phi(t)) + m_0^2\phi(t)\Big]\delta\phi(t). \tag{A.159}$$

2. Let $f(t) = \langle \phi(t)\phi(t_0)\rangle$. Following Section A.5, we know $f(t)$ must satisfy the equations of motion of the action $S(\phi) - \phi(t_0)$. Show that this implies that

$$-\frac{1}{\epsilon^2}(f(t+\epsilon)+f(t-\epsilon)-2f(t)) + m_0^2 f(t) = \frac{1}{\epsilon}\delta_{t,t_0}. \tag{A.160}$$

3. Show that the solution to this equation is

$$\langle \phi(t)\phi(t_0)\rangle = \frac{1}{T}\sum_{\omega\in\tilde{\mathcal{M}}} \frac{e^{i\omega(t-t_0)}}{\frac{4\sin(\omega\epsilon/2)^2}{\epsilon^2} + m_0^2}. \tag{A.161}$$

Hint: You may find useful to use the Fourier transform

$$f(t) = \frac{1}{N_t} \sum_{\omega \in \tilde{\mathcal{M}}} e^{i\omega t} \tilde{f}(\omega), \quad \tilde{\mathcal{M}} := \frac{2\pi}{T}\mathbb{Z} \diagup \frac{2\pi}{\epsilon}\mathbb{Z}. \tag{A.162}$$

4. Taking the limit as $\epsilon \to 0$, show that on $\mathcal{M} = S^1$ we have

$$\langle \phi(t)\phi(t_0) \rangle = \frac{1}{T} \sum_{\omega \in \frac{2\pi}{T}\mathbb{Z}} \frac{e^{i\omega(t-t_0)}}{\omega^2 + m^2}, \tag{A.163}$$

5. Taking the limit $L \to \infty$, show that on $\mathcal{M} = \mathbb{R}$

$$\langle \phi(t)\phi(t_0) \rangle = \int \frac{\mathrm{d}\omega}{2\pi} \frac{e^{i\omega(t-t_0)}}{\omega^2 + m^2} \tag{A.164}$$

6. Show that (A.164) coincides with (A.155). Hint: You may find it useful to use the residue theorem.

7. Show that (A.163) coincides with (A.153). Hint: You may find it useful to use the Poisson summation formula

$$\frac{1}{T} \sum_{\omega \in \frac{2\pi}{T}\mathbb{Z}} f(\omega) = \sum_{n \in \mathbb{Z}} \int \frac{\mathrm{d}\omega}{2\pi} e^{in\omega T} f(\omega). \tag{A.165}$$

   This is a general tool that we will use in order to relate infinite and finite volume calculations.

8. Show that (A.161) coincides with (A.154). Hint: This is considerably harder than the other problems. In order to do it, first note that (A.161) is a sum over the N_t-roots of unity. Then use the residue theorem to show that a sum of a function $f(z)$ over the N_t-roots of unity can be written as an integral of $N_t f(z)/(z(z^{N_t} - 1))$. The contour of that integral can be taken to be any union of a circle of radius bigger than one in the counter-clockwise direction, and a circle of radius smaller than one in the clockwise direction. Then use the residue theorem to deform this contour so that it encloses only the poles coming from $f(z)$.

A.9 2D Ising Model

We now return to the study of models that begin on the lattice. We will however move to the two-dimensional case, where the physics is much richer. We return to the Ising model,

first explore in Section A.7. Our spacetime lattices will now be of the form $\mathcal{M} = \underline{N_t}\epsilon \times \Sigma$, where $\Sigma \in \left\{ \underline{N_s}a, {}^{a\mathbb{Z}}\!/_{L\mathbb{Z}} \right\}$ is the spatial lattice. In this section and through the remainder of this dissertation we will restrict to spacetimes in which the temporal extent is not periodic. As before, the number of temporal links is given by N_t, so that the total time extent is $T = N_t\epsilon$. But we now have N_s spatial links, so our lattice has a total spatial length $L = N_s a$. The fields are functions ϕ on $\mathcal{M}$ such that for all $x \in \mathcal{M}$ we have $\phi(x) \in \{\pm 1\}$. The resulting space of fields $\mathcal{E}(\mathcal{M})$ is thus finite and we can also use the counting measure on it. The description of the theory is then complete once we introduce the action

$$\begin{aligned} S(\phi) = -K_t \sum_{n=0}^{N_t-1} \sum_{\boldsymbol{x}\in\Sigma} \phi(n\epsilon, \boldsymbol{x})\phi((n+1)\epsilon, \boldsymbol{x}) \\ - K_s \sum_{t\in\underline{N_t-1}\epsilon} \sum_{\boldsymbol{r}=0}^{N_s-1} \phi(t, \boldsymbol{r}a)\phi(t, (\boldsymbol{r}+1)a). \end{aligned} \tag{A.166}$$

Note that at $t = T$ the spatial interactions are neglected. This is to maintain the pasting properties of path integrals, much like in (A.106). We will further restrict to the ferromagnetic case $K_t, K_s > 0$.

A.9.1 Hamiltonian

In the action (A.166) we have decided that temporal neighbors and spatial neighbors have different couplings K_t and K_s. This is due to the fact that our lattice has different temporal and spatial spacings ϵ and a. We did this so that we can build the Hamiltonian through the transfer matrix formalism, in which we will take $\epsilon \to 0$. This will leave us with a quantum theory in continuous time, but in which the discrete spatial lattice Σ survives.

At a fixed time t, the spatial slice is $\{t\} \times \Sigma$. The configurations on it are determined by functions φ on Σ, assigning to each $\boldsymbol{x} \in \Sigma$ a value $\varphi(\boldsymbol{x}) \in \{\pm 1\}$. The span yields the Hilbert space

$$\mathcal{H} = \mathrm{Span}\left\{ |\varphi\rangle \mid \varphi : \Sigma \to \{\pm 1\} \right\} \cong (\mathbb{C}^2)^{\otimes\Sigma}. \tag{A.167}$$

This Hilbert space can be thought of as that of a chain Σ of spins that are interacting with one another. Indeed, we will show that the Hamiltonian of the quantum theory is precisely that of a now *quantum* 1D Ising model, where the coupling between the spins is given by K_s. Moreover, much like in Section A.7.2, this chain of spins will be further embedded in a magnetic field along the z-axis. In fact, we will see that its relation to K_t is analogous to (A.72).

To do this we now build the transfer matrix on the lattice with $N_t = 1$ temporal link.

We want to find a Hamiltonian H for which

$$\langle\varphi_f|e^{-\epsilon H}|\varphi_i\rangle = e^{-S} = \prod_{\boldsymbol{x}\in\Sigma} e^{K_t\varphi_i(\boldsymbol{x})\varphi_f(\boldsymbol{x})} \\ e^{\sum_{\boldsymbol{r}=0}^{N_s-1} K_s\varphi_i(\boldsymbol{r}a)\varphi_i((\boldsymbol{r}+1)a)} \tag{A.168}$$

Much like in Section A.8.1, quantization of the field

$$\phi(\boldsymbol{x})\,|\varphi\rangle = \varphi(\boldsymbol{x})\,|\varphi\rangle\,, \tag{A.169}$$

immediately suggests we define a Hamiltonian H_0 by the formula

$$e^{-\epsilon H} = e^{-\epsilon H_0} e^{K_s\sum_{\boldsymbol{r}=0}^{N_s-1}\phi(\boldsymbol{r}a)\phi((\boldsymbol{r}+1)a)}. \tag{A.170}$$

Then H_0 must satisfy

$$\langle\varphi_f|e^{-\epsilon H_0}|\varphi_i\rangle = \prod_{\boldsymbol{x}\in\Sigma} e^{K_t\varphi_i(\boldsymbol{x})\varphi_f(\boldsymbol{x})}. \tag{A.171}$$

Fortunately, we can directly determine H_0 from the work we did in the $D = 1$ case in Section A.7.2. The reason is that we can express

$$H_0 = \sum_{\boldsymbol{x}\in\Sigma} H_0(\boldsymbol{x}). \tag{A.172}$$

The $H_0(\boldsymbol{x})$ are defined to be operators supported at $\boldsymbol{x}$, so that they commute with one another. They must then satisfy

$$\langle\varphi_f|e^{-\epsilon H_0(\boldsymbol{x})}|\varphi_i\rangle = e^{K_t\varphi_i(\boldsymbol{x})\varphi_f(\boldsymbol{x})}. \tag{A.173}$$

But this is entirely analogous to the transfer matrix of the 1D model (A.65). In particular, up to a constant, it is given by

$$H_0(\boldsymbol{x}) = -B\pi(\boldsymbol{x}). \tag{A.174}$$

Comparing against the magnetic field in (A.82) and (A.72), we have defined B by

$$2\epsilon B = \ln(\coth(K_t)). \tag{A.175}$$

On the other hand, the operator measuring the spin in the z-direction implements the $\mathbb{Z}_2$ action

$$\pi(\boldsymbol{x})\,|\varphi\rangle = |\pi(\boldsymbol{x})\varphi\rangle\,, \tag{A.176}$$

where

$$(\pi(\boldsymbol{x})\varphi)(\boldsymbol{y}) = \begin{cases}\varphi(\boldsymbol{y}), & \boldsymbol{y}\neq\boldsymbol{x},\\ -\varphi(\boldsymbol{x}), & \boldsymbol{y}=\boldsymbol{x},\end{cases} \tag{A.177}$$

in analogy to (A.83).

Finally, we need to extract the Hamiltonian H from

$$e^{-\epsilon H} = e^{\epsilon B \sum_{\boldsymbol{x}\in\Sigma} \pi(\boldsymbol{x})} e^{K_s \sum_{\boldsymbol{r}=0}^{N_s-1} \phi(\boldsymbol{r}a)\phi((\boldsymbol{r}+1)a)}. \tag{A.178}$$

We will not attempt to do this in the finite ϵ case, unlike the previous sections. But in the limit $\epsilon \to 0$ this can be achieved by demanding that K_s is renormalized as $K_s = \epsilon J$ in terms of a J independent of ϵ. Then in this limit we recover the Hamiltonian

$$H = -B \sum_{\boldsymbol{x}\in\Sigma} \pi(\boldsymbol{x}) - J \sum_{\boldsymbol{r}=0}^{N_s-1} \phi(\boldsymbol{r}a)\phi((\boldsymbol{r}+1)a). \tag{A.179}$$

This is the Hamiltonian of a 1D quantum Ising model in which the spins have a coupling strength J in the x-direction and the chain is embedded in a magnetic field along the z-direction determined by B.

A.9.2 Diagonalization of the Hamiltonian

We now turn to the exact solution of the quantum model, for which we will closely follow [172]. We will choose a periodic lattice $\Sigma = {}^{a\mathbb{Z}}\!/_{L\mathbb{Z}}$ to preserve translation invariance. We first perform a Jordan-Wigner transformation, which transforms this into a fermionic model. That this is a good thing to do can be seen by introducing operators $a^{\pm}(\boldsymbol{x})$, adjoint to one another, supported at $\boldsymbol{x} \in \Sigma$, and satisfying

$$[-\pi(\boldsymbol{x}), a^{\pm}(\boldsymbol{x})] = \pm 2 a^{\pm}(\boldsymbol{x}), \tag{A.180}$$

which are then the creation and annihilation operators for the $-B\pi(\boldsymbol{x})$ part of the Hamiltonian. Given that there can be at most a single excitation, they satisfy anticommutation relations resembling those of fermions

$$\begin{aligned} \{a^{\pm}(\boldsymbol{x}), a^{\pm}(\boldsymbol{x})\} &= 0, \\ \{a^{+}(\boldsymbol{x}), a^{-}(\boldsymbol{x})\} &= 1, \end{aligned} \tag{A.181}$$

However, in this form, the spins cannot be truly treated as fermions since the operators at different sites commute instead of anticommuting.

The Jordan-Wigner transformation solves this by attaching to each spin at the site $\boldsymbol{x} = \boldsymbol{r}a$ a defect extending all the way to $\boldsymbol{x} = 0$, for which we will have to choose a label $\boldsymbol{x} = 0, \ldots, (N_s - 1)a$ for each site,

$$\mathcal{L}(\boldsymbol{x}) := (-1)^{\sum_{\boldsymbol{y}<\boldsymbol{x}} N(\boldsymbol{y})}. \tag{A.182}$$

This defect is written by using the number operator $N(\boldsymbol{x}) = a^{+}(\boldsymbol{x})a^{-}(\boldsymbol{x})$ for the excitations of $-B\pi(\boldsymbol{x})$. These defects commute with one another and

$$\mathcal{L}(\boldsymbol{x}) a^{\pm}(\boldsymbol{y}) = \begin{cases} a^{\pm}(\boldsymbol{y})\mathcal{L}(\boldsymbol{x}), & \boldsymbol{y} \geq \boldsymbol{x}, \\ -a^{\pm}(\boldsymbol{y})\mathcal{L}(\boldsymbol{x}), & \boldsymbol{y} < \boldsymbol{x}. \end{cases} \tag{A.183}$$

This asserts that

$$\begin{aligned}\psi(\boldsymbol{x}) &:= \mathcal{L}(\boldsymbol{x})a^-(\boldsymbol{x}),\\ \psi^\dagger(\boldsymbol{x}) &= \mathcal{L}(\boldsymbol{x})a^+(\boldsymbol{x}).\end{aligned} \tag{A.184}$$

are fermionic creation and annihilation operators

$$\begin{aligned}\{\psi(\boldsymbol{x}),\psi(\boldsymbol{y})\} &= \{\psi^\dagger(\boldsymbol{x}),\psi^\dagger(\boldsymbol{y})\} = 0,\\ \{\psi^\dagger(\boldsymbol{x}),\psi(\boldsymbol{y})\} &= \delta_{\boldsymbol{xy}}.\end{aligned} \tag{A.185}$$

We can now rewrite the Hamiltonian (A.179) in terms of these operators. To do this, we first note that $N(\boldsymbol{x}) = (1-\pi(\boldsymbol{x}))/2$, as in (A.81). This is a local expression for $\pi(\boldsymbol{x})$ in terms of the fermionic operators since $N(\boldsymbol{x}) = \psi^\dagger(\boldsymbol{x})\psi(\boldsymbol{x})$. On the other hand, given that $\phi(\boldsymbol{x})$ flips the eigenvalue of $\pi(\boldsymbol{x})$, we have

$$\phi(\boldsymbol{x}) = a^+(\boldsymbol{x}) + a^-(\boldsymbol{x}) = \mathcal{L}(\boldsymbol{x})(\psi^\dagger(\boldsymbol{x}) + \psi(\boldsymbol{x})), \tag{A.186}$$

which is not local. Fortunately, for $\boldsymbol{x} < (N_s-1)a$ we have

$$\begin{aligned}\phi(\boldsymbol{x})\phi(\boldsymbol{x}+a) &= (\psi^\dagger(\boldsymbol{x}+a)+\psi(\boldsymbol{x}+a))(-1)^{N(\boldsymbol{x})}(\psi^\dagger(\boldsymbol{x})+\psi(\boldsymbol{x}))\\ &= (\psi^\dagger(\boldsymbol{x}+a)+\psi(\boldsymbol{x}+a))(-\psi^\dagger(\boldsymbol{x})+\psi(\boldsymbol{x})),\end{aligned} \tag{A.187}$$

is local. The only non-local piece comes from the Ising interaction winding around the circle

$$\begin{aligned}\phi(L-a)\phi(0) &= (\psi^\dagger(0)+\psi(0))\mathcal{L}(L-a)(\psi^\dagger(L-a)+\psi(L-a))\\ &= (\psi^\dagger(0)+\psi(0))(-1)^N(-\psi^\dagger(L-a)+\psi(L-a))\\ &= (-1)^{N+1}(\psi^\dagger(0)+\psi(0))(-\psi^\dagger(L-a)+\psi(L-a)),\end{aligned} \tag{A.188}$$

with

$$N = \sum_{\boldsymbol{x}} N(\boldsymbol{x}). \tag{A.189}$$

In order to solve this issue we note that $(-1)^N$ commutes with the Hamiltonian. Indeed, the magnetic term is, up to a constant, $2BN$, so that it commutes with N. The Ising interaction on the other hand is quadratic in the creation and annihilation operators. Thus the Hilbert space splits into two sectors, one with an even and one with an odd number of particles

$$\mathcal{H} = \mathcal{H}_{\mathrm{NS}} \oplus \mathcal{H}_{\mathrm{R}}. \tag{A.190}$$

On each of these sectors one can then write the Ising interaction uniformly in the form (A.187), as long as one imposes antiperiodic boundary conditions $\psi(L) = -\psi(0)$ on the even sector, and periodic boundary conditions $\psi(L) = \psi(0)$ on the odd one. For this

reason we will now call the even and odd sectors, the Neveu-Schwartz (NS) and Ramond (R) sectors. After doing this, we conclude that the Hamiltonian of this model is

$$H = -J \sum_{\boldsymbol{x} \in \Sigma} (\psi^\dagger(\boldsymbol{x}+a) + \psi(\boldsymbol{x}+a))(-\psi^\dagger(\boldsymbol{x}) + \psi(\boldsymbol{x})) + B(2N - N_s). \tag{A.191}$$

Having realized the fermionic nature of the model, we go ahead and exploit the translational invariance to obtain a representation that is more diagonal. Indeed, if $T(a)$ denotes the unitary translation operator, then

$$T(a) H T(a)^{-1} = H, \quad T(a)\psi(\boldsymbol{x})T(a)^{-1} = \psi(\boldsymbol{x}+a). \tag{A.192}$$

It is therefore more convenient to work with the operators

$$\psi(\boldsymbol{p}) := \sum_{\boldsymbol{x} \in \Sigma} e^{i\boldsymbol{p}\cdot\boldsymbol{x}} \psi(\boldsymbol{x}) \quad \text{and} \quad \psi^\dagger(\boldsymbol{p}) = \sum_{\boldsymbol{x} \in \Sigma} e^{-i\boldsymbol{p}\cdot\boldsymbol{x}} \psi^\dagger(\boldsymbol{x}). \tag{A.193}$$

which satisfy

$$\begin{aligned} T(a)\psi(\boldsymbol{p})T(a)^{-1} &= e^{-i\boldsymbol{p}a}\psi(\boldsymbol{p}), \\ T(a)\psi^\dagger(\boldsymbol{p})T(a)^{-1} &= e^{i\boldsymbol{p}a}\psi^\dagger(\boldsymbol{p}). \end{aligned} \tag{A.194}$$

In other words, the operators $\psi^\dagger(\boldsymbol{p})$ and $\psi(-\boldsymbol{p})$ have momentum $\boldsymbol{p}$. This momentum is defined modulo $2\pi/a$ and it can only take values that are integer multiples of $2\pi/L$. Thus, letting

$$\tilde{\Sigma} = \begin{cases} \frac{2\pi}{L}\mathbb{Z} \diagup \frac{2\pi}{a}\mathbb{Z}, & N \text{ odd} \\ \frac{2\pi}{L}\mathbb{Z} \diagup \frac{2\pi}{a}\mathbb{Z} + \frac{\pi}{L}, & N \text{ even}, \end{cases} \tag{A.195}$$

then we can reexpress the terms in the Hamiltonian as

$$\begin{aligned} \sum_{\boldsymbol{x} \in \Sigma} \psi^\dagger(\boldsymbol{x}+a)\psi^\dagger(\boldsymbol{x}) &= \frac{1}{N_s} \sum_{\boldsymbol{p} \in \tilde{\Sigma}} e^{i\boldsymbol{p}a} \psi^\dagger(\boldsymbol{p})\psi^\dagger(-\boldsymbol{p}) \\ &= \frac{i}{N_s} \sum_{\boldsymbol{p} \in \tilde{\Sigma}} \sin(\boldsymbol{p}a)\psi^\dagger(\boldsymbol{p})\psi^\dagger(-\boldsymbol{p}), \\ \sum_{\boldsymbol{x} \in \Sigma} \psi(\boldsymbol{x}+a)\psi(\boldsymbol{x}) &= \frac{i}{N_s} \sum_{\boldsymbol{p} \in \tilde{\Sigma}} \sin(\boldsymbol{p}a)\psi(-\boldsymbol{p})\psi(\boldsymbol{p}), \\ \sum_{\boldsymbol{x} \in \Sigma} \psi^\dagger(\boldsymbol{x}+a)\psi(\boldsymbol{x}) &= \sum_{\boldsymbol{p} \in \tilde{\Sigma}} e^{i\boldsymbol{p}a} N(\boldsymbol{p}), \\ \sum_{\boldsymbol{x} \in \Sigma} \psi(\boldsymbol{x}+a)\psi^\dagger(\boldsymbol{x}) &= -\sum_{\boldsymbol{p} \in \tilde{\Sigma}} e^{-i\boldsymbol{p}a} N(\boldsymbol{p}), \\ N = \sum_{\boldsymbol{x} \in \Sigma} N(\boldsymbol{x}) &= \sum_{\boldsymbol{p} \in \tilde{\Sigma}} N(\boldsymbol{p}), \end{aligned} \tag{A.196}$$

with $N(\boldsymbol{p}) = \frac{1}{N_s}\psi^\dagger(\boldsymbol{p})\psi(\boldsymbol{p})$ the number operator for the fermionic excitations of definite momentum. This leaves us with a Hamiltonian in momentum space given by

$$\begin{aligned} H &= \sum_{\boldsymbol{p}\in\tilde{\Sigma}} 2(B - J\cos(\boldsymbol{p}a))N(\boldsymbol{p}) - N_s B \\ &\quad + \frac{1}{N_s}\sum_{\boldsymbol{p}\in\tilde{\Sigma}} iJ\sin(\boldsymbol{p}a)(\psi^\dagger(\boldsymbol{p})\psi^\dagger(-\boldsymbol{p}) - \psi(-\boldsymbol{p})\psi(\boldsymbol{p}))) \\ &= \sum_{\boldsymbol{p}\in\tilde{\Sigma}} (2(B - J\cos(\boldsymbol{p}a))N(\boldsymbol{p}) - B) \\ &\quad + \frac{1}{N_s}\sum_{\boldsymbol{p}\in\tilde{\Sigma}} iJ\sin(\boldsymbol{p}a)(\psi^\dagger(\boldsymbol{p})\psi^\dagger(-\boldsymbol{p}) - \psi(-\boldsymbol{p})\psi(\boldsymbol{p}))). \end{aligned} \tag{A.197}$$

Let us now group the terms with $\boldsymbol{p}$ and $-\boldsymbol{p}$, for the terms in which they are different. For this we define the quotient under this action

$$\tilde{\Sigma}^+ = \tilde{\Sigma}/\mathbb{Z}_2 \setminus \left\{ 0, \frac{\pi}{a} \right\}. \tag{A.198}$$

We can then set

$$H = \frac{1}{N_s}\sum_{\boldsymbol{p}\in\tilde{\Sigma}^+} H_{\boldsymbol{p}} + H^{(0)}. \tag{A.199}$$

In here, the second term contains the potentially unpaired momenta. Assuming N_s is even, it is only non-zero in the odd sector, where

$$H^{(0)} = 2(B - J)N(0) + 2(B + J)N(\pi/a) - 2B. \tag{A.200}$$

On the other hand

$$\begin{aligned} H_{\boldsymbol{p}} &= 2(B - J\cos(\boldsymbol{p}a))(\psi^\dagger(\boldsymbol{p})\psi(\boldsymbol{p}) + \psi^\dagger(-\boldsymbol{p})\psi(-\boldsymbol{p})) - 2B \\ &\quad + 2iJ\sin(\boldsymbol{p}a)(\psi^\dagger(\boldsymbol{p})\psi^\dagger(-\boldsymbol{p}) - \psi(-\boldsymbol{p})\psi(\boldsymbol{p})) \\ &= 2(B - J\cos(\boldsymbol{p}a))(\psi^\dagger(\boldsymbol{p})\psi(\boldsymbol{p}) - \psi(-\boldsymbol{p})\psi^\dagger(-\boldsymbol{p})) - 2JN_s\cos(\boldsymbol{p}a) \\ &\quad + 2iJ\sin(\boldsymbol{p}a)(\psi^\dagger(\boldsymbol{p})\psi^\dagger(-\boldsymbol{p}) - \psi(-\boldsymbol{p})\psi(\boldsymbol{p})) \end{aligned} \tag{A.201}$$

We will from now on drop the term $2JN_s\cos(\boldsymbol{p}a)$, since after summing over $\boldsymbol{p}$ it vanishes.

It is instructive to introduce a fermionic tuple

$$\Psi_N(\boldsymbol{p}) = \begin{pmatrix} \psi(\boldsymbol{p}) \\ \psi^\dagger(-\boldsymbol{p}) \end{pmatrix} \quad \text{and} \quad \Psi_N^\dagger(\boldsymbol{p}) = \begin{pmatrix} \psi^\dagger(\boldsymbol{p}) & \psi(-\boldsymbol{p}) \end{pmatrix}. \tag{A.202}$$

We can then write $H_{\boldsymbol{p}} = \Psi_N^\dagger(\boldsymbol{p})h\Psi_N(\boldsymbol{p})$, with

$$h = \begin{pmatrix} 2(B - J\cos(\boldsymbol{p}a)) & 2iJ\sin(\boldsymbol{p}a) \\ -2iJ\sin(\boldsymbol{p}a) & -2(B - J\cos(\boldsymbol{p}a)) \end{pmatrix} = \boldsymbol{h}\cdot\boldsymbol{\sigma}, \tag{A.203}$$

for an effective magnetic field

$$\boldsymbol{h} = 2(0, -J\sin(\boldsymbol{p}a), B - J\cos(\boldsymbol{p}a)). \tag{A.204}$$

The eigenvalues of h are thus given by $\pm\epsilon(\boldsymbol{p})$, with

$$\epsilon(\boldsymbol{p}) = \|\boldsymbol{h}\| = 2\sqrt{B^2 + J^2 - 2BJ\cos(\boldsymbol{p}a)}. \tag{A.205}$$

To find the eigenvectors, note that

$$(\boldsymbol{h}\cdot\boldsymbol{\sigma})^2 = h_i h_j \sigma_i \sigma_j = \frac{1}{2} h_i h_j \{\sigma_i, \sigma_j\} = \boldsymbol{h}^2. \tag{A.206}$$

We then conclude that $\hat{\boldsymbol{h}}\cdot\boldsymbol{\sigma}$ is unitary. Since it shares eigenvectors with h, we conclude that the projectors onto the eigenvectors are

$$P_\pm = \frac{1 \pm \hat{\boldsymbol{h}}\cdot\boldsymbol{\sigma}}{2} = \frac{1}{2}\begin{pmatrix} 1 \pm \hat{h}_z & \mp i\hat{h}_y \\ \pm i\hat{h}_y & 1 \mp \hat{h}_z \end{pmatrix} = \frac{1}{2\epsilon(\boldsymbol{p})}\begin{pmatrix} \epsilon(\boldsymbol{p}) \pm h_z & \mp i h_y \\ \pm i h_y & \epsilon(\boldsymbol{p}) \mp h_z \end{pmatrix} \tag{A.207}$$

from which we can immediately read off the eigenvectors. It is useful to write the one associated to $-\epsilon(\boldsymbol{p})$ by normalizing $P_-(0,1)$

$$\begin{pmatrix} v(\boldsymbol{p}) \\ u(\boldsymbol{p}) \end{pmatrix} = \frac{1}{\sqrt{2\epsilon(\boldsymbol{p})(\epsilon(\boldsymbol{p}) + h_z)}}\begin{pmatrix} i h_y \\ \epsilon(\boldsymbol{p}) + h_z \end{pmatrix}, \tag{A.208}$$

while writing the one associated to $\epsilon(\boldsymbol{p})$ by normalizing $P_+(1,0)$

$$\frac{1}{\sqrt{2\epsilon(\boldsymbol{p})(\epsilon(\boldsymbol{p}) + h_z))}}\begin{pmatrix} \epsilon(\boldsymbol{p}) + h_z \\ i h_y \end{pmatrix} = \begin{pmatrix} u(\boldsymbol{p})^* \\ -v(\boldsymbol{p})^* \end{pmatrix}. \tag{A.209}$$

With these eigenvectors we can now define the new fermions

$$\begin{aligned} \Gamma(\boldsymbol{p}) &= u(\boldsymbol{p})\psi(\boldsymbol{p}) - v(\boldsymbol{p})\psi^\dagger(-\boldsymbol{p}) \\ \Gamma^\dagger(-\boldsymbol{p}) &= v(\boldsymbol{p})^*\psi(\boldsymbol{p}) + u(\boldsymbol{p})\psi^\dagger(-\boldsymbol{p}), \end{aligned} \tag{A.210}$$

through the inner product of $\Psi_N(\boldsymbol{p})$ with the eigenvectors. The Hamiltonian is therefore

$$H_{\boldsymbol{p}} = \epsilon(\boldsymbol{p})(\Gamma^\dagger(\boldsymbol{p})\Gamma(\boldsymbol{p}) - \Gamma(-\boldsymbol{p})\Gamma^\dagger(-\boldsymbol{p})). \tag{A.211}$$

Thus

$$H = \sum_{\boldsymbol{p}\in\tilde{\Sigma}^+} \epsilon(\boldsymbol{p})(\mathcal{N}(\boldsymbol{p}) + \mathcal{N}(-\boldsymbol{p})) + H^{(0)} - E_0, \tag{A.212}$$

where $\mathcal{N}(\boldsymbol{p}) = \frac{1}{N_s}\Gamma^\dagger(\boldsymbol{p})\Gamma(\boldsymbol{p})$ are the new number operators for these fermions and

$$E_0 := \sum_{\boldsymbol{p}\in\tilde{\Sigma}^+} \epsilon(\boldsymbol{p}) \tag{A.213}$$

Note that these number operators can also be used in H_0 since, extending trivially our previous formulae to $\boldsymbol{p} = 0, \pi/a$, we have

$$\Gamma(0) = \psi(0) \quad \text{and} \quad \Gamma(\pi/a) = \psi(\pi/a). \tag{A.214}$$

At this stage the Hamiltonian has been worked out to the point that its spectrum can be immediately extracted. We will discuss independently the three terms in the Hamiltonian. Let us begin with the E_0 term. This is the energy of the Bogoliubov vacuum $|0\rangle$ defined by

$$\Gamma(\boldsymbol{p})\,|0\rangle = 0. \tag{A.215}$$

This term is a negative constant on each term in the decomposition (A.190). But it is different depending on which sector we are in, coming from the difference in the allowed momenta $\tilde{\Sigma}^+$.

For the study of the next two terms, we note that a general state fermionic state will be of the form

$$|n : \tilde{\Sigma} \to \{0,1\}\rangle \propto \prod_{\boldsymbol{p}\in\tilde{\Sigma}} \Gamma^\dagger(\boldsymbol{p})^{n(\boldsymbol{p})}\,|0\rangle\,. \tag{A.216}$$

These satisfy

$$\mathcal{N}(\boldsymbol{p})\,|n\rangle = n(\boldsymbol{p})\,|n\rangle\,. \tag{A.217}$$

Then, the contribution of $H^{(0)}$ to the energy is given by

$$2(B-J)n(0) + 2(B+J)n(\pi/a) - 2B. \tag{A.218}$$

This can take the values $-2J$, $2J$, $-2B$ and $2B$. Finally, the remaining contribution to the energy is

$$\sum_{\boldsymbol{p}\in\tilde{\Sigma}^+} (n(\boldsymbol{p}) + n(-\boldsymbol{p}))\epsilon(\boldsymbol{p}). \tag{A.219}$$

Note that in the NS sector $H^{(0)}$ does not contribute and thus we can simply take

$$E(n) = \sum_{\boldsymbol{p}\in\tilde{\Sigma}} n(\boldsymbol{p})\epsilon(\boldsymbol{p}) - E_0 \tag{A.220}$$

Defining $\epsilon(0) := 2(B-J)$, we can write similarly for the odd parity sector

$$E(n) = \sum_{\boldsymbol{p}\in\tilde{\Sigma}} n(\boldsymbol{p})\epsilon(\boldsymbol{p}) - E_0 - 2B. \tag{A.221}$$

A.9.3 Spectrum

To discuss the physical spectrum, we note that not all of the fermionic states (A.216) correspond to physical states in the 2D Ising model. Only those for which

$$\sum_{\boldsymbol{p}\in\tilde{\Sigma}} n(\boldsymbol{p}) \tag{A.222}$$

has the correct parity as dictated by the momenta corresponding to $\tilde{\Sigma}$ are allowed. Since parity plays a key role in the discussion of the spectrum, we will add the NS and R labels to the rest of our calculations.

Disordered Phase

We first consider the phase in which $J < B$, which is the simplest to interpret in this language. This is because in this case all $\epsilon(\boldsymbol{p}) > 0$. Thus, we can build a simple picture in which each vacuum $|0;\mathrm{NS}\rangle$ and $|0;\mathrm{R}\rangle$ generates a tower of states $|n;\mathrm{NS}\rangle$ and $|n;\mathrm{R}\rangle$ of fermions. In the 2D Ising model, states with an even number of fermions should be taken from the NS sector, while states with an odd number of fermions from the R sector. As we will now show, for large L, the states from both towers have the same energy. Thus, in this phase, the theory is truly that of free fermions.

Proving that the two towers have the same energy levels is done by showing that the two vacua have the same energy. The one in the NS sector has energy $-E_0^{\mathrm{NS}}$, while the one in the R sector has energy $-E_0^{\mathrm{R}} - 2B$. We thus need to understand the difference

$$E_0^{\mathrm{NS}} - E_0^{\mathrm{R}} = \sum_{n=0}^{\frac{N_s}{2}-1} \epsilon\Big(\frac{\pi(2n+1)}{L}\Big) - \sum_{n=1}^{\frac{N_s}{2}-1} \epsilon\Big(\frac{2\pi n}{L}\Big). \tag{A.223}$$

Note that the first sum contains $N_s/2$ terms, while the second has $N_s/2-1$. To understand their difference, we need to interpret them as integrals, which can be done in the thermodynamic $L\to\infty$ limit. For this we multiply by the distance between the points in the sum

$$\frac{2\pi}{L}(E_0^{\mathrm{NS}} - E_0^{\mathrm{R}}) = \frac{2\pi}{L}\sum_{n=0}^{\frac{N_s}{2}-1} \epsilon\Big(\frac{\pi(2n+1)}{L}\Big) - \frac{2\pi}{L}\sum_{n=1}^{\frac{N_s}{2}-1} \epsilon\Big(\frac{2\pi n}{L}\Big). \tag{A.224}$$

We recognize the first immediately as an approximation to the integral

$$\int_0^{\frac{\pi}{a}} \mathrm{d}\boldsymbol{p}\,\epsilon(\boldsymbol{p}) = \lim_{L\to\infty} \frac{2\pi}{L}\sum_{n=0}^{\frac{N_s}{2}-1} \epsilon\Big(\frac{\pi(2n+1)}{L}\Big). \tag{A.225}$$

On the other hand, using the trapezoidal rule would have left us with the approximation

$$\int_0^{\frac{\pi}{a}} \mathrm{d}\boldsymbol{p}\, \epsilon(\boldsymbol{p}) = \lim_{L\to\infty} \frac{2\pi}{L}\left(\sum_{n=1}^{\frac{N_s}{2}-1} \epsilon\left(\frac{\pi(2n+1)}{L}\right) + \frac{1}{2}\epsilon(0) + \frac{1}{2}\epsilon(\pi/a)\right). \tag{A.226}$$

Therefore, for large L

$$E_0^{\mathrm{NS}} - E_0^{\mathrm{R}} = \frac{\epsilon(0)+\epsilon(\pi/a)}{2}, \tag{A.227}$$

up to the difference between two approximations to an integral of a continuous function. Such approximations converge exponentially fast as $L \to \infty$.

In our particular phase, we have $E_0^{\mathrm{NS}} - E_0^{\mathrm{R}} = 2B$. We thus conclude that the two vacua have the same energy, completing our proof of the spectrum of the theory.

The single particle states are $|\boldsymbol{p}\rangle := \Gamma^\dagger(\boldsymbol{p})\,|0;\mathrm{R}\rangle$, following the dispersion relation

$$E = \epsilon(\boldsymbol{p}) - E_0^{\mathrm{R}} - 2B + E_0^{\mathrm{NS}} \to \epsilon(\boldsymbol{p}). \tag{A.228}$$

Two particle states $|\boldsymbol{p},\boldsymbol{q}\rangle \propto \Gamma^\dagger(\boldsymbol{p})\Gamma^\dagger(\boldsymbol{q})\,|0;\mathrm{NS}\rangle$ can then be considered with an excitation energy of $\epsilon(\boldsymbol{p})+\epsilon(\boldsymbol{q})$, and we can follow suit to build states with a higher energy. The corresponding spectrum is shown in Fig. A.10.

Ordered Phase

Now we consider the case $J > B$. This is more complex because $2(B-J) = \epsilon(0) < 0$. Therefore, the vacuum state of the R tower is no longer the Bogoliubov vacuum, but the odd state $\Gamma^\dagger(0)\,|0;R\rangle$, which is odd and thus also appears in the spectrum of the 2D Ising model. It has energy $E_0^R - 2J$. Moreover, since $\epsilon(\boldsymbol{p})$ is no longer continuous

$$\lim_{\boldsymbol{p}\to 0^+} \epsilon(\boldsymbol{p}) = 2(J-B) = -\epsilon(\boldsymbol{p}), \tag{A.229}$$

we now have

$$E_0^{\mathrm{NS}} - E_0^{\mathrm{R}} = \frac{\lim_{\boldsymbol{p}\to 0^+}\epsilon(0)+\epsilon(\pi/a)}{2} = 2J. \tag{A.230}$$

Thus, the difference in energy between these two new vacua also vanishes as L goes to infinity. The ground state in this phase is doubly degenerate.

Some intuition of this result can be obtained by considering the $B = 0$ case. In there the vacuum states can immediately be found from the original Hamiltonian (A.179). They are given by the states in which the field is constant

$$|1,1,1,\cdots,1\rangle \quad \text{and} \quad |-1,-1,-1,\cdots,-1\rangle\,. \tag{A.231}$$

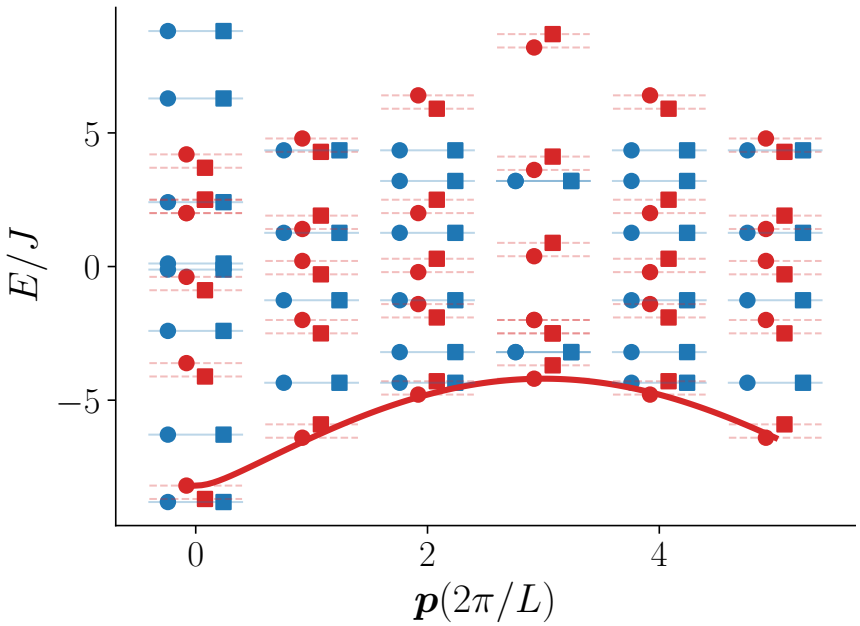


Figure A.10: Spectrum of the 2D Ising model in the disordered phase $B/J = 1.25$, with $N_s = 6$. Thin solid and dashed lines correspond to fermionic levels in the NS and R sectors. Scattered points correspond to those states that persist in the 2D Ising model. Scattered squares are the energies E/B of the states in the dual ordered phase with $J/B = 1.25$. The solid curved line corresponds to the dispersion relation of the single particle states. Only states with even total momenta are shown since all the states in the 2D Ising model satisfy this.

Since our Bogoliubov vacua have definite parity, we conclude that

$$\begin{aligned} |0;\mathrm{NS}\rangle &\propto |1,1,1,\cdots,1\rangle + |-1,-1,-1,\cdots,-1\rangle\,, \\ \Gamma^\dagger(0)\,|0;\mathrm{R}\rangle &\propto |1,1,1,\cdots,1\rangle - |-1,-1,-1,\cdots,-1\rangle \end{aligned} \tag{A.232}$$

On top of the R tower we can create the state $|0;\mathrm{R}\rangle = \Gamma(0)\Gamma^\dagger(0)\,|0;\mathrm{R}\rangle$, which adds an energy $|\epsilon(0)|$ on top of the vacuum of the sector and thus can be interpreted as the addition of a particle of momentum 0. This is not part of the spectrum of the 2D Ising model for it is even. Thus, we need to go further into the two particle sector, with states given by

$$|\boldsymbol{p},\boldsymbol{q}\rangle \propto \Gamma^\dagger(\boldsymbol{p})\Gamma^\dagger(\boldsymbol{q})\Gamma^\dagger(0)\,|0;\mathrm{R}\rangle\,, \tag{A.233}$$

when $\boldsymbol{p},\boldsymbol{q} \neq 0$, or

$$|\boldsymbol{p},0\rangle \propto \Gamma^\dagger(\boldsymbol{p})\,|0;\mathrm{R}\rangle\,. \tag{A.234}$$

The corresponding states in the NS tower are $|\boldsymbol{p},\boldsymbol{q}\rangle \propto \Gamma^\dagger(\boldsymbol{p})\Gamma^\dagger(\boldsymbol{q})\,|0;\mathrm{NS}\rangle$. This can be continued, leading to the realization that in this phase there are only state with an even number of particles. The resulting spectrum is found in Fig. A.10

The fact that an odd number of particles is disallowed can be understood from our solution of the 1D Ising model in Section A.7.1. There we saw that the elementary excitations of the model were given in terms of domain walls. The periodic boundary conditions then force us to have an even number of them. These qualitative considerations also explain the name of this phase.

Duality and Phase Transition

The energy in the NS sector (A.220) is trivially invariant under the change $J \leftrightarrow B$, which exchanges disordered and ordered phases. The same is true for the R sector, as our previous discussion shows. While the same is not true of the finite-volume spectrum of the 2D Ising model, due to the required projection, this distinction disappears as $L \to \infty$. This duality between these two phases is known as the Kramers-Wannier duality.

At the transition between these two phases, the mass of the particles, given by

$$\lim_{\boldsymbol{p}\to 0^+} \epsilon(\boldsymbol{p}) = 2|B - J|, \tag{A.235}$$

disappears. At this point the correlation length in the theory becomes infinite, a characteristic property of phase transitions. At this point the theory becomes conformal, having no characteristic length scale. If we for the moment consider a uniform spacetime lattice with $\epsilon = a$, and thus $K_t = K_s \equiv K$, this corresponds to the point in which

$$\frac{1}{2}\ln(\coth(K)) = K \Rightarrow K = \frac{1}{2}\ln(1+\sqrt{2}). \tag{A.236}$$

In the statistical mechanical interpretation, the action is $S = E/T$, with T the temperature of the system. Writing $K = \kappa/T$, we see that this corresponds to the temperature

$$\frac{T}{\kappa} = \frac{2}{\ln(1+\sqrt{2})} = 2.269\ldots \tag{A.237}$$

Below this temperature, the coupling between spins dominates, leading to ordered states where the spins tend to point in the same direction. Above this temperature, entropy dominates and typical configurations have their spins pointing in random directions.

A.9.4 Renormalization

In our previous models, the transfer matrix formalism required us to take the continuum limit. The resulting parameters were thus already physical. In this model, however, even after the transfer matrix formalism was implemented, we were still left with a spatial lattice. From a field-theoretic point of view, the resulting parameters J and B are unphysical and a function of the lattice spacing. We must therefore renormalize them.

We have so far used the energy gap, corresponding to the mass m of the first excitation to do this. But since we now have two parameters, we must include a new renormalization condition. Fortunately, having $d > 0$ yields N_s of these, in the form of the relativistic dispersion relation

$$E^2 = m^2 + \boldsymbol{p}^2. \tag{A.238}$$

Comparison against the dispersion relation (A.205)

$$\epsilon(\boldsymbol{p})^2 = 4|B-J|^2 + 4BJa^2\boldsymbol{p}^2 + \mathcal{O}(\boldsymbol{p}^4), \tag{A.239}$$

shows then that

$$m = 2|B-J| \quad \text{and} \quad 4BJa^2 = 1. \tag{A.240}$$

This fixes

$$B = \frac{\sqrt{m^2+4/a^2}+m}{4} \quad \text{and} \quad J = \frac{\sqrt{m^2+4/a^2}-m}{4} \tag{A.241}$$

in the disordered phase. In the continuum limit $a \to 0$, both diverge as $1/a$. On the other hand, in the limit $m \to \infty$ we have $B \to m/2$ and $J \to 0$. The renormalization conditions in the ordered phase are obtained by Kramers-Wannier duality $J \leftrightarrow B$. These are shown in Fig. A.11.

Although we were able to solve this problem analytically, it is still interesting to consider how one might do this numerically. Such a study would require a dimensionless version of the Hamiltonian. For example, we can define an effective temporal scale $\epsilon = 1/J$ and a dimensionless coupling $g = B/J$, which have continuum limits $\epsilon \to 0$ and $g \to 1$. Their renormalization is in Fig. A.12. This temporal scale should not be confused with the

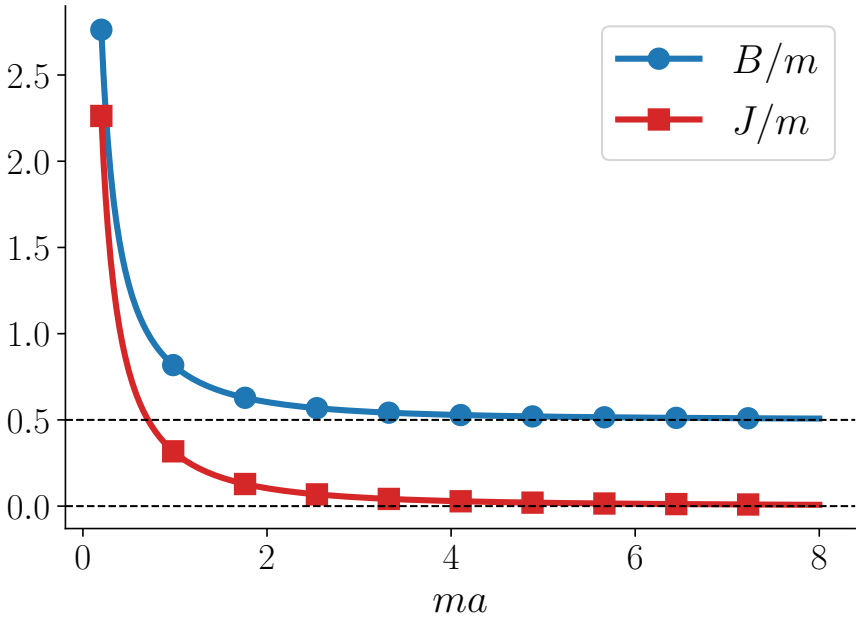


Figure A.11: Renormalization group flow of the parameters B and J in the disordered phase.

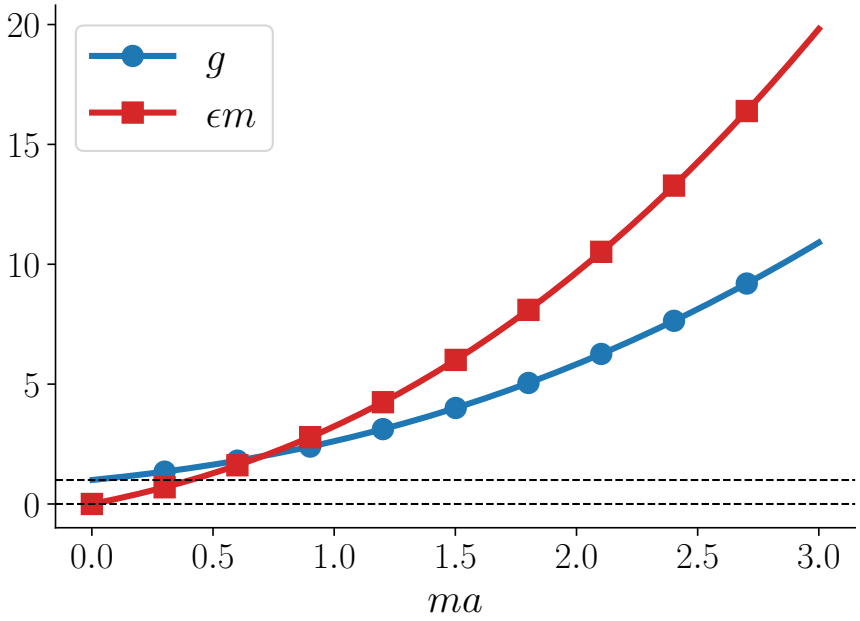


Figure A.12: Renormalization group flow of the parameters g and ϵ in the disordered phase.

temporal lattice spacing of the Euclidean theory, which has already been set to 0. We can then write a dimensionless Hamiltonian

$$\epsilon H = -g \sum_{\boldsymbol{x} \in \Sigma} \pi(\boldsymbol{x}) - \sum_{\boldsymbol{r}=0}^{N_s - 1} \phi(\boldsymbol{r}a)\phi((\boldsymbol{r}+1)a). \tag{A.242}$$

Numerical exploration, say through diagonalization, would lead to the mass ϵm and more generally the dispersion ϵE. Comparison against the physical mass would then lead to a determination of

$$\epsilon = \frac{\epsilon m}{m}. \tag{A.243}$$

In terms of the anisotropy $\xi = a/\epsilon$, the relativistic dispersion relation can be written as

$$(\epsilon E)^2 = (\epsilon m)^2 + \frac{1}{\xi^2}\left(\frac{2\pi \boldsymbol{n}}{N_s}\right)^2. \tag{A.244}$$

In light of this equality, ξ^{-1} is often called the speed of light [173]. However, since ξ is a spatial scale divided by a temporal one, it is also often referred to as the speed of light

[174]. We do not do either of these, preferring an interpretation in which the speed of light is always 1.

Bibliography

[1] S. Navas et al. "Review of particle physics". In: *Phys. Rev. D* 110.3 (2024), p. 030001. DOI: 10.1103/PhysRevD.110.030001.

[2] X. Fan et al. "Measurement of the Electron Magnetic Moment". In: *Phys. Rev. Lett.* 130.7 (2023), p. 071801. DOI: 10.1103/PhysRevLett.130.071801. arXiv: 2209.13084 [physics.atom-ph].

[3] H. Fritzsch, Murray Gell-Mann, and H. Leutwyler. "Advantages of the Color Octet Gluon Picture". In: *Phys. Lett. B* 47 (1973), pp. 365–368. DOI: 10.1016/0370-2693(73)90625-4.

[4] Y. Fukuda et al. "Evidence for oscillation of atmospheric neutrinos". In: *Phys. Rev. Lett.* 81 (1998), pp. 1562–1567. DOI: 10.1103/PhysRevLett.81.1562. arXiv: hep-ex/9807003.

[5] Jihn E. Kim and Gianpaolo Carosi. "Axions and the Strong CP Problem". In: *Rev. Mod. Phys.* 82 (2010). [Erratum: Rev.Mod.Phys. 91, 049902 (2019)], pp. 557–602. DOI: 10.1103/RevModPhys.82.557. arXiv: 0807.3125 [hep-ph].

[6] Michael Dine and Alexander Kusenko. "The Origin of the matter - antimatter asymmetry". In: *Rev. Mod. Phys.* 76 (2003), p. 1. DOI: 10.1103/RevModPhys.76.1. arXiv: hep-ph/0303065.

[7] B. Abi et al. "Long-baseline neutrino oscillation physics potential of the DUNE experiment". In: *Eur. Phys. J. C* 80.10 (2020), p. 978. DOI: 10.1140/epjc/s10052-020-08456-z. arXiv: 2006.16043 [hep-ex].

[8] G. C. Branco, R. Gonzalez Felipe, and F. R. Joaquim. "Leptonic CP Violation". In: *Rev. Mod. Phys.* 84 (2012), pp. 515–565. DOI: 10.1103/RevModPhys.84.515. arXiv: 1111.5332 [hep-ph].

[9] Babak Abi et al. "Deep Underground Neutrino Experiment (DUNE), Far Detector Technical Design Report, Volume II: DUNE Physics". In: (Feb. 2020). DOI: 10.2172/1599307. arXiv: 2002.03005 [hep-ex].

[10] L. Alvarez-Ruso et al. "NuSTEC White Paper: Status and challenges of neutrino–nucleus scattering". In: *Prog. Part. Nucl. Phys.* 100 (2018), pp. 1–68. DOI: 10.1016/j.ppnp.2018.01.006. arXiv: 1706.03621 [hep-ph].

[11] J. Schechter and J. W. F. Valle. "Neutrinoless Double beta Decay in SU(2) x U(1) Theories". In: *Phys. Rev. D* 25 (1982), p. 2951. DOI: 10.1103/PhysRevD.25.2951.

[12] Matteo Agostini et al. "Toward the discovery of matter creation with neutrinoless $\beta\beta$ decay". In: *Rev. Mod. Phys.* 95.2 (2023), p. 025002. DOI: 10.1103/RevModPhys.95.025002. arXiv: 2202.01787 [hep-ex].

[13] Murray Gell-Mann. "A Schematic Model of Baryons and Mesons". In: *Phys. Lett.* 8 (1964), pp. 214–215. DOI: 10.1016/S0031-9163(64)92001-3.

[14] Jacob J. Ethier and Emanuele R. Nocera. "Parton Distributions in Nucleons and Nuclei". In: *Ann. Rev. Nucl. Part. Sci.* 70 (2020), pp. 43–76. DOI: 10.1146/annurev-nucl-011720-042725. arXiv: 2001.07722 [hep-ph].

[15] R. Abdul Khalek et al. "Science Requirements and Detector Concepts for the Electron-Ion Collider: EIC Yellow Report". In: *Nucl. Phys. A* 1026 (2022), p. 122447. DOI: 10.1016/j.nuclphysa.2022.122447. arXiv: 2103.05419 [physics.ins-det].

[16] Wolfgang Ochs. "The Status of Glueballs". In: *J. Phys. G* 40 (2013), p. 043001. DOI: 10.1088/0954-3899/40/4/043001. arXiv: 1301.5183 [hep-ph].

[17] Colin J. Morningstar and Mike J. Peardon. "The Glueball spectrum from an anisotropic lattice study". In: *Phys. Rev. D* 60 (1999), p. 034509. DOI: 10.1103/PhysRevD.60.034509. arXiv: hep-lat/9901004.

[18] Nora Brambilla et al. "The XYZ states: experimental and theoretical status and perspectives". In: *Phys. Rept.* 873 (2020), pp. 1–154. DOI: 10.1016/j.physrep.2020.05.001. arXiv: 1907.07583 [hep-ex].

[19] Roel Aaij et al. "Observation of $J/\psi p$ Resonances Consistent with Pentaquark States in $\Lambda_b^0 \to J/\psi K^- p$ Decays". In: *Phys. Rev. Lett.* 115 (2015), p. 072001. DOI: 10.1103/PhysRevLett.115.072001. arXiv: 1507.03414 [hep-ex].

[20] Raul A. Briceno, Jozef J. Dudek, and Ross D. Young. "Scattering processes and resonances from lattice QCD". In: *Rev. Mod. Phys.* 90.2 (2018), p. 025001. DOI: 10.1103/RevModPhys.90.025001. arXiv: 1706.06223 [hep-lat].

[21] Kazuo Abe et al. "Evidence for X(3872) —> gamma J / psi and the sub-threshold decay X(3872) —> omega J / psi". In: *22nd International Symposium on Lepton-Photon Interactions at High Energy (LP 2005)*. May 2005. arXiv: hep-ex/0505037.

[22] P. Adlarson et al. "Measurement of the $np \to np\pi^0\pi^0$ Reaction in Search for the Recently Observed $d^*(2380)$ Resonance". In: *Phys. Lett. B* 743 (2015), pp. 325–332. DOI: 10.1016/j.physletb.2015.02.067. arXiv: 1409.2659 [nucl-ex].

[23] Maxim V. Polyakov and Peter Schweitzer. "Forces inside hadrons: pressure, surface tension, mechanical radius, and all that". In: *Int. J. Mod. Phys. A* 33.26 (2018), p. 1830025. DOI: 10.1142/S0217751X18300259. arXiv: 1805.06596 [hep-ph].

[24] Ryan Abbott et al. "Gravitational form factors of glueballs in Yang-Mills theory". In: *PoS* LATTICE2024 (2025), p. 459. DOI: 10.22323/1.466.0459. arXiv: 2410.02706 [hep-lat].

[25] Jean Zinn-Justin. "Perturbation Series at Large Orders in Quantum Mechanics and Field Theories: Application to the Problem of Resummation". In: *Phys. Rept.* 70 (1981), p. 109. DOI: 10.1016/0370-1573(81)90016-8.

[26] David J. Gross and Frank Wilczek. "Ultraviolet Behavior of Nonabelian Gauge Theories". In: *Phys. Rev. Lett.* 30 (1973), pp. 1343–1346. DOI: 10.1103/PhysRevLett.30.1343.

[27] H. David Politzer. "Reliable Perturbative Results for Strong Interactions?" In: *Phys. Rev. Lett.* 30 (1973), pp. 1346–1349. DOI: 10.1103/PhysRevLett.30.1346.

[28] Andreas S. Kronfeld et al. "Lattice QCD and Particle Physics". In: (July 2022). arXiv: 2207.07641 [hep-lat].

[29] Martin Luscher. "Lattice QCD: From quark confinement to asymptotic freedom". In: *Annales Henri Poincare* 4 (2003). Ed. by V. Rivasseau, S197–S210. DOI: 10.1007/s00023-003-0916-z. arXiv: hep-ph/0211220.

[30] Konrad Osterwalder and Robert Schrader. "AXIOMS FOR EUCLIDEAN GREEN'S FUNCTIONS". In: *Commun. Math. Phys.* 31 (1973), pp. 83–112. DOI: 10.1007/BF01645738.

[31] S. Durr et al. "Ab-Initio Determination of Light Hadron Masses". In: *Science* 322 (2008), pp. 1224–1227. DOI: 10.1126/science.1163233. arXiv: 0906.3599 [hep-lat].

[32] M. Luscher. "Volume Dependence of the Energy Spectrum in Massive Quantum Field Theories. 1. Stable Particle States". In: *Commun. Math. Phys.* 104 (1986), p. 177. DOI: 10.1007/BF01211589.

[33] R. Aliberti et al. "The anomalous magnetic moment of the muon in the Standard Model: an update". In: *Phys. Rept.* 1143 (2025), pp. 1–158. DOI: 10.1016/j.physrep.2025.08.002. arXiv: 2505.21476 [hep-ph].

[34] Huey-Wen Lin et al. "Parton distributions and lattice QCD calculations: a community white paper". In: *Prog. Part. Nucl. Phys.* 100 (2018), pp. 107–160. DOI: 10.1016/j.ppnp.2018.01.007. arXiv: 1711.07916 [hep-ph].

[35] M. Luscher. "Volume Dependence of the Energy Spectrum in Massive Quantum Field Theories. 2. Scattering States". In: *Commun. Math. Phys.* 105 (1986), pp. 153–188. DOI: 10.1007/BF01211097.

[36] Martin Luscher. "Two particle states on a torus and their relation to the scattering matrix". In: *Nucl. Phys. B* 354 (1991), pp. 531–578. DOI: 10.1016/0550-3213(91)90366-6.

[37] Martin Luscher and Ulli Wolff. "How to Calculate the Elastic Scattering Matrix in Two-dimensional Quantum Field Theories by Numerical Simulation". In: *Nucl. Phys. B* 339 (1990), pp. 222–252. DOI: 10.1016/0550-3213(90)90540-T.

[38] K. Rummukainen and Steven A. Gottlieb. "Resonance scattering phase shifts on a nonrest frame lattice". In: *Nucl. Phys. B* 450 (1995), pp. 397–436. DOI: 10.1016/0550-3213(95)00313-H. arXiv: hep-lat/9503028.

[39] Song He, Xu Feng, and Chuan Liu. "Two particle states and the S-matrix elements in multi-channel scattering". In: *JHEP* 07 (2005), p. 011. DOI: 10.1088/1126-6708/2005/07/011. arXiv: hep-lat/0504019.

[40] C. h. Kim, C. T. Sachrajda, and Stephen R. Sharpe. "Finite-volume effects for two-hadron states in moving frames". In: *Nucl. Phys. B* 727 (2005), pp. 218–243. DOI: 10.1016/j.nuclphysb.2005.08.029. arXiv: hep-lat/0507006.

[41] Norman H. Christ, Changhoan Kim, and Takeshi Yamazaki. "Finite volume corrections to the two-particle decay of states with non-zero momentum". In: *Phys. Rev. D* 72 (2005), p. 114506. DOI: 10.1103/PhysRevD.72.114506. arXiv: hep-lat/0507009.

[42] Raul A. Briceño et al. "Two-nucleon systems in a finite volume. II. ${}^3S_1 - {}^3D_1$ coupled channels and the deuteron". In: *Phys. Rev. D* 88.11 (2013), p. 114507. DOI: 10.1103/PhysRevD.88.114507. arXiv: 1309.3556 [hep-lat].

[43] Raul A. Briceno et al. "Two-Baryon Systems with Twisted Boundary Conditions". In: *Phys. Rev. D* 89.7 (2014), p. 074509. DOI: 10.1103/PhysRevD.89.074509. arXiv: 1311.7686 [hep-lat].

[44] Raul A. Briceno. "Two-particle multichannel systems in a finite volume with arbitrary spin". In: *Phys. Rev. D* 89.7 (2014), p. 074507. DOI: 10.1103/PhysRevD.89.074507. arXiv: 1401.3312 [hep-lat].

[45] Andria Agadjanov et al. "The $B \to K^*$ form factors on the lattice". In: *Nucl. Phys. B* 910 (2016), pp. 387–409. DOI: 10.1016/j.nuclphysb.2016.07.005. arXiv: 1605.03386 [hep-lat].

[46] Laurent Lellouch and Martin Luscher. "Weak transition matrix elements from finite volume correlation functions". In: *Commun. Math. Phys.* 219 (2001), pp. 31–44. DOI: 10.1007/s002200100410. arXiv: hep-lat/0003023.

[47] Raul A. Briceno and Zohreh Davoudi. "Moving multichannel systems in a finite volume with application to proton-proton fusion". In: *Phys. Rev. D* 88.9 (2013), p. 094507. DOI: 10.1103/PhysRevD.88.094507. arXiv: 1204.1110 [hep-lat].

[48] Raúl A. Briceño, Maxwell T. Hansen, and André Walker-Loud. "Multichannel $1 \to 2$ transition amplitudes in a finite volume". In: *Phys. Rev. D* 91.3 (2015), p. 034501. DOI: 10.1103/PhysRevD.91.034501. arXiv: 1406.5965 [hep-lat].

[49] Raúl A. Briceño and Maxwell T. Hansen. "Multichannel $0 \to 2$ and $1 \to 2$ transition amplitudes for arbitrary spin particles in a finite volume". In: *Phys. Rev. D* 92.7 (2015), p. 074509. DOI: 10.1103/PhysRevD.92.074509. arXiv: 1502.04314 [hep-lat].

[50] Harvey B. Meyer. "Lattice QCD and the Timelike Pion Form Factor". In: *Phys. Rev. Lett.* 107 (2011), p. 072002. DOI: 10.1103/PhysRevLett.107.072002. arXiv: 1105.1892 [hep-lat].

[51] V. Bernard et al. "Matrix elements of unstable states". In: *JHEP* 09 (2012), p. 023. DOI: 10.1007/JHEP09(2012)023. arXiv: 1205.4642 [hep-lat].

[52] Raúl A. Briceño and Maxwell T. Hansen. "Relativistic, model-independent, multichannel $2 \to 2$ transition amplitudes in a finite volume". In: *Phys. Rev. D* 94.1 (2016), p. 013008. DOI: 10.1103/PhysRevD.94.013008. arXiv: 1509.08507 [hep-lat].

[53] Alessandro Baroni et al. "Form factors of two-hadron states from a covariant finite-volume formalism". In: *Phys. Rev. D* 100.3 (2019), p. 034511. DOI: 10.1103/PhysRevD.100.034511. arXiv: 1812.10504 [hep-lat].

[54] Raúl A. Briceño et al. "On-shell representations of two-body transition amplitudes: Single external current". In: *Phys. Rev. D* 103.11 (2021), p. 114512. DOI: 10.1103/PhysRevD.103.114512. arXiv: 2012.13338 [hep-lat].

[55] Keegan H. Sherman et al. "Two-current transition amplitudes with two-body final states". In: *Phys. Rev. D* 105.11 (2022), p. 114510. DOI: 10.1103/PhysRevD.105.114510. arXiv: 2202.02284 [hep-lat].

[56] Raúl A. Briceño et al. "Prospects for $\gamma\star\gamma\star\to\pi\pi$ via lattice QCD". In: *Phys. Rev. D* 107.3 (2023), p. 034504. DOI: 10.1103/PhysRevD.107.034504. arXiv: 2210.08051 [hep-lat].

[57] K. Polejaeva and A. Rusetsky. "Three particles in a finite volume". In: *Eur. Phys. J. A* 48 (2012), p. 67. DOI: 10.1140/epja/i2012-12067-8. arXiv: 1203.1241 [hep-lat].

[58] Maxwell T. Hansen and Stephen R. Sharpe. "Relativistic, model-independent, three-particle quantization condition". In: *Phys. Rev. D* 90.11 (2014), p. 116003. DOI: 10.1103/PhysRevD.90.116003. arXiv: 1408.5933 [hep-lat].

[59] Maxwell T. Hansen and Stephen R. Sharpe. "Expressing the three-particle finite-volume spectrum in terms of the three-to-three scattering amplitude". In: *Phys. Rev. D* 92.11 (2015), p. 114509. DOI: 10.1103/PhysRevD.92.114509. arXiv: 1504.04248 [hep-lat].

[60] H. -W. Hammer, J. -Y. Pang, and A. Rusetsky. "Three particle quantization condition in a finite volume: 2. general formalism and the analysis of data". In: *JHEP* 10 (2017), p. 115. DOI: 10.1007/JHEP10(2017)115. arXiv: 1707.02176 [hep-lat].

[61] Raúl A. Briceño, Maxwell T. Hansen, and Stephen R. Sharpe. "Relating the finite-volume spectrum and the two-and-three-particle S matrix for relativistic systems of identical scalar particles". In: *Phys. Rev. D* 95.7 (2017), p. 074510. DOI: 10.1103/PhysRevD.95.074510. arXiv: 1701.07465 [hep-lat].

[62] M. Mai and M. Döring. "Three-body Unitarity in the Finite Volume". In: *Eur. Phys. J. A* 53.12 (2017), p. 240. DOI: 10.1140/epja/i2017-12440-1. arXiv: 1709.08222 [hep-lat].

[63] Raúl A. Briceño, Maxwell T. Hansen, and Stephen R. Sharpe. "Three-particle systems with resonant subprocesses in a finite volume". In: *Phys. Rev. D* 99.1 (2019), p. 014516. DOI: 10.1103/PhysRevD.99.014516. arXiv: 1810.01429 [hep-lat].

[64] Tyler D. Blanton and Stephen R. Sharpe. "Equivalence of relativistic three-particle quantization conditions". In: *Phys. Rev. D* 102.5 (2020), p. 054515. DOI: 10.1103/PhysRevD.102.054515. arXiv: 2007.16190 [hep-lat].

[65] Maxwell T. Hansen, Fernando Romero-López, and Stephen R. Sharpe. "Incorporating DDπ effects and left-hand cuts in lattice QCD studies of the $\mathrm{T}_{cc}(3875)^{+}$". In: *JHEP* 06 (2024), p. 051. DOI: 10.1007/JHEP06(2024)051. arXiv: 2401.06609 [hep-lat].

[66] S. Aoki et al. "Lattice QCD Calculation of the rho Meson Decay Width". In: *Phys. Rev. D* 76 (2007), p. 094506. DOI: 10.1103/PhysRevD.76.094506. arXiv: 0708.3705 [hep-lat].

[67] Jozef J. Dudek, Robert G. Edwards, and Christopher E. Thomas. "Energy dependence of the ρ resonance in $\pi\pi$ elastic scattering from lattice QCD". In: *Phys. Rev. D* 87.3 (2013). [Erratum: Phys.Rev.D 90, 099902 (2014)], p. 034505. DOI: 10.1103/PhysRevD.87.034505. arXiv: 1212.0830 [hep-ph].

[68] Jozef J. Dudek et al. "Resonances in coupled $\pi K - \eta K$ scattering from quantum chromodynamics". In: *Phys. Rev. Lett.* 113.18 (2014), p. 182001. DOI: 10.1103/PhysRevLett.113.182001. arXiv: 1406.4158 [hep-ph].

[69] Gunnar S. Bali et al. "ρ and K^* resonances on the lattice at nearly physical quark masses and $N_f = 2$". In: *Phys. Rev. D* 93.5 (2016), p. 054509. DOI: 10.1103/PhysRevD.93.054509. arXiv: 1512.08678 [hep-lat].

[70] Giorgio Silvi et al. "P-wave nucleon-pion scattering amplitude in the $\Delta(1232)$ channel from lattice QCD". In: *Phys. Rev. D* 103.9 (2021), p. 094508. DOI: 10.1103/PhysRevD.103.094508. arXiv: 2101.00689 [hep-lat].

[71] John Bulava et al. "Lattice QCD study of $\pi\Sigma$-K^-N scattering and the $\Lambda(1405)$ resonance". In: *Phys. Rev. D* 109.1 (2024), p. 014511. DOI: 10.1103/PhysRevD.109.014511. arXiv: 2307.13471 [hep-lat].

[72] R. Abbott et al. "Direct CP violation and the $\Delta I = 1/2$ rule in $K \to \pi\pi$ decay from the standard model". In: *Phys. Rev. D* 102.5 (2020), p. 054509. DOI: 10.1103/PhysRevD.102.054509. arXiv: 2004.09440 [hep-lat].

[73] Xu Feng et al. "Timelike pion form factor in lattice QCD". In: *Phys. Rev. D* 91.5 (2015), p. 054504. DOI: 10.1103/PhysRevD.91.054504. arXiv: 1412.6319 [hep-lat].

[74] Felipe G. Ortega-Gama, Jozef J. Dudek, and Robert G. Edwards. "Timelike meson form factors beyond the elastic region from lattice QCD". In: *Phys. Rev. D* 110.9 (2024), p. 094505. DOI: 10.1103/PhysRevD.110.094505. arXiv: 2407.20617 [hep-lat].

[75] Constantia Alexandrou et al. "$\pi\gamma \to \pi\pi$ transition and the ρ radiative decay width from lattice QCD". In: *Phys. Rev. D* 98.7 (2018). [Erratum: Phys.Rev.D 105, 019902 (2022)], p. 074502. DOI: 10.1103/PhysRevD.98.074502. arXiv: 1807.08357 [hep-lat].

[76] Chris Culver et al. "Three pion spectrum in the $I = 3$ channel from lattice QCD". In: *Phys. Rev. D* 101.11 (2020), p. 114507. DOI: 10.1103/PhysRevD.101.114507. arXiv: 1911.09047 [hep-lat].

[77] Matthias Fischer et al. "Scattering of two and three physical pions at maximal isospin from lattice QCD". In: *Eur. Phys. J. C* 81.5 (2021), p. 436. DOI: 10.1140/epjc/s10052-021-09206-5. arXiv: 2008.03035 [hep-lat].

[78] Maxwell T. Hansen et al. "Energy-Dependent $\pi^+\pi^+\pi^+$ Scattering Amplitude from QCD". In: *Phys. Rev. Lett.* 126 (2021), p. 012001. DOI: 10.1103/PhysRevLett.126.012001. arXiv: 2009.04931 [hep-lat].

[79] Maxim Mai et al. "Three-Body Dynamics of the a1(1260) Resonance from Lattice QCD". In: *Phys. Rev. Lett.* 127.22 (2021), p. 222001. DOI: 10.1103/PhysRevLett.127.222001. arXiv: 2107.03973 [hep-lat].

[80] Raúl A. Briceño et al. "Role of boundary conditions in quantum computations of scattering observables". In: *Phys. Rev. D* 103.1 (2021), p. 014506. DOI: 10.1103/PhysRevD.103.014506. arXiv: 2007.01155 [hep-lat].

[81] Raul A. Briceño et al. "Accessing scattering amplitudes using quantum computers". In: *PoS* LATTICE2021 (2022), p. 315. DOI: 10.22323/1.396.0315. arXiv: 2112.01968 [hep-lat].

[82] Marco A. Carrillo, Raúl A. Briceño, and Alexandru M. Sturzu. "Inclusive reactions from finite Minkowski spacetime correlation functions". In: *Phys. Rev. D* 110.5 (2024), p. 054503. DOI: 10.1103/PhysRevD.110.054503. arXiv: 2406.06877 [hep-lat].

[83] Ivan M. Burbano et al. "Real-time estimators for scattering observables: A full account of finite-volume errors for quantum simulation". In: *Phys. Rev. D* 113.7 (2026), p. L071502. DOI: 10.1103/dc17-4zjy. arXiv: 2506.06511 [hep-lat].

[84] Richard P. Feynman. "Simulating Physics with Computers". In: *Int. J. Theor. Phys.* 21 (1982), pp. 467–488. DOI: 10.1007/BF02650179.

[85] Seth Lloyd. "Universal Quantum Simulators". In: *Science* 273.5278 (1996), p. 1073. DOI: 10.1126/science.273.5278.1073.

[86] Christian W. Bauer et al. "Quantum Simulation for High-Energy Physics". In: *PRX Quantum* 4.2 (2023), p. 027001. DOI: 10.1103/PRXQuantum.4.027001. arXiv: 2204.03381 [quant-ph].

[87] John Preskill. "Quantum Computing in the NISQ era and beyond". In: *Quantum* 2 (2018), p. 79. DOI: 10.22331/q-2018-08-06-79. arXiv: 1801.00862 [quant-ph].

[88] Erez Zohar and Michele Burrello. "Formulation of lattice gauge theories for quantum simulations". In: *Phys. Rev. D* 91.5 (2015), p. 054506. DOI: 10.1103/PhysRevD.91.054506. arXiv: 1409.3085 [quant-ph].

[89] Andrei Alexandru et al. "Gluon Field Digitization for Quantum Computers". In: *Phys. Rev. D* 100.11 (2019), p. 114501. DOI: 10.1103/PhysRevD.100.114501. arXiv: 1906.11213 [hep-lat].

[90] Angus Kan and Yunseong Nam. "Lattice Quantum Chromodynamics and Electrodynamics on a Universal Quantum Computer". In: (July 2021). arXiv: 2107.12769 [quant-ph].

[91] Christian W. Bauer and Dorota M. Grabowska. "Efficient representation for simulating U(1) gauge theories on digital quantum computers at all values of the coupling". In: *Phys. Rev. D* 107.3 (2023), p. L031503. DOI: 10.1103/PhysRevD.107.L031503. arXiv: 2111.08015 [hep-ph].

[92] Zohreh Davoudi, Indrakshi Raychowdhury, and Andrew Shaw. "Search for efficient formulations for Hamiltonian simulation of non-Abelian lattice gauge theories". In: *Phys. Rev. D* 104.7 (2021), p. 074505. DOI: 10.1103/PhysRevD.104.074505. arXiv: 2009.11802 [hep-lat].

[93] Anthony Ciavarella, Natalie Klco, and Martin J. Savage. "Trailhead for quantum simulation of SU(3) Yang-Mills lattice gauge theory in the local multiplet basis". In: *Phys. Rev. D* 103.9 (2021), p. 094501. DOI: 10.1103/PhysRevD.103.094501. arXiv: 2101.10227 [quant-ph].

[94] Manu Mathur and T. P. Sreeraj. "Canonical Transformations and Loop Formulation of SU(N) Lattice Gauge Theories". In: *Phys. Rev. D* 92.12 (2015), p. 125018. DOI: 10.1103/PhysRevD.92.125018. arXiv: 1509.04033 [hep-lat].

[95] Indrakshi Raychowdhury and Jesse R. Stryker. "Solving Gauss's Law on Digital Quantum Computers with Loop-String-Hadron Digitization". In: *Phys. Rev. Res.* 2.3 (2020), p. 033039. DOI: 10.1103/PhysRevResearch.2.033039. arXiv: 1812.07554 [hep-lat].

[96] Indrakshi Raychowdhury and Jesse R. Stryker. "Loop, string, and hadron dynamics in SU(2) Hamiltonian lattice gauge theories". In: *Phys. Rev. D* 101.11 (2020), p. 114502. DOI: 10.1103/PhysRevD.101.114502. arXiv: 1912.06133 [hep-lat].

[97] Saurabh V. Kadam, Indrakshi Raychowdhury, and Jesse R. Stryker. "Loop-string-hadron formulation of an SU(3) gauge theory with dynamical quarks". In: *Phys. Rev. D* 107.9 (2023), p. 094513. DOI: 10.1103/PhysRevD.107.094513. arXiv: 2212.04490 [hep-lat].

[98] Irian D'Andrea et al. "New basis for Hamiltonian SU(2) simulations". In: *Phys. Rev. D* 109.7 (2024), p. 074501. DOI: 10.1103/PhysRevD.109.074501. arXiv: 2307.11829 [hep-ph].

[99] Dorota M. Grabowska, Christopher F. Kane, and Christian W. Bauer. "Fully gauge-fixed SU(2) Hamiltonian for quantum simulations". In: *Phys. Rev. D* 111.11 (2025), p. 114516. DOI: 10.1103/PhysRevD.111.114516. arXiv: 2409.10610 [quant-ph].

[100] Ivan M. Burbano and Christian W. Bauer. "Gauge loop-string-hadron formulation on general graphs and applications to fully gauge fixed Hamiltonian lattice gauge theory". In: *JHEP* 12 (2025), p. 060. DOI: 10.1007/JHEP12(2025)060. arXiv: 2409.13812 [hep-lat].

[101] Saurabh V. Kadam et al. "Loop-string-hadron approach to SU(3) lattice Yang-Mills theory: Hilbert space of a trivalent vertex". In: *Phys. Rev. D* 111.7 (2025), p. 074516. DOI: 10.1103/PhysRevD.111.074516. arXiv: 2407.19181 [hep-lat].

[102] Saurabh V. Kadam et al. "Loop-string-hadron approach to SU(3) lattice Yang-Mills theory, II: Operator representation for the trivalent vertex". In: (Dec. 2025). arXiv: 2512.11796 [hep-lat].

[103] Ali Hamed Moosavian, James R. Garrison, and Stephen P. Jordan. "Site-by-site quantum state preparation algorithm for preparing vacua of fermionic lattice field theories". In: (Nov. 2019). arXiv: 1911.03505 [quant-ph].

[104] Anthony N. Ciavarella and Ivan A. Chernyshev. "Preparation of the SU(3) lattice Yang-Mills vacuum with variational quantum methods". In: *Phys. Rev. D* 105.7 (2022), p. 074504. DOI: 10.1103/PhysRevD.105.074504. arXiv: 2112.09083 [quant-ph].

[105] Roland C. Farrell et al. "Scalable Circuits for Preparing Ground States on Digital Quantum Computers: The Schwinger Model Vacuum on 100 Qubits". In: *PRX Quantum* 5.2 (2024), p. 020315. DOI: 10.1103/PRXQuantum.5.020315. arXiv: 2308.04481 [quant-ph].

[106] Matteo D'Anna, Marina Krstic Marinkovic, and Joao C. Pinto Barros. "Adiabatic state preparation for digital quantum simulations of QED in 1+1D". In: *Phys. Rev. D* 111.9 (2025), p. 094514. DOI: 10.1103/PhysRevD.111.094514. arXiv: 2411.01079 [hep-lat].

[107] Yasar Y. Atas et al. "SU(2) hadrons on a quantum computer via a variational approach". In: *Nature Commun.* 12.1 (2021), p. 6499. DOI: 10.1038/s41467-021-26825-4. arXiv: 2102.08920 [quant-ph].

[108] Roland C. Farrell et al. "Preparations for quantum simulations of quantum chromodynamics in 1+1 dimensions. II. Single-baryon β-decay in real time". In: *Phys. Rev. D* 107.5 (2023), p. 054513. DOI: 10.1103/PhysRevD.107.054513. arXiv: 2209.10781 [quant-ph].

[109] Ali Hamed Moosavian and Stephen Jordan. "Faster Quantum Algorithm to simulate Fermionic Quantum Field Theory". In: *Phys. Rev. A* 98.1 (2018), p. 012332. DOI: 10.1103/PhysRevA.98.012332. arXiv: 1711.04006 [quant-ph].

[110] Zohreh Davoudi, Chung-Chun Hsieh, and Saurabh V. Kadam. "Scattering wave packets of hadrons in gauge theories: Preparation on a quantum computer". In: *Quantum* 8 (2024), p. 1520. DOI: 10.22331/q-2024-11-11-1520. arXiv: 2402.00840 [quant-ph].

[111] Roland C. Farrell et al. "Quantum simulations of hadron dynamics in the Schwinger model using 112 qubits". In: *Phys. Rev. D* 109.11 (2024), p. 114510. DOI: 10.1103/PhysRevD.109.114510. arXiv: 2401.08044 [quant-ph].

[112] Elizabeth R. Bennewitz et al. "Simulating Meson Scattering on Spin Quantum Simulators". In: *Quantum* 9 (2025), p. 1773. DOI: 10.22331/q-2025-06-17-1773. arXiv: 2403.07061 [quant-ph].

[113] Henry Lamm, Scott Lawrence, and Yukari Yamauchi. "General Methods for Digital Quantum Simulation of Gauge Theories". In: *Phys. Rev. D* 100.3 (2019), p. 034518. DOI: 10.1103/PhysRevD.100.034518. arXiv: 1903.08807 [hep-lat].

[114] Alexander F. Shaw et al. "Quantum Algorithms for Simulating the Lattice Schwinger Model". In: *Quantum* 4 (2020), p. 306. DOI: 10.22331/q-2020-08-10-306. arXiv: 2002.11146 [quant-ph].

[115] Zohreh Davoudi, Alexander F. Shaw, and Jesse R. Stryker. "General quantum algorithms for Hamiltonian simulation with applications to a non-Abelian lattice gauge theory". In: *Quantum* 7 (2023), p. 1213. DOI: 10.22331/q-2023-12-20-1213. arXiv: 2212.14030 [hep-lat].

[116] Siddharth Hariprakash et al. "Strategies for simulating the time evolution of Hamiltonian lattice field theories". In: *Phys. Rev. A* 111.2 (2025), p. 022419. DOI: 10.1103/PhysRevA.111.022419. arXiv: 2312.11637 [quant-ph].

[117] Mason L. Rhodes, Michael Kreshchuk, and Shivesh Pathak. "Exponential Improvements in the Simulation of Lattice Gauge Theories Using Near-Optimal Techniques". In: *PRX Quantum* 5.4 (2024), p. 040347. DOI: 10.1103/PRXQuantum.5.040347. arXiv: 2405.10416 [quant-ph].

[118] Stephen P. Jordan, Keith S. M. Lee, and John Preskill. "Quantum Algorithms for Quantum Field Theories". In: *Science* 336 (2012), pp. 1130–1133. DOI: 10.1126/science.1217069. arXiv: 1111.3633 [quant-ph].

[119] Stephen P. Jordan, Keith S. M. Lee, and John Preskill. "Quantum Computation of Scattering in Scalar Quantum Field Theories". In: *Quant. Inf. Comput.* 14 (2014), pp. 1014–1080. arXiv: 1112.4833 [hep-th].

[120] Erik Gustafson et al. "Real-time quantum calculations of phase shifts using wave packet time delays". In: *Phys. Rev. D* 104.5 (2021), p. 054507. DOI: 10.1103/PhysRevD.104.054507. arXiv: 2103.06848 [hep-lat].

[121] Nikita A. Zemlevskiy. "Scalable quantum simulations of scattering in scalar field theory on 120 qubits". In: *Phys. Rev. D* 112.3 (2025), p. 034502. DOI: 10.1103/qr72-51v1. arXiv: 2411.02486 [quant-ph].

[122] Roland C. Farrell et al. "Digital quantum simulations of scattering in quantum field theories using W states". In: (May 2025). arXiv: 2505.03111 [quant-ph].

[123] Zohreh Davoudi, Chung-Chun Hsieh, and Saurabh V. Kadam. "Quantum computation of hadron scattering in a lattice gauge theory". In: (May 2025). arXiv: 2505.20408 [quant-ph].

[124] Julian Schuhmacher et al. "Observation of hadron scattering in a lattice gauge theory on a quantum computer". In: (May 2025). arXiv: 2505.20387 [quant-ph].

[125] Yahui Chai et al. "Resource-efficient simulations of particle scattering on a digital quantum computer". In: *npj Quantum Inf.* 12.1 (2026), p. 100. DOI: 10.1038/s41534-026-01311-1. arXiv: 2507.17832 [quant-ph].

[126] Irene Papaefstathiou, Johannes Knolle, and Mari Carmen Bañuls. "Real-time scattering in the lattice Schwinger model". In: *Phys. Rev. D* 111.1 (2025), p. 014504. DOI: 10.1103/PhysRevD.111.014504. arXiv: 2402.18429 [hep-lat].

[127] Raghav G. Jha et al. "Real-time scattering in Ising field theory using matrix product states". In: *Phys. Rev. Res.* 7.2 (2025), p. 023266. DOI: 10.1103/9dxz-k5wb. arXiv: 2411.13645 [hep-th].

[128] Tianyin Li et al. "Scattering amplitude from quantum computing with reduction formula". In: *Phys. Rev. D* 109.3 (2024), p. 036025. DOI: 10.1103/PhysRevD.109.036025. arXiv: 2301.04179 [hep-ph].

[129] Raúl A. Briceño et al. "Toward coherent quantum computation of scattering amplitudes with a measurement-based photonic quantum processor". In: *Phys. Rev. Res.* 6.4 (2024), p. 043065. DOI: 10.1103/PhysRevResearch.6.043065. arXiv: 2312.12613 [quant-ph].

[130] A. P. Balachandran et al. "Emergent Gauge Symmetries and Quantum Operations". In: *J. Phys. A* 53.6 (2020), 06LT01. DOI: 10.1088/1751-8121/ab6143. arXiv: 1906.05464 [quant-ph].

[131] Ivan M. Burbano, T. Rick Perche, and Bruno de S. L. Torres. "A path integral formulation for particle detectors: the Unruh-DeWitt model as a line defect". In: *JHEP* 03 (2021), p. 076. DOI: 10.1007/JHEP03(2021)076. arXiv: 2012.14912 [hep-th].

[132] Ivan M. Burbano and Francisco Calderón. "Self-Normalizing Path Integrals". In: *Found. Phys.* 54.5 (2024), p. 60. DOI: 10.1007/s10701-024-00779-1. arXiv: 2109.00517 [hep-th].

[133] Ivan M. Burbano, Justin Kulp, and Jonas Neuser. "Duality defects in E_8". In: *JHEP* 10 (2022), p. 186. DOI: 10.1007/JHEP10(2022)187. arXiv: 2112.14323 [hep-th].

[134] Anthony N. Ciavarella, Ivan M. Burbano, and Christian W. Bauer. "Efficient truncations of SU(Nc) lattice gauge theory for quantum simulation". In: *Phys. Rev. D* 112.5 (2025), p. 054514. DOI: 10.1103/ylqb-phv5. arXiv: 2503.11888 [hep-lat].

[135] Iván Mauricio Burbano. *ivanmbur/dissertation_supplementary_material*. Aug. 14, 2026. DOI: 10.5281/zenodo.21935845.

[136] Michael Creutz. "Gauge Fixing, the Transfer Matrix, and Confinement on a Lattice". In: *Phys. Rev. D* 15 (1977). Ed. by J. Julve and M. Ramón-Medrano, p. 1128. DOI: 10.1103/PhysRevD.15.1128.

[137] Michael Creutz. *Quarks, Gluons and Lattices*. Oxford University Press, 1983. ISBN: 978-0-521-31535-7. DOI: 10.1017/9781009290395.

[138] Brian C. Hall. *Lie Groups, Lie Algebras, and Representations*. Vol. 222. Graduate Texts in Mathematics. Cham: Springer, 2015. ISBN: 978-3-319-13467-3. DOI: 10.1007/978-3-319-13467-3.

[139] Yao Ji, Henry Lamm, and Shuchen Zhu. "Gluon Field Digitization via Group Space Decimation for Quantum Computers". In: *Phys. Rev. D* 102.11 (2020), p. 114513. DOI: 10.1103/PhysRevD.102.114513. arXiv: 2005.14221 [hep-lat].

[140] M. Sohaib Alam et al. "Primitive quantum gates for dihedral gauge theories". In: *Phys. Rev. D* 105.11 (2022), p. 114501. DOI: 10.1103/PhysRevD.105.114501. arXiv: 2108.13305 [quant-ph].

[141] Andrei Alexandru et al. "Spectrum of digitized QCD: Glueballs in a S(1080) gauge theory". In: *Phys. Rev. D* 105.11 (2022), p. 114508. DOI: 10.1103/PhysRevD.105.114508. arXiv: 2112.08482 [hep-lat].

[142] Yao Ji, Henry Lamm, and Shuchen Zhu. "Gluon digitization via character expansion for quantum computers". In: *Phys. Rev. D* 107.11 (2023), p. 114503. DOI: 10.1103/PhysRevD.107.114503. arXiv: 2203.02330 [hep-lat].

[143] Erik J. Gustafson, Henry Lamm, and Felicity Lovelace. "Primitive quantum gates for an SU(2) discrete subgroup: Binary octahedral". In: *Phys. Rev. D* 109.5 (2024), p. 054503. DOI: 10.1103/PhysRevD.109.054503. arXiv: 2312.10285 [hep-lat].

[144] Erik J. Gustafson et al. "Primitive quantum gates for an SU(3) discrete subgroup: $\Sigma(36\times3)$". In: *Phys. Rev. D* 110.3 (2024), p. 034515. DOI: 10.1103/PhysRevD.110.034515. arXiv: 2405.05973 [hep-lat].

[145] Benoît Assi and Henry Lamm. "Digitization and subduction of SU(N) gauge theories". In: *Phys. Rev. D* 110.7 (2024), p. 074511. DOI: 10.1103/PhysRevD.110.074511. arXiv: 2405.12204 [hep-lat].

[146] Henry Lamm et al. "Block encodings of discrete subgroups on a quantum computer". In: *Phys. Rev. D* 110.5 (2024), p. 054505. DOI: 10.1103/PhysRevD.110.054505. arXiv: 2405.12890 [hep-lat].

[147] Sebastian Osorio Perez et al. "Primitive Quantum Gates for an $SU(3)$ Discrete Subgroup: $\Sigma(72 \times 3)$". In: (Nov. 2025). arXiv: 2511.17437 [hep-lat].

[148] Tobias Hartung et al. "Digitising SU(2) gauge fields and the freezing transition". In: *Eur. Phys. J. C* 82.3 (2022), p. 237. DOI: 10.1140/epjc/s10052-022-10192-5. arXiv: 2201.09625 [hep-lat].

[149] Simone Romiti and Carsten Urbach. "Digitizing lattice gauge theories in the magnetic basis: reducing the breaking of the fundamental commutation relations". In: *Eur. Phys. J. C* 84.7 (2024), p. 708. DOI: 10.1140/epjc/s10052-024-13037-5. arXiv: 2311.11928 [hep-lat].

[150] David B. Kaplan and Jesse R. Stryker. "Gauss's law, duality, and the Hamiltonian formulation of U(1) lattice gauge theory". In: *Phys. Rev. D* 102.9 (2020), p. 094515. DOI: 10.1103/PhysRevD.102.094515. arXiv: 1806.08797 [hep-lat].

[151] Jan F. Haase et al. "A resource efficient approach for quantum and classical simulations of gauge theories in particle physics". In: *Quantum* 5 (2021), p. 393. DOI: 10.22331/q-2021-02-04-393. arXiv: 2006.14160 [quant-ph].

[152] Julian Bender and Erez Zohar. "Gauge redundancy-free formulation of compact QED with dynamical matter for quantum and classical computations". In: *Phys. Rev. D* 102.11 (2020), p. 114517. DOI: 10.1103/PhysRevD.102.114517. arXiv: 2008.01349 [quant-ph].

[153] G. Burgio et al. "The Basis of the physical Hilbert space of lattice gauge theories". In: *Nucl. Phys. B* 566 (2000), pp. 547–561. DOI: 10.1016/S0550-3213(99)00533-7. arXiv: hep-lat/9906036.

[154] Kevin Costello. *Renormalization and Effective Field Theory*. Mar. 2011. DOI: 10.1090/surv/170.

[155] Manu Mathur. "Harmonic oscillator prepotentials in SU(2) lattice gauge theory". In: *J. Phys. A* 38 (2005), pp. 10015–10026. DOI: 10.1088/0305-4470/38/46/008. arXiv: hep-lat/0403029.

[156] Manu Mathur. "The loop states in lattice gauge theories". In: *Phys. Lett. B* 640 (2006), pp. 292–296. DOI: 10.1016/j.physletb.2006.08.022. arXiv: hep-lat/0510101.

[157] Manu Mathur. "Loop Approach to Lattice Gauge Theories". In: *Nucl. Phys. B* 779 (2007), pp. 32–62. DOI: 10.1016/j.nuclphysb.2007.04.031. arXiv: hep-lat/0702007.

[158] Indrakshi Raychowdhury and Ramesh Anishetty. "Prepotential Formulation of Lattice Gauge Theory". In: *PoS* LATTICE2014 (2014), p. 313. DOI: 10.22323/1.214.0313. arXiv: 1411.3068 [hep-lat].

[159] J. Schwinger. "On angular momentum". In: (Jan. 1952). DOI: 10.2172/4389568.

[160] Henry Froland, Dorota M. Grabowska, and Zhiyao Li. "Simulating Fully Gauge-Fixed SU(2) Hamiltonian Dynamics on Digital Quantum Computers". In: (Dec. 2025). arXiv: 2512.22782 [quant-ph].

[161] R. Haag. "Quantum field theories with composite particles and asymptotic conditions". In: *Phys. Rev.* 112 (1958), pp. 669–673. DOI: 10.1103/PhysRev.112.669.

[162] R. Haag. *Local quantum physics: Fields, particles, algebras*. 1992.

[163] Sidney Coleman. *Lectures of Sidney Coleman on Quantum Field Theory*. Ed. by Bryan Gin-ge Chen et al. Hackensack: WSP, Dec. 2018. ISBN: 978-981-4632-53-9. DOI: 10.1142/9371.

[164] A. Dixit and A. Roy. "Analogue of a Fock-type integral arising from electromagnetism and its applications in number theory". In: *Research in the Mathematical Sciences* 7 (2020), p. 25. DOI: 10.1007/s40687-020-00223-6. arXiv: 1907.03650 [math.NT].

[165] Zohreh Davoudi and Martin J. Savage. "Improving the Volume Dependence of Two-Body Binding Energies Calculated with Lattice QCD". In: *Phys. Rev. D* 84 (2011), p. 114502. DOI: 10.1103/PhysRevD.84.114502. arXiv: 1108.5371 [hep-lat].

[166] Igor Khavkine. "Covariant phase space, constraints, gauge and the Peierls formula". In: *Int. J. Mod. Phys. A* 29.5 (2014), p. 1430009. DOI: 10.1142/S0217751X14300099. arXiv: 1402.1282 [math-ph].

[167] Michael F. Atiyah. "Topological quantum field theory". en. In: *Publications Mathématiques de l'IHÉS* 68 (1988), pp. 175–186. DOI: 10.1007/BF02698547. URL: https://pmihes.centre-mersenne.org/articles/10.1007/BF02698547/.

[168] R. P. Feynman. "Space-time approach to nonrelativistic quantum mechanics". In: *Rev. Mod. Phys.* 20 (1948), pp. 367–387. DOI: 10.1103/RevModPhys.20.367.

[169] Kasia Rejzner. *Perturbative Algebraic Quantum Field Theory: An Introduction for Mathematicians*. Mathematical Physics Studies. New York: Springer, 2016. ISBN: 978-3-319-25899-7. DOI: 10.1007/978-3-319-25901-7.

[170] K. Osterwalder and E. Seiler. "Gauge Field Theories on the Lattice". In: *Annals Phys.* 110 (1978), p. 440. DOI: 10.1016/0003-4916(78)90039-8.

[171] Owen Gwilliam and Theo Johnson-Freyd. "How to derive Feynman diagrams for finite-dimensional integrals directly from the BV formalism". In: (Feb. 2012). arXiv: 1202.1554 [math-ph].

[172] Glen Bigan Mbeng, Angelo Russomanno, and Giuseppe E. Santoro. "The quantum Ising chain for beginners". In: *SciPost Phys. Lect. Notes* 82 (2024), p. 1. DOI: 10.21468/SciPostPhysLectNotes.82. arXiv: 2009.09208 [quant-ph].

[173] Marcela Carena et al. "Gauge theory couplings on anisotropic lattices". In: *Phys. Rev. D* 106.11 (2022), p. 114504. DOI: 10.1103/PhysRevD.106.114504. arXiv: 2208.10417 [hep-lat].

[174] Christopher F. Kane, Siddharth Hariprakash, and Christian W. Bauer. "Obtaining continuum physics from dynamical simulations of Hamiltonian lattice gauge theories". In: (June 2025). arXiv: 2506.16559 [hep-lat].